MARTIN MARIETTA ENERGY SYSTEMS LIBRARIES
3 4456 0049751 2

CENTRAL RESEARCH LIBRARY
DOCUMENT COLLECTION

ORNL-2879
Reactors-Power

HOMOGENEOUS REACTOR PROGRAM

PROGRESS REPORT

FOR PERIOD MAY 1 THROUGH OCTOBER 31, 1959

CENTRAL RESEARCH LIBRARY
DOCUMENT COLLECTION
LIBRARY LOAN COPY
DO NOT TRANSFER TO ANOTHER PERSON
If you wish someone else to see this document, send in name with document and the library will arrange a loan.

OAK RIDGE NATIONAL LABORATORY
operated by
UNION CARBIDE CORPORATION
for the
U.S. ATOMIC ENERGY COMMISSION

Printed in USA. Price $4.00. Available from the

Office of Technical Services
Department of Commerce
Washington 25, D.C.

LEGAL NOTICE

This report was prepared as an account of Government sponsored work. Neither the United States, nor the Commission, nor any person acting on behalf of the Commission:

A. Makes any warranty or representation, expressed or implied, with respect to the accuracy, completeness, or usefulness of the information contained in this report, or that the use of any information, apparatus, method, or process disclosed in this report may not infringe privately owned rights; or

B. Assumes any liabilities with respect to the use of, or for damages resulting from the use of any information, apparatus, method, or process disclosed in this report.

As used in the above, "person acting on behalf of the Commission" includes any employee or contractor of the Commission, or employee of such contractor, to the extent that such employee or contractor of the Commission, or employee of such contractor prepares, disseminates, or provides access to, any information pursuant to his employment or contract with the Commission, or his employment with such contractor.

ORNL-2879
Reactors-Power
TID-4500 (15th ed.)

Contract No. W-7405-eng-26

HOMOGENEOUS REACTOR PROGRAM

PROGRESS REPORT

for Period May 1 Through October 31, 1959

Program Director - R. B. Briggs

Homogeneous Reactor Test - S. E. Beall
Reactor Analysis and Engineering Development - R. N. Lyon
Reactor Materials Research - E. G. Bohlmann
Chemical Engineering Development - D. E. Ferguson
Supporting Chemical Research - H. F. McDuffie
Analytical Chemistry - M. T. Kelley

DATE ISSUED

JAN 27 1960

OAK RIDGE NATIONAL LABORATORY
Oak Ridge, Tennessee
operated by
UNION CARBIDE CORPORATION
for the
U.S. ATOMIC ENERGY COMMISSION

MARTIN MARIETTA ENERGY SYSTEMS LIBRARIES
3 4456 0049751 2

SUMMARY

PART I. HOMOGENEOUS REACTOR TEST

1. HRT Operations

In this report period the reactor was in operation for over 2500 hr, including a continuous run of 1364 hr. Over 3200 Mwhr(th) were generated. Experimental effort was directed principally at the problem of fuel instability. It was learned that the instability is especially sensitive to system pressure; the reactor is completely stable below 1400 psig but exhibits power disturbances and reactivity losses when at high power with the pressure at 1400 psig or above. The relatively sharp division between stable and unstable performance may be associated with the formation and separation of a heavy liquid phase in fuel solution. Since acid concentration affects this phenomenon, experiments are being planned with various acidity levels.

Measurements were made to determine the reactivity loss resulting from buildup of xenon in the high-pressure system. Although a small amount of poisoning (1% or less) is indicated, final results are not yet available.

A series of experiments is presently in progress to determine the activity of copper as a D_2-O_2 recombination catalyst in the fuel solution.

2. HRT Processing Plant

The multiple hydroclone, designed to increase solids removal rates through faster processing, was tested, installed in the reactor cell prior to HRT run 20, and operated throughout the run. Solids concentrated in the multiclone underflow are routed to the original cell C hydroclone feed line for collection in the underflow receiver. Removal rates decreased from 5 g/hr initially to an equilibrium value of 0.5 g/hr after 500 hr. These rates average 50-80% greater than those obtained previously with the single hydroclone under comparable operating conditions. Prior to operation, equilibrium removal rates in excess of 1 g/hr were predicted. The lower rates are attributed to uncertainties about the solids particle size, which had led to an incorrect estimate of hydroclone efficiency.

Removal rates dropped drastically in the final three operating periods during run 20. A malfunction of the single hydroclone was suspected, and this unit was replaced following run 20. Removal rates in the first 88 hr of run 21 were a factor of 5 below those in the comparable period of run 20; thus the condition of the system is still uncertain.

In the past year, corrosion-product solids have been produced at a rate no higher than 1.6 g/hr and removed at an average rate of 1.1 g/hr.

A substantial holdup of iodine in the reactor high-pressure system was confirmed by methods previously described and from a comparison of calculated and measured heat generation rates on the iodine trap in the low-pressure system. Calculations based on Cs^{137}/Cs^{135} mass ratios showed that xenon is also being held up longer than had been anticipated.

3. HRT Remote Operations

In a period of maintenance prior to run 20, the fuel-circulating pump was replaced, the blanket sampling mechanism was removed and repaired, and a new multiple hydroclone was installed in the reactor piping, connected to the chemical plant.

Several remote operations were performed at the HRT after run 20. These included: (1) determination that four diffuser screens were detached from the core, (2) photography of the hole and core interior, (3) measurement of the core-tank thickness, and (4) exposure of some plastics in the core gamma field of 40,400 to 82,900 r/hr.

Tools for modification of the HRT core were designed and fabricated, and testing was completed in the HRT-maintenance mockup. Detailed operating instructions were prepared for the use of the tools at the HRT.

A 2-in.-dia television camera was adapted for viewing the inside of the core. A core-access-flange reamer was developed to permit full use of the nominal 2-1/8-in. port. A core-access standpipe, which will simplify some core remote operations, was designed.

Tests were performed on the HRT flow model to develop a procedure for flushing solids out of the core following screen removal.

4. HRT Engineering Development

A test of two HRT prototype feed-pump heads was discontinued after 19,256 hr of operation; one head was installed in the reactor. A test titanium impeller with high wear-ring clearance was not burned after use as an oxygen-steam blower. A rotation-speed and rotation-direction indicator was built for HRT-type circulating pumps.

The HRT mockup was operated for 1050 hr in run CS-25, which was an investigation of inventory control during stable and unstable chemical conditions.

5. HRT Design

The activity hazards in the HRT steam system associated with a ruptured heat exchanger tube were re-evaluated.

The HRT fuel primary and secondary recombiners were redesigned to provide for more adequate heating and easier reactivation.

Several details of the HRT samplers were redesigned to improve operation and increase reliability.

The design of thimbles to permit replacement of the Victoreen gamma monitors in the steam-drum pit and instrument cubicles during reactor operation was completed.

6. HRT Controls and Instrumentation

The feasibility of using a Laub Electrocaloric flowmeter for measurement of HRT fuel feed flows is being investigated.

A miniature television camera was modified for use in viewing the impeller of the blanket circulating pump.

The presently installed reactor letdown valve continues to give satisfactory performance; it has operated for 5657 hr. A similar valve has operated satisfactorily in the HRT mockup for 4780 hr.

The HRT fuel feed shutoff valve was replaced. Preliminary tests indicate that failure was due to mechanical binding between the valve stem and its guide bushing.

A second generator was installed to provide standby power for the d-c control circuitry. The emergency block control system was extensively revised. Instrumentation and control for the fuel recombiner superheater was designed and installed.

An emergency a-c power supply for the public-address system was installed.

PART II. REACTOR ANALYSIS AND ENGINEERING DEVELOPMENT

7. Reactor Analysis

A study was made of the nuclear statics characteristics of small, two-region reactors containing 1000 g of Th per liter in the blanket region, a solution core, and a water moderator with various percentages of D_2O. In order to maintain a core fuel concentration less than 10 g of U per liter at 280°C with a blanket region less than 1 ft thick and containing less than 40 g of U^{235} per kg of Th, the core diameter must be greater than about 24 in. At larger core diameters there is an increase in the combinations of blanket thicknesses and blanket fuel concentrations which give core critical concentrations less than 10 g of U per liter; for a 30-in.-dia core, this condition is satisfied by a 1-ft-thick blanket containing 20 or more grams of U^{235} per kg of Th and also by an 8-in.-thick blanket containing 40 g of U^{235} per kg of Th. The moderator composition associated with minimum critical mass was usually in the range of 60 to 80% D_2O. About 50% of the reactor power was generated in the blanket for either a 12-in.-thick blanket containing 20 g of U^{235} per kg of Th or an 8-in.-thick blanket containing 40 g of U^{235} per kg of Th. For blanket fuel concentrations greater than about 10 g of U^{235} per kg of Th, the core-wall power density was greater on the blanket side of the wall.

Studies were made of the effect of region composition on the power generated within in-pile loops. In present ORR in-pile loops a 1/2-in. void annulus surrounds the core region of the loop, and the region adjacent to the rear of the loop core contains little neutron-reflecting material. Based on the results of calculations, filling the annular void region with reflecting material will about double the power generated in the loop; if a 6-in. graphite reflector were placed at the rear of the loop core, the loop power would increase about 20% above that associated with no reflector and no annular void. Use of beryllium instead of graphite would change the 20% increase to about 50%; however, capture gamma heating in the beryllium would generate about 0.13 kw of energy compared with

about 0.013 kw in graphite. Again based on results from computations, replacement of the H_2O in the region surrounding the in-pile loop with D_2O would not appreciably increase the power generated in the loop core.

8. Development of Fuel- and Slurry-System Components

A 2500-hr operating test at 1500 psi was completed successfully by the natural-circulation recombiner.

Testing of a 20-cfm canned-motor blower was terminated by a stator failure after a long period of successful performance at 225°C and 1500 psi. An irradiated stator maintained satisfactory electrical properties after 5.4×10^9 rad exposure. Excellent performance of aluminum oxide bearings and a nitrided-titanium floating-bushing shaft seal were demonstrated in the 300A slurry pump.

Testing of diaphragm oxygen compressors, increased-capacity solution pumps, and slurry pumps continued with only minor difficulties. Simplifications in the coupling of feed pumps to feed tanks were demonstrated. Various grades of alumina were tested as check-valve trim; fracture of the valve seats as a result of inadequate mounting designs was frequent.

Tests of a 4-ft-dia spherical re-entrant core model were completed with measurement of the velocity distribution near the core wall. The distribution was in excellent agreement with the universal velocity law, and heat transfer coefficients computed from the observed velocities were in excellent agreement with those measured.

Preliminary tests of a cylindrical core with swirling flow were promising from the standpoint of blanketing the core wall with cool fluid. The mechanical design of a full-scale vessel with such a core was initiated. Qualitative indications that similar conditions could be achieved in a spherical annular-entry core were obtained from small model tests.

Unstable flow conditions were generated in the 30-in. slurry core vessel at flow rates below 100 gpm, at various concentrations. The design appeared adequate for slurry suspension at the rated 300 gpm.

9. Development of Reactor Slurry Systems

A new 50-gpm Byron-Jackson canned-motor pump circulated an 800°C-fired, digested thoria in the 200A loop successfully. The slurry behavior was judged to be inferior to that of 1600°C-fired thoria. The formation of a cake on a surface from which heat was being removed was noted in the 200B loop; a mixed-oxide slurry (8% uranium) was being circulated at the time at 230 to 280°C. When cake was absent, the heat transfer coefficients at the cooled surface were close to those observed earlier for water.

A general relationship was derived for predicting the effect of temperature on the settled-bed density and the yield stress of slurries in small tubes.

Run SM-7, during which slurry distribution inside the 300-SM system core vessel was investigated at 150 to 200°C, was completed. A primary objective of a new run, SM-8, was to extend the temperature range investigated to 300°C. The vessel appeared to perform satisfactorily at flow rates above 130 gpm.

During run SM-8, the 300-SM low-pressure system was operated in conjunction with the high-pressure system for the first time. The system performed successfully as a charging device, and it received several dumps of the high-pressure system.

10. Instrument and Valve Development

The differential transformer developed for use at high temperatures and in radiation fields was operated for three months at 300°C without change of characteristics.

A new design for a transistorized electropneumatic converter was developed.

A new Foxboro Instrument Company electric transmission system for process instrumentation was evaluated and found to be satisfactory.

No slurry plugging difficulties or other malfunctions have been experienced with a Norwood Controls Division pressure transmitter installed on the 300 Slurry Mockup Loop.

An analog computer was acquired for use in training personnel and for solution of simple HRP problems.

A Branson-type ceramic ultrasonic transducer for detecting the interface of a falling slurry was tested in a beaker at room temperature and in an autoclave up to 150°C. While the interface could be detected during the initial stages of an experiment, gas bubbles collected on the transducer face, causing the signal to become weak and erratic.

A Zircaloy-2 trim installed in a flush-bellows Hammel-Dahl valve was in good condition after 2064 hr of operation in slurry service.

After 22 hr of slurry flow, the tungsten carbide trim in a High Pressure Equipment handwheel valve, used for letting down slurry from 1500 to 500 psig was severely eroded.

Five Ti-55 bellows assemblies have been cycled to destruction in uranyl sulfate at 280°C. Performance exceeded design specifications.

Three HRT-type stem-sealing bellows were cycled to destruction in a slurry consisting of 400 g of ThO_2 per kg of H_2O. Results indicate that bellows life is not adversely affected by ThO_2 slurry.

The use of handwheels incorporating Saginaw ball bearing assemblies reduces friction and permits manual operation of general-purpose sampling valves where pressures as high as 2000 psig are applied to the bellows.

11. Heat Transfer Studies

Heat transfer measurements were made using an electrically heated stainless steel tube in degassed and in oxygenated H_2O, D_2O, and uranyl sulfate solution circulated at 100 to 250°C and at pressures from 300 to 1000 psia. No difference was observed between light and heavy water, but electrolytic effects obscured the results for uranyl sulfate solution. The oxygen decreased the boiling point of water as predicted from Henry's law constants and also decreased the heat-transfer coefficient in the nucleate-boiling region.

PART III. SOLUTION FUELS

12. Reactions in Aqueous Solutions

Reaction rates were measured for the four combinations of H_2 and D_2 with H_2O and D_2O in 0.1 M $Cu(ClO_4)_2$ solutions at acidities of 0.01 and 1.0 M and at temperatures of 100, 120, and 130°C. The calculated energies of activation decreased with increasing acidity but appeared to be independent of the choice of solute or solvent.

The effectiveness of cupric ion as a catalyst in a UO_3-HNO_3-H_2O fuel system was investigated. Comparisons were made of the catalytic activity of cupric ion in the nitrate fuel solution and in the presently used sulfate system. Using reasonable assumptions, permissible power densities at several temperatures were calculated for the nitrate system.

13. Heterogeneous Equilibria in Aqueous Systems

Study of the boundaries of the liquid-liquid immiscibility regions of systems having compositions related to that of the HRT fuel reveals that, upon concentration by removal of water, the two-liquid-phase temperatures pass through minimal values at concentration factors of 2X to 10X. For the HRT fuel the minimum temperature was 305°C; this temperature corresponds closely to that pressurizer temperature below which stable reactor operation has been achieved and above which power-dependent instability has been observed. If local boiling, from the presence of localized hot spots, occurs above this temperature, the slow concentration of surrounding solution can lead to the sudden formation of a very concentrated second-liquid-phase with its attendant increase in fission-energy density. If local boiling is forced to take place below the minimal two-liquid-phase temperature, then no amount of slow concentration by boiling can lead to the sudden hundredfold concentration increase provided by the appearance of a second-liquid phase.

The second-liquid-phase temperatures of solutions initially 1.25, 2.5, 5, and 10 times as concentrated as the core solution in HRT run 20 were determined in a titanium loop equipped with a hydroclone. Agreement with quartz-tube data was obtained.

The temperature of two-liquid-phase formation for a sample of radioactive HRT fuel solution was determined. There appeared to be little reason to believe that the high radiation level to which the fuel solution was exposed in the reactor exerted a significant effect on its phase behavior.

Preliminary experiments indicate a reversible adsorption of uranium on metal oxides which increases with increasing temperature. The observation suggests that a similar phenomenon may account for some of the operational anomalies of the HRT.

Determinations from 300 to 350°C were made of the compositions of light and heavy phases in the systems UO_3-SO_3-H_2O and UO_3-SO_3-D_2O. The heavy phase in equilibrium with a light phase approximating HRT fuel in SO_3 concentration contained nearly stoichiometric UO_2SO_4 at concentrations from 5 to 9 m, which varied with temperature. Copper and nickel, in solutions of similar total SO_3 concentration, appeared to occur in the heavy phase as approximately stoichiometric $CuSO_4$ and $NiSO_4$. There was little difference between D_2O and H_2O in solubility relationships in the heavy phase, but some difference was found in the light-phase relationships.

Two additional binary curves at 300°C were established in the sytem UO_3-CuO-NiO-SO_3-$H_2O(D_2O)$. These binaries were determined for SO_3 concentrations varying from 0.02 to 0.2 m. The first binary curve showed stable solids, $CuO \cdot 3UO_3$ and $UO_3 \cdot H_2O$, up to an invariant at 0.12 m SO_3 at which point the heavy-liquid phase appeared. The second binary showed stable solids, $UO_3 \cdot H_2O$, and a compound possibly containing both nickel and uranium. Based on these and previous data, it is anticipated that the liquid-liquid immiscibility region at constant m_{SO_3} will engulf considerable portions of the five-component system at temperatures higher than 300°C.

The effect of the UO_3/SO_3 molar ratio on immiscibility temperatures of 0.10 m SO_3 solutions was determined. A plot of temperature vs UO_3/SO_3 gave an approximately linear relationship down to a ratio of 0.18. Below this ratio the UO_3 component appeared to be soluble in the supercritical fluid.

Temperatures of formation of two-liquid phases were determined in the system UO_3-SO_3-N_2O_5-H_2O. The data indicate that there is probably little advantage in using mixed nitrate-sulfate anions in uranyl solutions as compared to UO_2SO_4-H_2SO_4 solutions.

The investigation of the system UO_3-N_2O_5-H_2O at 150 to 300°C was extended up to 2 m and down to 0.00025 m N_2O_5. Further studies were carried out in the middle concentration range in order to improve the over-all precision of previous data. An exploratory investigation at 300°C of the system UO_3-CuO-NiO-N_2O_5-H_2O indicated no markedly lowered solubilities which might adversely affect its use as a reactor fuel.

Liquid-salt-bath equipment for the determination of phase equilibria in sealed tubes was improved considerably and is yielding more precise data. An all-titanium pressure vessel of 50-ml capacity has been developed for routine use from 100 to 500°C. Also an all-platinum-lined vessel of similar capacity is approaching satisfactory completion. Upon final modification of these two vessels, additional ones are to be constructed for routine use in high-temperature solubility measurements for the most part above 300°C.

14. Solution Corrosion

Corrosion rates of several alloys and the critical velocity of type 347 stainless steel in a solution containing 0.03 m $UO_2(NO_3)_2$, 0.02 m $Cu(NO_3)_2$, and 0.10 m DNO_3 at 250°C were found to be about the same as those observed in uranyl sulfate solutions similar to HRT fuel used in run 20. With the volume ratio of solution to vapor equal to 4, approximately 1% of the nitric acid originally in solution was in the vapor phase.

Deoxidine-170 diluted 50% with water descaled a stainless steel loop effectively and was not excessively corrosive to titanium.

Stress-corrosion-cracking tests with cast type 347 stainless steel have confirmed previous data to the effect that the alloy is resistant to stress-corrosion cracking in chloride environments so long as the material is not permanently deformed. Preliminary tests with other alloys have indicated that cast types 316 and 309SCb stainless steels may be as resistant, or even more so, than type 347 stainless steel in chloride environments.

15. Radiation Corrosion

The first ORR in-pile loop, 0-1-25, was inserted in beam hole HN-1 of the ORR on May 18, 1959. The loop operated continuously at a mainstream temperature of 280°C until a scheduled removal on Sept. 8, 1959. During this period 2741 hr of loop operation and 36,895 Mwhr of reactor energy were accumulated. The loop was fully inserted during 30,159 Mwhr, fully retracted during 6100 Mwhr, and partially retracted during 636 Mwhr.

With a few exceptions, the performance of the components of loop and auxiliary equipment was good. Both the core cooler and the bypass line from the pressurizer to the back of the pump ceased functioning, presumably because of stoppages in the lines. These lines are being examined.

The effect of reactor radiation on the over-all corrosion rate of the loop components was continuously monitored by measurement of the oxygen consumed and by frequent removal of solution samples for chemical analyses. The loop also contained a number of corrosion specimens which are currently being removed from the loop for examination.

Except for qualitative and metallographic examinations, in-pile loop experiment L-2-22 was completed and is reported. This experiment was designed with the primary objective of determining the effects of inclusion of Li_2SO_4-H_2SO_4 additives in a 0.04 m UO_2SO_4 solution on the radiation-induced corrosion of Zircaloy-2 at 280°C, in comparison with the corrosion observed in a previous loop experiment, L-2-10, which employed a solution of similar UO_2SO_4 concentration but low concentrations of additives (0.02 m H_2SO_4 and 0.008 m $CuSO_4$).

Zircaloy-2 specimens of commercially annealed material with as-machined surfaces, similar to those employed in L-2-10, were included in the core. The solution initially charged and used during most of the in-pile exposure was 0.036 m UO_2SO_4, 0.002 m $CuSO_4$, 0.18 m Li_2SO_4, and 0.09 m H_2SO_4 in D_2O. (H_2O was employed in L-2-10.) The test with this solution was interrupted when a laboratory power failure led to conditions which required that the solution be drained. The replacement solution was of a composition similar to that employed in the previous L-2-10 experiment, except that the solvent was D_2O rather than H_2O, as in L-2-10. This replacement solution was in turn replaced with a solution similar in composition to the initial solution for the final portion of the run.

As reported previously, experiments for studying the deposition of uranium in the core under conditions of low solution-flow rate and low overpressure were carried out during the periods of operation with the replacement solutions. Thus, the over-all experiment was not a straightforward test of Zircaloy-2 corrosion in the solution which contained additives.

In addition to the primary objective, the test was used to gain information on the radiation-induced corrosion of some other materials and of the effects on Zircaloy-2 corrosion brought about by different types of heat treatment and chemical polishing of the specimen surfaces.

The results of quantitative analyses of metallic constituents in films and scales found on various specimen surfaces showed that core as well as in-line specimens of zirconium-alloys retained the film or scale in amounts which must be taken into consideration in making accurate evaluations of the zirconium-alloy corrosion rates according to specimen-weight data. Consequently, the

analytical results were used to estimate the total amount of oxide on each of the core specimens. About 2 mg/cm^2 was estimated for each specimen, regardless of material or location.

The average corrosion rates of the commercially annealed, as-machined, Zircaloy-2 specimens at given solution power densities were substantially less than those observed in the previous experiment, L-2-10, which contained no additives. Because of the scale on the core specimens, the results of the present experiment do not provide a direct test of the previously proposed hypothesis that the beneficial action is due to a reduction or elimination of uranium sorption on Zircaloy-2 surfaces during radiation-exposure. However, they are consistent with this hypothesis.

The corrosion rates of commercially annealed and chemically polished Zircaloy-2 specimens in this experiment were less than those for the as-machined specimens.

Different heat treatments of Zircaloy-2 had no apparent effects on the corrosion rates. Core specimens of crystal-bar zirconium, Zr-5% Sn, Zr-15% Nb, Zr-15% Nb-5% Mo, and Zr-15% Nb-2% Mo exhibited corrosion rates which, with two exceptions, were from 1.4 to 2.5 times greater than those for similarly located Zircaloy-2 specimens. For the exceptions, the similarly determined factors were 1.0 and 4.3, respectively, for the two specimens of crystal-bar zirconium. The corrosion rates for the niobium core specimens were about twenty times greater than those for Zircaloy-2.

A new rocking-autoclave experiment assembly has been designed and constructed which will permit an experiment to be operated in any one of three beam holes of the LITR. The new design is an attempt to improve the reliability, safety, and flexibility of this apparatus which has been in use for a number of years for obtaining information on the effect of reactor radiation on the corrosion of materials of interest in the aqueous Homogeneous Reactor Program.

The results of several autoclave experiments which were exposed in-pile several months ago have become available and are being studied and reported. The results of three of these experiments are summarized in this report.

A Zr-1% Cr alloy, reported to be more resistant than Zircaloy-2 to 900°F steam, was tested along with Zircaloy-2 control specimens under irradiation in contact with a uranyl sulfate solution (300 g uranium per liter) at 275°C. The data indicate that insignificant amounts of uranium deposited on the specimen surfaces and, thus, that the Zr - 1% Cr alloy and the Zircaloy-2 samples were both exposed to the same effective fission power density of 36 w/ml. That is to say, the deposited uranium provided practically no additional radiation over that provided by the fissioning uranium in the solution. The corrosion rates observed were practically the same for both alloys, 12.4 mpy for the Zr - 1% Cr alloy and 12.0 mpy for Zircaloy-2.

A scouting experiment dealing with the $Cr(III) \rightleftharpoons Cr(VI)$ equilibrium in uranyl sulfate solution under irradiation was carried out. The reduction of Cr(VI) to the subsequently insoluble Cr(III) may be largely responsible for the apparent insolubility of Cr(VI) in uranyl sulfate solutions under irradiation. Ruthenium, which catalyzes the oxidation of Cr(III) to Cr(VI), was added, along with 200 ppm of Cr(VI), to the solution in an effort to determine if a significant concentration of Cr(VI) could be stabilized under irradiation and what effects the additives have on the corrosion of type 347 stainless steel and Zircaloy-2.

The results indicate that the chromium remained as Cr(III) during the irradiation, but was converted to Cr(VI) after radiation was terminated. The type 347 stainless steel corrosion rate was probably not affected by the addition. Zircaloy-2 corroded somewhat faster than in a comparable previous test, apparently because of a high concentration of uranium in the corrosion scale.

Corrosion at a heated Zircaloy-2 surface was studied in an autoclave, using a hollow pin specimen filled with enriched UO_2, and sealed. The heat flux through the specimen surface ranged from 3.5 w/cm^2 at one end to 5.7 w/cm^2 at the other. The experiment was exposed to radiation at solution temperatures of 250, 280, 300, and 320°C. The pressure data indicate a possible high rate of corrosion during the 250°C period. The weight data show that the scale on the hot pin was more tenacious than that on the control specimen, and indicate that the total corrosion penetration on the hot pin was about 20% less than the corrosion expected for a non-fission-heated control coupon at the location of the specimen.

Measurements of the adsorptive capacity of hydrous zirconium oxide for uranium from uranyl sulfate solutions at high temperature (250°C) have been continued. Minor changes in the technique have led to somewhat better reproducibility than could be obtained previously. Two uranium concentrations have been studied, 5 and 25 g/liter, with all solutions 0.02 m in H_2SO_4.

The adsorption results for the 5-g/liter solution were fairly reproducible and showed capacities of about 15 mg of uranium per gram of zirconium oxide, for oxide preheated in water at 250°C overnight. Measurements with the 25-g/liter solution, and using oxide similarly pretreated or oxide preheated in the solution overnight at 250°C, showed poor reproducibility; capacities ranged from 50 to 160 mg of uranium per gram of oxide. In general, sulfate was adsorbed to a greater extent than uranium, on a molar basis. The uranium and sulfate adsorptions from one of the 5 g/liter solutions which also contained 0.02 m HNO_3 were comparable to those from solutions without added HNO_3. However, the nitrate ion was almost completely adsorbed from the first 50 ml of solution passing through the oxide.

Electrochemical measurements of Zircaloy-2 corrosion in oxygenated H_2SO_4 at 208°C were continued. The corrosion of rod stock obtained from Westinghouse several years ago and measured in the as-received but cleaned condition is significantly different from that previously found for rod stock obtained, within the past few years, from Firth-Sterling. The corrosion rates of the Westinghouse material are satisfactorily represented by a hyperbolic rate-time expression during exposure times up to 48 hr, the duration of the longest run. The source of the difference is unknown. An additional, short-term, experiment performed on the Westinghouse alloy in the same solution at 267°C resulted in periodic potential oscillations similar in character to those reported for other metals (Fe, Cr, Ni, steels) in aqueous acids, where the oscillations are interpreted as representing alternating activation-passivation phenomena.

PART IV. SLURRY FUELS

16. Engineering and Physical Properties

An extension of the Bingham-plastic model for interpreting laminar-flow data with thorium oxide slurries was attempted by relating other factors such as slurry concentration, particle size, and method of oxide preparation to the

suspension yield stress. It is found that the yield stress can be related directly to the cube of the volume fraction solids and inversely to the particle size to the 1.42 power. The constant of proportionality shows a wide variation, implying that other unconsidered factors may be of importance. The calcining temperature and the previous pumping history of the slurry do not appear to have a consistent bearing on the yield stress.

A study of data for suspensions of glass beads, steel and lead shot, sand, and ThO_2 in water indicates that a single relationship describes the noncompaction region for both flocculated and unflocculated slurries over a wide range of particle diameters, settling rates, particle densities, and pipe diameters. Additional data are required for verification.

The effect of delaying electrolyte additions for prevention of cake formation until initial ThO_2 particle degradation has occurred was studied in a series of runs in the 30-gpm loop at 275°C. Results with late additions of CrO_3 in amounts ranging from 500 to 10,000 ppm were not definitive. Similar tests are being made with $NaAlO_2$ additions.

A circulation test demonstrated that cake formation is possible even in low-concentration slurries (11 to 52 g of Th per kg of H_2O) and that degradation by particle-particle interaction is only of secondary importance in the caking phenomenon. A copper-disc heat meter installed in the wall of the 30-gpm loop appeared sensitive to deposited ThO_2 films as thin as 1 to 2 mils.

Evidences of chemisorption on ThO_2 prepared by oxalate precipitation with calcination at 800°C were found in water-vapor adsorption studies. The pore-size distribution, as computed from desportion curves, shows a sharp peak at 10 Å and an over-all range extending up to 200 Å. Electron micrographs of thorium oxide calcined at 800°C revealed that the particles consist of aggregates of minute crystals having predominatly octahedral structure. Similar micrographs of 1600°C-calcined ThO_2 showed edge-rounding of the particles as the result of circulation.

17. Slurry Irradiation Studies

A slurry of thorium oxide (500 g per kg of D_2O) containing 8% natural uranium and fired at 1050°C was irradiated 370 hr at 300°C in the LITR. No radiolytic gas was observed. This slurry and two previously irradiated slurries were recovered and analyzed for fission and corrosion products.

Three experiments in the ORNL Graphite Reactor with 500 and 250 g of Th per kg of D_2O slurries of 650°C-fired Th-2.8% U^{235} oxide and a 250-g/kg D_2O slurry of 1000°C-fired Th-3% U^{235} oxide irradiated under oxygen atmospheres showed gas production rates corresponding to G values of ~0.8. First-order recombination rate constants calculated from equilibrium pressures and measured during reactor shutdowns (for the 250-g/kg D_2O slurry of 650°C-fired oxide) agreed with each other and with previous data. In the case of the high-fired oxide the initial oxygen overpressure was consumed by corrosion, and a deuterium atmosphere accumulated, resulting in very low gas production rates for the rest of the experiment.

The solubility of hydrogen on aqueous slurries was determined, and the data are in good agreement with data from Battelle Memorial Institute, except at 150 and 200°C.

18. Development of Gas-Recombination Catalysts

Development of a catalyst for the internal recombination of radiolytic gas in thorium and thorium-uranium oxide continued. An uncatalyzed slurry of 1050°C-fired Th - 8% uranium oxide in D_2O pumped at 200°C in a D_2 atmosphere showed low recombination rates 0.005-0.06 mole D_2/liter-hr, at 280°C and 100 psi D_2 partial pressure. Two palladium catalyst preparations were investigated: one prepared by reduction of palladium on thoria suspended in an acetone-alcohol solution of palladium nitrate and a second by dispersion of thoria in an aqueous palladium nitrate solution and subsequent reduction with hydrogen. The first preparation was the least active, with a catalyst-performance index of 1.4-4.8 w/ml per 100 psi D_2 per millimolal concentration of palladium; the dispersed preparation was 10 to 20 times more active.

A new gas-injection apparatus, which permits the addition of measured quantities of the gases to a reaction autoclave at high temperatures, was developed for gas-recombination measurements. An apparatus to study the properties of slurry catalyst systems under steady-state operating conditions is under development. The apparatus consists of an electrolysis cell to produce hydrogen and oxygen, a separate recombiner vessel, and a connection for the return of the condensed recombined gases to the electrolysis cell. Continuous operation was demonstrated for periods of 26 and 99 hr.

19. Slurry Corrosion

In a series of six 100A-loop tests of 400 to 800 hr duration which were conducted to evaluate the chemical, circulation, and corrosion-erosion properties of heavy-water slurries of mixed Th-U oxides containing 8.8 and 15% U/Th, no change in the $U^{+4}/\Sigma U$ ratio of the oxides was observed in tests conducted at 200 and 280°C, using oxygen atmospheres. Under deuterium atmospheres in tests at 200°C, the ratios changed from an initial value of ~0.3 to 0.8, although recirculation of the slurry in an oxygen atmosphere resulted in restoring the ratio to essentially the initial value of ~0.3. The ΣU/Th ratio of the oxides remained constant during circulation at the test conditions. Reduction of particle and crystallite size of the oxides occurred in the oxygenated tests; however, no significant changes in rheological properties of the slurries were detected.

At a mean slurry concentration of 500 g of uranium-bearing thorium per kg of D_2O, corrosion-erosion attack closely approximated attack by slurries of pure thoria. In general the effect of increasing the uranium content of the oxides from 8.8 to 15% U/Th was to lower the attack by an average factor of 0.4. Attack rates were in some cases strongly affected by changing from an operating atmosphere of oxygen to deuterium. Stainless and alloy steels suffered severe localized attack under reducing conditions at the higher velocity, whereas attack of titanium and Zircaloy-2 was little affected by changes in atmosphere, and the attack of Inconel was diminished. These effects were most noticeable at the higher velocity.

In a toroid-test series, the effects of uranium content, calcination conditions, operating temperature, and atmosphere on the corrosive-erosive attack of materials was examined by using D_2O slurries of experimental Th-U oxides containing from 5 to 33% U/Th which had been calcined at 1050°C in air and in hydrogen. Attack of a group of selected alloys, Inconel, type 347 stainless steel, titanium, and Zircaloy-2, was increased by factors of 2 to 5 when the operating temperature was increased from 200 to 280°C. There was a notable

effect produced by oxides that had been fired in hydrogen, the general result being to lower the attack when oxygenated slurries and to increase the attack in tests employing deuterium atmospheres. Attack of all materials except Inconel was increased with a deuterium atmosphere. No pronounced effect was observed due to changing the U/Th ratios of the mixed oxides, although the 33% U/Th oxide generally gave lowest attack.

In tests made for studying the variables associated with the hydriding of zirconium alloys in toroids, substantial massive hydride formation was noted under reducing atmospheres, and hydride needles were found under oxygen atmosphere. The rate and extent of hydriding were found to be influenced by the overpressure of oxygen or deuterium employed during slurry circulation, the general aggressiveness of the test system, the test duration, and the composition of the alloy. A time-overpressure relationship was indicated. Hydrogen produced as a by-product of corrosion by slurries appeared sufficient to promote hydriding of some zirconium alloys.

Autoclave experiment L6S-151S has been successfully operated and removed from the HB-6 facility of the LITR. The type 347 stainless steel autoclave was loaded with slurry at a concentration of 1100 g of Th per kg of D_2O, with 4.8 wt % enriched uranium based on thorium, 0.017 m Pd catalyst, and an excess oxygen atmosphere. Experiment Y6Z-128S, an out-of-pile control experiment for experiment L6Z-127S, has been completed. The Zircaloy-2 autoclave was loaded with slurry at a concentration of 410 g of Th per kg of D_2O with 5.1 wt % enriched uranium, based on thorium, 0.011 m MoO_3, and an excess oxygen atmosphere. Oxygen-consumption data indicated a lower rate in the unirradiated experiment, thus confirming an effect of radiation on the corrosion of Zircaloy-2. A comparison of the postrun examination of the slurry and corrosion-pin specimens in experiments L6Z-127S, Y6Z-128S, and L6Z-129S is presented.

The use of neutron activation of Zircaloy-2 or other corrosion specimens to determine the maximum and mean flux and exposure in in-pile experiments in which a considerable time variation of flux occurred, has been facilitated by the development of an IBM-704 computer program for the reduction of data associated with this procedure.

Generalized time-corrosion data from a number of experiments related to the effect of radiation on the corrosion of Zircaloy-2 by high-temperature aqueous slurries have been correlated. It has appeared that a small amount of corrosion, of the order of zero to 30 μ in. occurred for various samples and was different for each experiment. In the absence of radiation, the incremental corrosion rate was inversely proportional to total time at temperature, thus following the classical logarithmic law when integrated. In the presence of a fissioning slurry, the incremental corrosion rate was still inversely proportional to the total time at temperature but was increased. The increase in corrosion rate above the unirradiated value was correlated as being proportional to the cube root of the fission-power density as well as the reciprocal of total time at temperature.

Based on satisfactory operation of a developmental model of a 5-gpm slurry loop, a new loop was constructed which is dimensionally suitable for in-pile operation in beam hole HB-2 of the LITR. Seven hundred hours of operation at temperatures to 280°C with a thorium oxide slurry containing 1/2 wt % uranium, have been accumulated. Inventory control of the circulating slurry at concentrations to 600 g of Th per kg of D_2O has been excellent. Several batchwise additions of deuterium gas to the loop, which was operated with oxygen and

steam in the vapor space of the pressurizer, indicated that the kinetics of the recombination of deuterium and oxygen gas can be studied in the loop.

Satisfactory operation of the loop with thoria slurries depends on maintaining the pressurizer and pump-rotor cavity free of thoria. This is accomplished by means of thoria-free filtrate from a sintered-metal filter. Thus, testing and evaluation of various sintered materials suitable for filtering thoria slurries at elevated temperature is an important part of the in-pile slurry-loop development. Plugging of these filters to various degrees has occurred in slurry at elevated temperatures but has not prevented loop operating times to 2000 hr.

Mathematical models relating to the analysis of pressure transients and equilibria in the D_2-O_2 recombination kinetics is proposed in-pile slurry loops have been set up. Solutions to some of the appropriate equations have been obtained by use of a small electronic analog computer. The solutions offer guides to the preparation and analysis of loop experiments.

PART V. FUEL MANUFACTURE AND PROCESSING

20. Uranyl Sulfate Fuel Processing

Procedures were demonstrated by using HRT-scale equipment for the electrolytic removal (mercury cathode) of nickel from UO_2SO_4 fuel solution and the regeneration of the resulting amalgam with 1 M HNO_3 and 1.5% H_2O_2 in order to remove the copper and nickel. The electrolysis was conducted in a glass-lined cell with a platinum anode and a mercury cathode. The cell solution, fuel concentrated by evaporation, was 0.34 M in UO_2SO_4, 0.27 M in $CuSO_4$, and 0.045 M in Ni. The nickel was removed with a 1% current efficiency.

Soluble corrosion and fission products were removed from a simulated fuel solution by the precipitation of uranium dioxide and metallic copper with hydrogen at 250°C in situ in a titanium loop and the draining off the uranium- and copper-free solution. The fuel, less the soluble impurities, was reconstituted by circulating new, oxygenated 0.075 m D_2SO_4 at 250°C in the loop in order to dissolve the UO_2 and the copper as UO_2SO_4 and $CuSO_4$.

21. Thorium Oxide Preparation and Production

Studies were carried out on the properties of thorium-uranium oxides prepared by the adsorption of uranium from an ammonium uranyl carbonate solution by preformed thoria (650°C fired), followed by firing at 1100°C. Principal preparation variables investigated were uranium content and firing atmosphere. The species of oxide produced by firing in oxidizing and in reducing atmospheres appeared to differ both chemically and physically. The mixed oxides fired in H_2 also appeared to be less homogeneous than those fired in air. The percentage of uranium leached by 8 N HNO_3 from the mixed oxides fired at 1100°C in air decreased with increasing uranium content and was proportional to the surface area of the mixed oxide.

Work on the development of oxide preparation methods continued, with emphasis on the production of spherical particles by flame denitration of alcoholic solutions of nitrates and by a gel technique. Spherical oxide particles 0.9 to 2.9 μ in average size and containing 82 to 99 wt % ThO_2, 1 to 10 wt % Al_2O_3, and 0 to 8 wt % uranium oxides were prepared and calcined

up to 1800°C by flame denitration. Spherical thorium oxide particles in the size range 0.5 to 30 μ were prepared by the partial neutralization of a thorium nitrate solution with ammonia, setting the resulting sol to a gel by mixing with isopropyl alcohol, drying, and then firing the resulting solids.

Fifteen oxalate precipitations were made in the new oxide-preparation equipment in order to prepare approximately 2150 lb of thorium oxide. A total of 1041 lb of oxide prepared in the new equipment was shipped to REED. Of this total, 524 lb was thorium - 8% uranium oxide, while the remainder was thorium oxide.

PART VI. METALLURGY

22. Metallurgy

The macro- and microexaminations of the specimens removed from the HRT core tank after run 17 have been completed. The only change in previously reported conclusions has been the determination that the deuterium pickup which occurred in the titanium specimen holder was not general but was confined to the region of the burned surfaces.

Electrolytic dissolution in 6 N HNO_3 and induction and arc-melting tests of portions of the specimen discs cut from the screens of the HRT core tank after run 17 have shown that radioactive material of two types, particulate and gaseous, is released during the melting or dissolving of the screen specimens.

The thickness of the HRT core vessel has been measured ultrasoncially. By using a new positioning rig and measuring with the Immerscope, a study was made of the spherical portion of the vessel. Only a moderate attack had occurred in the equatorial region, but thin spots were found near the cones.

The fabrication study of Zircaloy-2 has been essentially completed insofar as the preparation and testing of specimens are concerned. The data are now being examined and correlated. A new evaluation technique has been developed for determining and characterizing the anisotropy of mechanical properties in plate and sheet Zircaloy-2 by examination of the cross sections of fractured tensile specimens and correlating the axial strain with the contractile strains. Additional fabrication schedules have been studied to show the effects of cross rolling and the degree of final reduction on the resulting anisotropy of mechanical properties.

Transformation kinetic and transformation sequence studies in Zr-Nb-X alloys, of interest to the HRP as high-strength corrosion-resistant alloys, have shown that below 525°C the sequence of beta quench and reheat transformations in the Zr-15Nb alloys is the decomposition of the retained body-centered cubic (bcc) beta matrix to a metastable hexagonal omega phase containing 5 to 7% Nb plus a niobium-enriched bcc beta phase which is continuously and progressively enriched in niobium with increased aging time. The omega phase is eventually replaced with the close-packed-hexagonal (cph) equilibrium alpha phase. The martensitic Widmanstätten platelet phase observed in all beta-quenched Zr-Nb-X alloys containing more than 12% Nb has been identified as a body-centered monoclinic phase which forms only on the (100) type planes of the bcc matrix. The phase will redissolve in the bcc matrix without decomposition on reheating to 250°C or higher.

PART VII. ANALYTICAL CHEMISTRY

23. Analytical Chemistry

A method is described for the determination of microgram quantities of molybdenum in slurries of $ThO_2 \cdot UO_x$. Procedures are outlined for the separation of fluoride from HNO_3-$Al(NO_3)_3$ solutions or H_2SO_4 solutions by pyrolysis and subsequent titration of the fluoride without interference from decomposition products of the matrix materials. Improved flame spectra of all rare-earth elements except cerium and promethium have been recorded, and additional data for use in fixing the wave lengths of characteristic lines and bands have been collected. A further study was made of a colorimetric method for osmium. Optimum operating conditions were established for the attainment of maximum sensitivity, and the extent to which a number of elements interfere was ascertained. Work was also continued on improvements of a coulometric method for the estimation of U(VI) and U(IV) in ThO_2-UO_x slurries which contain corrosion products.

An improved method is described for the determination of free acid in the fuel solution of a homogeneous reactor. After separating the acid from interferences by means of a cation-exchange column, the acid is titrated photometrically. Coulometric methods are also outlined for the estimation of nickel, copper, and uranium in homogeneous reactor fuels, and the precision attained is indicated in a table. The compositions of HRT off-gas and shield gas in HRT run 20, as determined by a gas chromatographic method, are given in some detail.

CONTENTS

SUMMARY iii

PART I. HOMOGENEOUS REACTOR TEST

1. HRT OPERATIONS 3
   1.1 Reactor Operations 3
      1.1.1 Stability Investigations 3
      1.1.2 Operations Analysis 5
      1.1.3 Equipment Problems 7

2. HRT PROCESSING PLANT 8
   2.1 Hydroclone System 8
      2.1.1 Corrosion-Product Solids Removal in Run 20 8
      2.1.2 Chemical Analysis of Solids 10
      2.1.3 Comparison of Solids Removal Rates and Production Rates 10
   2.2 Iodine Behavior 10

3. HRT REMOTE OPERATIONS 13
   3.1 Maintenance and Other Activities 13
      3.1.1 Maintenance Prior to Run 20 13
      3.1.2 Maintenance Prior to Run 21 13
   3.2 Operations Performed in the HRT Core After Run 20 14
      3.2.1 Diffuser-Screen Manipulation and Position Measurements 14
      3.2.2 Viewing of the Core 14
      3.2.3 Core-Wall Thickness Measurements 14
      3.2.4 Irradiation of Nonmetallic Materials in the HRT Core .. 17
   3.3 Modification of the HRT Core 17
      3.3.1 Separation of Diffuser Screens from Core Tank 17
      3.3.2 Loose-Screen Manipulation 18
      3.3.3 Removal of Screens from Core 18
      3.3.4 Core-Hole Definition and Patch Installation in the HRT 24
   3.4 Remote Viewing Equipment 24
   3.5 Core-Access-Flange Reamer 24
   3.6 HRT Core-Access Standpipe 28
   3.7 Off-Gas Control During Screen Cutting 28
   3.8 HRT Core Flush Tests 28

4. HRT ENGINEERING DEVELOPMENT 31
   4.1 Feed-Pump Endurance Testing 31
   4.2 Test and Pretreatment of the Replacement Fuel-Circulating Pump for HRT 31
   4.3 Circulating-Pump Tests Under Adverse Flow Conditions 31

4.4 Pump Rotation and Speed Indicator 32
4.5 HRT Mockup 32

5. HRT DESIGN 34
5.1 Effects of Stopping Circulating Pumps During a Dump 34
5.2 Replacement Pressure Vessel, Summary Report 34
5.3 Containment of Reactor Steam System 34
5.4 Recombiner 35
5.4.1 Fuel Primary Recombiner 35
5.4.2 Fuel Secondary Recombiner 35
5.5 Samplers 38
5.6 Radiation Monitors 38

6. HRT CONTROLS AND INSTRUMENTATION 39
6.1 Component Development 39
6.1.1 Fuel Feed Flowmeter 39
6.1.2 Remote Viewing Equipment 39
6.1.3 HRT Letdown Valves 40
6.2 Maintenance and Modification 40
6.2.1 Control Valves 40
6.2.2 Control-System Revisions 40
6.2.3 Emergency A-C Power for Public-Address System 42

PART II. REACTOR ANALYSIS AND ENGINEERING DEVELOPMENT

7. REACTOR ANALYSIS 45
7.1 Nuclear Characteristics of Small Solution-Core, Slurry-Blanket Spherical Reactors (HRE-3) 45
7.2 Studies of Improvement of Power Densities in ORR Loops 47

8. DEVELOPMENT OF FUEL- AND SLURRY-SYSTEM COMPONENTS 51
8.1 High-Pressure Recombiner Loop 51
8.2 Centrifugal Pumps 51
8.2.1 20-cfm Allis-Chalmers Blower 51
8.2.2 Reliance 6000-gpm Pump 51
8.2.3 300A Slurry Pump and Loop 52
8.2.4 200Z Slurry Pump and Loop 52
8.2.5 Test Program for Slurry-Pump Bearings 53
8.3 Feed Pumps 53
8.3.1 Oxygen Compressors 53
8.3.2 Increased-Capacity Solution Pumps 53
8.3.3 Slurry Feed Pumps 53
8.4 Slurry Low-Pressure System 55
8.5 Valve Trim 55
8.5.1 Dump-Valve Trim for Solutions 55
8.5.2 Slurry Valves 55
8.5.3 Slurry Letdown Chokes 57
8.6 Heat Exchanger Test Facility 57
8.7 Core and Blanket Development 57
8.7.1 Re-entrant Core Model 57
8.7.2 Cylindrical Core with Swirling Flow 60
8.7.3 Reactor-Vessel Design 60
8.7.4 Spherical Annular Re-entrant Core 61
8.7.5 Slurry Core Vessel 61

9. DEVELOPMENT OF REACTOR SLURRY SYSTEMS 64
9.1 Circulating-Slurry Experiments 64

9.1.1 200A-Loop Operation 64
9.1.2 200B-Loop Operation 65
9.1.3 200B Heat-Transfer and Viscometry Data 65
9.1.4 Properties of Slurry Settled Beds 67
9.2 300-SM Blanket-System Development 68
9.2.1 30-in.-dia Core-Vessel Tests 68
9.2.2 The 300-SM Low-Pressure System 69
9.2.3 Pump and Valve Failures in Run SM-8 71

10. INSTRUMENT AND VALVE DEVELOPMENT 74
10.1 Instrument Development 74
10.1.1 High-Temperature, Radiation-Resistant, Differential Transformer 74
10.1.2 Transistorized Electropneumatic Converter 74
10.1.3 Evaluation of a Magnetic-Amplifier Instrumentation System 76
10.1.4 Evaluation of Pressure Transmitters 79
10.1.5 Analog Computer 79
10.1.6 Ultrasonic Detection of the Interface of a Falling Slurry 79
10.2 Valve and Actuator Development 81
10.2.1 Valve Trim for Slurry Service 81
10.2.2 Valve Stem-Sealing Bellows 81
10.2.3 Solution-Sampling Valve 81

11. HEAT TRANSFER STUDIES 85
11.1 Heat Transfer from Stainless Steel to Oxygenated H_2O, D_2O, and Uranyl Sulfate at 100 and 250°C 85

PART III. SOLUTION FUELS

12. REACTIONS IN AQUEOUS SOLUTIONS 93
12.1 Rate of Oxidation of Dissolved H_2 or D_2 Catalyzed by $Cu(ClO_4)_2$ in Light and Heavy Water 93
12.2 Cupric Ion as a Homogeneous Catalyst in the UO_3-HNO_3-H_2O System 96

13. HETEROGENEOUS EQUILIBRIA IN AQUEOUS SYSTEMS 99
13.1 Two-Liquid-Phase-Boundary Temperatures for the HRT Fuel Solution and Its Concentrates 99
13.2 Two-Liquid-Phase Studies in a Titanium Loop 100
13.3 Phase Stability of Radioactive HRT Fuel Solutions 102
13.4 Behavior of Synthetic HRT Fuel Solution in the Presence of Metal Oxides 104
13.5 The Two-Liquid-Phase Regions of the Systems UO_3-SO_3-H_2O and UO_3-SO_3-D_2O 104
13.6 Solid-Liquid Equilibria: The System UO_3-CuO-NiO-SO_3-$H_2O(D_2O)$ 107
13.7 Effect of UO_3/SO_3 Molar Ratio on Immiscibility Temperature of 0.10 Molal Sulfate Solutions 110
13.8 Liquid-Liquid Immiscibility in the System UO_3-SO_3-N_2O_5-H_2O 110
13.9 Systems Based on Nitrate 119
13.9.1 The System UO_3-N_2O_5-H_2O at 150-300°C 119
13.9.2 The Multicomponent System UO_3-CuO-NiO-N_2O_5-$H_2O(D_2O)$ and Its Relation to Homogeneous Reactors 122

13.10 Apparatus Development for High-Temperature Aqueous Studies 122
13.10.1 Liquid-Salt Bath 122
13.10.2 Pressure Vessels for Use from 100 to 500°C 123

14. SOLUTION CORROSION 126
14.1 Dynamic Solution Corrosion 126
14.1.1 Corrosion in Uranyl Nitrate Solution 126
14.1.2 Loop Descaling with Deoxidine-170 127
14.2 Laboratory Corrosion Studies 128
14.2.1 Stress-Corrosion Cracking of Cast Austenitic Stainless Steels 128

15. RADIATION CORROSION 130
15.1 In-Pile Loops 130
15.1.1 Development, Construction, and Operation 130
15.1.2 In-Pile Loop Experiment L-2-22 133
15.2 In-Pile Solution Rocking-Autoclave Tests, LITR 141
15.2.1 Development, Construction, and Operation 141
15.2.2 Results of In-Pile Autoclave Experiments 143
15.2.3 A Comparison of the Radiation Corrosion of a Zr - 1% Cr Alloy with That of Zircaloy-2: Experiment L6Z-139 143
15.2.4 A Qualitative Test of Possible Cr(III) $\rightleftharpoons$ Cr(VI) Equilibria in Fuel Solution Under Irradiation: Experiment L6Z-142 144
15.2.5 Corrosion of a Heated Zircaloy-2 Surface Under Irradiation: Experiment L52T-145 146
15.3 Supporting Research 148
15.3.1 Adsorption of Uranium on Hydrous Zirconium Oxide from UO_2SO_4 Solutions 148
15.3.2 Electrochemical Studies of Zircaloy-2 Corrosion 149

PART IV. SLURRY FUELS

16. ENGINEERING AND PHYSICAL PROPERTIES 159
16.1 Rheology of Aqueous Thorium Oxide Suspensions 159
16.2 Slurry Resuspension and Dropout Studies 161
16.3 Thoria Caking Studies 161
16.3.1 Test with Electrolyte Additives 161
16.3.2 Low-Concentration Slurry 163
16.3.3 Detection of ThO_2 Cake Formation 163
16.4 Surface Chemistry of ThO_2 164

17. SLURRY IRRADIATION STUDIES 168
17.1 Slurry Irradiations in the LITR 168
17.2 Postirradiation Examination 168
17.3 In-Pile Gas Production and Recombination Studies 169
17.4 Hydrogen Solubility in Aqueous Slurries 171

18. DEVELOPMENT OF GAS-RECOMBINATION CATALYSTS 173
18.1 Effect of Pumping on Catalysis in Thorium-Uranium Oxide Slurry 173
18.2 Palladium as a Catalyst 174
18.2.1 Westinghouse Type of Preparation 174
18.2.2 Dispersion Preparation Method 175
18.3 Gas-Injection Apparatus for Catalyst Studies 175

18.4 Development of Continuous Gas Production-Recombination Apparatus 177

19. SLURRY CORROSION 180
19.1 Pump Loops 180
19.1.1 Introduction to Pump-Loop Tests; Circulation of Th-U Oxide Fuel Slurries 180
19.1.2 Loop Operating Characteristics 180
19.1.3 Uranium Redox and Solubility 182
19.1.4 Slurry Circulation Properties 182
19.1.5 Slurry Rheological Properties 185
19.1.6 Corrosion-Erosion 185
19.2 Toroids 186
19.2.1 Introduction 186
19.2.2 Tests with Slurries of Thorium-Uranium Oxides 186
19.2.3 Hydriding of Zirconium-Base Alloys 191
19.3 In-Pile Autoclave Slurry Corrosion Tests 195
19.3.1 Introduction 195
19.3.2 Out-of-Pile Control Experiment 195
19.3.3 Post-Experiment Examinations 197
19.3.4 Computation of Experiment Flux from Specimen Activation 200
19.3.5 Time Correlation of Zircaloy-2 Radiation Corrosion Data from Slurry Autoclave Experiments 201
19.4 In-Pile Slurry Loop 203
19.4.1 Loop Development 205
19.4.2 Loop Tests at Elevated Temperatures 205
19.4.3 Analysis of Loop Recombination Kinetics 208

PART V. FUEL MANUFACTURE AND PROCESSING

20. URANYL SULFATE FUEL PROCESSING 215
20.1 Nickel Removal from Fuel Solution by Electrolysis 215
20.2 Purification of Reactor Fuel Solutions by Precipitation of Uranium with Hydrogen 218

21. THORIUM OXIDE PREPARATION AND PRODUCTION 220
21.1 Thorium-Uranium Oxide: Adsorption Preparation Method 220
21.1.1 Experimental 220
21.1.2 Effect of Preparation Variables on Lattice Parameters 220
21.1.3 Uranium Content, Surface Area, and Crystallite Size Relation 223
21.1.4 Oxygen-Uranium Relation 223
21.1.5 Leachability of Uranium from Thorium-Uranium Oxides 223
21.2 Oxide Preparation Development 223
21.2.1 Flame Denitration 227
21.2.2 Preparation of Spherical Particles by a Gel Technique 227
21.3 Oxide Preparation 231

PART VI. METALLURGY

22. METALLURGY 237
22.1 HRT Repair and Examination 237
22.1.1 Examination of Specimens Removed from the HRT after Run 17 237
22.1.2 Measurement of HRT Zircaloy-2 Core-Vessel Thickness 238

22.2 Zircaloy-2 Fabrication Study 240
22.3 Forming of Zircaloy-2 242
22.4 Zirconium Alloy Development 242

PART VII. ANALYTICAL CHEMISTRY

23. ANALYTICAL CHEMISTRY 247
23.1 Determination of Molybdenum by Derivative Polarography 247
23.2 Pyrolytic Separation of Fluoride from Nitrate or Sulfate Solutions 247
23.3 Flame-Photometric Determination of Rare-Earth Elements 248
23.4 Further Study of the Determination of Osmium by a Colorimetric Method 248
23.5 Coulometric Determination of U(IV) and U(VI) in ThO_2-UO_x 248
23.6 Determination of Free Acid in the HRT Feed Solution 248
23.7 Coulometric Analysis of Homogeneous Reactor Fuel 249
23.8 Analysis of HRT Off-Gas and Shield Gas by Gas Chromatography 249

ORGANIZATION CHART 251

Part I

HOMOGENEOUS REACTOR TEST

1. HRT OPERATIONS

S. E. Beall P. N. Haubenreich J. W. Hill, Jr.

H. F. Bauman
N. C. Bradley
J. R. Buchanan
S. R. Buxton
J. R. Engel
J. D. Flynn
D. F. Frech
R. H. Guymon
R. J. Harvey
J. Hirota[1]
J. O. Kolb
J. L. Redford
D. M. Richardson
H. C. Roller
D. Scott
W. Terry

1.1 REACTOR OPERATIONS

In this report period (June 1 to Nov. 1), the reactor was in operation for over 2500 hr, generating over 3200 Mwhr(th). The longest period of continuous operation was 1364 hr. Nearly all of this period was spent studying the problem of fuel instability and learning how to prevent it. Some experiment time was devoted to xenon-iodine and to recombination studies.

1.1.1 Stability Investigations

(a) Run 20.--In run 20 the HRT operated at pressures of 1150, 1250, 1400, 1600, and 1750 psig, at temperatures of 240 and 260°C, and at power levels as high as 5 Mw. The parameters of pressure and temperature were used to explore stability limits. The purpose of these explorations was to block out areas where power operations resulted in uranium loss or power disturbances. The results are presented in Fig. 1.1; the curve is located to separate, approximately, the stable and unstable areas.

There was a striking difference in the stable power level that could be attained when system pressure was the variable. Whereas the threshold for uranium loss was reached at about 1.5 Mw at pressures of 1600 and 1750 psig, the reactor could be operated to 5 Mw at pressures of 1150 or 1250 psig without the indications of uranium loss seen at the higher pressures. At 1400 psig the uranium-loss threshold is seen to be about 2.5 Mw.

Power disturbances were encountered in the "unstable" area while operating at pressures of 1400, 1600, and 1750 psig. Although there were 33 disturbances during the run, ranging from 3.5 to 22% of the operating power level, only two exceeded 10%.

Most of the investigations were started with a reactor temperature of 260°C. The temperatures of 240°C and 270°C were also investigated while the reactor pressure was 1750 psig. Over this range of temperature there appeared to be little difference in the power level at which fuel loss occurred.

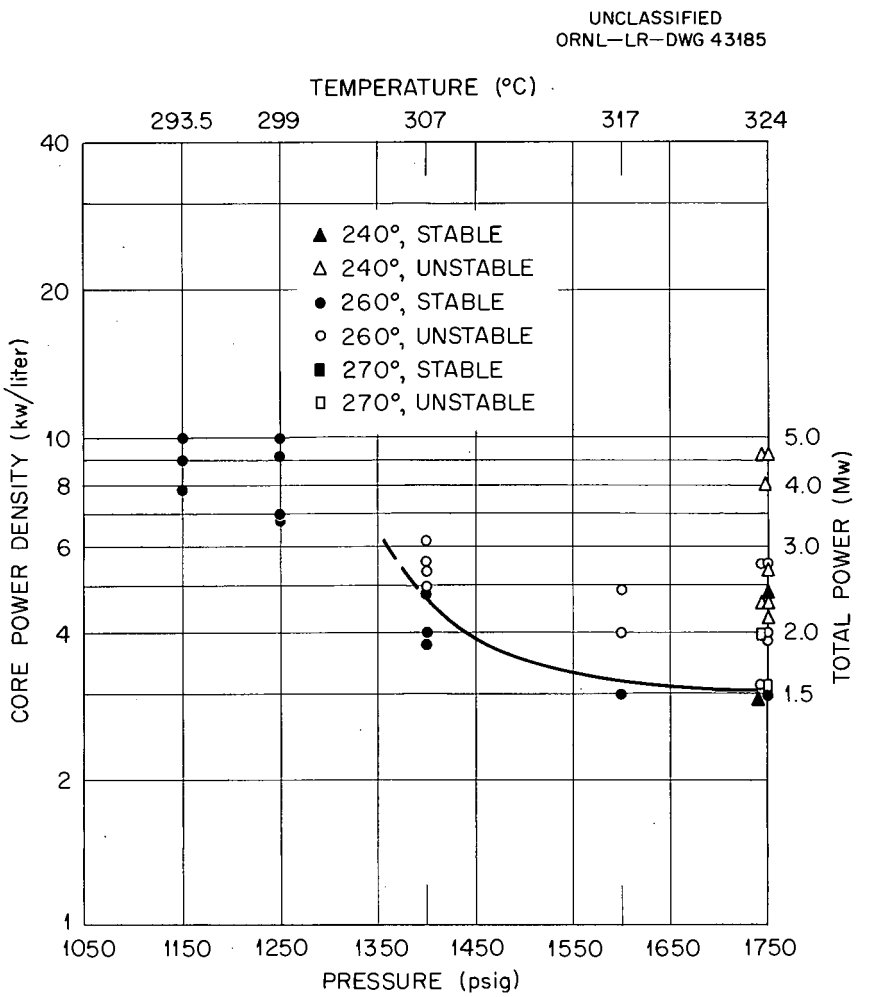

Fig. 1.1. Core Power Density vs Pressure.

Since all of these tests were relatively short term (the total time spent above 4 Mw was only 30 hr), longer-term stability tests were planned for run 21.

One explanation for the great difference in fuel stability with change in pressure is based on the relationship of the two-liquid phase-separation point with temperature. It is presumed that the indicated loss of uranium and the power disturbances are related to the phase-separation phenomenon. Experiments reported elsewhere (see Sec. 13.1) have provided evidence that the separation of a heavy phase containing a high percentage of the uranium can occur at a temperature as low as 305°C, if the concentration of the fuel solution is increased several times. The 305°C minimum temperature corresponds to a pressure of 1400 psig; it can be argued that if the reactor is operating at a pressure below approximately 1400 psig, boiling can occur before 305°C is reached, thus limiting the temperature and preventing the separation of the heavy phase. On the other hand, pressures above approximately 1400 psig can result in unstable conditions because they permit the existence of temperatures above the heavy-phase-formation temperature (305°C). The problem is complicated by the fact that the second liquid phase may exist for only a short time, perhaps going back into solution or changing to a solid phase by further hydrolysis. It is known that the appearance of the second liquid phase is strongly dependent on the acid concentration of the fuel solution, and experiments are being planned to vary the acid concentration in an effort to determine the effect on reactor performance.

(b) Run 21 (In Progress).--The reactor has operated a total of 225 hr at full power (5 Mw), with a system pressure of 1250 psig and a temperature of 260°C. This relatively long period of operation has verified the stability evidence obtained in the previous short periods: no loss of uranium and no power excursions are observed at 1250 psig, 260°C. Fuel-stability studies will continue throughout the run. The reactivity loss from xenon poisoning is being studied also (see Sec. 3.2).

Fifty-nine small power disturbances of 2 to 5% of the power level were observed in the first 170 hr of run 21. They are distinguished from normal power oscillations in that they result in a noticeable rapid power increase above the nominal power. The frequency gradually decreased, and since the 170th hour, none have been observed.

1.1.2 Operations Analysis

(a) Mixing Between Core and Blanket.--Although the distribution of uranium between core and blanket remains fairly steady for long periods of operation, the concentration ratio has shifted at times for no apparent reason. Blanket-to-core concentration ratios during normal operation have ranged from 0.20 to 0.47. (During run 19, when circulation rates were about one-third of normal, the concentration ratio was 0.10.) The behavior of the concentration ratio suggests infrequent but abrupt changes in backmixing through the core-tank hole. It is believed that these are caused by shifts in the position of the loose screen at the elevation of the hole in the core entrance cone.

(b) Critical Concentrations.--Improvements in sampling and analytical procedures during runs 18 through 21 enabled accurate measurement of critical concentrations at temperatures from 220 to 280°C and at blanket-to-core concentration ratios from 0.10 to 0.36. The observed concentrations have been used to normalize the results of critical calculations in order to obtain curves for use in operations analysis (see Fig. 1.2). About 80% of the concentrations

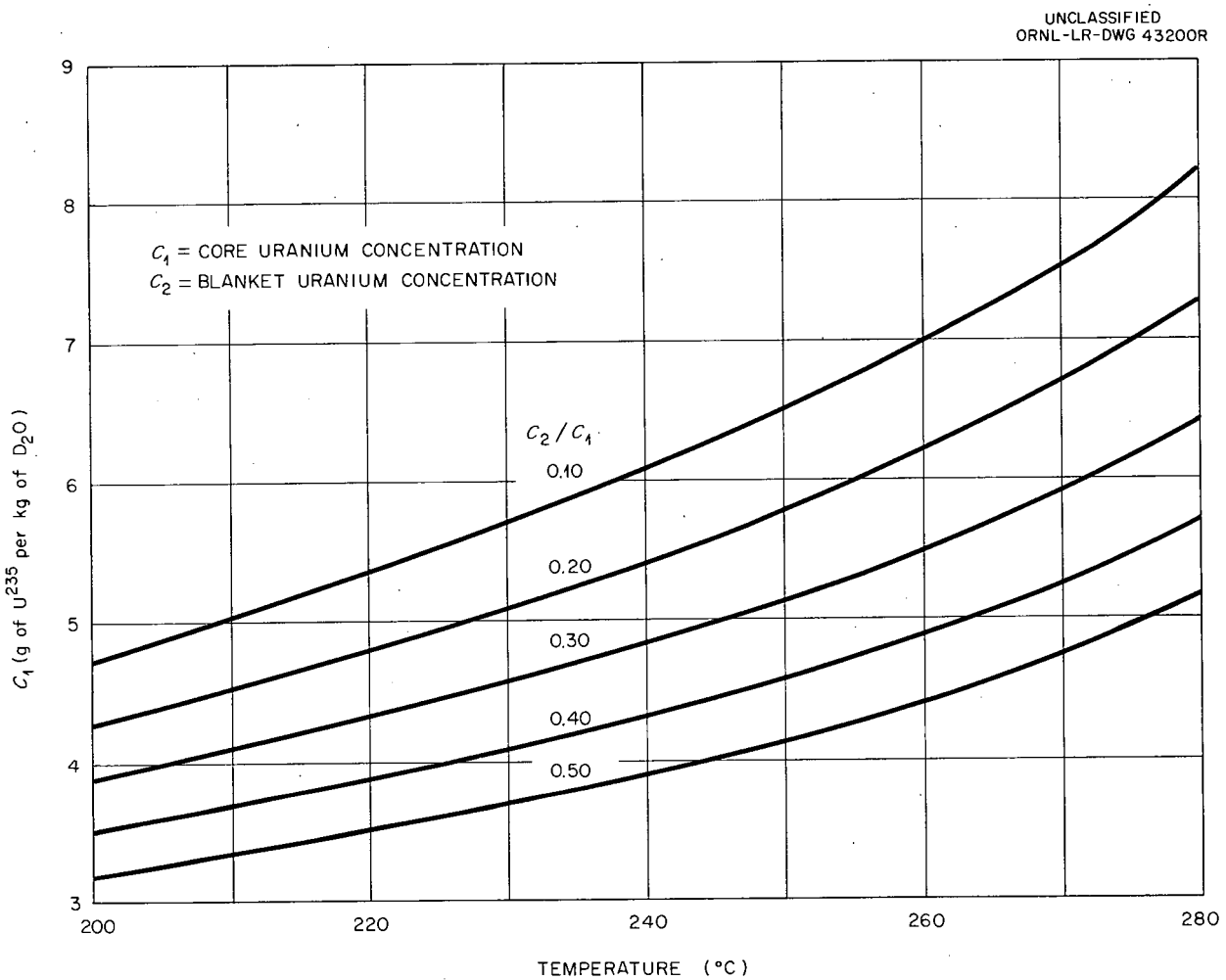

Fig. 1.2. Core Critical Concentration vs Temperature. Based on runs 12, 18, and 19, with Wanda results normalized to those runs.

measured at low power fall within ±1% of the normalized curves. (Only the low-power data were used in the normalization since, at high power, the buildup of noncirculating uranium affects the critical concentrations.)

The observed critical concentrations ranged from 15 to 25% higher than predicted by the Wanda two-group calculation. The error was greater at lower blanket-to-core concentration ratios, indicating that the importance of uranium in the blanket is underestimated by the Wanda calculation.

(c) Internal Recombination.--Data on internal recombination during early runs indicated solution rate constants slightly higher than predicted from the copper concentrations in the fuel.[2,3] It appears, from the absence of bubble letdown at the low pressures and high powers attained in runs 20 and 21, that solution rate constants are over twice as great as previously observed. Experiments to determine threshold conditions for bubble evolution are in progress to measure the effects of temperature and power level on internal recombination.

1.1.3 Equipment Problems

(a) Recombination.--At the start of run 20, the efficiency of the catalytic recombiners was found to be low (90%, estimated), with the 240-lb heating steam normally supplied. To attain a satisfactory recombination, it was necessary to superheat the steam to temperatures in the range 400 to 450°C. Replacement catalyst beds are being prepared for installation in a future shutdown if needed.

(b) Fuel Feed.--The stability investigations in run 20 were complicated at times by difficulties in maintaining a constant rate of fuel feed from the dump-tank reservoir to the high-pressure system. (A decreasing feed rate has the same effect on the reactor temperature as uranium loss due to chemical instability.) On several occasions faulty operation of the block valve (HCV-337) in the fuel feed line caused a decrease in fuel feed with a resultant decrease in reactor temperature.

In the course of the run, the diaphragms in the heads of both fuel feed pumps failed and leaked radioactive liquid into the intermediate system of the pump. When the second (spare) head failed on August 30, it became necessary to end run 20. The cause of failure is unknown, at present. The expected life of these pumping units is 4000 to 8000 hr, compared with 2000 hr for each of the failed heads. They will be cut open remotely and examined to determine the cause of failure.

In the shutdown between runs, the faulty valve and both feed-pump heads were replaced or repaired, and the performance of the fuel feed system in run 21 has been satisfactory.

(c) Core Dump Valve.--During run 20 the core dump valve leaked. Although the leak rate was less than 3 lb/min and did not seriously interfere with reactor operation, the valve was replaced at the end of the run.

REFERENCES

1. Japanese Atomic Energy Research Institute.

2. J. R. Engel et al., Summary of HRE-2 Run 13, ORNL CF-58-10-115, p 45 (Oct. 29, 1958).

3. J. R. McWherter et al., HRP Quar. Prog. Rep. Apr. 30, 1959, ORNL-2743, p 36.

2. HRT PROCESSING PLANT

W. D. Burch

L. B. Shappert O. O. Yarbro

2.1 HYDROCLONE SYSTEM

2.1.1 Corrosion-Product Solids Removal in Run 20

Prior to HRT run 20 the multiple hydroclone, or multiclone, described previously[1] was tested[2] and was installed in the reactor cell as shown in Fig. 2.1. Solids concentrated in the multiclone are routed to the original hydroclone in the processing cell for final solids collection. The purpose of the device is to increase solids removal rates by faster processing. With the original single hydroclone the core processing period was 1-1/2 hr; with flows through the multiclone at 10 gpm, this was reduced to about 12 min. Unfortunately, it is not possible to evaluate the effect of higher processing rates, independent of other variables, because the pressure drop across the multiclone is much lower than across the hydroclone (48 ft, compared with 125 ft).

The performance of this system was clearly established in a series of six short runs. Removal rates are seen in Fig. 2.2 to decrease from a high in excess of 5 g/hr in the first 50 hr of operation to an apparent equilibrium value of 0.5 g/hr after 500 hr. This drop is typical of previous runs, and in all cases the removal rate appears to be about 50-80% higher with the multiclone installation. Prior to operation, an increase in the removal rate by a factor of 3 was predicted.[2] A re-analysis of all available data leads to the conclusion that the factor of 3 was not obtained probably because the solids particle size was slightly smaller than that used in predicting performance. Hydroclone efficiencies are extremely sensitive to particle size in this range, decreasing by a factor of 2 in going from 1-μ to 0.8-μ particles.

The multiclone efficiency measured with sized ThO_2 was somewhat lower than would be predicted for individual hydroclones of the same design, although the difference may be within the experimental error.

An improvement in the performance should be achieved by directing the cell C hydroclone overflow stream back to the multiclone underflow pot, thus recycling any solids not removed on the first pass. This was attempted in runs CP-20-18 and CP-20-19 by recycling internally in cell C a part of the hydroclone overflow to the feed stream. For reasons still not understood, the removal rate dropped drastically to about 0.1 g/hr. The final run (CP-20-20) was made under the original operating conditions, but the rate was still extremely low. Since removal rates with the single hydroclone had always exceeded 0.3 g/hr, some malfunction of this unit was suspected.

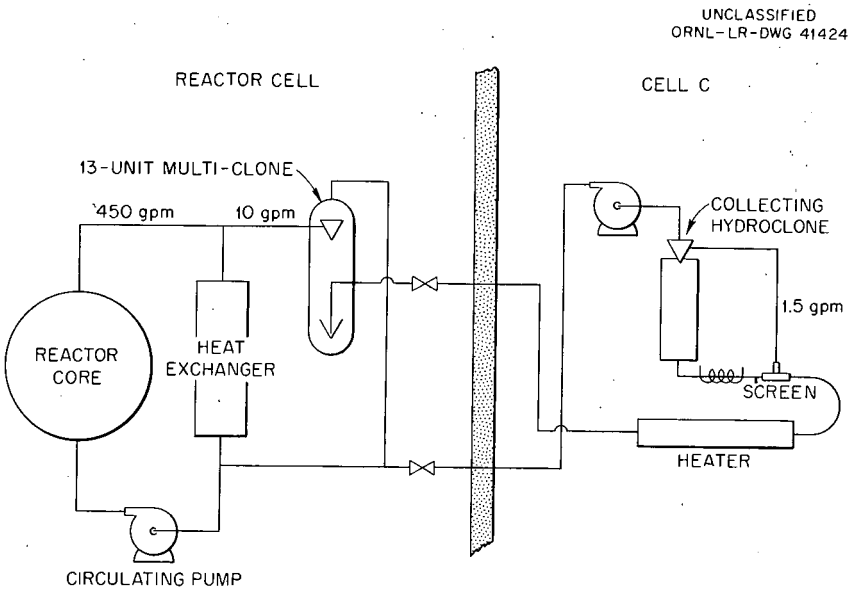

Fig. 2.1. Multiclone Installation to Increase Processing Rates for Solids Removal.

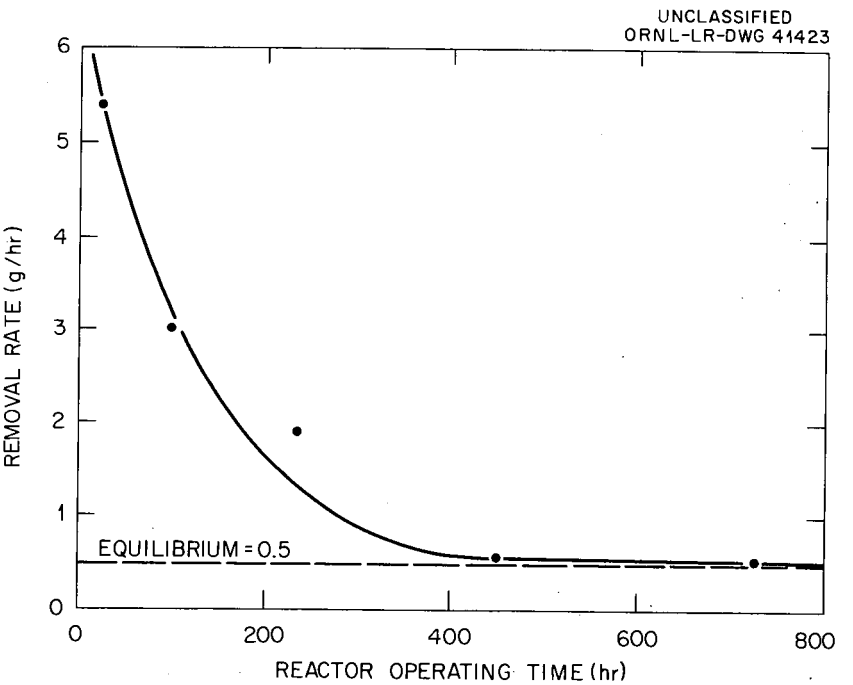

Fig. 2.2. Solids Removal Rates in HRT Run 20.

The hydroclone was removed and replaced with a spare following run 20, by use of the special dry-maintenance tools designed for this operation. A bolt on the access flange seized, was broken, and had to be drilled out and replaced, but the hydroclone and retainer-plug assembly were replaced with little difficulty. No obvious damage was seen in a short, direct examination; the hydroclone will be sectioned and inspected in hot-cell facilities.

The new hydroclone was operated during the first 88 hr of run 21. The removal rate of 0.8 g/hr obtained was again very low, compared with 4.5 g/hr in the same period of run 20. Some unknown malfunction of the system may still exist.

2.1.2 Chemical Analysis of Solids

Chemical composition of the corrosion products collected in run 20 was similar to that of previous runs, averaging as follows: Fe, 21%; Zr, 40%; Cr, 8.7%; Ti, 2.5%; U, 10.5%; and Cu, 1.8%. The higher titanium percentage (0.7% in run 18) resulted from the burning of the circulating-pump impellers at the end of runs 18 and 19.

2.1.3 Comparison of Solids Removal Rates and Production Rates

Based on the concentration of soluble nickel in the fuel solution, corrosion rates of stainless steel surfaces have been less than 0.5 mpy, and recent core-thickness measurements showed the Zircaloy corrosion rate to be substantially less than 10 mpy. Converted to oxide production rates, these maximum rates correspond to 0.6 g/hr of stainless steel oxides and 1 g/hr of zirconium oxide for a total maximum production of 1.6 g/hr. Hydroclone removal rates for the year have averaged 1.1 g/hr.

2.2 IODINE BEHAVIOR

In circulating-fuel reactors the behavior of iodine is important because the concentration in the fuel strongly affects the neutron poison level of the Xe^{135} daughter, and because radio-iodine is especially dangerous biologically.

A critical review of iodine data obtained from previous runs and in run 20 substantiated earlier evidence that, although the iodine which is let down to the low-pressure system is completely removed by the silver bed, some iodine is held-up in the high-pressure system; this permits a large fraction of the short-lived isotopes to decay before being let down to the low-pressure system. In the case of I^{131}, with an 8-day halflife, 3% of the total production remains in the high-pressure system. However, only 10% of this amount, or 0.3%, is circulating with the fuel. It is assumed that most of the iodine is sorbed in scale on the pipe walls.

Iodine behavior was analyzed by the following methods:

1. direct radiochemical analyses,
2. comparison of I^{133}/I^{131} activity ratios,
3. comparison of blanket/core concentration of both I^{131} and I^{133},
4. measurement of heat release due to iodine on the silver bed, and

5. measurement of Cs^{137}/Cs^{135} mass ratios in the present fuel batch.

The first three methods gave results in reasonable agreement. Until recently, heat balances on the silver-bed iodine trap indicated that more than 10% of the iodine in the high-pressure system was circulating, but the heat balances were in error because of gamma-ray heating of the thermocouples in the bed. Using the thermocouples located in the recombiner to measure the true steam temperature, the heat load from the iodine trap indicated the same iodine behavior as the other methods.

Ratios of Cs^{137} to Cs^{135}, obtained by mass-spectrographic methods, provide information about the combined holdup of xenon and iodine. The ratio of 3.3 obtained indicates that xenon, in addition to iodine, is being held up somewhere in the reactor system. In Fig. 2.3, the effect of xenon holdup, if in the high-pressure system, is shown. The fractions plotted are the fractions which are still in the high-pressure system and circulating with the solution. The xenon not circulating is presumably held up on the walls outside the core in a manner similar to the iodine holdup. This figure indicates that only about 25% of the xenon is circulating. The holdup could be in the low-pressure system; it is not possible to locate definitely the holdup by means of the cesium mass-ratio data. Other attempts will be made to determine the location of the holdup and, at the same time, to measure the xenon poison fraction by analyzing the reactor off-gas stream for Xe^{136} concentration. The increase (due to capture in Xe^{135}) above the direct yield should be sufficient to define accurately the xenon poison level and provide additional knowledge of the behavior of xenon in the reactor.

REFERENCES

1. W. D. Burch et al., HRP Quar. Prog. Rep. Apr. 30, 1959, ORNL-2743, p 10.

2. P. A. Haas and E. L. Youngblood, HRT-CP Results to Be Expected from Operation of the Multiple Hydroclone with the HRT, ORNL CF-59-7-49 (July 1, 1959).

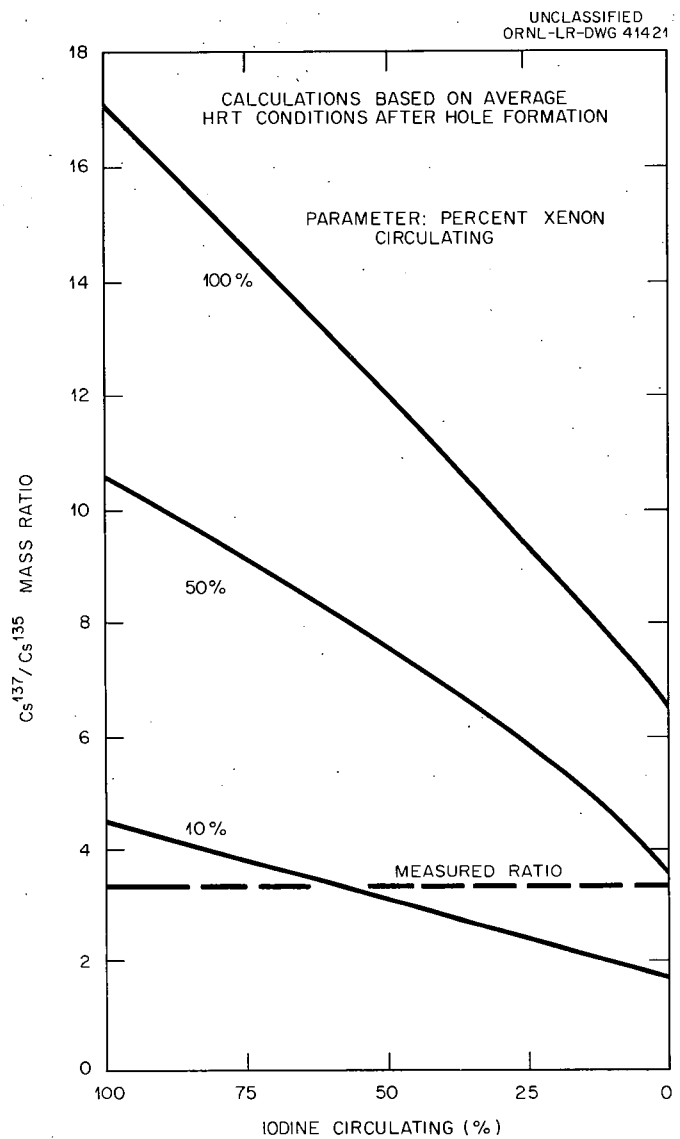

Fig. 2.3. Xenon and Iodine Behavior from Cesium Mass Ratios.

3. HRT REMOTE OPERATIONS

S. E. Beall W. R. Gall R. L. Moore I. Spiewak

J. R. Buchanan B. D. Draper J. E. Jones, Jr.
R. Blumberg J. D. Flynn D. M. Shepherd
C. A. Burchsted E. C. Hise W. Terry
J. S. Culver P. P. Holz F. C. Zapp

3.1 MAINTENANCE AND OTHER ACTIVITIES

3.1.1 Maintenance Prior to Run 20

In preparation for run 20 the following activities were performed.

The fuel-circulating pump was replaced. It had stopped rotating simultaneously with a sudden surge (200 psig) in system pressure. The titanium impeller of this pump apparently ignited, as had the blanket-circulating pump impeller earlier.[1] The pump replacement was made under water, with excellent results. Less than 1 lb of light water entered the reactor system during the entire operation. The pump will be remotely disassembled for inspection.

A multiple-hydroclone assembly intended for increasing the solids-removal rate of the single hydroclone in the chemical plant was installed in the reactor piping.[2] At the same time, the chemical plant intake line was removed from inside the reactor core and reattached to the fuel heat-exchanger inlet line.

The blanket sampler was removed to replace a valve-stem adapter which had failed.[3]

During a routine hydrostatic pressure test of the high-pressure system, flange A-146 was tightened to reduce the leak rate to an acceptable level.

All the maintenance work was accomplished during the 25-day shutdown, requiring about 600 man-hours of craft labor.

3.1.2 Maintenance Prior to Run 21

As mentioned in Sec. 1.1.3 (b), run 20 was terminated by failure of the diaphragm in both of the fuel-feed pumping heads. This initiated a period of maintenance activities in which both pump heads were replaced. During the replacement of the pump heads, the fuel-feed block valve and core dump valve were also replaced.

All the replacements were made under water. However, due to faulty refrigerant lines it was not possible to freeze ice plugs on either side of the feed

block valve or on the low-pressure side of the dump valve. To minimize the amount of flooding water that would enter the fuel low-pressure system, gas pressure was maintained in the system to approximately balance the head of flooding water. Excellent results were obtained. Less than 7 lb of light water entered the reactor system during all of the replacement operations. This water was transferred from the reactor to the waste system, and the reactor piping was rinsed with heavy water to remove all trace of the flooding water.

During a routine 2600-lb hydrotest of the reactor high-pressure system, five flanges (B-100, A-102, A-103, LE-145, and A-146) required tightening.

These repairs were accomplished in 20 days, requiring about 800 man-hours of craft labor.

3.2 OPERATIONS PERFORMED IN THE HRT CORE AFTER RUN 20

Remote operations performed within the HRT core after run 20 included: (1) manipulation of the loose diffuser screens to determine which remain attached and measurement of the distance between the attached screens, (2) viewing of the core tank surface, (3) measurement of the core-wall thickness, and (4) irradiation of nonmetallic-material specimens to be used in tools for remote operation. The tools used in these operations performed satisfactorily.

3.2.1 Diffuser-Screen Manipulation and Position Measurements

Long-handle tools were inserted into the core through the 2-in. access opening and used to check all diffuser screens for detachment by working through the 2-in. holes drilled in the center of the top six screens. The first, second, fourth, and fifth screens were determined to be definitely loose. The spacing between the attached third and sixth screens is as observed previously, and agrees well with core-tank manufacturer's dimensions.

To provide better viewing of the core, the pawl clamp[4] was used to suspend the two top diffuser screens in a vertical position.

3.2.2 Viewing of the Core

The 7/8-in. Omniscope was used to view the interior of the core. This periscope permits fields of observation as wide as 180°. Figure 3.1 shows the third screen and core wall in the lower hemisphere, as viewed with the Omniscope field limited to 120° by a contamination-protection sleeve.

Additional viewing between the screens was done with the piggy-back periscope, a 1-3/4-in.-dia tilting-mirror device with its own light source. Figure 3.2 shows the hole in the core tank after run 20. The fifth diffuser screen is seen edgewise across the hole.

3.2.3 Core-Wall Thickness Measurements

The ultrasonic core-wall-thickness gauge was checked out in the HRT maintenance mockup, and then used in the HRT core for wall-thickness determination. Results from these measurements are reported in Sec. 22.1.2.

Fig. 3.1. HRT Third Screen and Lower Core-Tank Wall Obtained with the 120° Field Omniscope.

UNCLASSIFIED
PHOTO 48018

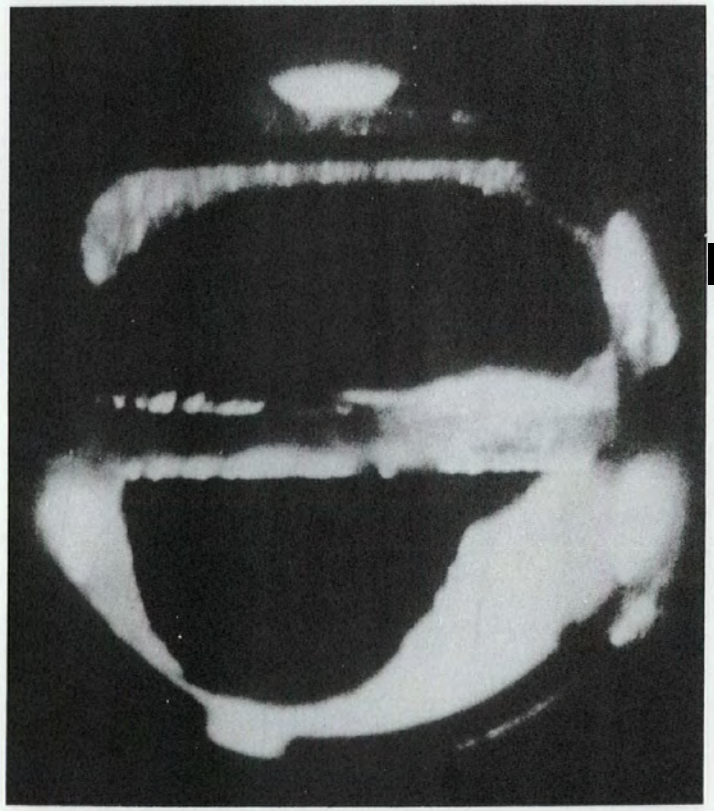

Fig. 3.2. Hole in the HRT Core-Tank Wall After Run 20.

3.2.4 Irradiation of Nonmetallic Materials in the HRT Core[5]

The underwater Heliarc torch which has been developed for cutting the diffuser screens utilizes plastic and rubber parts, generally not considered resistant to damage in the intense radiation field of the HRT core. Samples of nylon, Teflon, Neoprene and natural rubber were lowered into the HRT core, approximately 250 hr after run 20, and exposed for 8.8 hr, to determine the extent of radiation damage which might be incurred during normal tool life. No measurable weight change and only a slight increase in hardness of the samples were detected.

Several ceric sulfate solution gamma-radiation dosimeters were irradiated along with the nonmetallic material samples, for periods of 2 to 8.8 hr. Analysis of the ceric sulfate solutions indicated gamma radiation levels in the HRT core of 40,500 to 82,900 r/hr. The variation in radiation-level data is probably a result of differences in the location of samples during exposure and inaccuracies in the ceric sulfate dosimeters for this level of radiation.

3.3 MODIFICATION OF THE HRT CORE

Tools for modification of the HRT, according to the general procedure reported previously[6] were designed, fabricated, and tested in the HRT maintenance mockup.

Since the proposed core modifications have now been deferred for some time, the tools and spares were placed in standby readiness. It is believed that only minor refinements of the tools will be required to carry out satisfactorily the various remote operations. Detailed operating procedures for each tool are being prepared for use as operator training manuals at the time the core modifications are performed. A listing of tools (description, drawings, and photographic references) associated with the core repair operation has been issued.[7]

Following are descriptions of the tools as developed for removing the core diffuser screens and for plugging the hole in the core tank.

3.3.1 Separation of Diffuser Screens from Core Tank

The third and sixth diffuser screens, of the top six, remain attached to the core-tank wall. The other four screens are loose and will not require detachment. Different tools are needed to cut the two attached screens, because of the change in cutting radius at the two elevations in the conical section of the core tank.

The remote milling cutter[8] is the preferred tool for detachment of the third screen, and the final design is essentially that previously reported. This tool is preferred to the remote fly cutter, an alternative for cutting the third screen, because an extra tool insertion and contaminated tool withdrawal are required to preplace a bearing for the fly cutter.

Figure 3.3 shows the remote fly cutter developed for cutting the sixth screen. This cutter also requires a preplaced bearing.

The radius of the cutting path of the remote milling cutter and the fly cutter for the sixth screen is dimensioned to leave a 3/8-in. shelf around the edge to ensure that no damage to the core wall results from the screen cutting operations.

3.3.2 Loose-Screen Manipulation

A tool was fabricated to support the screens from the core-tank-to-pressure-vessel joint without restricting the 2-in. access opening. Figure 3.4 shows, on the left, the tool with the screen-support hook attached for insertion into the core; at the right, the tool has the hook unscrewed and offset, supported in the trunnions of the tool; and, in the center, the screen support hook is shown hanging on the groove of the transition flange model. The tool permits an operator to pass the hook through the 2-in. hole in the center of the screens, pick up the screens, and, by offsetting the tool, hang the hook with screens on the transition flange groove.

3.3.3 Removal of Screens from Core*

An improved design of the remotely operated manipulator and underwater Heliarc cutting torch[9] for cutting detached screens into strips less than 2 in. wide was fabricated and tested successfully. Cutting will be done under water in the core tank by the constricted, tungsten-arc method. The torch is used in conjunction with modified commercial arc-cutting equipment.

It was established that considerable leeway existed in the design of the torch. Figure 3.5 shows a cross section of the latest design of the torch head and its nylon spacer shoe. Conditions considered in adapting the torch to intended reactor use are:

1. Special cooling of the cutting tip may be eliminated, since cooling from the surrounding water is sufficient.

2. Insulation of the torch head is necessary to prevent erratic arc starting due to loss of the high-frequency current.

3. Concentricity of electrode and the cutting orifice must be preserved.

4. The torch and lines must be gas-tight.

5. Arc length must be constant and the cutting tip must be prevented from shorting onto the screen. For this purpose shoes or skids of Teflon or nylon are attached to the torch and ride on the screens.

Recommended conditions for underwater cutting are summarized in Table 3.1. Details as to cutting sequence, photographs of the torch in action, of the cut plate, and of the small, spherical particles produced by the cutting have been presented in another report.[10] Figure 3.6 shows the maximum speed that may be used with a given amperage to completely cut the Zircaloy-2 screens. Settings near the curve will result in narrow cuts. Wider cuts and increased metal removal will result with settings away from the curve. Using the conditions outlined, it was possible to make cuts totaling over 190 ft (in steel) and still have the torch in usable condition. Techniques were developed to detect an incomplete strip cut and to monitor the arc operation during a cut, by means of meters in the power circuit.

---

*Part of this section was contributed by G. M. Adamson and C. H. Wodtke of the HRP Metallurgy Group, Chap. 22.

UNCLASSIFIED
PHOTO 35053

Fig. 3.3. Remote Fly Cutter for Detaching Sixth Diffuser Screen.

UNCLASSIFIED
PHOTO 35048

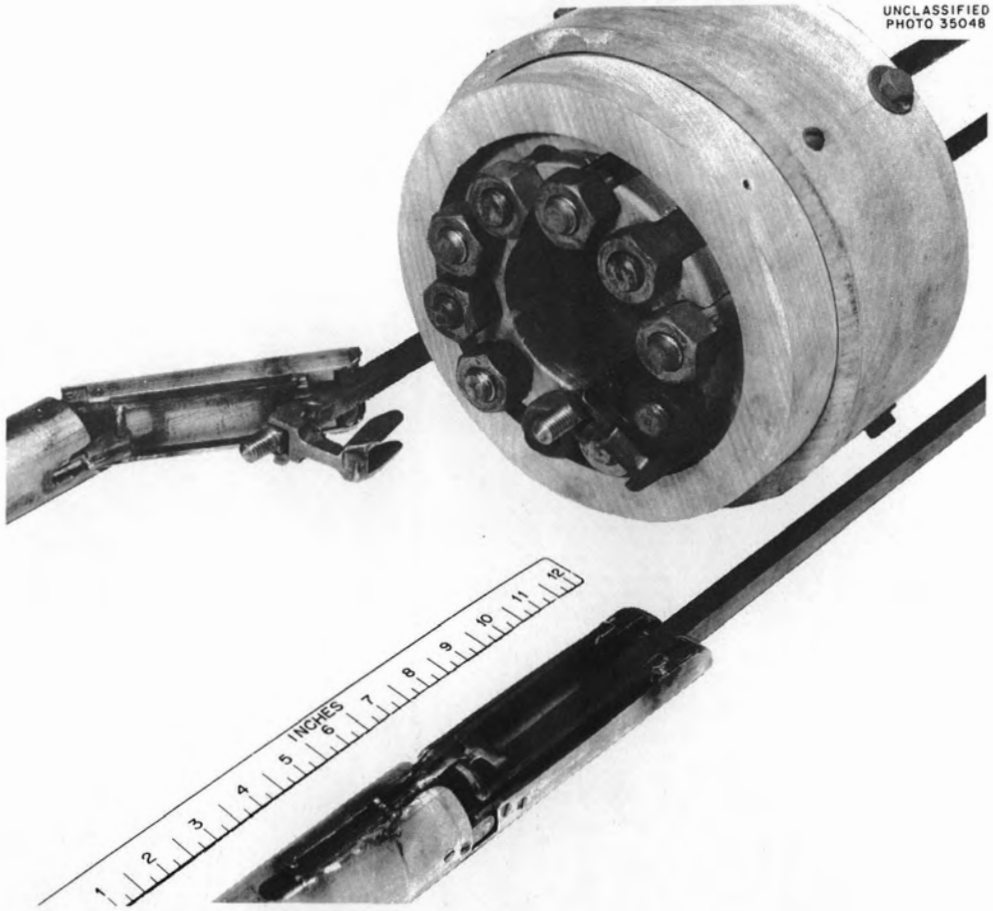

Fig. 3.4. Tool for Remote Manipulation of Diffuser-Screen Support.

UNCLASSIFIED
ORNL-LR-DWG 44255

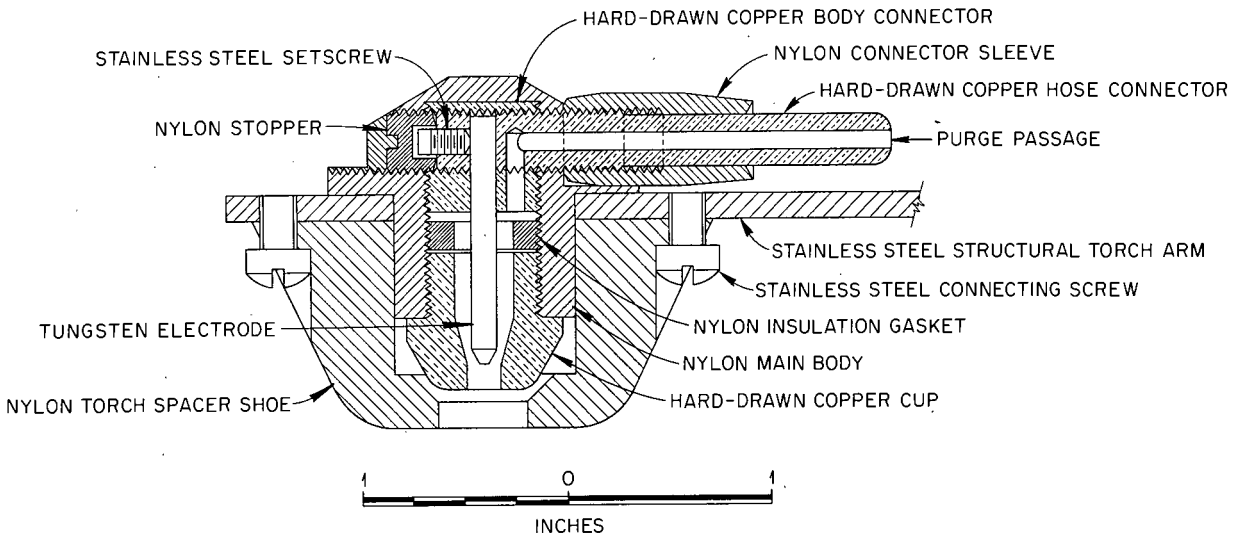

Fig. 3.5. Underwater Electric-Arc Cutting Torch and Rider Shoe.

UNCLASSIFIED
ORNL-LR-DWG 44256

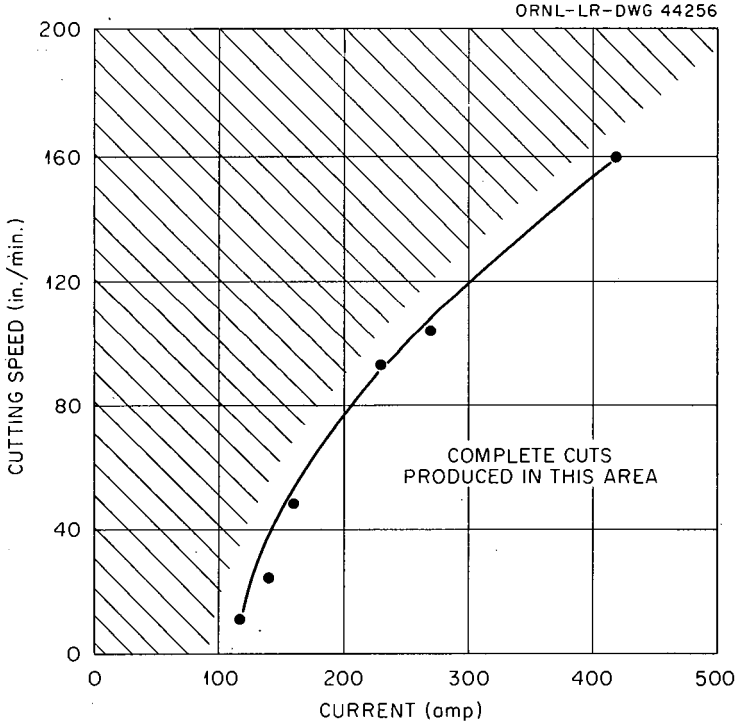

Fig. 3.6. Maximum Cutting Speed for a Set Current; Underwater Constricted-Arc Cutting of $\frac{1}{8}$-in.-Thick Perforated Zircaloy-2 Plate.

Although the molten Zircaloy-2 drops remained white hot for several seconds, there was no visible indication of self-ignition or other self-sustaining reactions with the water.

Table 3.1. Recommended Conditions* for Underwater Cutting of Zircaloy-2

Current DCSP, amp	350 to 425
Volts, open circuit	155
Volts, cutting	80
Argon flow, cutting, cfh	60
Argon flow, between cuts, cfh	5
Tungsten electrode dia, in.	1/8
Electrode inset, in.	1/8
Arc length (cutting tip to base metal), in.	1/4
Cutting-tip orifice dia, in.	5/32
Cutting speed, in./min	90

*Limited-duty cycle.

Figure 3.7 shows the lower end of the manipulator and torch assembly, with marks on the screen where cuts would be made. Figure 3.8 shows the motor drive for the torch traverse and upper end of the manipulator. Calibrated gage blocks are used, as shown, to move the torch position horizontally and to ensure strips small enough to be removed through the 2-in. core-access flange. The manipulator is sufficiently compact to allow simultaneous insertion of the 7/8-in. Omniscope through the access flange.

Development of the electrolytic dissolution method for removing detached screens from the HRT core was brought to a close after partial feasibility was established. This development was stopped primarily because of the success of the underwater cutting method and the additional development required to control pickup of hydrogen by the Zircaloy-2 core wall during the screen dissolution.

During the report period, further laboratory and bench-scale tests of electrolytic dissolution were made to investigate the effectiveness of biasing the potential of mockup core tanks in eliminating hydrogen pickup. Finally, a replica of the top diffuser screen was dissolved in a full-scale stainless steel mockup of the core vessel. The optimum operating conditions were: acid concentration, 8 $\underline{M}$ HNO_3; acid temperature, 60°C; dissolution rate, 44.5 g/hr or about 1 g/amp-$\overline{hr}$; core-vessel potential bias, +0.5 to +0.9 v.

In the full-scale mockup dissolution, 0.018-in.-thick vacuum-annealed Zircaloy-2 specimens attached to the vessel wall picked up 18 to 34 ppm hydrogen. The specimens exposed for varying times showed no time dependence for the amount of hydrogen pickup. Those specimens nearest the anodic screen being dissolved showed the highest hydrogen contents.

UNCLASSIFIED
PHOTO 35046

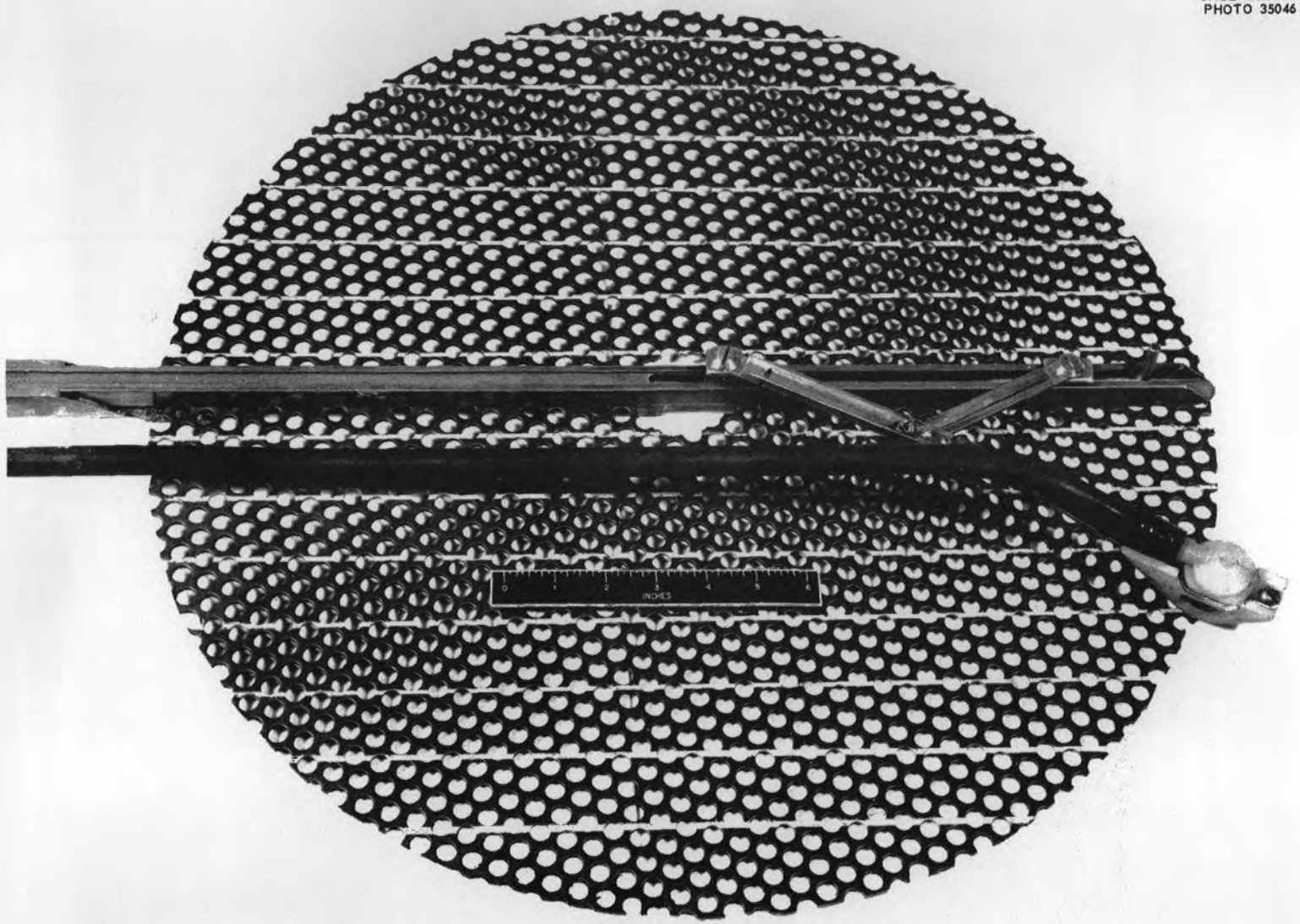

Fig. 3.7. Underwater-Cutting-Torch Manipulator and Torch Assembly.

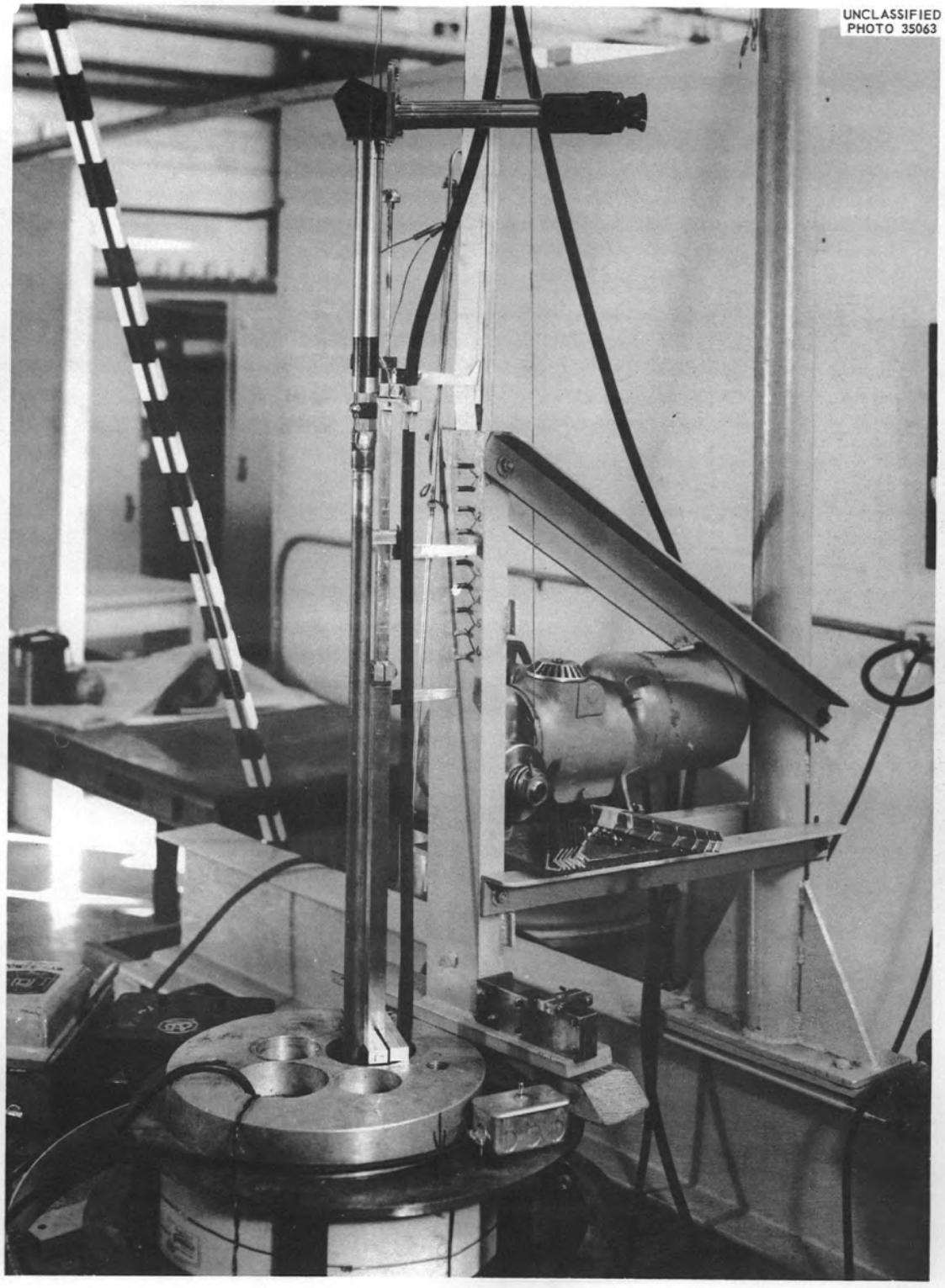

Fig. 3.8. Motor-Drive Device for Underwater-Cutting-Torch Manipulator.

In addition to the problem of hydrogen pickup by Zircaloy-2, an improved design for the anode clamp is required before the electrolytic process can be used in a reactor. With the present design, high contact resistance has caused overheating, with attendant burnup of tantalum hooks and severe embrittlement of a type 347 stainless steel clamp having a platinum contacting surface.

3.3.4 Core-Hole Definition and Patch Installation in the HRT

The core-hole-impression device shown in Fig. 3.9 will be used to provide an impression of the HRT core defect, from which a contour patch can be machined. The tool carries a cone of Dip Seal strippable plastic which has a Nichrome wire heater embedded in its surface. When inserted, the tool is retracted so that it will pass through the access flange, and after entry into the core, it is extended, as shown, and positioned opposite the hole by visual observation through the hole from the blanket side. When properly positioned, the plastic is heated on a predetermined schedule to provide proper plasticity, and is then forced into the hole by means of the spring-loaded air cylinder behind the plug. Upon cooling, the impression is retracted from the hole, and the tool is collapsed and removed from the core. The cone assembly can then be cut off the tool and placed in a shielded container for shipment to a hot cell in order to prepare a contour model for the patch.

A process was developed, in cooperation with personnel of the Solid State Physics Division, for first preparing a silicone-rubber mold of the core-hole impression, then coating the mold to reduce the spread of contamination, and finally making an epoxy resin casting of the impression. The casting will be used as a template to machine a contour patch of Zircaloy-2. A model, prepared by this replication process, and using a sample of HRT screen removed from the reactor, was only slightly contaminated, 3 mr/hr.

Installation of the patch in the HRT core will be made with the tools and procedure reported previously.[11]

3.4 REMOTE VIEWING EQUIPMENT

A 2-in.-dia television camera was adapted for viewing the inside of the HRT core vessel. Figure 3.10 illustrates the camera manipulator and use within the core. Remote lighting, focusing, and positioning were provided. There is space for insertion of small tools through the core access opening when the camera is installed for viewing. A nonbrowning lens has been obtained for the camera and should give a reasonable time for viewing.

3.5 CORE-ACCESS-FLANGE REAMER

The maximum tool diameter which can be inserted through the core access flange is 1.9 in., because of some shrinkage and weld push-through at the 2-1/8-in.-ID flange. Figure 3.11 shows the cutter of a tool for boring the flange to the full diameter of 2-1/8 in. The mill cutter is attached to a 12 ft shaft and is driven by an air motor.

UNCLASSIFIED
PHOTO 34179

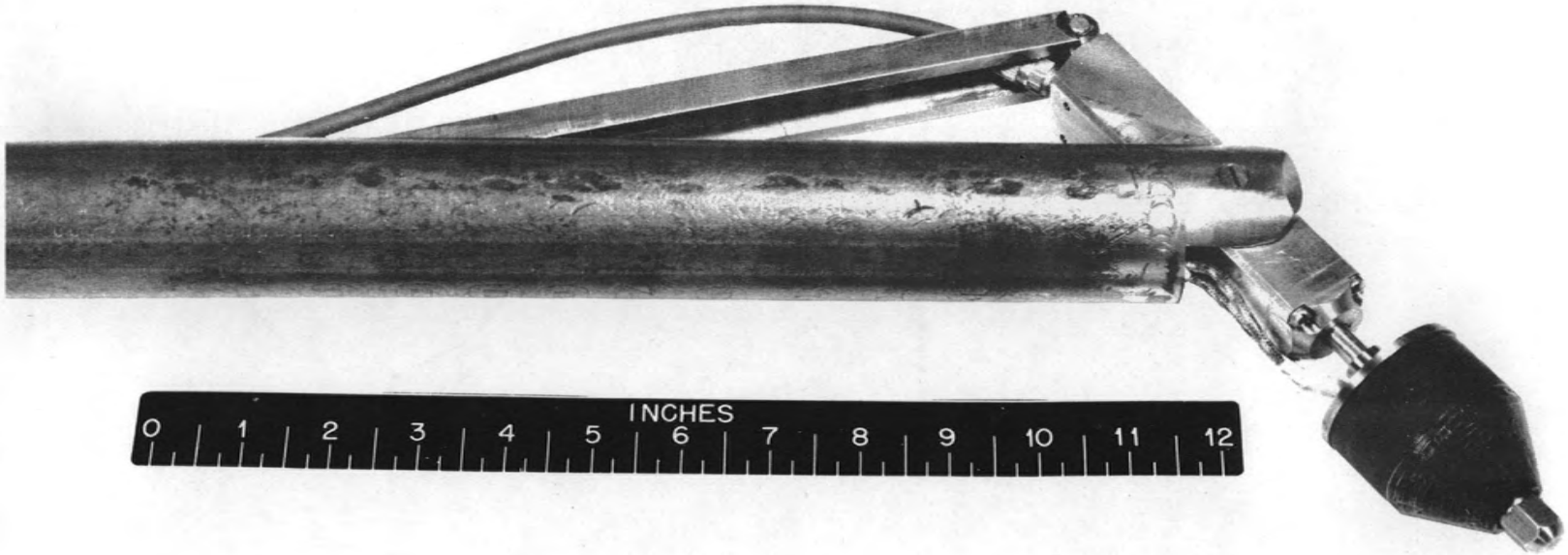

Fig. 3.9. Core-Hole Impression Tool.

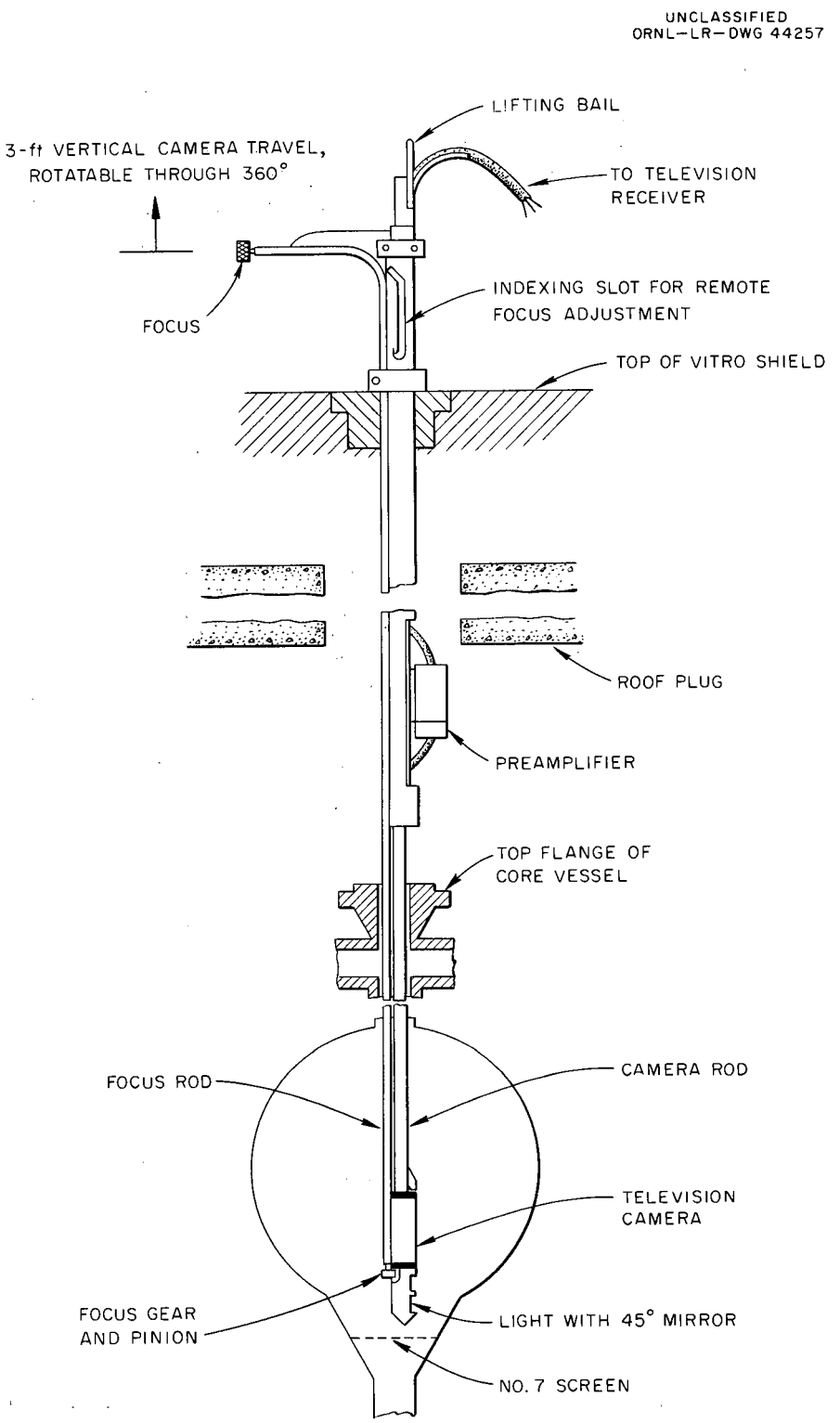

Fig. 3.10. Television-Camera Manipulator.

UNCLASSIFIED
PHOTO 35061

Fig. 3.11. Lower End of Tool for Reaming the HRT Core Access Flange.

3.6 HRT CORE-ACCESS STANDPIPE

A standpipe assembly, 12 in. in diameter and 44 in. high, was designed for installation at the core access flange face. This unit permits flooding of the cell to levels above the access flange face, and by providing for temporary storage of items removed from the core, it eliminates the necessity of completely removing the retrieving tools through the access plugs at each operation.

3.7 OFF-GAS CONTROL DURING SCREEN CUTTING

A system (see Fig. 3.12), consisting of an air-driven jet and a filter assembly packaged for installation through the blanket access plug, was designed for control of the gases associated with the screen cutting operation. The gases will be drawn through the lower flange of the core access standpipe and discharged to the cell for disposal through the cell air exhaust system via the east valve pit, the stack filter, and the stack.

3.8 HRT CORE FLUSH TESTS

Tests were performed to determine the amount of fluid and flow rate required to flush from the HRT core the solids produced in the screen dissolution or underwater screen-cutting processes. Representative solids produced by the two processes were added to the full-scale, low-temperature mockup of the HRT core, and attempts were made to remove the solids by water flushing.

Beads produced in the underwater screen-cutting operations could be removed by flushing at 50 gpm for about 3 min, followed by a short flush of 1 min duration at 300 gpm, with flow entering the top of the vessel.

Scale produced in the electrolytic dissolution of screens could not all be removed by flushing. The scale not removed was larger than the holes of the lower screens in the 30° conical section of the core vessel.

REFERENCES

1. S. E. Beall et al., HRP Quar. Prog. Rep. Apr. 30, 1959, ORNL-2743, p 5.
2. W. D. Burch et al., HRP Quar. Prog. Rep., Apr. 30, 1959, ORNL-2743, p 10.
3. F. W. Cooke, Examination and Remedy of HRT Sample Valve Stem Adapter Failure, HRP-MET-98 (Sept. 10, 1959).
4. I. Spiewak et al., HRP Quar. Prog. Rep. Apr. 30, 1959, ORNL-2743, p 16.
5. P. P. Holz and R. Blumberg, Measurement of Gamma Activity and Irradiation of Plastics, HRP-59-175 (Sept. 17, 1959).
6. I. Spiewak et al., HRP Quar. Prog. Rep. Apr. 30, 1959, ORNL-2743, p 13.
7. J. E. Jones and F. C. Zapp to Distribution, Maintenance Tool Listing, (Sept. 16, 1959).
8. I. Spiewak et al., HRP Quar. Prog. Rep. Apr. 30, 1959, ORNL-2743, p 13.

9. Ibid., p 16.

10. G. M. Adamson, Met. Div. Ann. Prog. Rep. Oct. 1959, ORNL-2839, p 127-129.

11. I. Spiewak et al., HRP Quar. Prog. Rep. Apr. 30, 1959, ORNL-2743, p 20.

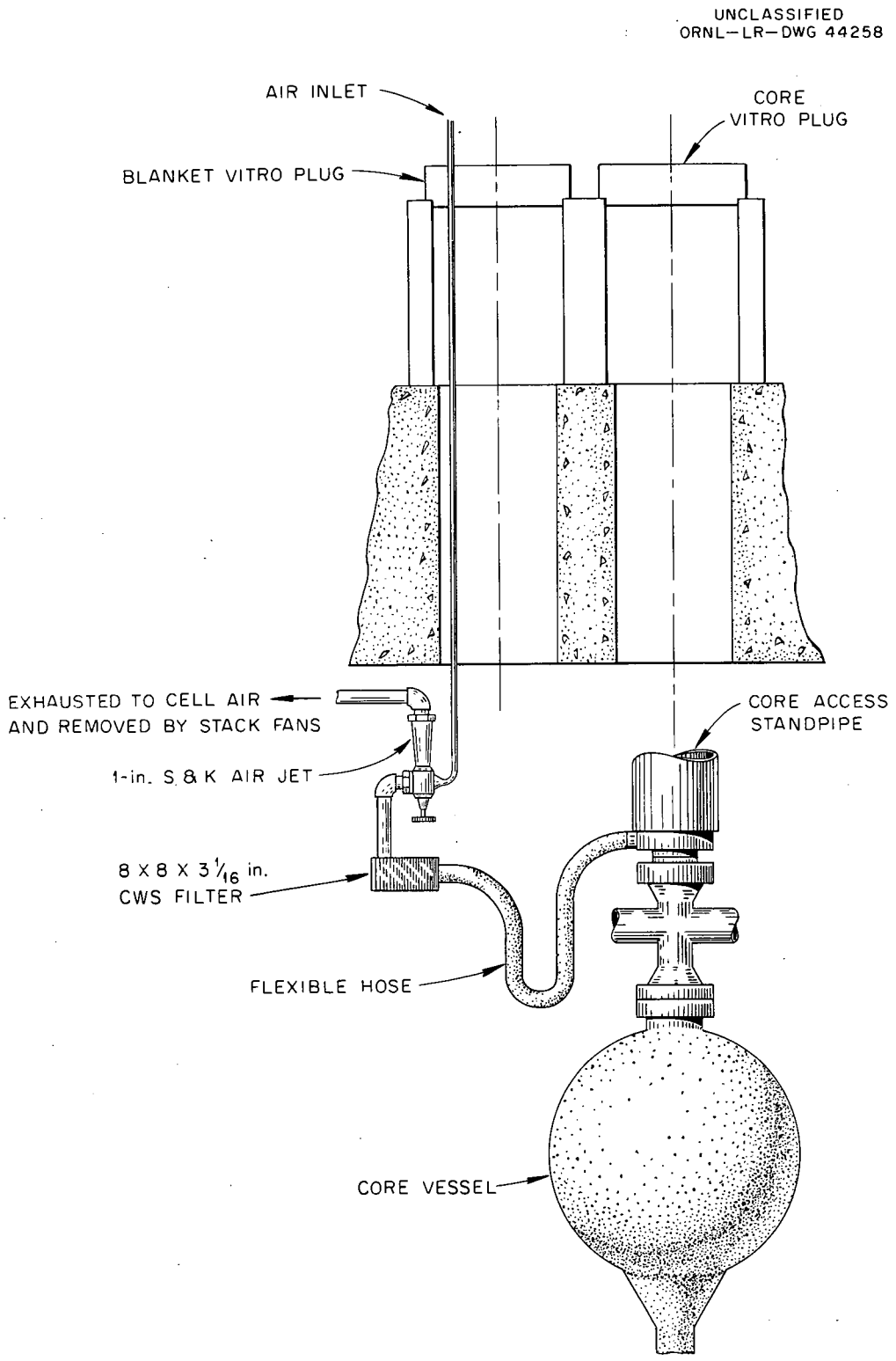

Fig. 3.12. Off-Gas System for HRT Core Vessel.

4. HRT ENGINEERING DEVELOPMENT

I. Spiewak F. N. Peebles

C. H. Gabbard E. C. Hise J. C. Moyers
P. H. Harley H. R. Payne

4.1 FEED-PUMP ENDURANCE TESTING

Endurance testing of the two HRT prototype feed-pump heads was discontinued after 19,256 hr of satisfactory operation. One of the heads was installed in the HRT; the other will be available as a spare. A hydrostatic test of the suction and discharge check valves of the unit that was installed in the HRT showed acceptably low leakage rates of 0.9 and 0.5 cc/hr of water at 2000 psi ΔP.

4.2 TEST AND PRETREATMENT OF THE REPLACEMENT FUEL-CIRCULATING PUMP FOR THE HRT

The replacement for the HRT fuel-circulating pump was fitted with a 400-gpm stainless steel impeller. The upper and lower impeller hubs were machined to the maximum clearance permitted by the manufacturer's tolerances, thus reducing the possibility of contact in the wear rings.

Complete hydraulic performance data were obtained with the pump over its operating range while circulating cold water at low pressure. Similar performance data were also taken for reverse rotation at the estimated operating point. The pump was then given a short pretreatment run in oxygenated water to establish a corrosion film prior to installation in the HRT.

4.3 CIRCULATING-PUMP TESTS UNDER ADVERSE FLOW CONDITIONS

A pump loop was constructed and operated to investigate the cause of titanium impeller fires and to test corrective measures. A 50-gpm Byron-Jackson pump fitted with titanium wear rings having a radial clearance of 0.040 in. (normal clearance = 0.020 in.) was run at the following conditions without damage:

1. normal operation in oxygenated water at 250°C, 48 hr;

2. operation with oxygen-saturated water at 250°C, 48 hr;

3. cavitation run at 250°C and 577 psi
   (5 to 10% decrease in pump power), 48 hr;

4. operation with loop half full of water at 250°C and 1250 psi (oxygen pressure), 48 hr;

5. operation as oxygen blower at 250°C and 1250 psi, 48 hr.

Similar tests with a set of Zircaloy-2 wear rings having a clearance of 0.010 in. were also run with no damage to the pump. Zircaloy-2 and titanium wear rings will be run with light contact in the near future.

4.4 PUMP ROTATION AND SPEED INDICATOR

An indicator was designed and built to indicate the direction of rotation of the HRT circulating pumps. The device consists of a pickup coil mounted in the back plug of the motor, and three iron slugs mounted in the rotor at 0°, 45°, and 135°. The direction of rotation can be determined by observing the impulse pattern on an oscilloscope or other high-speed recorder. The pump speed can also be determined by timing the impulses.

4.5 HRT MOCKUP

During the report period, the HRT mockup was operated for 1050 hr in run CS-25. The major objective of this run was to study the inventory of fuel components (uranium, copper, sulfate, and free acid) as revealed from chemical analyses of samples, as compared to the "book" values computed from addition and withdrawal of materials from the system. It was expected that the information obtained in the nonradioactive HRT mockup would indicate a limit of precision obtainable in HRT inventory control.

Run CS-25 consisted of two parts: (1) a 655-hr period of chemically "stable" operation at loop temperatures of 280 to 300°C, pressures of 1500 to 1670 psi, and feed rates from 0.6 to 1 gpm, and (2) a 395-hr period of "unstable" operation during which a heavy liquid phase was formed periodically by cycling the titanium pressurizer between 336°C (2000 psi) and 315°C (1500 psi). The results of the run are summarized in Table 4.1, which gives the ratio of observed to "book" inventories, and lists also the variation obtained in control samples.

The results demonstrate that U, Cu, SO_4, and H_2O were always within 3% of the expected value within both the stock-solution control group and the samples withdrawn from the loop at "stable" conditions. On the other hand, the free acid was between -2.6% and +7.3% of the expected value. Following instabilities, U, Cu, and SO_4 did not appear to be completely recovered until after the run. One might infer from these data that material balances may be used during periods of chemical stability to prove stability; however, following instabilities material recovery may be slow.

During the chemical instabilities, almost stoichiometric U, Cu, and Ni sulfates were removed from circulation. The excess-acid level in the circulating light phase increased slightly, causing an increase of loop corrosion rate from 0.84 mpy to 1.54-2.75 mpy.

Table 4.1. Ratio of Inventories Computed from Sample Analyses to "Book" Inventories, Run CS-25

Sample Series	U	Cu	SO_4	Free Acid	H_2O
Stock-solution control samples*	0.995 to 1.006	0.983 to 1.021	0.984 to 1.023	0.974 to 1.056	
Solution charged into mockup	1.00	1.00	1.00	1.00	1.00
Run-hours 0 to 655 (stable conditions)	0.991 to 1.020	0.978 to 1.025	0.966 to 1.005	1.035 to 1.073	0.995 to 1.013
Run-hours 655 to 1050 (following instabilities)	0.949 to 0.984	0.957 to 0.979	0.938 to 0.960	1.030 to 1.071	0.994 to 1.00
Postrun solution drained	1.012	1.015	0.990	0.964	

*"Book" inventory of stock solution is taken equal to the mean of all analyses of the stock solution.

5. HRT DESIGN

W. R. Gall M. I. Lundin

C. A. Burchsted E. H. Gift
C. J. Claffey J. E. Jones, Jr.
F. C. Zapp

5.1 EFFECTS OF STOPPING THE CIRCULATING PUMPS DURING A DUMP

A study was made[1] of afterheat removal in the HRT system during an emergency dump, to help evaluate the advisability of de-energizing the circulating pumps at the time the dump valve opens, rather than having them de-energized by low current when they become vapor bound. An earlier study[2] on heat removal after shutdown indicated that no appreciable increase in system pressure would be caused by shutoff of the pump at the time the dump valve opens. The present review indicates that the conclusions of the earlier study still apply.

5.2 REPLACEMENT PRESSURE VESSEL, SUMMARY REPORT

The effort devoted to the replacement of the HRT reactor pressure vessel was suspended as a result of a review of the Laboratory's fluid-fuel reactor program.[3] Work on the design studies for replacement of the vessel was summarized[4] to provide a convenient reference to the drawings and memoranda pertaining to the study.

5.3 CONTAINMENT OF REACTOR STEAM SYSTEM

The activity hazard which would arise as a result of a ruptured heat exchanger tube was re-evaluated using more realistic assumptions than those reported previously.[5] These most recent calculations[6] are based on the additional assumptions: (1) that the pressure in the external steam system is determined by the rate of leakage through the steam stop valves and the cooling capacity of the steam killer, (2) that the entrainment separator is effective in removing from the exit stream 90% of the non-gaseous fission products in the heat exchanger, (3) that the rate of leakage of fission products through the steam stop valves is a time-dependent function of the fuel transfer through the ruptured heat exchanger tube, and (4) that during the 4-min delay (built into the control circuits) before dumping the reactor system, 1020 lb of fuel solution may be transferred to the steam side through the ruptured tube.

Two cases were considered for cooling in the steam killer: (1) the

cooling-air blower continues to operate, and (2) the blower is off and the steam killer is cooled by natural convection of air.

The calculations indicate that the radiation hazard from fission products being dissipated to the atmosphere through the steam-system vents is negligible if the steam-killer air blower continues operating. If, however, the air blower is not operating, natural convection of air through the steam killer will condense a minimum of 4 lb/min of steam (equivalent to 1.8 liters of liquid H_2O per minute) at atmospheric pressure. In this case the inhalation hazard will be negligible at all reactor power levels unless the steam stop valves have combined leak rates greater than 4 lb/min. Radioactive iodine is the controlling ingestion hazard since the entrainment separators inside the heat exchanger shells effectively remove a major portion of the nongaseous fission products from the steam leaving the exchangers. Figure 5.1 shows the product of exposure time and reactor power that would produce an emergency thyroid dose of 50 rem as a function of steam-stop-valve leak rate for the case of the steam-killer blower being inoperative.

Although the whole-body external radiation hazard is not controlling, it can become serious in certain situations. For instance, if the steam-killer blower continues to function, the unit will be operating at subatmospheric pressures, and there should be no fission products released to the atmosphere. However, under these conditions the radiation emitted from the fission products contained within the steam pipes, condensate lines, etc., may become a hazard to people in the vicinity of these sources. Figure 5.2 shows the product of exposure time and reactor power that would produce an emergency whole-body dose of 25 rem from steam and condensate lines as a function of distance away from the lines.

5.4 RECOMBINERS

Recent difficulties with the HRT recombiners suggested a review for a design that could be adequately heated, more easily reactivated, and installed with a minimum of changes to the existing system.

5.4.1 Fuel Primary Recombiner

A replacement catalyst bed was designed for the fuel primary recombiner. This bed contains approximately 180 ft^2 of surface area per cubic foot at a density of 20 to 24 lb/ft^3 and is 10-1/2 in. in diameter by 12 in. high. Incoloy or stainless steel ribbon (1/16 in. x 0.005 in.) is used as the support material and is plated with a total of 10 g (15 g/ft^3) of platinum. The process-side pressure drop is approximately 5 in. of H_2O at a flow rate of 10 lb/min.

Two flat coils of stainless steel tubing are located within the bed for cooling or for heating by superheated steam for reactivation. A superheater section was designed to heat saturated steam (at 225 to 250 psi) to approximately 500°C for this purpose.

5.4.2 Fuel Secondary Recombiner

The fuel secondary recombiner assembly was redesigned in the form of a removable piping loop (see Fig. 5.3) that can be installed between existing system flanges which now serve valve HCV-344 in line 116. The recombiner

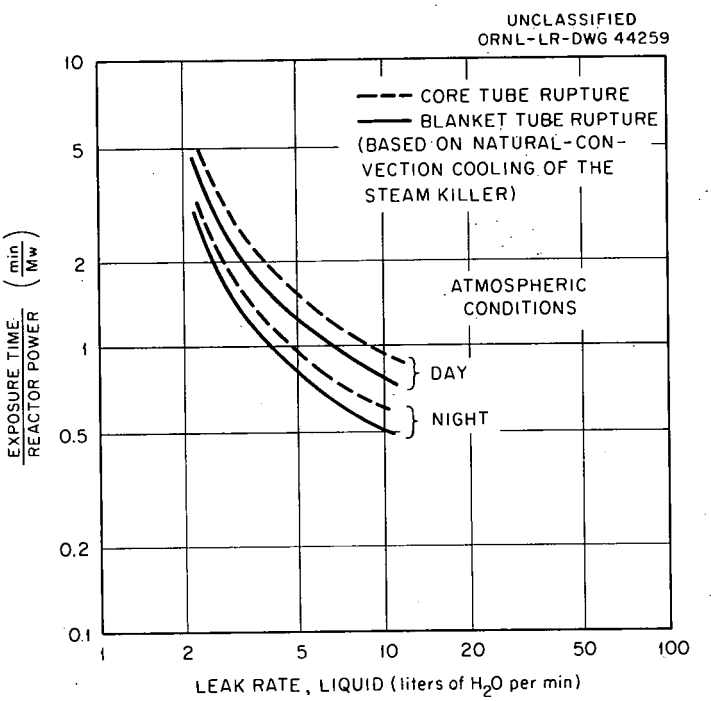

Fig. 5.1. Exposure Time Required to Give 50 rem to the Thyroid as a Function of Leak Rate Through HRT Steam Valve 537 or 538 Following a Heat Exchanger Tube Rupture.

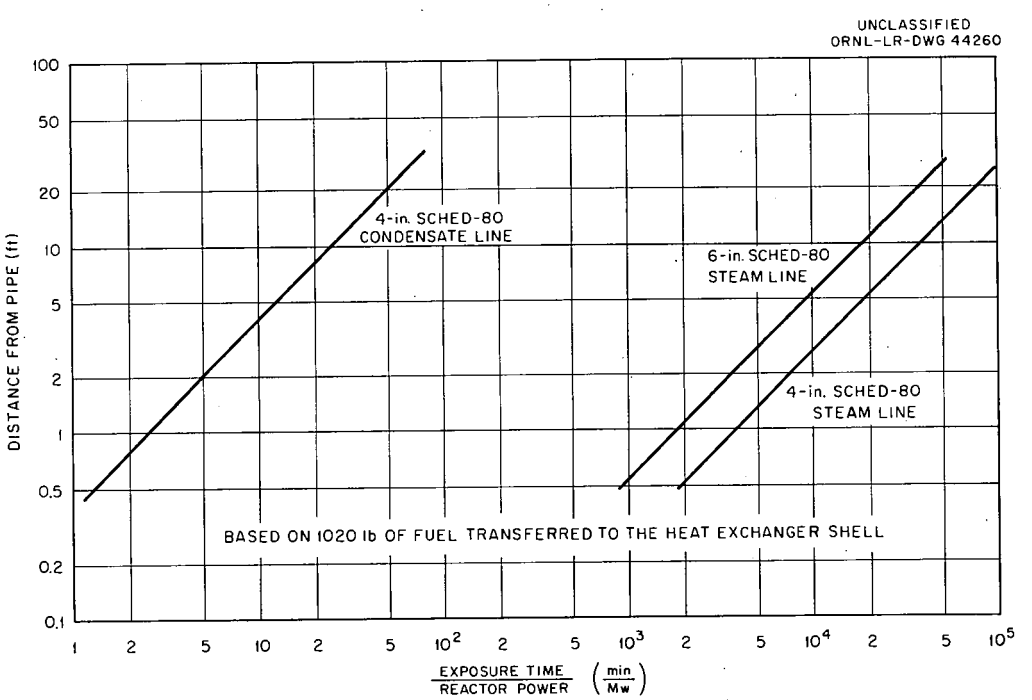

Fig. 5.2. Exposure Time Required to Receive 25 rem Whole-Body Dose as a Function of Distance from Contaminated HRT Steam and Condensate Lines Following a Heat Exchanger Tube Rupture.

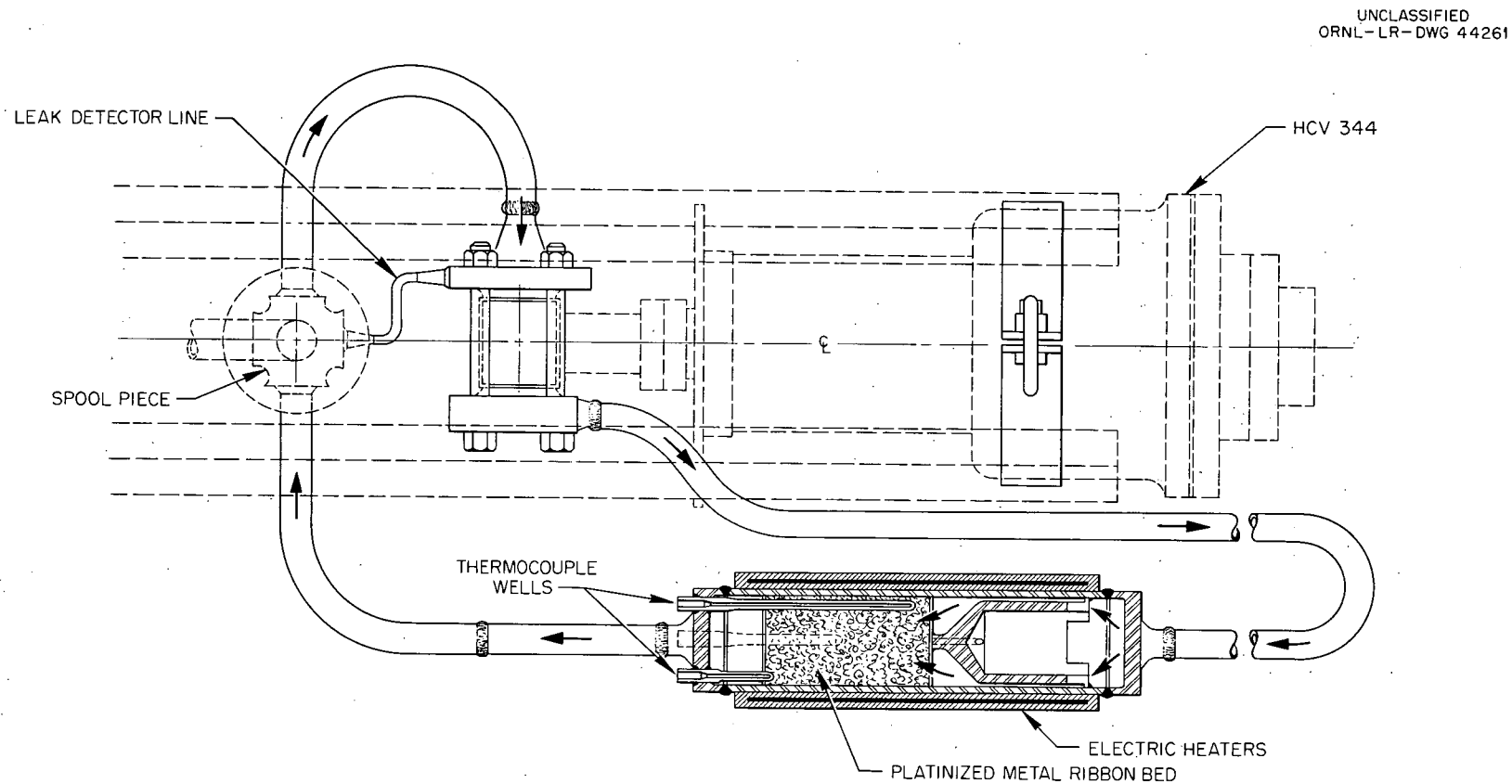

Fig. 5.3. HRT Fuel Secondary Recombiner.

contains a cylindrical bed (approximately 3 in. in diameter by 5-1/2 in. long) of platinized Chromel ribbon. Electrical strip heaters are available for heating and reactivating the bed.

5.5 SAMPLERS

Because of occasional difficulties with stripped threads in process-line disconnects installed in the HRT samplers, portions of the samplers were redesigned to incorporate floating disconnect adapters, new hold-down bolts, a new plug alignment system, and new shielding plugs. A new male jig was also designed for use in aligning the adapters with respect to the connectors on the main plug.

The position-sensing device for the sampler isolation chamber was revised to strengthen the microswitch brackets, since weaknesses in both the support and actuating brackets decreased the effectiveness and reliability of the present device.

5.6 RADIATION MONITORS

The Victoreen gamma monitors located in the steam-drum pit and in the east and west instrument cubicles are relatively inaccessible for replacement without shutting-down the reactor. Since these units require frequent replacement, thimbles are being designed to permit installation or replacement of the monitors without moving the shielding blocks over the steam-drum pit or opening the cubicles during operation.

The thimbles for the instrument cubicles are designed to withstand 50 psi external pressure and will be seal welded to the top plate of the cubicles. The steam-drum-pit shielding blocks will be drilled through for a 6-in.-dia thimble (not pressure-tight). This access hole will normally be filled with a carbon-steel plug except while the monitors are being replaced.

REFERENCES

1. E. H. Gift, "Effects of Stopping the HRT Circulating Pumps During an Emergency Dump," memorandum to S. E. Beall, May 1, 1959.

2. M. W. Rosenthal and H. C. Claiborne, Effects of Heat Generation and Heat Removal on HRT Shutdown and Dump, ORNL CF-56-2-128 (Feb. 8, 1956).

3. R. B. Briggs, "Program for the Homogeneous Reactor Project," memorandum to HRP technical personnel, April 23, 1959.

4. R. H. Chapman, HRT Replacement Reactor Vessel Study, ORNL CF-59-8-110 (Aug. 5, 1959).

5. W. R. Gall, et al., Monthly Report - Design Section - December 1958 and January 1959, ORNL CF-59-1-150 (Jan. 30, 1959).

6. E. H. Gift, Determination of Maximum Permissible Leakage from the HRT Process Steam System, ORNL CF-59-1-143 (Mar. 11, 1959).

6. HRT CONTROLS AND INSTRUMENTATION

R. L. Moore

A. M. Billings
J. R. Brown
P. H. Harley
P. G. Herndon
J. L. Redford
D. S. Toomb

6.1 COMPONENT DEVELOPMENT

6.1.1 Fuel Feed Flowmeter

Recent experience in HRT operations has indicated the need for a method of measuring continuously the fuel feed-pump flow rate. Knowledge of the flow rate is required for accurate determination of fuel inventories in the reactor system under operating conditions.

Measurement of the fuel feed flow is complicated by the pulsing nature of the flow, the high radiation level of the fuel solution, and the necessity for absolute containment of fuel solution. Also, it is desirable that the instrument be self-draining and present minimum obstruction to fluid flow.

In an effort to provide a flowmeter for this service, a Laub Electrocaloric flowmeter (heat-balance type, manufactured by Industrial Development Laboratories, Inc.) was installed and operated in the fuel feed system of the HRT mockup. The instrument was calibrated for a pulsing-flow range of 0.5 to 1.5 gpm at 100°C. During operation the Electrocaloric indication was compared with the flow indicated on a variable-area type of flowmeter installed in a part of the system not subjected to pulsing flow. At all flow rates, fluctuations in the Electrocaloric indication resulted in an uncertainty in the measurement, the magnitude of the fluctuations being 8% of full scale at low flows and 2% of full scale at 1.5 gpm. No change in the indicated flow rate was observed when the temperature of the process fluid was varied from 99 to 106°C.

In order to study the fluctuations, the indicator presently used with the system will be replaced with a recorder. The information obtained should permit averaging of the fluctuations and should result in an improvement in the accuracy of measurement.

6.1.2 Remote Viewing Equipment

The Dage miniature television camera previously described[1] was modified for use in viewing the impeller of the blanket circulating pump. In this service, the camera was required to pass through the 3-in.-ID inlet pipe of the pump assembly with sufficient clearance to allow passage around the two 45° bends

in the pipe. Also it was required that:

1. a means for pushing, pulling, and twisting the camera be provided,

2. provisions be made for shadowless illumination of the impeller by lights outside the field of view of the camera,

3. an air purge be provided to cool the camera,

4. protection be provided to prevent contamination of those parts of the camera which could not be easily decontaminated or which would be costly to replace.

The camera (Fig. 6.1) was tested on the bench by viewing impellers in spare blanket and fuel circulating pumps; the pictures obtained were clear and sharp. The portions of the impeller seen were the same as would be seen by eye, looking into the center of the impeller, with the eye 3 in. from the edge of the impeller hub. It was not necessary to use the camera on the reactor blanket pump because of the success of the seal-weld cutting operation, which permitted direct viewing.

6.1.3 HRT Letdown Valves

Testing of letdown valves in the HRT mockup was continued. Valve No. 23,[1] with a 1/8-in.-dia port, was returned to service in the mockup and has since operated satisfactorily for 1350 hr. Total service time for this valve is 4780 hr.

The 1/4-in.-dia port valve in the reactor continues to give satisfactory performance; it has operated for 5657 hr.

6.2 MAINTENANCE AND MODIFICATION

6.2.1 Control Valves

The fuel feed shutoff valve (HCV-337, serial No. K-03), which was replaced during October, has been examined. Although radioactive contamination has prevented disassembly of the valve, preliminary tests indicate that mechanical binding occurred between the valve stem and its guide bushing. Plug-to-seat leakage was found to be negligible. This is the first low-pressure-system valve to require replacement since the valves were installed in the reactor approximately 2 years ago.

Requirements for steam-system valve sizes were studied to determine the changes necessary to permit 10-Mw operation of the HRT. No changes appear necessary.[2]

6.2.2 Control-System Revision

A second generator was installed to provide standby power for the 48-v d-c control circuitry. As part of this installation a jumper board was installed which gives operating personnel the option of running either generator separately or both generators in parallel. Also, the design of this board is such as to permit replacement of banks of batteries without control-power interruption.

UNCLASSIFIED
PHOTO 35145

Fig. 6.1. Miniature Television Camera Modified for Pump Inspection.

Extensive revisions to the emergency air-line block system were made in order to allow the instrument-cubicle vent and instrument air systems to be blocked separately. These revisions to the control system have necessitated extensive revision of the jumper board. Design and fabrication of the revised board was completed, but the board has not been installed as yet.

Instrumentation and control required for operation of the fuel recombiner superheater was designed and installed. Control of the heaters in this system is manual, with protection against excessive heater temperature being provided by a high-temperature interlock.

6.2.3 Emergency A-C Power for Public-Address System

A d-c to a-c converter was installed which will provide emergency power for the public-address system in the event that total loss of a-c power is experienced. This system is designed to provide power automatically for a period of 1 min after loss of service power. If it is necessary to operate the public-address system after this period, power may be restored by operation of a key switch located in the control console. When service power is restored, the converter network automatically becomes de-energized.

REFERENCES

1. D. S. Toomb, et al., HRP Quar. Prog. Rep., April 30 and July 31, 1958, ORNL-2561, p 50.

2. A. M. Billings, "Steam System Valve Capacities for HRT 10 MW Operation," memorandum to R. L. Moore, HRP-59-184.

Part II

REACTOR ANALYSIS AND ENGINEERING DEVELOPMENT

7. REACTOR ANALYSIS

P. R. Kasten

M. L. Tobias D. R. Vondy

7.1 NUCLEAR CHARACTERISTICS OF SMALL SOLUTION-CORE, SLURRY-BLANKET SPHERICAL REACTORS (HRE-3)

Some of the nuclear statics characteristics of small, spherical, solution-core, slurry-blanket reactors were studied to provide information for the design of HRE-3. The following requirements form the bases for the investigation:

1. The core diameter is less than 3 ft.
2. The blanket thickness is less than 1 ft.
3. The core fuel concentration is to be made less than 10 g of U^{235} per liter. A poison fraction of 6% is to be assumed.
4. The blanket thorium concentration is 1000 g of Th per liter.
5. The moderator is to be a mixture of D_2O and H_2O.
6. The blanket fuel concentration is to be less than 40 g of U^{235} per kg of Th. Blanket poisons are neglected.
7. The reactor is to operate at 280°C.

Subject to these restrictions, the critical concentrations, core-wall power densities, breeding ratios, and ratios of core-to-blanket power were determined as functions of moderator composition, reactor dimensions, and blanket fuel concentration.

The calculations were performed using an IBM-704 code for the spherical harmonics method of Edlund and Noderer.[1] The results of the calculations are displayed in the accompanying figures. Figure 7.1 shows how the moderator composition for minimum core critical concentration varies with core diameter and blanket thickness. This composition is not a strong function of blanket fuel concentration; for a given core diameter the per cent of D_2O in the moderator rises as blanket thickness increases, and for a given blanket thickness the D_2O concentration likewise rises with increasing core diameter. Figure 7.2 shows the effect of varying moderator composition, blanket uranium-to-thorium ratios, and blanket thickness upon the core concentration of reactors having a

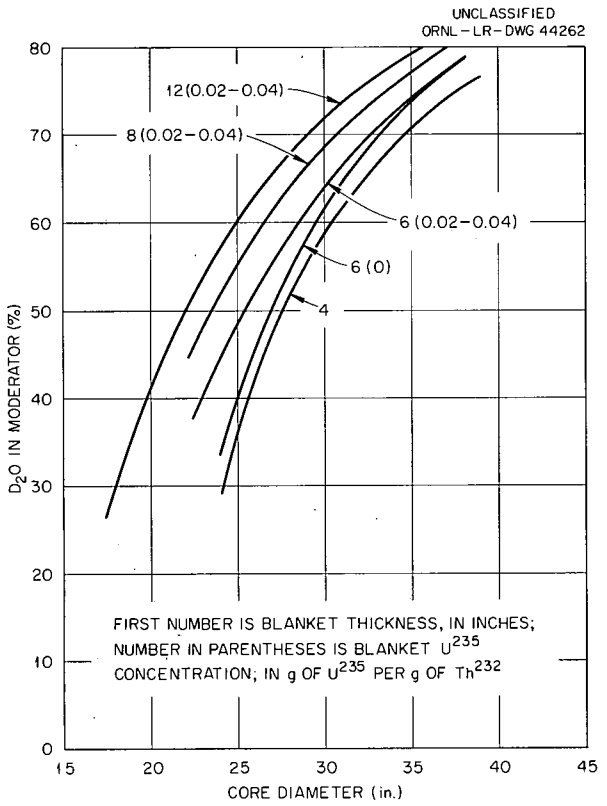

Fig. 7.1. Moderator Composition for Minimum Critical Core Fuel Concentration.

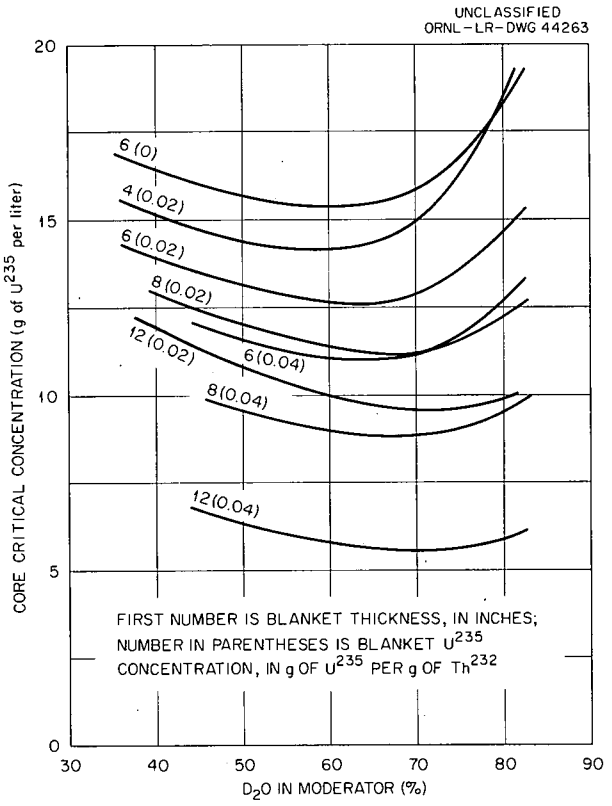

Fig. 7.2. Core Critical Concentration vs Moderator Composition for Reactors Having a 30-in.-dia Core and Various Blanket Thicknesses and U^{235}/Th^{232} Ratios.

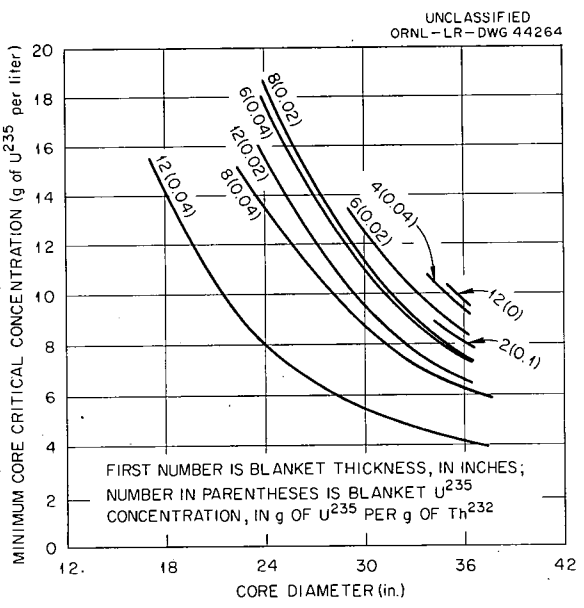

Fig. 7.3. Minimum Core Critical Concentration as a Function of Core Diameter, Blanket Thickness, and Blanket Uranium Concentration.

30-in. core diameter. Figure 7.3 gives the minimum fuel concentration associated with the optimum D_2O-H_2O mixtures as a function of core diameter, blanket thickness, and the U^{235}/Th ratio in the blanket. For a 36-in.-dia reactor core, moderator compositions exist for which many combinations of blanket thickness and blanket fuel concentration result in core critical concentrations of less than 10 g of U^{235} per liter. As the core diameter is decreased, larger blanket thicknesses and blanket fuel concentrations are needed. For the 24-in.-dia core, a 1-ft-thick blanket and 40 g of U^{235} per kg of Th are needed; for the 18-in.-dia core, no combination achieved the desired result. Minimum critical concentrations usually corresponded to moderator compositions in the 60 to 80% D_2O range.

Breeding ratios were generally low, mostly less than 0.5, and fairly insensitive to moderator composition and core diameter. They were principally dependent upon blanket fuel concentration and blanket thickness, increasing with larger blanket thickness and decreasing with higher fuel concentration.

Core-wall power density and core power fraction vary strongly with blanket fuel concentration. Figure 7.4 gives the fraction of the reactor power generated in the core for various parameter values and a moderator composition of 60% D_2O. Figure 7.5 gives the core-wall power density for various parameter values, a moderator composition of 60% D_2O, and a blanket thickness of 1 ft; the variation shown is typical of the variation for other blanket thicknesses and moderator compositions. Above about 10 g of U^{235} per kg of Th in the blanket, the wall power density on the blanket side is larger than that on the core side. Blanket-side wall power densities may range up to 4 kw/liter per megawatt of total power for reactors of interest (i.e., those with low core concentrations); the core-side wall power density was usually less than 2 kw/liter per megawatt.

7.2 STUDIES OF IMPROVEMENT OF POWER DENSITY IN ORR LOOPS

Although fluxes obtainable in the ORR are much higher than those in the LITR, the power density in a fuel-solution loop operated in the ORR was not markedly greater than that in loops operated in the LITR. The principal point of contrast between these loops appears to lie in one important construction difference, namely, that the fuel-solution containers in the LITR loops were surrounded by graphite whereas the container in the ORR loop was not. Further, in the ORR loop there was an air gap about $\frac{1}{2}$ in. thick between the outer shell and the fuel-solution container; no gap was present in the LITR loops. Behind the fuel container in both loops, neutron reflection is afforded only by the piping and other hardware associated with the fuel loop which are heavily intersphersed with air gaps. It appeared that in the ORR loop the power was being lowered by two interconnected effects. First, the air gaps lower the reactor flux in the loop vicinity due to neutron streaming through these passages, and second, fission neutrons generated in the fuel container are poorly reflected and moderated by surrounding material because of the high percentage of nearby void space.

Only the second of these effects has been studied here, but the results indicate that a substantial improvement in power density is possible if the voids are replaced by moderator material. A simple geometrical model was used to represent the actual situation; namely, the fuel container was assumed to be cylindrical and surrounded in the radial direction by a $\frac{1}{2}$-in. air gap. The flux at the fuel-container face in contact with the reactor was assumed to be constant, with the ratio of the fast to slow fluxes used as a parameter.

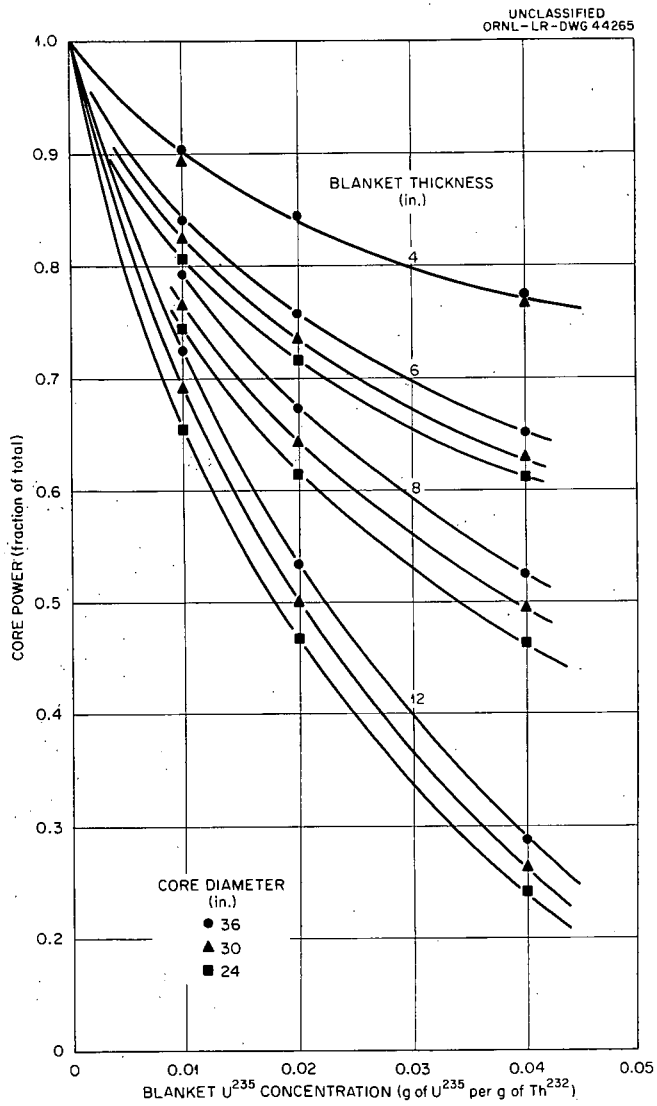

Fig. 7.4. Fraction of Total Reactor Power Generated in the Core vs U^{235}/Th^{232} Ratio for Various Core Diameters and Blanket Thicknesses at a Moderator Composition of 60% D_2O.

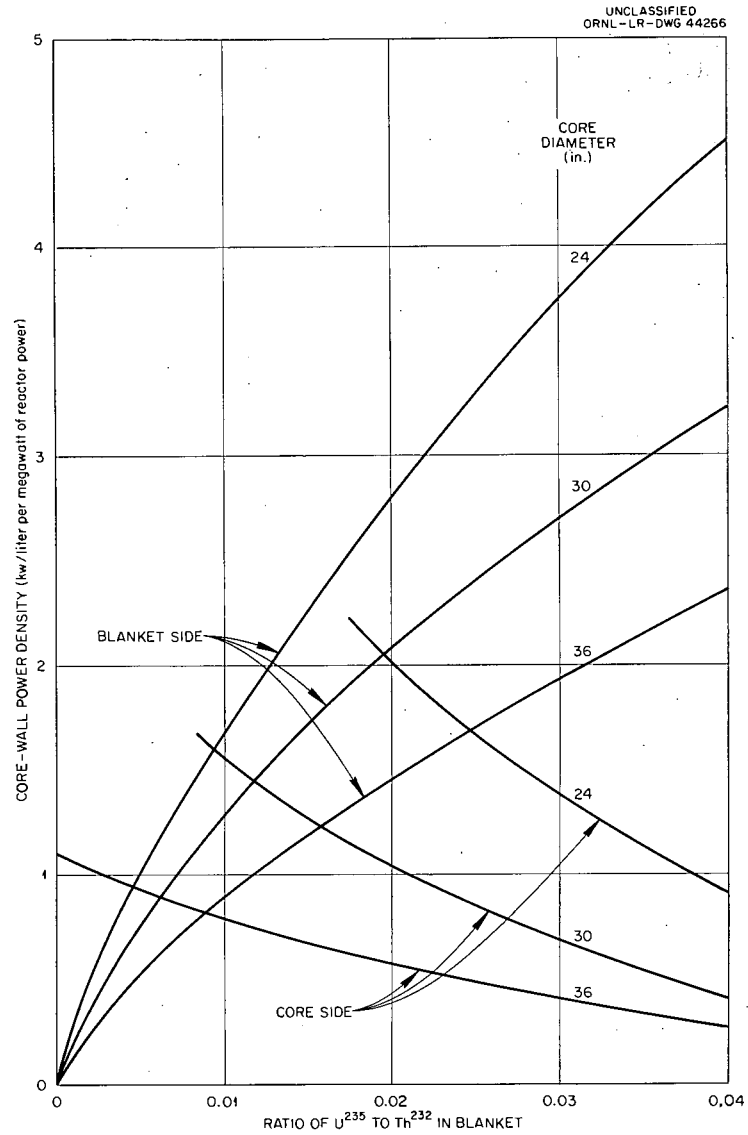

Fig. 7.5. Power Densities at the Core Wall vs Ratio of U^{235}/Th^{232} in the Blanket for Various Core Diameters. (Blanket thickness, 12 in.; moderator, 60% D_2O.)

The nuclear calculations were two-group diffusion calculations, which were handled in two ways and gave results in good agreement. The first method assumed that the effect of the $\frac{1}{2}$-in. gap around the fuel container was the same as if the void were homogeneously dispersed in the fuel solution. The second way likewise dispersed the void throughout the fuel solution, but included the geometry effects as well as the dilution effects of the void by the methods of Behrens.[2] In addition, the effects of placing a graphite or beryllium reflector 6 in. thick at the cylinder face away from the reactor were computed. The results are shown in Fig. 7.6. It is seen that the average power density per unit thermal flux at the reactor face varied linearly with the fast-to-thermal flux ratio. This ratio is in the neighborhood of 2 for the ORR but varies with the reactor core configuration and is quite variable with position as well. The equivalent void fraction in the present case was about 40%; good agreement was found between the results from Behren's theory and those from the simple dilution method. The best reflector from the standpoint of power improvement was beryllium; however, the heat generation rate from capture gammas would be about 10 times that in graphite and would be about 0.13 kw.

The question of whether any benefit may be obtained from surrounding the loop with heavy water instead of light water (as at present) has also been examined. Again on the basis of a simplified physical model of the actual situation, the variation of power per unit thermal flux was determined as a function of fast-to-slow flux ratio at the reactor face. Figure 7.7 gives the results of the calculations; light water is seen to be superior at high values of the fast-to-slow flux ratio, while heavy water is better at low values. Near a ratio of 2, the in-pile loop powers obtainable are quite close. For reasonable flux ratios, no great advantage in loop power appears to be associated with the use of heavy water.

REFERENCES

1. M. C. Edlund and L. C. Noderer, An Harmonics Method Applied to D_2O Moderated Reactors, ORNL CF-54-3-120.

2. D. J. Behrens, The Effect of Holes in a Reacting Material on the Passage of Neutrons, with Special Reference to the Critical Dimensions of a Reactor, AERE-T/R-103, 1958.

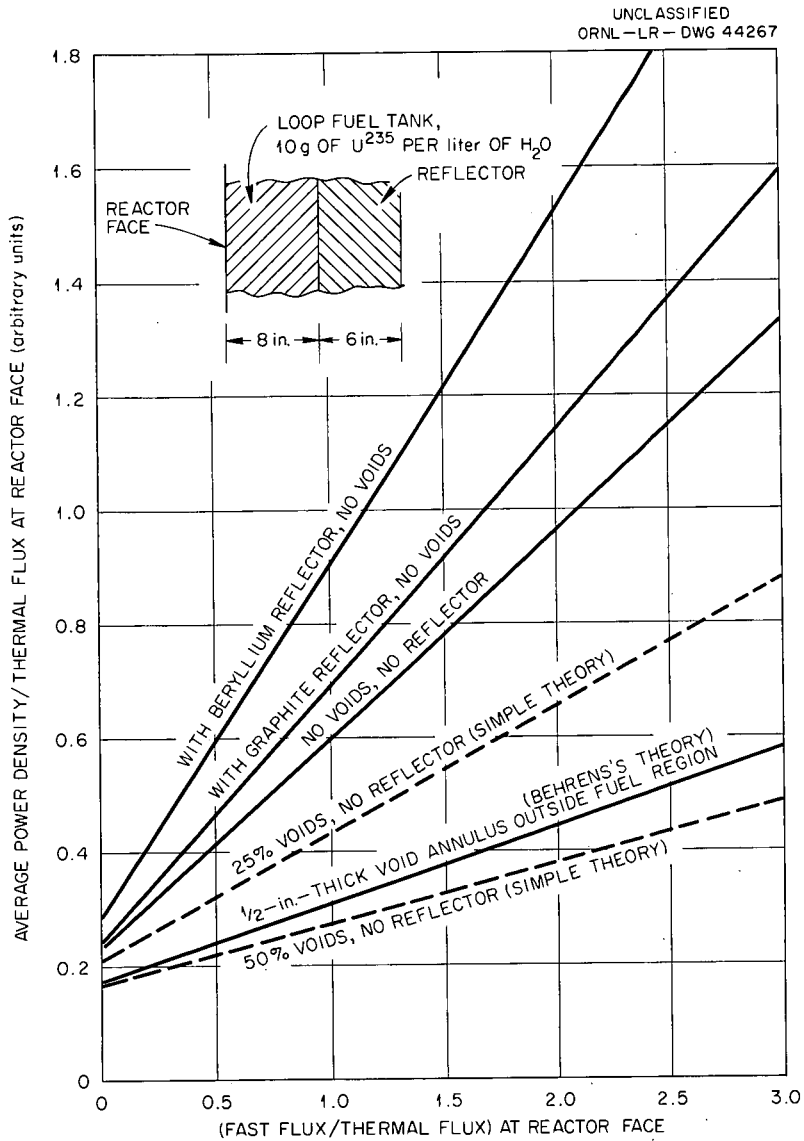

Fig. 7.6. Effect of Voids and End Reflector on the Relative Power Density in ORR In-Pile Loops.

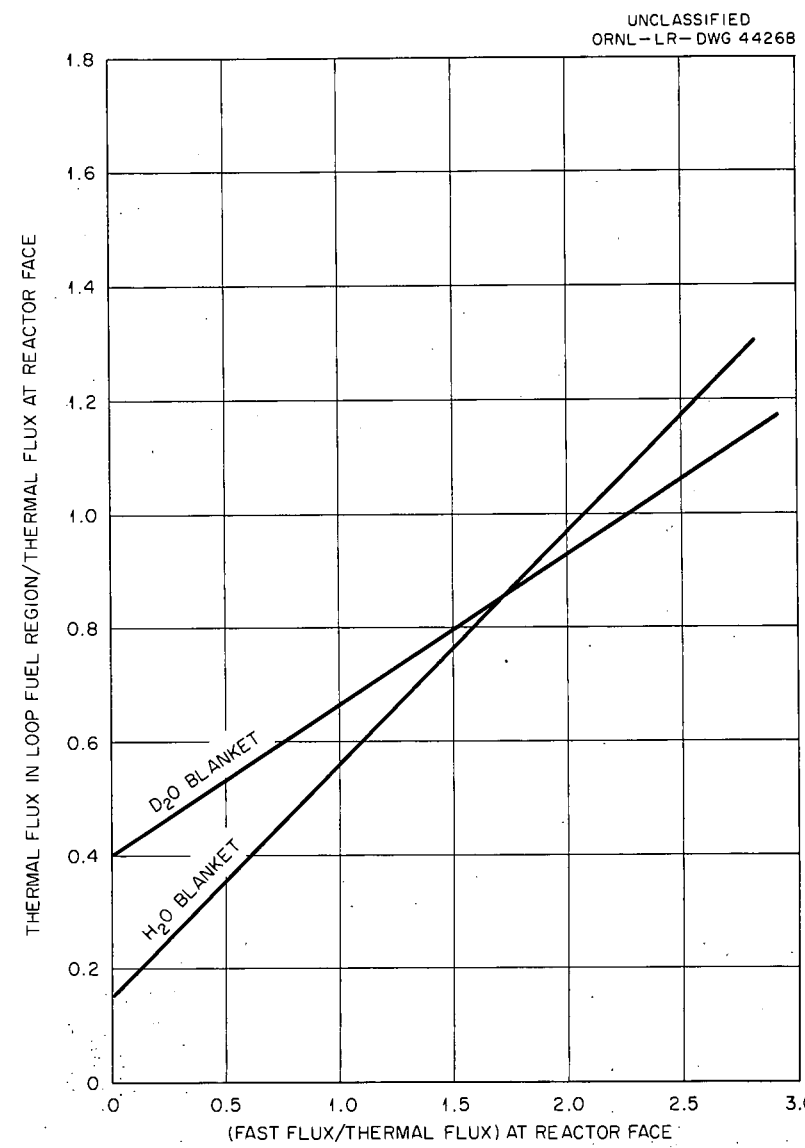

Fig. 7.7. Effect of Moderator Composition in Region Adjacent to Loop on Thermal Flux in Loop Fuel Region.

8. DEVELOPMENT OF FUEL- AND SLURRY-SYSTEM COMPONENTS

I. Spiewak F. N. Peebles

C. H. Gabbard C. G. Lawson H. R. Payne
B. A. Hannaford J. C. Moyers M. Richardson
E. C. Hise R. P. Wichner

8.1 HIGH-PRESSURE RECOMBINER LOOP

A natural-circulation, high-pressure catalytic recombiner has been tested to determine the feasibility of eliminating continuous letdown of radiolytic gases in future homogeneous reactors. Routine operation proceeded during the report period for 1000 hr at 1500 psi and an average stoichiometric gas input of 0.6 scfm. The test was then terminated after 2500 hr of successful operation. No further operation of this loop is planned at this time.

8.2 CENTRIFUGAL PUMPS

8.2.1 20-cfm Allis-Chalmers Blower

A test to evaluate the 20-cfm canned-motor blower for pumping a steam-gas mixture at 225°C and 1500 psi was terminated after 1228 hr by an electrical failure in the blower motor. Investigation revealed that cooling water had entered the stator-winding cavity, evidently from a leak in the stator cooling coil. The primary high-pressure system remained intact.

Total operating time accumulated by the blower prior to the failure was 10,744 hr, including 8730 hr at elevated temperature and pressure. It is believed that these tests demonstrate the feasibility of the canned-motor blower for high-temperature gas circulation. The additional development required to reduce the heat losses to the blower motor will not be carried out at the present time.

8.2.2 Reliance 6000-gpm Pump

Termination of the contract for the Reliance 6000-gpm pump was reported previously.[1] A report was issued covering the design of the pump and the problems which require further investigation.[2]

The insulation-test stator in the Co-60 source has received approximately 5.4×10^9 rad. Although there is a marked increase in leakage current at voltages above 1600, the leakage current at operating voltages has decreased slightly from the original value.

8.2.3 300A Slurry Pump and Loop

Runs with the 300A slurry pump were continued to test improved designs of pump parts. During run 300A-8 (ref. 3) the pump was operated for 2862 hr at 280°C and 1500 psi, with an average slurry concentration of approximately 450 g of Th per kg of H_2O. Attack on the titanium impeller was very slight, and no measurable wear of any of the aluminum oxide bearings occurred. A longitudinal, full-length crack was found in the lower journal, evidently caused by the inability of the conical mounting system to compensate for the differential thermal expansion.

A test of the pump with bearings having flame-plated aluminum oxide wear surfaces had to be terminated after 48 hr of operation with water at 280°C and 1500 psig. Inspection revealed that the flame-plated aluminum oxide coating had failed on the lower journal and bearing. There seems to be insufficient bond strength between the coating and the stainless steel base metal for this application.

The pump was reassembled with the cone-mounted bearings and a nitrided-titanium floating-bushing shaft seal, and was operated for 410 hr with water at 280°C and 1500 psi. Subsequent disassembly and inspection revealed no wear of the nitrided-titanium seal parts.

A stainless steel 300-gpm impeller, of standard design except for four of the seven vanes having modified exit angles, was installed, and the pump was operated for 329 hr in slurry containing 1000 g of Th per kg of H_2O. The slurry was a long-digested 800°C-fired oxide which had been shown to produce high impeller attack rates in other loops. Inspection after the run revealed an impeller weight loss of approximately 41 g. It appeared that the attack on the modified vane exits was slightly less severe than on the standard vanes. No wear was detected on the bearings or the shaft seal. However, both bearing journals were slightly loose on their mounts.

A new set of hydraulic parts for the 300A pump was designed and fabricated. The following features were designed into the impeller in an attempt to reduce slurry damage of the lower wear ring and on the vane inlet edge:

1. lower shroud ribs to give zero pressure differential across the suction wear ring at rated capacity,

2. smoothly contoured flow passages and a smooth transition from the axial flow direction to the radial direction,

3. a constant angle of attack across the inlet edge,

4. convergent flow passages to prevent flow separation.

Testing of the new hydraulic end will be started soon.

8.2.4 200Z Slurry Pump and Loop

Repair of the 200Z pump stator was completed, and the pump was performance-tested while circulating water with the standard diffuser and with a vaneless diffuser. The vaneless design gave slightly greater head and efficiency, and it should be very erosion-resistant. A test will be carried out to observe the extent of slurry attack on the diffuser surface and the suction wear ring.

8.2.5 Test Program for Slurry-Pump Bearings

The bearing test program with the Franklin Institute to investigate hydrodynamic-bearing performance with thoria slurry was terminated because of the lack of funds. No actual bearing tests were made, but the bearing test machine was completed and will be shipped to ORNL. The test program will be resumed at a later date.

The mechanically mounted aluminum oxide bearings in the 300A pump have operated satisfactorily for approximately 3300 hr with no measurable wear despite the longitudinal crack and the loosening of the journals. A new mounting system, which will load the journals in compression at all times, has been designed, and its parts are on order.

8.3 FEED PUMPS

8.3.1 Oxygen Compressors[4]

Development work and testing were continued on oxygen compressors for feeding cylinder oxygen to high-pressure systems, and for recycling oxygen from low- to high-pressure systems.

The Pressure Products Industries single-stage diaphragm compressor with the Scott & Williams P1 drive unit has performed satisfactorily in the HRT mockup. The diaphragm, in intermittent service, operated 448 hr during the report period. On two occasions the compressor was used at the HRT to provide 3000-psi oxygen for pre-operational leak testing.

The Pressure Products Industries three-stage contaminated-service oxygen compressor operated approximately 400 hr during the report period. A 0.019-in. stainless steel third-stage diaphragm cracked at a dent after 210 hr. The compressor has now operated continuously for 160 hr with a 0.016-in., 1/8-hard, type 302 stainless steel third-stage diaphragm.

8.3.2 Increased-Capacity Solution Pumps

The double-diaphragm 10-3/4-in. head and the single-diaphragm 12-in. head have continued on test for 10,870 and 6,248 hr, respectively, at an average of 60 strokes/min. Endurance testing of these heads will be continued, but no new development work is believed to be required for feed pumps of this type. Experimental and analytical information is available which permits confident design of units over a wide range of output.[5]

8.3.3 Slurry Feed Pumps

The remote-leg and the single-contour diaphragm pumps were disassembled after pumping to 1500 psi for 6200 hr various 1600°C-fired thoria slurries of specific gravities of 1.5 to 2.1. Neither diaphragm had failed. Some solids had entered the remote-leg head, which is protected by a vertical settling leg and 20-μ screening, and had dented and eroded the diaphragm. No effort was made to keep solids out of the single-contour head; however, its diaphragm was completely undamaged (see Fig. 8.1). Either head appears to be a satisfactory device for injecting slurries into a high-pressure system, although the single-contour head is expected to have somewhat longer life.

UNCLASSIFIED
PHOTO 34822

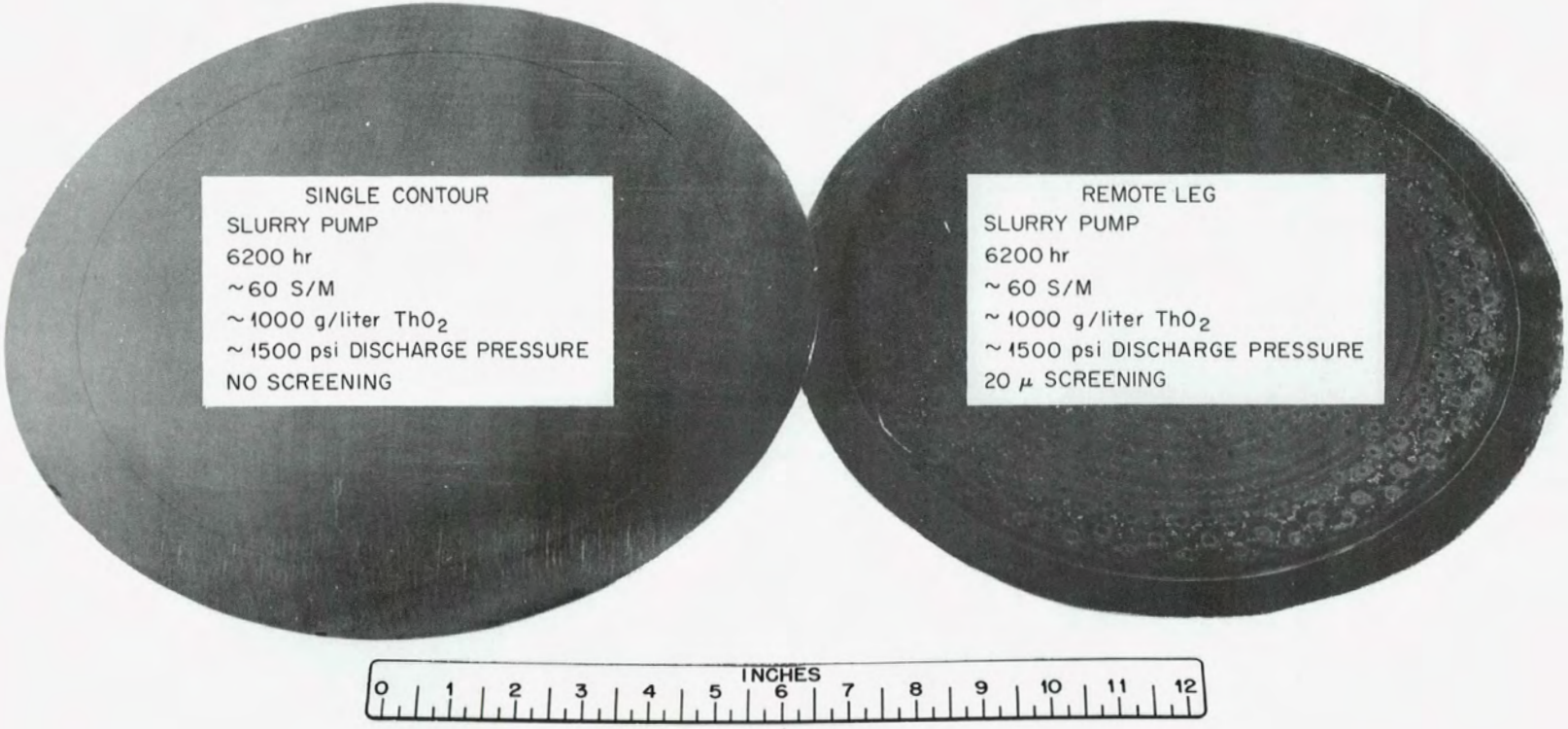

Fig. 8.1. Stainless Steel Diaphragms After Slurry Feed-Pump Test.

The duplex, single-contour feed-pump unit furnished to the 300-SM loop has been successfully operated to fill, concentrate, and dilute the high-pressure system.

8.4 SLURRY LOW-PRESSURE SYSTEM

The slurry feed-pump test loop was modified to eliminate the small circulating pump that was being used to agitate the supply tank and provide a positive suction head to the feed pump. Previously reported difficulty[6] with slurry settling in a 3/4-in. horizontal feed-pump line was overcome by using closely coupled, inclined suction lines, illustrated in Fig. 8.2.

The loop has since operated for over 2000 hr with no difficulties attributable to the supply tank or suction lines. The pump restarted readily after settling periods as long as 24 hr. Static pressurization of the tank was varied from 0 to 40 psig. The pump output increased with suction head up to 20 psig, and then remained constant.

To study further the requirements of a slurry low-pressure system, a larger feed-pump loop was constructed. The loop consists principally of two vertical, cylindrical tanks 2 ft in diameter by 6 ft high and a duplex feed pump. The supply tank has three steam jackets for agitation and/or pressurization by boiling. The feed-pump suction line is inclined at a 45° angle running upward from the bottom center of the tank out through the wall. Various configurations of poison rods or baffles can be inserted in the supply tank to determine their effect upon agitation and transport. A condenser can be connected to determine limitations on the slurry concentration which can be handled. The initial test is to determine the practicality of operating the 300-SM low-pressure system[7] without a transfer pump.

8.5 VALVE TRIM

8.5.1 Dump-Valve Trim for Solutions

A report[8] was issued which describes the testing program and the operational experience with solution dump valves in the HRT.

8.5.2 Slurry Valves

H.P. Alundum 687 balls and seats made by Norton Laboratories, Inc., operated for 804 hr in the slurry check-valve-material test. The seats failed by cracking apparently as a result of an experimental mounting technique. A replacement set of balls and suction seat of the same material, and a discharge seat of Alsimag 614, have now operated 2100 hr and are still pumping satisfactorily.

A set of check-valve trim of American Lava Corp. Alsimag 576 balls and Thermal Refractories Co. 99% purity Alox seats were operated for 3200 hr in the slurry feed-pump test loop. This trim was examined[9] after 1135 hr and returned to operation. At the end of 3200 hr the balls had lost an average of 0.004 in. in diameter. Several of the seats had failed completely by fracture, and the others had suffered considerable widening of the seating area and mild-to-severe channeling. An improved mounting, which is ready for testing, supports and confines the ceramic completely, and should reduce the number of mechanical failures.

UNCLASSIFIED
ORNL-LR-DWG 44269

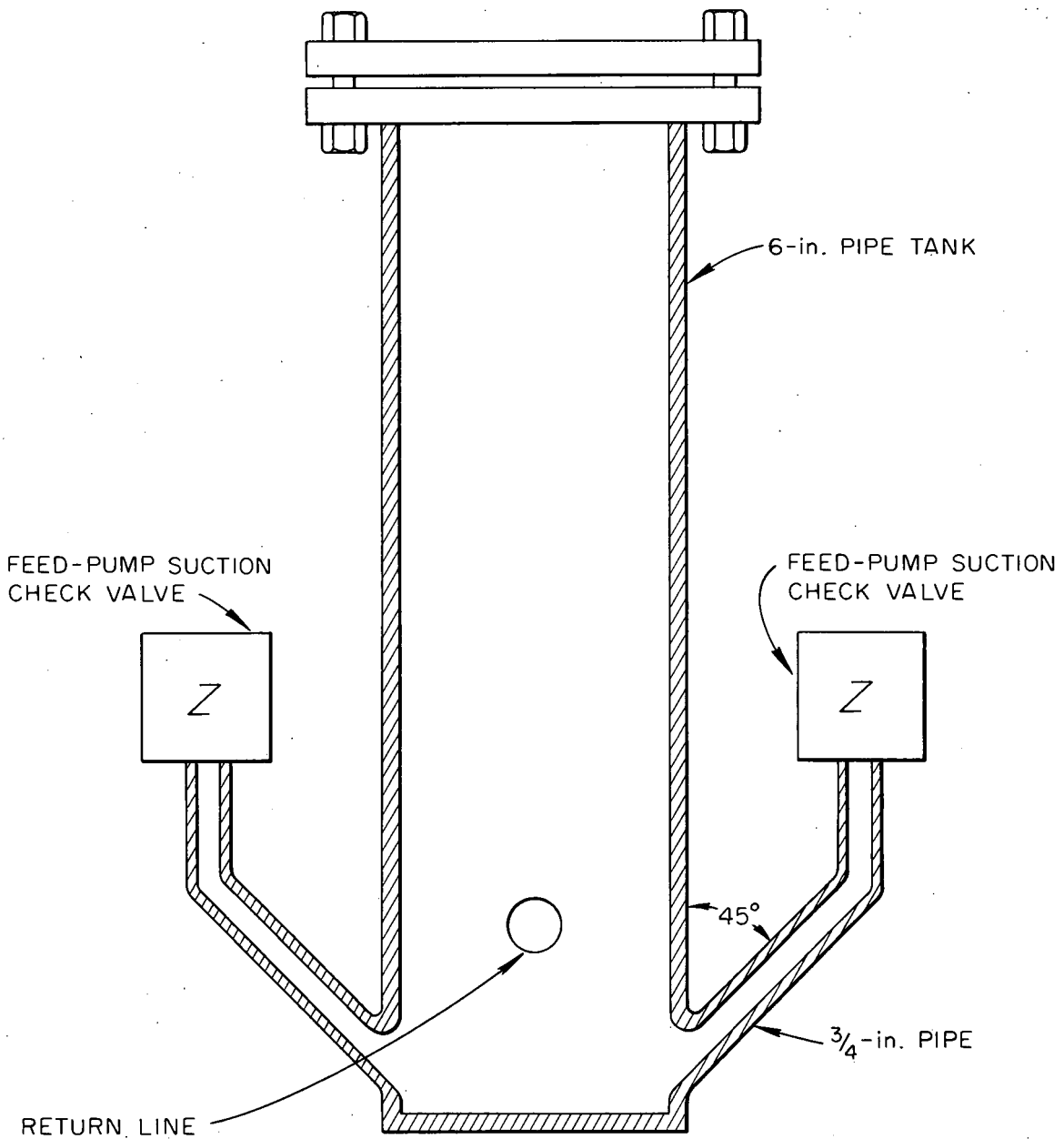

Fig. 8.2. Slurry Feed-Pump Supply Tank and Suction Line.

8.5.3 Slurry Letdown Chokes

Both the 0.063-in.-ID and the 0.125-in.-ID tubes are still intact after respective service periods of 8656 hr at 40 fps and 5298 hr at 25 fps.

8.6 HEAT EXCHANGER TEST FACILITY

The design of the heat exchanger test facility (shown schematically in Fig. 8.3) was completed; fabrication of the primary loop is approximately 80% complete. The remaining work is being delayed until the steam-generator units and the condenser are completed by Griscom-Russell.

The carbon-steel steam-side components of the steam generators and condenser were completed. The fabrication of the tube bundles and the main-flange transition-joint welds are required to complete the units. All the tubing was received and tube-joint weld development was completed. The tube-joint weld samples were submitted for metallographic examination. Final approval for construction will be made if the results of the pending examination are satisfactory.

Both types of composite tubing (carbon steel - stainless steel and Inconel - stainless steel) were accepted from the vendor, following ultrasonic tests which indicated conformance to minimum standards.

8.7 CORE AND BLANKET DEVELOPMENT

The problem of controlling temperatures in the core and blanket of aqueous homogeneous reactors is an important one. Excessive temperatures at the core-tank wall can lead to excessive corrosion rates, while excessive temperatures in the fuel solution can lead to chemical instability. At the present time the core hydrodynamics program includes investigation of geometrical configurations which may be useful in commercial reactors, and particularly an attempt is being made to develop experimental and analytical methods which will be used to prove the attainment of a feasible design.

8.7.1 Re-entrant Core Model

A correlation of heat transfer coefficients existing between the core fluid and the core wall in a polar-entry concentric-annular-exit sphere was presented previously.[10] Additional experiments were completed in which the detailed velocity distribution of the fluid adjacent to the core wall was measured. From such measurements it is possible (1) to perform an independent evaluation of the heat transfer correlation, (2) to calculate the temperature rise of the core wall above stream temperature due to the fluid volume heat source, (3) to calculate the wall shear stress, (4) to determine whether the bulk flow rate is increasing or decreasing with position along the wall, and (5) to detect regions of flow separation.

The dimensions of the particular model tested are shown in Fig. 8.4. A typical velocity profile near the wall is shown in Fig. 8.5. The data are in excellent agreement with the universal velocity law.[11] The distance from the wall to the position of maximum velocity varied from 1/4 in. to 3/8 in., and the ratio of average to peak velocity was about 0.9 in all cases. The ratio of maximum boundary velocity to inlet jet velocity varied from 0.25 near the jet impingement area to 0.11 near the outlet.

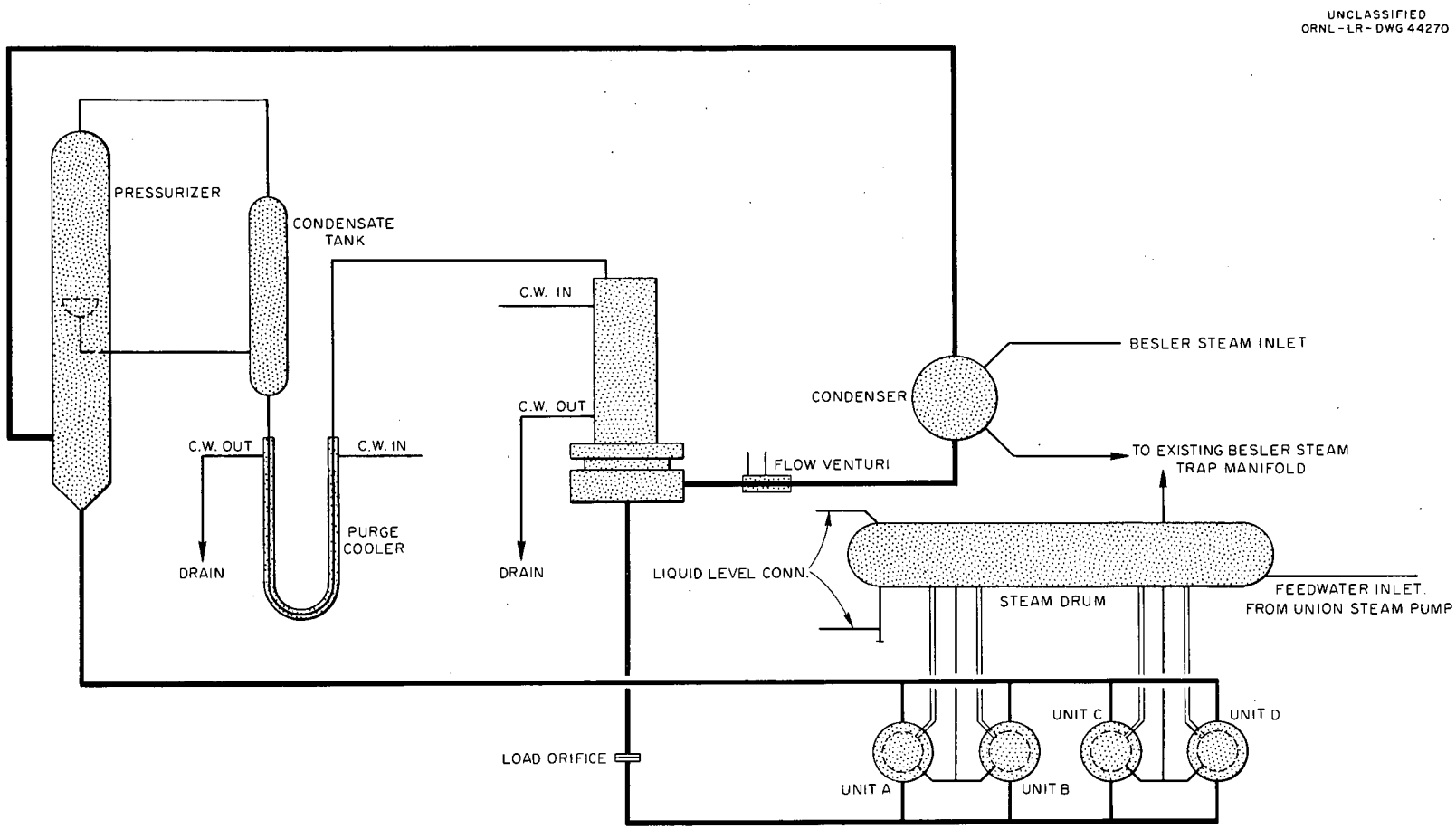

Fig. 8.3. Flow Diagram for Heat Exchanger Test Loop.

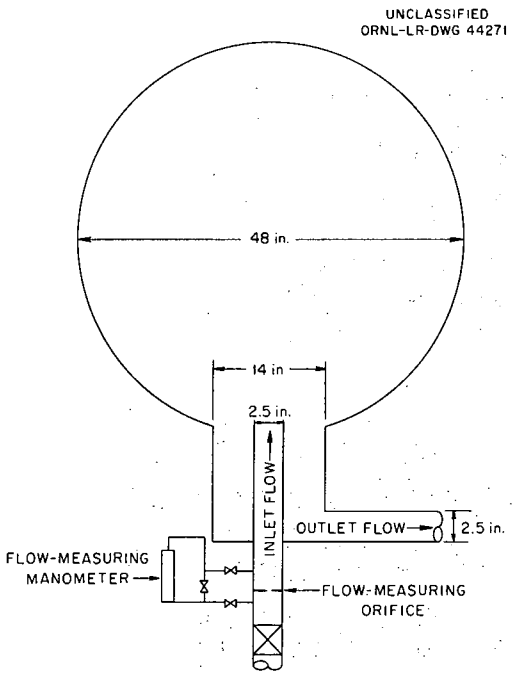

Fig. 8.4. The 48-in. Polar Re-entrant Core Model.

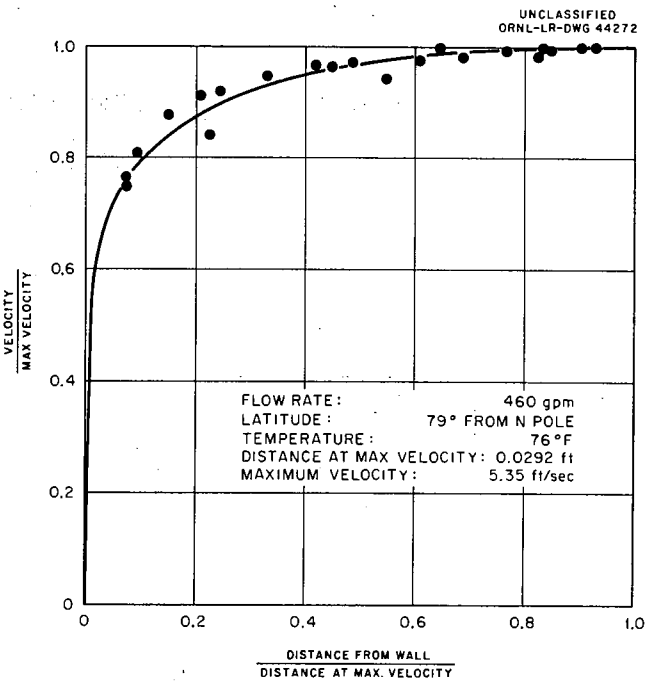

Fig. 8.5. Velocity Profile in the Boundary Layer of the 48-in. Polar Re-entrant Core Model.

Heat transfer coefficients were calculated from the Colburn equation,[12] using the measured average velocity in an equivalent parallel-plate geometry. Corrections for entrance effects were made by the method of Aladyev[13] to experimentally measured heat transfer coefficients from the model; these were within 15% of the predictions from the Colburn equation. Agreement between the present predictions and the earlier heat transfer correlation was within 30%.

No regions of flow separation of fluid from the wall were found by these measurements. The flow rate within the region between the surface of maximum velocity and the wall was found to decrease as the fluid moved around the wall.

Further work on this type of core will be discontinued since the core wall tends to approach the outlet temperature of the reactor. At these temperatures the corrosion rates of Zircaloy would be about 50 mpy and therefore too high for economic reactors.

8.7.2 Cylindrical Core with Swirling Flow

The need of power densities in the range of 100 kw/liter requires that the core wall be maintained at some temperature near the core inlet temperature in order to limit the corrosion rate to an acceptable level. One method for accomplishing this has been proposed wherein the stabilizing influence of a swirl in a cylindrical geometry is used to keep the cooler fluid flowing near the wall. The fluid is introduced through swirl-promoting vanes at the periphery in the top of the vessel, flows downward along the wall, turns around at the bottom of the vessel, and is removed through a pipe centered at the top of the vessel.

A 5-in.-dia model employing this principle has been set up for flow visualization studies, to develop a vessel configuration for more intensive study. The model has 45° angle swirl-generator vanes located in an annulus 3/8 in. thick. It was found that the vanes must impart a radial outward component of flow in order to prevent fluid from short-circuiting the core. The residence time of fluid in the bottom of the core is higher than in the major portion of the vessel. The higher residence time may be caused by recirculation of fluid near the turn-around point. Different configurations of turn-around are being tried in an attempt to decrease the residence time of the fluid at the bottom of the vessel.

8.7.3 Reactor-Vessel Design

Work was started on the mechanical design of a reactor vessel for a 380-Mw(th) two-region breeder reactor. The preliminary design has the following features: (1) 4 ft x 12 ft re-entrant cylindrical core tank similar to that described in Sec. 8.7.2, (2) provision for internal core-wall cooling, and (3) a removable core tank.

Preliminary calculations indicate that the core wall on the fuel side can be maintained below 260°C by using a counterflow cooling-water system of 200 gpm and an inlet temperature of 186°C. The flow rate was selected to give a coolant temperature equal to the fuel inlet temperature at the transition joint between the core tank and pressure vessel, which reduces the thermal-expansion problem in the transition joint. The temperatures stated above are achieved in a core wall consisting of two 1/4-in.-thick Zircaloy plates separated by a 1/8-in. coolant gap. A double transition-joint between the stainless steel piping and the vessel is being designed, using laminated cylindrical gaskets similar to those used in the HRT.[14] The double joint is required by the double-walled core vessel.

Calculations are in progress to determine the thermal stresses in the pressure vessel, and to design a thermal shield if necessary.

8.7.4 Spherical Annular Re-entrant Core

The spherical annular re-entrant core[15] is closely related to the cylindrical core described above, except that less rotation of the inlet fluid is needed to achieve a stable flow pattern. Several small two- and three-dimensional models of this type were operated to determine how to ensure that the entire wall is covered by a stable boundary layer, how to eliminate local regions having high residence time, and how to minimize the entrainment of interior core fluid into the boundary stream.

Qualitative observations made of the two-dimensional models with a birefringent fluid suggested that high inlet velocity and low average residence time were desirable. A typical observation is illustrated in Fig. 8.6, which shows the presence of a relatively less turbulent "doldrum" region.

Several small three-dimensional models were tested which were constructed from glass and consequently of unknown dimensional tolerances. No irrotational model demonstrated a desirable flow pattern. A satisfactory flow pattern was achieved in a model with 30° (with the vertical) inlet fluid rotation when the mean residence time was reduced to 1 to 2 sec.

8.7.5 Slurry Core Vessel

The 30-in. slurry core vessel[16] was operated at concentrations between 150 and 1000 g of Th per kg of H_2O and temperatures between 25 and 80°C, to determine in what flow situations and in what manner the slurry core vessel begins to malfunction. The following characteristics were used to determine malfunction: (1) slurry nonuniformity as determined by core samplers, (2) low or erratic local wall heat transfer coefficients, (3) visual observation of gross ThO_2 dropout, and (4) very slow moving or immobile slurry in the core interior as detected by a heated thermocouple probe.

At 1000 g of Th per kg of H_2O, malfunction was first noted at 100 gpm, independent of temperature, because of irregular and low heat transfer coefficients on the conical wall. The concentration at this time appeared to be uniform to within 0.6%. As the flow rate was lowered to 56 gpm at 80°C and to 38 gpm at 30°C, instability was apparent at the upper viewing ports, and was confirmed by sampling. When the flow rate was further lowered to 32 gpm at 80°C or to 22 gpm at 30°C, gross dropout was visible. The heated thermocouple indicated quiescent slurry in a toroidal region at those conditions.

At 500 g of Th per kg of H_2O the first malfunction, sample nonuniformity, was observed at 60 gpm. Gross dropout was noted at about half that flow. At 150 g of Th per kg of H_2O nonuniformity was very evident at 76 gpm.

It is concluded from this investigation that adequate suspension of slurry is achievable in this design at the rated 300-gpm flow over the concentration range tested.

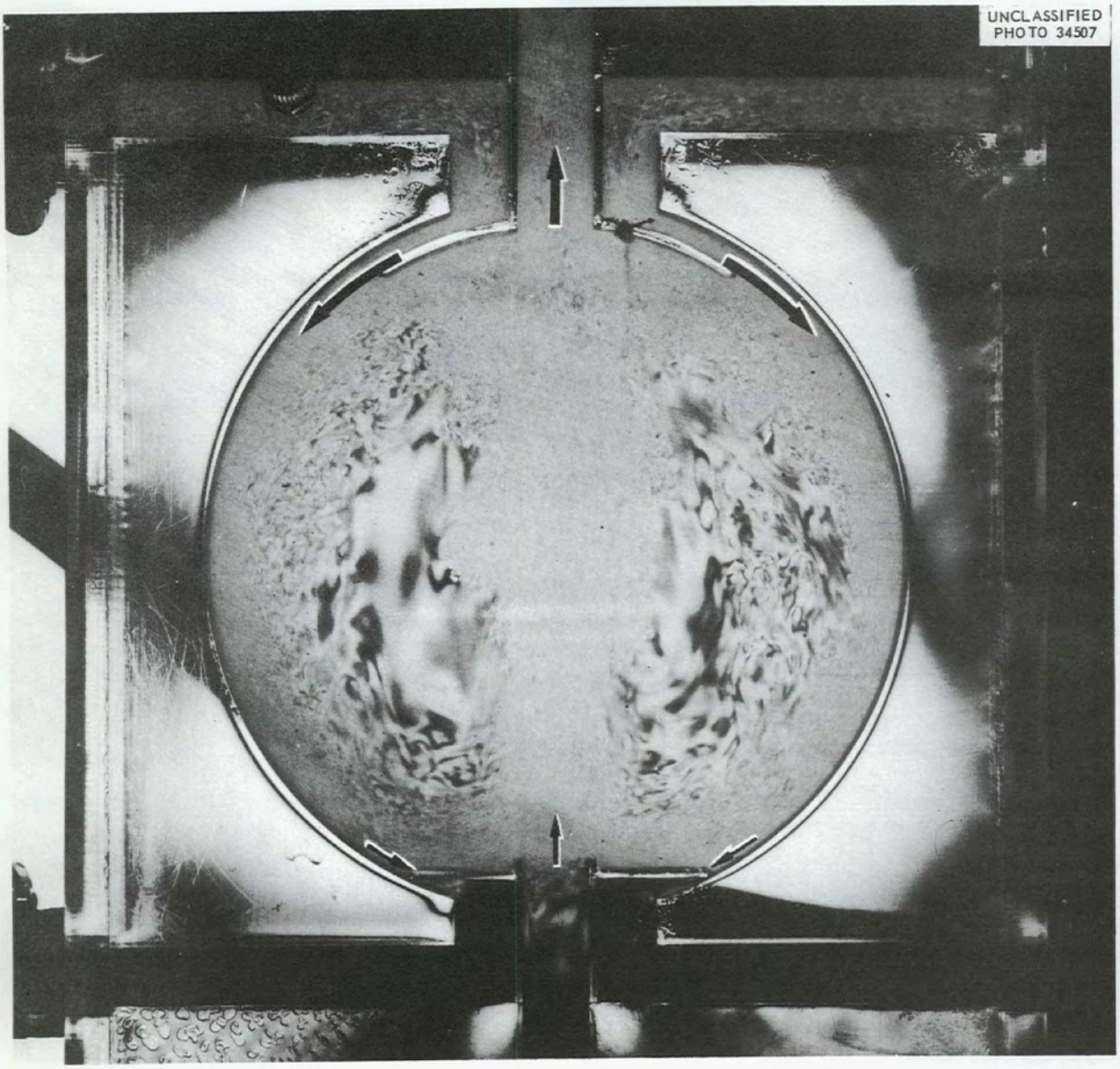

Fig. 8.6. Two-Dimensional Model of Annular Re-entrant Core.

REFERENCES

1. I. Spiewak et al., HRP Quar. Prog. Rep. April 30, 1959, ORNL-2743, p 73.

2. J. C. Moyers, Summary Report of 6000 gpm Reactor-Prototype Circulating Pump Contract with Reliance Electric and Engineering Company, ORNL CF-59-8-49, (Aug. 3, 1959).

3. J. C. Moyers, Run 300A-8, Initial Slurry Run of 300A Pump and Loop, ORNL CF-59-7-35 (July 2, 1959).

4. E. C. Hise, Interim Report of Development of Contaminated Oxygen Compressors for Aqueous Homogeneous Reactors, ORNL CF-59-9-109 (Sept. 29, 1959).

5. E. C. Hise, Design, Development and Operation of Metal-Diaphragm Reactor Service Pumps, ORNL-2841 (to be published)

6. I. Spiewak et al., HRP Quar. Prog. Rep. April 30, 1959, ORNL-2743, p 76.

7. Refer to Chap. 9 of this report.

8. E. C. Hise, Testing of Dump Valve Trim in the Valve Test Loop and the Performance of Dump Valves in the HRT, ORNL CF-59-8-86 (Aug. 3, 1959).

9. I. Spiewak et al., HRP Quar. Prog. Rep. April 30, 1959, ORNL-2743, p 76.

10. I. Spiewak et al., HRP Quar. Prog. Rep. Oct. 31, 1959, ORNL-2654, p 87.

11. H. Schlichting, Boundary Layer Theory, Chap. 20, p 400, McGraw-Hill, New York.

12. A. P. Colburn, Trans. Am. Inst. Chem. Eng., 29, pp 174-210 (1933).

13. I. T. Aladyev, Experimental Determination of Mean and Local Coefficients of Heat Transfer for Turbulent Flow in Pipes, NACA TM 1356 (translation).

14. J. A. Lane, H. G. MacPherson and F. Maslin, Eds., Fluid Fuel Reactors, p 432, Addison-Wesley, Reading, Mass., 1958.

15. I. Spiewak et al., HRP Quar. Prog. Rep. April 30, 1959, ORNL-2743, p 30.

16. Ibid., p 77.

9. DEVELOPMENT OF REACTOR SLURRY SYSTEMS

I. Spiewak
D. M. Eissenberg
P. H. Harley
R. J. Kedl
L. F. Parsly
F. N. Peebles
H. B. Piper
M. Richardson
A. N. Smith
R. Van Winkle

9.1 CIRCULATING-SLURRY EXPERIMENTS

The 200A and 200B slurry loops are operated to investigate the high-temperature engineering properties of thoria slurries and to provide a basis for improving the specifications for oxide production and for slurry-handling components. Important characteristics being studied include rheology, long-term oxide stability, attack rate on components, heat-transfer coefficients and settling.

9.1.1 200A-Loop Operation

Run 20A was primarily a performance test of one of the new 50-gpm, 15-hp Byron Jackson liner motor pumps and secondarily a test of an 800°C-fired, long-digested thoria, with a mean particle size of 1.8 μ. The oxide was potentially of interest as a cheap substitute for 1600°C-fired material. The average flow rate was 88 gpm, equivalent to 5 fps in the 3-in. pipe; concentration was 625 g of ThO_2 per liter. The run was terminated after 264 hr at 300°C and 30 hr at 225°C. Operation of the pump was judged to be satisfactory with respect to capacity and durability, within the limited scope of the test.

During run 20A a concentration gradient was noted in the piping while operating at 300°C. Samples drawn from the top of the horizontal 3-in. pipe were much lower in concentration than samples drawn from the bottom of the pipe at the same cross-section. The ratio of top to bottom concentration was as low as 0.5 in some cases. The effect appeared to be more pronounced as distance from the pump discharge increased. The existence of a top-to-bottom gradient was confirmed by the use of a gamma-ray densitometer. The concentration gradient could not be noted when the loop was operating at 225°C.

It is not known whether the dropout occurs with most slurries at these particular loop conditions; this will be determined in future runs.

The corrosion-erosion rate during run 20A was 4 mpy, as determined by chemical analysis of the slurry. Thirty per cent of the total pickup of corrosion products came from the impeller. The mean particle size of the oxide decreased from 1.8 to 1.3 μ during the run. The slurry tested was judged

inferior to 1600°C-fired oxides, from the standpoints of erosion and degradation.

During the latter part of the report period, the loop was shut down to permit some changes, including installation of a hydroclone system. This system will be tested as a means of charging and withdrawing slurry during startups and shutdowns, and also for the adjustment of oxide concentration as may be required for the performance of various tests. Additional gamma-densitometer equipment was installed for slurry dropout tests, which are to be run at various velocities, temperatures, and oxide concentrations. The 200A pump was re-installed in the loop and the system subjected to a hydrostatic test.

9.1.2 200B-Loop Operation

The 200B loop was operated for 915 hr during the report period. The purpose of the run, 3B, was to obtain high-temperature rheological measurements by using the capillary-tube viscometer sampler and to study the heat transfer and scale-forming characteristics of a mixed-oxide slurry (8% uranium) by using a cooled copper disk. The loop concentration ranged from 280 to 1080 g of Th-U per kg of H_2O, and the operating temperature was varied from 100 to 280°C. Average particle size was 2.2 μ. The attack rate, as has been observed before with mixed oxides[1] was low (less than 1 mpy), and there was no measurable particle degradation.

9.1.3 200B Heat-Transfer and Viscometry Data

The heat-transfer coefficients measured from the copper-disk heat meter[2] indicated evidence of buildup of cake during the run, on three occasions. The coefficients obtained when there was no cake continued to be higher than those usually predicted for non-Newtonian slurries[3] and close to those observed for water.

The first indication of cake buildup occurred shortly after startup. The charge consisted of a mixture containing both fresh and previously pumped oxide; the concentration was approximately 280 g of Th-U per kg of H_2O; and the loop temperature varied between 230 and 250°C. The measured heat-transfer coefficient dropped by a factor of 3 during the first 250 hr and then returned to its original value of 6000 Btu/hr·ft^2·°F in the next 75 hr. The coefficient remained steady for the next 400 hr of operation at 250 to 280°C. The heat meter was examined at that time and found to be free of cake.

The concentration of the loop was increased to about 820 g of Th-U per kg of H_2O by addition of fresh oxide, and the loop was brought to 270 to 275°C. There was a gradual decrease in heat-transfer coefficients; however, the loop was shut down temporarily as the result of a sampler leak.

Upon startup, the loop concentration was increased to 1250 g of Th-U per kg of H_2O by addition of a fresh urania-thoria mixture, and the loop was brought to 200 to 280°C. The initial heat-transfer coefficient was again approximately 6000 Btu/hr·ft^2·°F. This was followed by a sharp decrease in coefficient and the loop was shut down by stopping the pump and then cooling gradually, at a time when the coefficient had dropped to 500 Btu/hr·ft^2·°F.

Examination of the disk revealed a soft cake covering the entire exposed surface of the disk (Fig. 9.1). Its density was 5.1 g/cm^3 after drying, and its thickness varied from 0.012 in. at the upstream edge to 0.025 in. at the

UNCLASSIFIED
PHOTO 35042

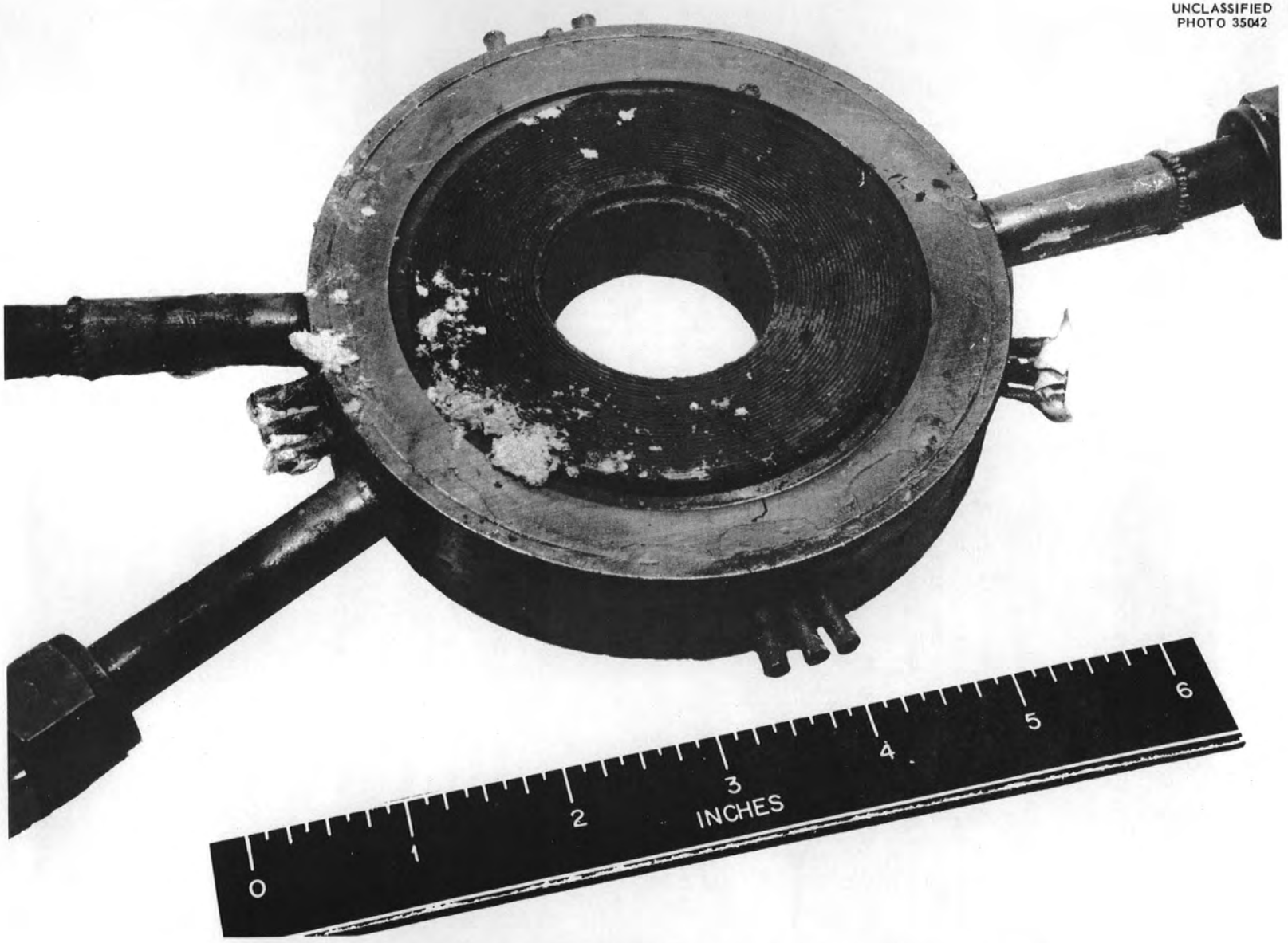

Fig. 9.1. Copper-Disk Heat Meter, Showing Part of a Slurry Cake on the Inside Surface.

downstream end of the disk. The cake contained substantially more fines and more uranium than the circulating slurry.

Examination of the interior of the loop, upstream and downstream of the disk, revealed no evidence of cake. The pipe-line velocity at the disk was approximately 15 fps.

Several runs were made with the capillary-tube viscometer at high temperature and pressure. The observations are reported in Table 9.1; the indicated yield stress is quite low.

Table 9.1 Rheology at Elevated Temperature, Run 3B

Run Time (hr)	Temp. (°C)	Solids Concentration (vol. fraction)	Coefficient of Rigidity (centipoise)	Yield Stress (lb/ft^2)
180	230 ± 3	0.045	0.93	0.003
200	230 ± 2	0.045	0.93	0.003
445	270 ± 5	0.039	0.85	0.003
750	225 ± 3	0.064	1.00	0.008
766*	290	0.110	2.69	0.143
795*	205 ± 3	0.092	2.69	0.023
850*	255 ± 5	0.095	2.34	0.084
850*	270 ± 5	0.090	2.47	0.052

*These measurements were made following the addition of new slurry: 1, 30, 85, and 85 hr, thereafter, respectively.

Run 3B will be continued in order to study more closely the reasons for the cake formation, as well as to make further rheological measurements.

9.1.4 Properties of Slurry Settled Beds

The settled-bed concentrations of various thoria and thoria-urania slurries, in 6-mm quartz tubes, were found to vary linearly with temperature in the range 18 to 225°C. Since the weight of a slurry settled bed in a small tube is supported by bridging to the tube wall, a static yield stress may be computed from the dimensions and weight of the settled bed. Expressed mathematically:

$$\frac{c_1}{c_2} = 1 + A\,(T_2 - T_1), \tag{1}$$

$$\frac{\tau_2}{\tau_1} = \left[1 + A\,(T_2 - T_1)\right]^2, \tag{2}$$

where

T = temperature, °C,

c = concentration,

τ = yield stress at constant concentration,

$A = (0.0035 \pm 0.005)/°C$ for all slurries investigated in the particle-size range of 1 to 3 μ average,

subscript 1 refers to conditions at T_1,

subscript 2 refers to conditions at T_2.

Thus the yield value of a slurry at an elevated temperature can be predicted if the yield value at room temperature is known. For example, Eq. (2) predicts the yield stress at 200°C to be 2.37 times that at 18°C.

9.2 300-SM BLANKET-SYSTEM DEVELOPMENT

The 300-SM system is a complex slurry-circulating facility simulating the slurry core or blanket system of a 5-Mw reactor. Important activities during the report period were the continued investigation of slurry circulation through a 30-in.-dia core vessel at elevated temperatures and the preliminary operation of a low-pressure system which regulates the concentration of slurry in the high-pressure circulating stream. It is intended, by further testing and development, to demonstrate in the 300-SM system a working prototype of a reactor slurry system.

Run SM-7, which had been in progress at temperatures below 200°C and at 500 psi loop pressure,[4] was completed.

The primary objective of a new run, SM-8, was to extend the operating temperature range studied in the 300-SM system from 200 to 300°C and the concentration range to 1000 g of Th-U per liter if possible, using the low-pressure system to make concentration increases from time to time. Alterations which were considered necessary for operation at 2000 psi and 300°C were made in the interim between runs SM-7 and SM-8, and a hydrostatic proof test at 3750 psi was completed. Run SM-8 was interrupted after 653 hr of slurry circulation because of a pump-bearing failure; a concentration of 750 g of Th-U per liter was reached before the failure occurred.

9.2.1 30-in.-dia Core-Vessel Tests

For run SM-7, vessel samplings at 150 to 200°C, at concentrations of 325 to 425 g of Th-U per liter, and at flow rates of 130 to 380 gpm were reported earlier.[4] Additional samplings were made at a slurry concentration of 200 g of Th-U per liter and at the above-mentioned temperatures and flow rates. At the higher flow rates an apparent low-concentration region, 23% below that circulating, was again observed at the center of the large toroidal eddy set up in the core vessel. At 130 gpm, an appreciable increase in concentration was noted at the lower conical vessel surface, and an appreciable solids decrease was noted in the stream withdrawn from the north pole of the vessel; this was believed to signal the onset of dropout. That

dropout was indeed becoming important was confirmed by decreasing the flow rate further to 78 gpm.

The core vessel was sampled also at 200 g of Th-U per liter, at 380 gpm, and at 40 to 100°C. As the temperature was decreased, the concentration of samples from different points became more uniform. At 40°C, the concentration was almost the same at all sample positions, varying within 3.6% of that circulating.

During the early part of run SM-8, the effect of changing the sample-withdrawal rate from 6.8 to 14.1 fps was investigated. Other conditions at the time were 200°C, 380 gpm, and 300 g of Th-U per liter. At the higher sampling rate, the indicated concentration in the low-concentration region was 13% below the circulating concentration, compared with 20% below at the lower sampling rate. This confirms that sampling errors are present, but unfortunately it is not possible to conclude whether the apparent concentration gradient is real.

Continuing run SM-8, the concentration was retained at 300 g of Th-U per liter, and the temperature was increased gradually to 300°C, at variable flow rate. Dropout was initiated only at 275 to 300°C, at 130 gpm. The slurry loading was increased to 500 g of Th-U per liter, and a similar flow-temperature range investigated. Dropout was again observed to start at 275°C and 130 gpm.

9.2.2 The 300-SM Low-Pressure System

The low-pressure section of the 300-SM system was completed, tested on water, and placed in service; Fig. 9.2 is a flowsheet of this system. Its major components are:

1. A 30-in.-dia, vertical cylindrical dump tank with a 90° included-angle cone bottom; its volume is 1200 liters. Steam jackets are provided at the cone bottom and at the lower third of the cylindrical shell. Steam sparge connections are also provided. The tank is mounted on three Emery hydraulic weigh cells connected to a totalizer unit. The liquid level is indicated at four elevations by heated thermocouple probes.

2. A vapor entrainment separator and U-tube condenser rated at 1258 lb/hr of steam, and a condensate receiver.

3. An auxiliary steam-generating system to supply 100 lb/hr of 100-psi steam for sparging the dump tank or for line blowouts.

4. A 600-liter rinse-water tank.

5. A 4-gpm centrifugal transfer pump to supply suction head to:

6. A diaphragm feed pump rated at 1.5 gpm, and 2000 psi.

Subsequent to the water tests, the tie lines to the high-pressure system were installed, and the system was operated as an auxiliary to the high-pressure system for storing slurry, receiving dumps, and providing a source of feed. It was found that the original slurry outlet at the bottom of the tank plugged frequently. The center steam-sparge line, which goes vertically up for about 2 ft inside the tank and out through the wall of the cylinder, was converted to a slurry outlet line and has worked well. Slurry has been handled at concentrations up to 2100 g of Th-U per liter, to date. It is often necessary to use the steam generator to back-flush the feed line before starting flow.

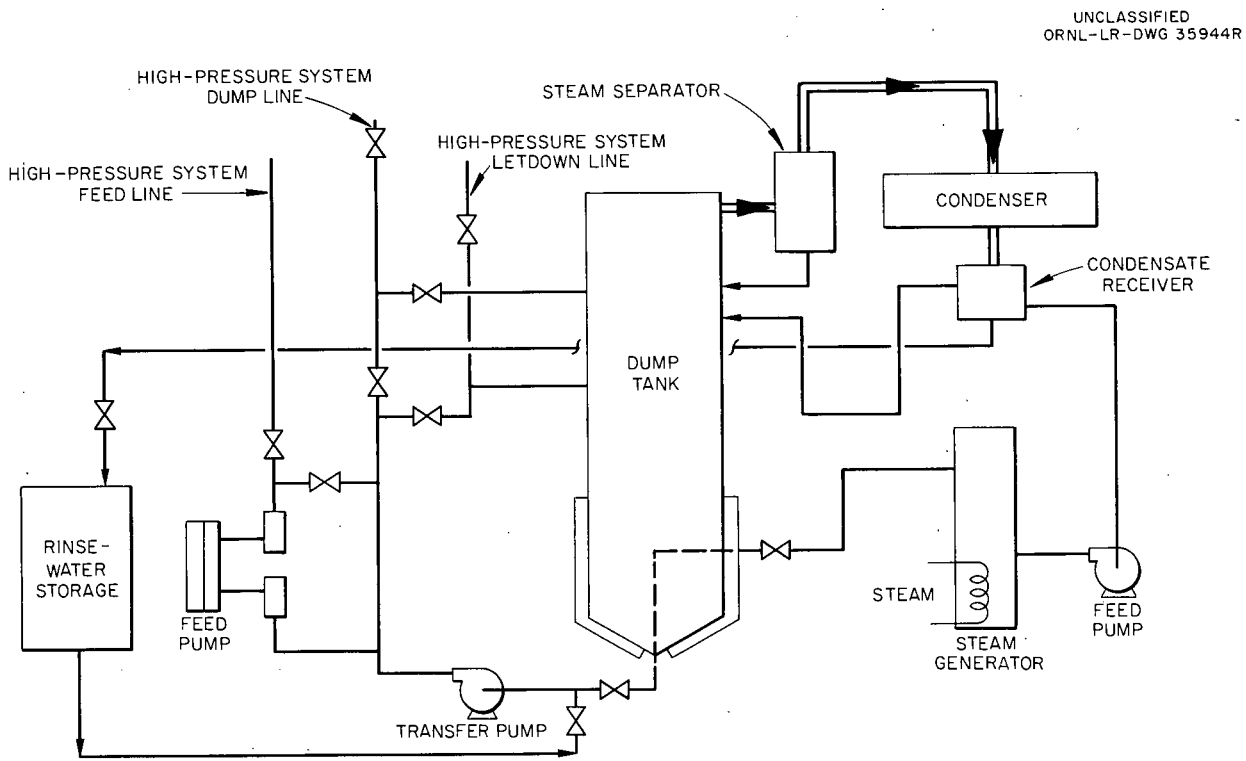

Fig. 9.2. Flowsheet of 300-SM Low-Pressure System.

Simple boiling of the dump-tank contents by heating with the steam jackets has proved adequate for keeping the slurry in suspension. Of the four jacket sections, only that on the cone appears effective in keeping the slurry in suspension. There are indications that the centrifugal transfer pump has insufficient net positive-suction head at low tank level; an attempt will be made to correct this condition by improved temperature control.

The diaphragm feed pump has been used to pump water into the loop during the dilution operation and to increase the circulating loop concentration to 750 g of Th-U per liter. During one charging operation, pumping stopped; subsequently, the suction check valves were found packed full of pasty thoria. Some changes in operating technique are being tried in an effort to avoid a recurrence.

Since the low-pressure system began operation, three dumps of the high-pressure system have been made. In all cases, the initial high-pressure-system temperature was 225°C. The initial pressures were 1250, 1400, and 750 psig, respectively, and the circulating slurry concentrations were 2, 500, and 750 g of Th-U per liter. The dump-tank condenser has worked well in limiting the dump-tank pressure. The highest pressure in any of the three dumps (28 psig, in the third) developed before the steam had displaced the noncondensables from the condenser. The pressure dropped to 2 psig about 2 min after condensation started.

A 46-in. length of 1/8-in. sched-80 pipe is used as a flow restrictor in the dump line; this is intended to reduce the velocities past the dump-valve trims. The valves have indicated a slight leakage after each dump, but no visible damage. Slight lapping was used in every case to eliminate the leak.

After both the second and third dumps, approximately 40 kg of Th-U remained in the high-pressure system, based on the concentration of the slurry resuspended in subsequent rinsing operations. An inspection of the pressure vessel after the second dump showed that very little residual solids remain in the vessel. Figure 9.3 is a photograph of the bottom of the vessel.

In preparation for the first dump, the high-pressure system was diluted by pumping up water with the feed pump and then draining the slurry. The concentration was reduced from 180 to 2 g of Th-U per liter in 20 hr.

Experience with the low-pressure system has been generally favorable. At least one anticipated problem, foaming in the dump tank, has not been experienced. Minor alterations in the flowsheet and piping layout are desired to give improved operation, and the limitations of the system and the possibility of major improvements need to be explored more fully than has been possible to date.

9.2.3 Pump and Valve Failures in Run SM-8

The Westinghouse 300A slurry-circulating pump failed after 3580 hr of operation since its last major overhaul. The first signs of pump trouble were a 90 cycle/min oscillation in current, with a corresponding noise. Shortly thereafter there were indications that excessive thoria from the loop plus graphite from a bearing were circulating in the motor bearing water. Subsequent examination showed that the lower radial bearing of the pump had worn excessively, although the other bearings were still in good condition. The pump was repaired without difficulty.

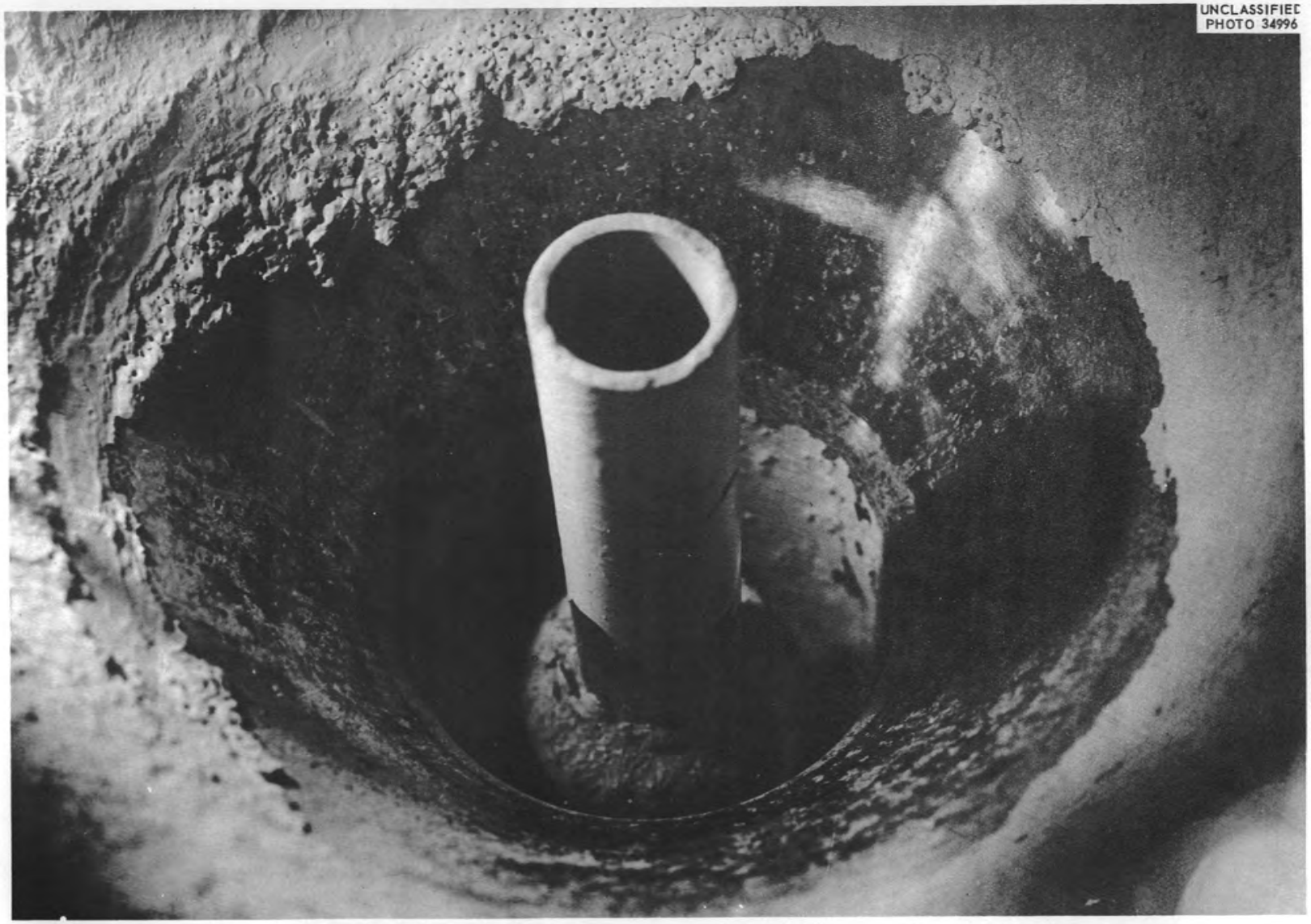

Fig. 9.3. Bottom of 300-SM Core Vessel Following Dump.

During the 653 hr of slurry circulation in run SM-8, the Zircaloy impeller lost 5.8 g of metal. A calculation indicates that this loss is almost entirely accounted for by abrasion of the hub against its wear ring, following the bearing failure.

Nine valves of various types failed during run SM-8, which was the first 300-SM loop operation above 500 psi pressure. In all cases, severe erosion of the valve trim was observed; presumably most of the visible damage had occurred after the failures. Also, full system pressure was across each valve at the time of failure.

Six of the valves were small hand valves, used in taking samples. These are arranged in two series of three valves, including two stainless steel bar stock shutoff valves and a third toggle valve which contains a Teflon seat. The latter valve is the primary sample valve and must close while slurry is flowing through it. Upon failure of the toggle valves, which had each been used for about 250 samples, the other two series of valves failed in sequence while the operator was attempting to stop flow through the sample line.

The air-operated letdown valve (Annin 1/2-in. 1500-psi angle valve with Stellite throttling trim) failed during a dilution operation carried out just prior to run SM-8. At the time that failure became evident, the valve had carried flow for 16 hr and had been operated about 10 times with the high-pressure loop at 750 psi. Both the plug and seat were eroded.

An unintentional dump occurred during run SM-8 as the result of simultaneous failure of two air-operated block valves in the feed-pump discharge piping. Both valves contained 17-4 PH stainless steel trim.

Revised operating procedures, piping rearrangements, and the procurement of other trim materials are being considered as means of preventing future valve failures.

REFERENCES

1. R. B. Korsmeyer et al., HRP Quar. Prog. Rep. Apr. 30, 1959, ORNL-2743, p 80.

2. R. B. Korsmeyer et al., HRP Quar. Prog. Rep. Jan. 31, 1959, ORNL-2696, p 60-67.

3. C. G. Lawson, Heat Transfer to Bingham Plastics ThO_2 Slurries Flowing Turbulently in Tubes: An Exploratory Study, ORNL CF-56-9-132, (Sept. 30, 1956).

4. R. B. Korsmeyer et al., HRP Quar. Prog. Rep. Apr. 30, 1959, ORNL-2743, p 84-93.

10. INSTRUMENT AND VALVE DEVELOPMENT

R. L. Moore

S. J. Ball
A. M. Billings
E. H. Bell
D. G. Davis
D. S. Toomb
H. D. Wills

10.1 INSTRUMENT DEVELOPMENT

10.1.1 High-Temperature, Radiation-Resistant, Differential Transformers

The development of differential transformers for sensing the primary-element motions of instruments and capable of operating for long periods at high temperatures and in radiation fields was continued.

The transformer described previously[1] was operated for three months at 300°C and subsequently temperature-cycled several times between 25 and 300°C. A zero drift of approximately 5% was accumulated over the three months period. This drift was determined to be due to expansion of the test jig. No other changes in characteristics were noted. A second transformer was constructed and has performed satisfactorily.

10.1.2 Transistorized Electropneumatic Converter

The transistorized electropneumatic converter described previously[2] was redesigned to eliminate recurrent zero shift and drift troubles experienced with this prototype instrument. Analysis of the circuitry and bench tests of the prototype model indicated that the basic circuit design of the instrument was satisfactory and that the shifts and drift were due to such factors as poor contacts in printed-board connectors, leaky and intermittently open condensers, bad solder joints, and the arrangement of the wiring.

The redesigned model illustrated in Fig. 10.1 is designed for rack mounting of the main chassis in a standard 19-in. relay rack. The associated electropneumatic and pneumatic-to-electric transducers are connected to the main chassis by cables and may be field mounted. Printed wiring has been eliminated, and the number of plug-in connections has been reduced to one connector which is located at the rear of the chassis. High-grade components, including silicon transistors and tantalum capacitors, are used throughout.

Basic operation of the instrument is the same as that of the University of Virginia prototype except that the automatic phasing feature of the prototype model has been eliminated and the d-c amplifier is now of the direct-coupled type instead of the chopper type. A block diagram of the revised circuitry is shown in Fig. 10.2.

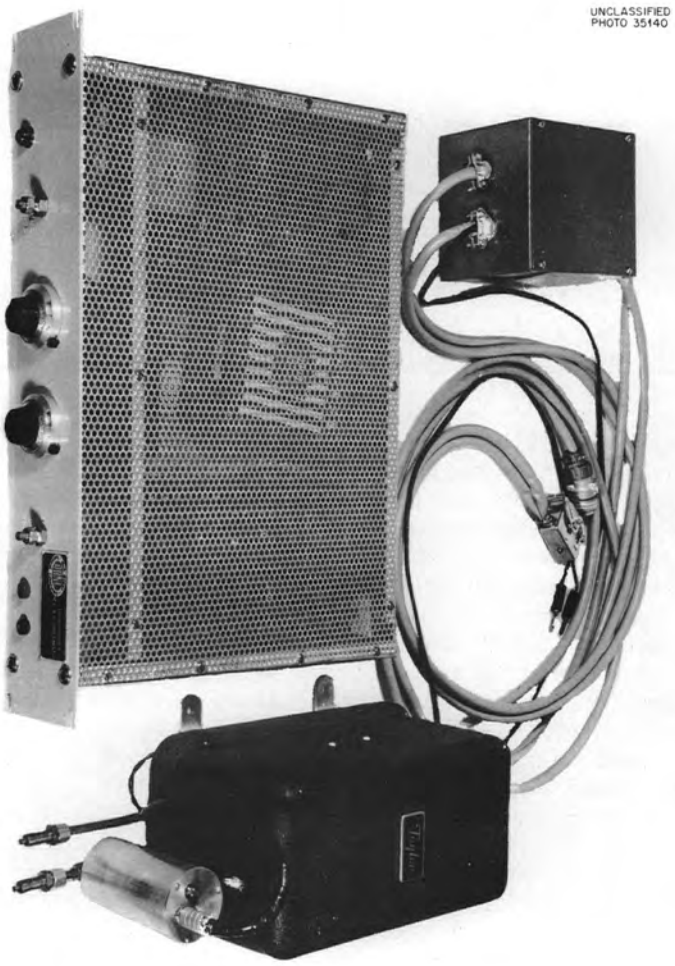

Fig. 10.1. Transistorized Electropneumatic Converter.

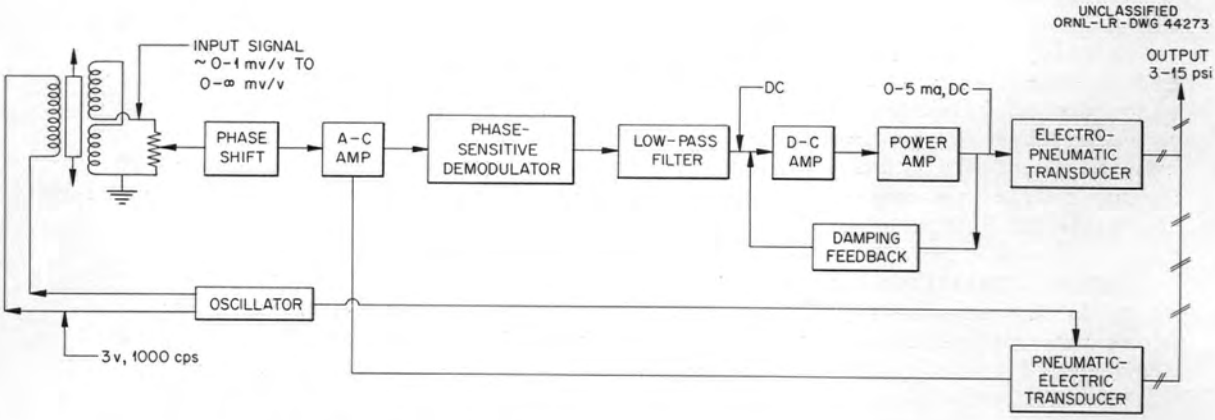

Fig. 10.2. Block Diagram of Transistorized Electropneumatic Converter.

The redesigned model utilizes 18 transistors, compared with 26 transistors required in the prototype. This reduction resulted from the elimination of the automatic phasing circuitry and from redesign of the d-c amplifier circuit. Significant reductions were also made in the number of other components.

Tests to date indicate that the redesigned instrument has an accuracy of ±1/2% of span under the following conditions:

Range: 5 mv/v, full scale (1000 cps)
Output: 3 to 15 psig air
Supply Voltage: 40 to 50 v, dc
Ambient Temperature: 50 to 120°F

10.1.3 Evaluation of a Magnetic-Amplifier Instrumentation System

A new Foxboro Company electric system for process instrumentation was tested to determine its suitability for HRP applications and was satisfactory. The system is unique in that magnetic components and static rectifiers are used to amplify low-level signals and to derive the control functions. Previously, commercial equipment for general process instrumentation has been pneumatically powered or has utilized vacuum tubes, which do not have the inherent reliability of electric static-component systems.

A block diagram of the pressure-measuring and control system tested is shown in Fig. 10.3. The 0 to 2500 psi measured pressure is applied to a stainless steel, helical sensing element which alters the position of a copper coupling ring and thereby the flux linkage and output electric signal in a differentially connected electromechanical transducer, the Dynaformer. The low-level a-c output signal proportional to pressure is rectified and then amplified by a magnetic amplifier to provide a 10- to 50-ma d-c signal for the transmission line to the recorder or indicator, function-generating controller, and adjustable electric alarm-deriving chassis. An electric-to-air converter, to provide a pneumatic pressure signal for powering diaphragm control valves, is also available as part of the system. These components are pictured in Fig. 10.4.

The laboratory test of set-point stability, with the system connected as a closed loop, resulted in less than 1% change in control point when the line voltage was varied from 105 to 125 v ac, and no drift was observed during two weeks of operation with constant line voltage.

Frequency response analysis of the controller indicated a characteristic curve, flat to approximately 1 cps. It was also noted that the minimum reset valve obtainable with the two-element flow controller was about 2 min/reset, and the minimum proportional band setting was 50%. A general purpose three-element controller has been designed by Foxboro and placed on order but is not yet available for testing. Figure 10.5 indicates how the magnetic amplifier components of the controller are arranged on a printed-circuit wiring board. The controller assembly is connected to its housing by an easily removable plug-in connector.

After completion of laboratory tests, the system was installed as a pressure control loop in a high-pressure test stand in order to evaluate long-term stability and reliability. Five months of operation in this service have been accumulated to date. No malfunctions or difficulties have been experienced during this period.

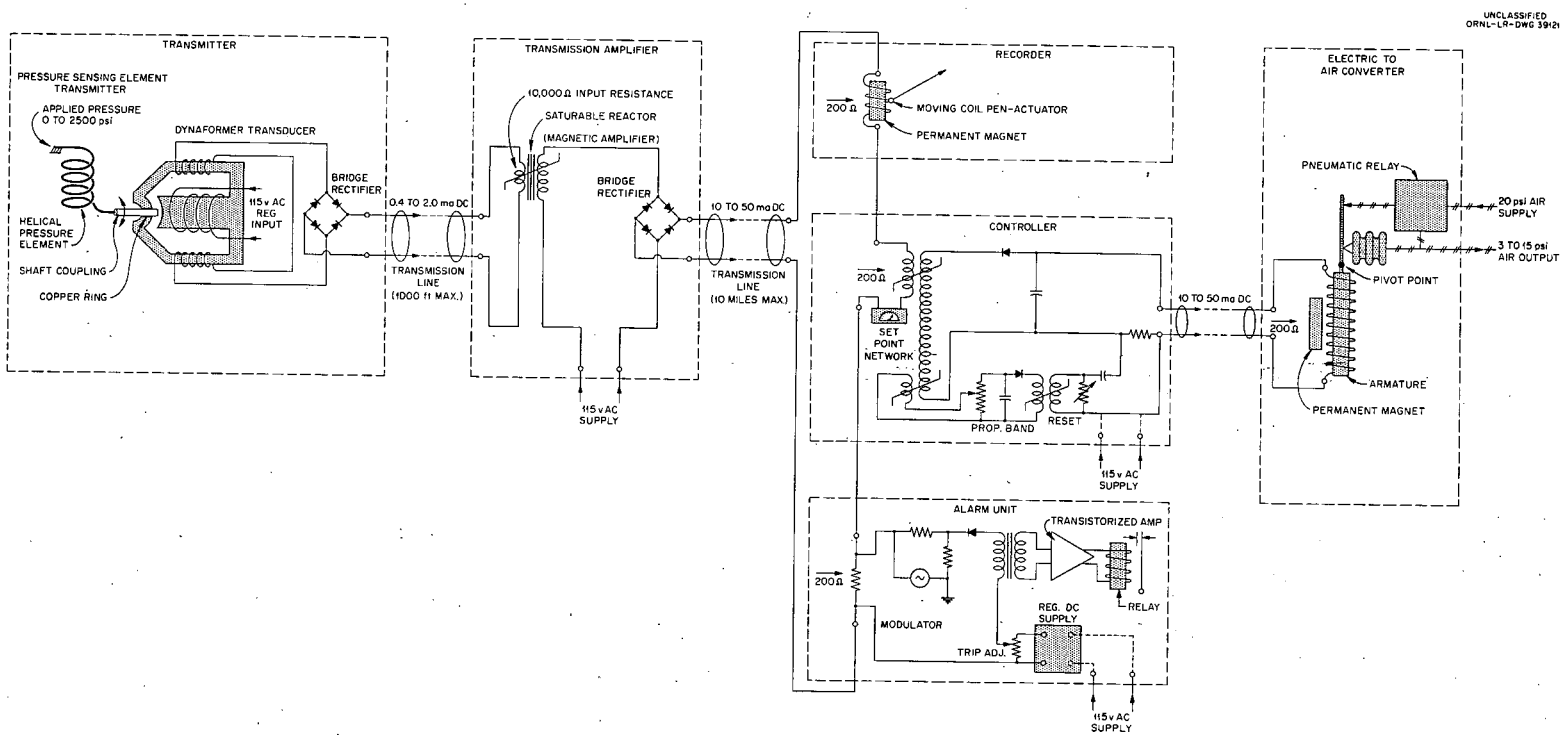

Fig. 10.3. Block Diagram Foxboro Electronic Consotrol Instrumentation: Pressure Recording-Controlling-Alarm System.

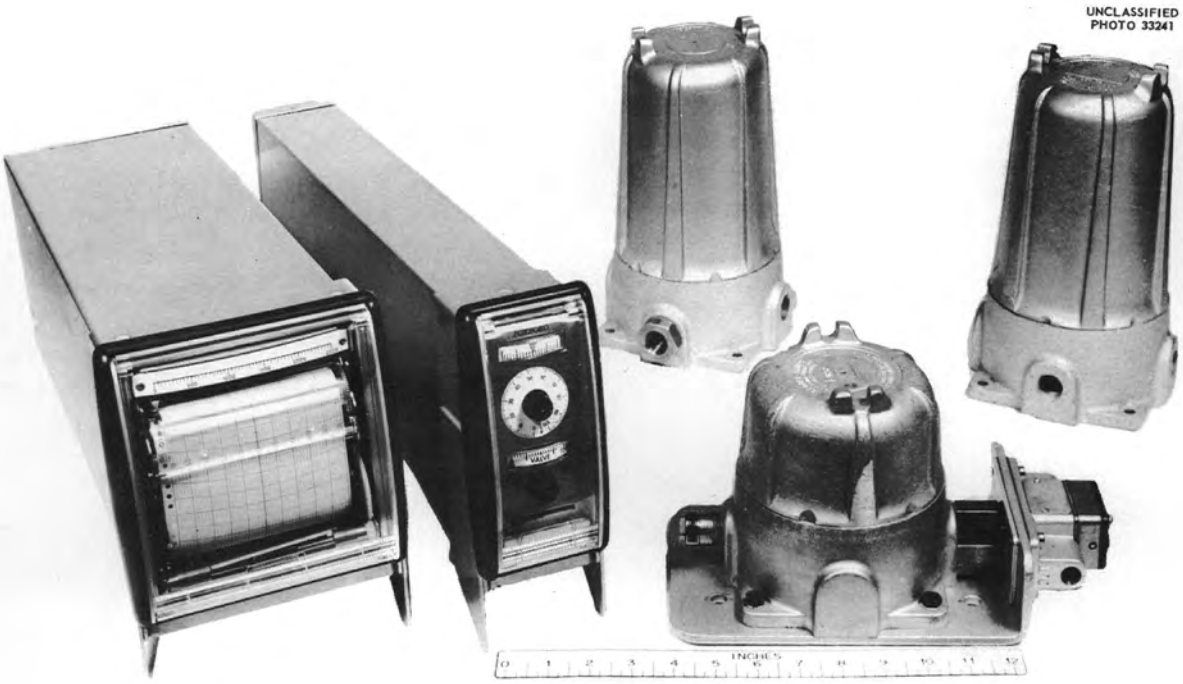

Fig. 10.4. Foxboro Electronic Consotrol Instrumentation: Pressure Recorder-Controlling System.

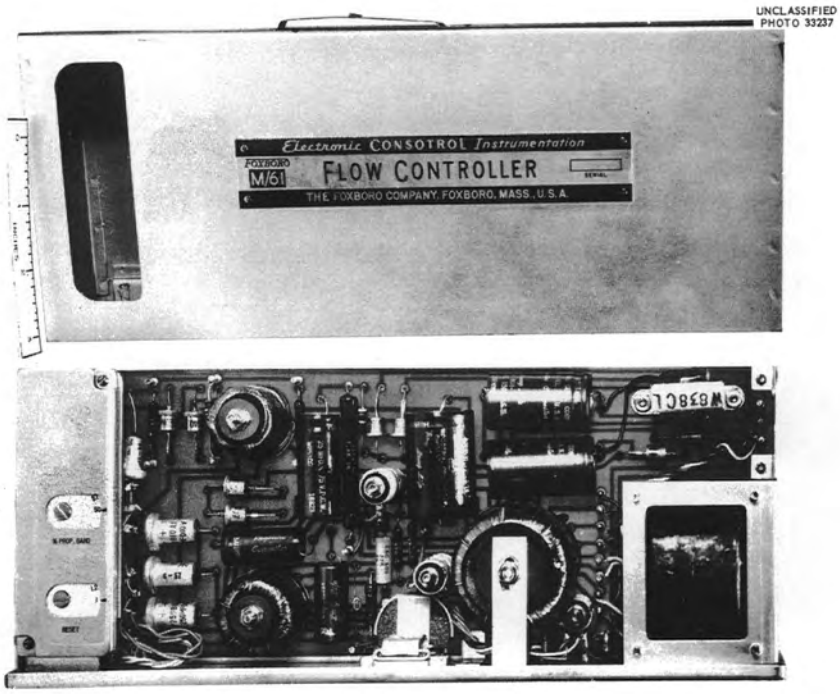

Fig. 10.5. Foxboro Model M/61 Flow Controller.

Additional components of the Foxboro ECI (Electronic Consotrol Instrumentation) system, including an alarm unit and a millivolt-to-current converter, have been ordered for test and evaluation.

10.1.4 Evaluation of Pressure Transmitters

The Norwood Controls Division pressure transmitter described previously[3] was installed on the slurry-mockup high-pressure system in order to obtain long-term operation experience with this instrument in a slurry system. The process connection was a 1/4-in. pipe connection into the top of a circulating slurry stream. To date, the instrument has operated approximately 2300 hr, with no indication of slurry plugging or other malfunction.

10.1.5 Analog Computer

A Donner model 3400 electronic analog computer, illustrated in Fig. 10.6, was acquired for use in training personnel in the uses of analog computers and in closed-loop process-control theory.

This computer incorporates ten stabilized operational amplifiers, two electronic multipliers, and one diode function generator. The computer is also finding use in solving HRP problems.

10.1.6 Ultrasonic Detection of the Interface of a Falling Slurry*

A Branson-type ceramic ultrasonic transducer,[6] which was mounted in an end plug for the dash-pot bomb, was tested with thoria slurries in a beaker at room temperature and in an autoclave at temperatures up to 150°C.

The transducer was demonstrated to produce a signal showing, within ±0.5 in., the position of the interface produced by a 400-g/liter aqueous slurry of preparation DT-7-650 to a distance of approximately 4 in. below the transducer face in an open beaker at room temperature. Occasional wiping of the transducer face was necessary to free it of small gas bubbles collected from entrained or dissolved gases in the slurry. Such gas bubbles were capable of absorbing the entire power output of the transducer.

When the transducer was installed in an autoclave, it became impossible to free the face from the gas bubbles, which caused the signal to be weak and erratic. Attempts to heat the bomb resulted consistently in disappearance of the signal at temperatures below 100°C. Full signal power could be restored temporarily by disassembling the bomb and wiping the transducer face.

Although it is possible to detect the interface ultrasonically, the apparatus must be provided with means for keeping the face of the transducer free of gas bubbles.

---

*This section was contributed by K. H. McCorkle of Chemical Development Section A, Chemical Technology Division.

UNCLASSIFIED
PHOTO 35148

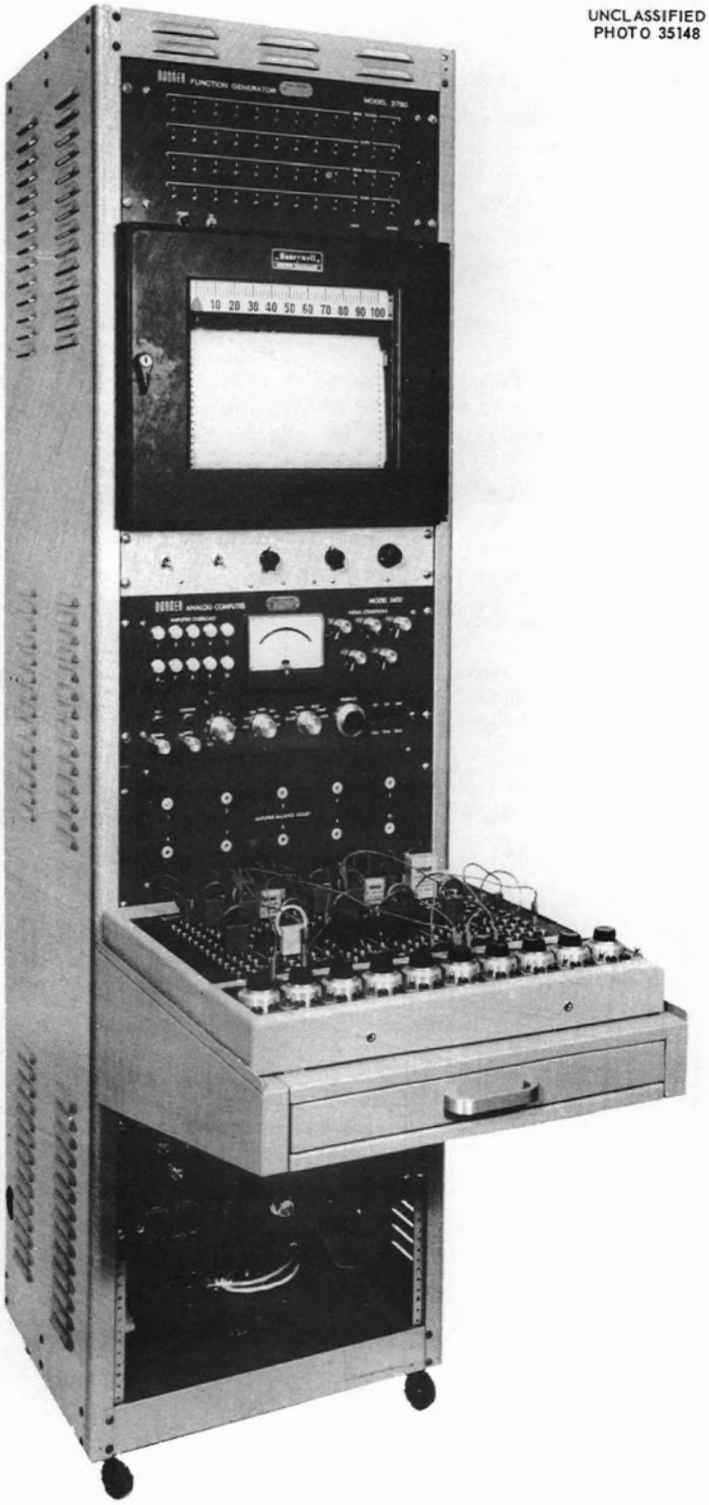

Fig. 10.6. Donner Model 3400 Electronic Analog Computer.

10.2 VALVE AND ACTUATOR DEVELOPMENT

10.2.1 Valve Trim for Slurry Service

After operating satisfactorily for 2064 hr, the Zircaloy-2 trim installed in the flushed-bellows Hammel-Dahl valve in the 30-gpm loop was in good condition, as shown in Fig. 10.7. The time included 125 hr with the valve 65% closed and 94 hr with the valve 30 to 40% closed. All operation was at a loop pressure of 1600 to 1700 psig at 270°C. Slurry concentration varied from 400 to 500 g ThO_2 per kg of H_2O. Flow through the valve was varied from 10 to 30 gpm, with a pressure differential across the valve of 25 to 40 psi.

Since examination, this valve has accumulated an additional 2015 hr of operation for a total operating time of approximately 4079 hr. The valve will be removed and inspected again when the test-loop operating schedule permits.

A High Pressure Equipment Company handwheel valve fitted with tungsten carbide trim was used for letting down slurry from 1500 to 500 psig. Total operating time was 45 hr, including 22 hr of slurry flow. The valve had to be removed because of severe attack on the plug and seat. Figure 10.8 illustrates the eroded condition of the plug and seat following this operation.

10.2.2 Valve Stem-Sealing Bellows

Five Ti-55 titanium bellows[5] assemblies have been cycled to destruction in uranyl sulfate at 280°C. Stroke length was 1/8 in., with 2300 psi applied externally to the assembly. Results are as follows:

Bellows No.	No. of Strokes
P2-1 (prototype)	13,480
P2-2 (prototype)	11,611
P2-3	39,420
P2-4	28,067
P2-5	24,143

The Fulton Sylphon Division, Robertshaw-Fulton Controls Company, developed this unit for a minimum life expectancy of 10,000 cycles under the conditions described above. Following the acceptance testing of assembly P2-2, 12 units were procured for life testing. Four additional assemblies were purchased fitted with a smaller-diameter flange to facilitate inclusion in a future all-titanium valve.

Three HRT-type valve-stem sealing bellows (Fulton Sylphon No. 10716-R3) have been cycled to destruction in 400 g of ThO_2 per kg of H_2O at 2300 psig, 285°C, with a 1/8-in. stroke. Average life of the three units was 75,598 strokes. No further testing is planned since bellows life does not seem adversely affected by the ThO_2 slurry.

10.2.3 Solution-Sampling Valve

The handwheels of the general-purpose sampling valves[6] procured from Fulton Sylphon were replaced with handwheels incorporating Saginaw ball-bearing assemblies as illustrated in Fig. 10.9. This has reduced friction, that is, closing torque, sufficiently to permit manual operation of the valves with

UNCLASSIFIED
PHOTO 33844

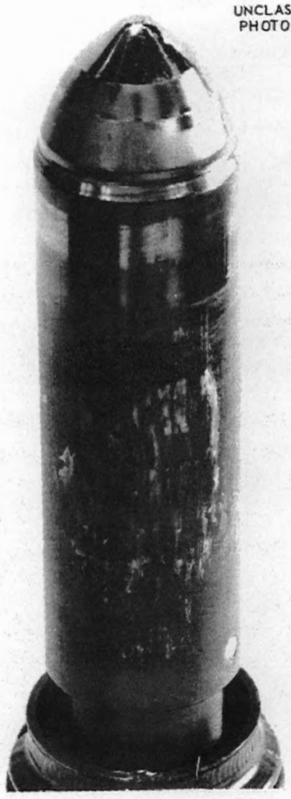

Fig. 10.7. Zircaloy-2 Valve Trim After Slurry Service.

UNCLASSIFIED
PHOTO 33686

Fig. 10.8. Plug and Seat from Valve 253, After Test.

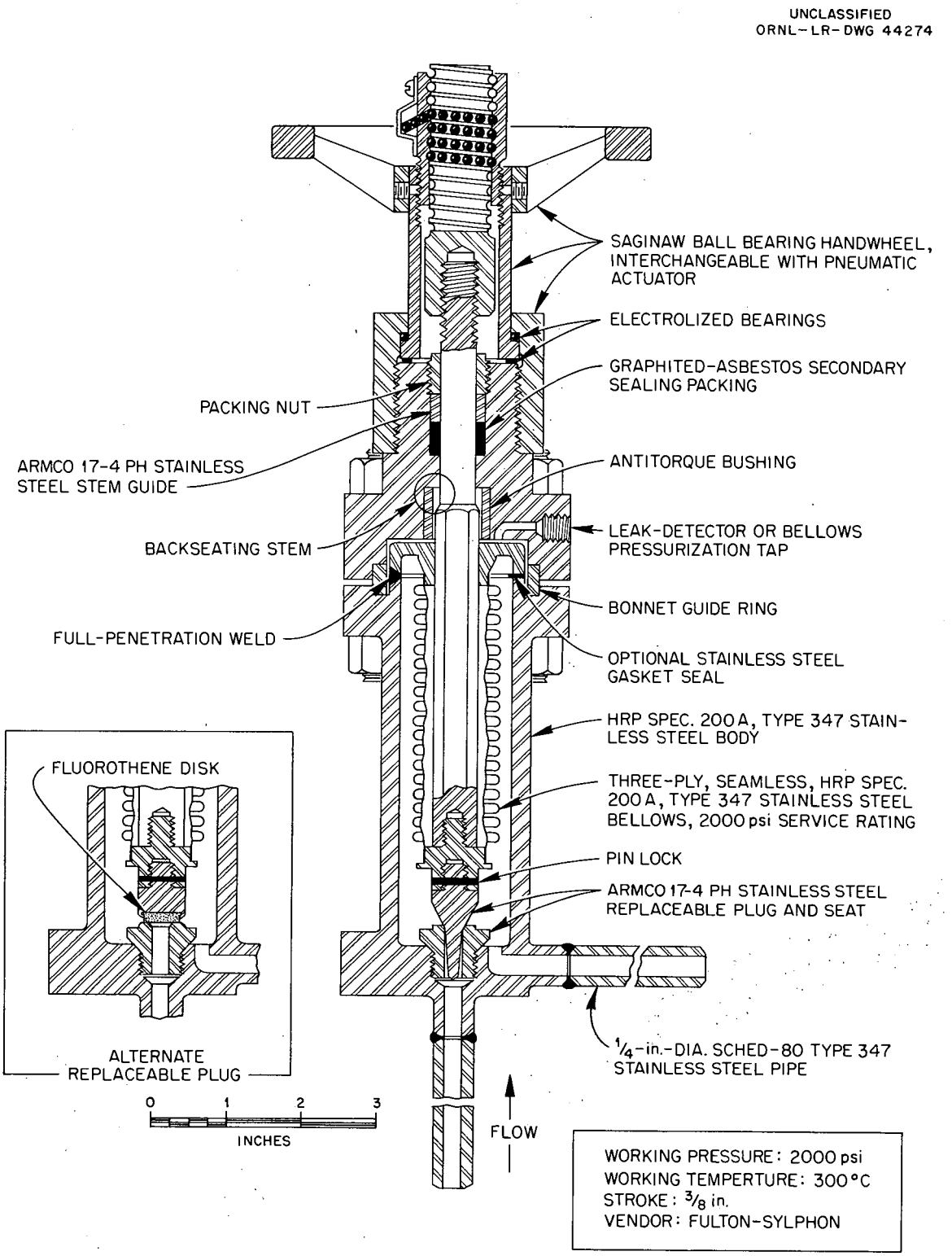

Fig. 10.9. Saginaw Ball-Bearing Handwheel Operator for Fulton Sylphon Valve.

2000 psig applied to the bellows. The new handwheels retain the feature of being interchangeable with penumatic actuators.

REFERENCES

1. D. S. Toomb, et al., HRP Quar. Prog. Rep. Apr. 30, 1959, ORNL-2743, p 95.
2. D. S. Toomb, et al., HRP Quar. Prog. Rep. July 31, 1958, ORNL-2561, p 131.
3. D. S. Toomb, et al., HRP Quar. Prog. Rep. Jan. 31, 1959, ORNL-2696, p 70.
4. J. P. McBride, et al., HRP Quar. Prog. Rep. Jan. 31, 1959, ORNL-2696 pp 177-195.
5. D. S. Toomb, et al., HRP Quar. Prog. Rep. Apr. 30, 1959, ORNL-2743, p 100.
6. D. S. Toomb, et al., HRP Quar. Prog. Rep. Oct. 31, 1958, ORNL-2654, p 104.

11. HEAT TRANSFER STUDIES

J. C. Griess H. C. Savage

R. S. Greeley W. C. Ulrich
C. B. Wooldridge[1]

11.1 HEAT TRANSFER FROM STAINLESS STEEL TO OXYGENATED H_2O, D_2O, AND URANYL SULFATE SOLUTION AT 100 TO 250°C

In previous quarterly reports experiments were described concerning the deposition of salts from loop fuel solutions on heated surfaces.[2] During those experiments rough measurements were made of the heat transfer from the heated surface to the solution. In order to study more precisely the variables involved in heat transfer from a hot metal wall to solution, a new experimental facility was constructed. The apparatus consisted of a loop equipped with a window for the observation of an electrically heated type 347 stainless steel capillary tube containing a central thermocouple for determining the tube-interior temperature. The heated capillary tube was observed through a modified boiler-gauge-glass assembly containing Pyrex windows sealed with Teflon gaskets. The loop was hydraulically pressurized by means of a pulse pump. Heat-flux and wall-temperature measurements were made in degassed and oxygenated H_2O, D_2O, and uranyl sulfate solution at 100 to 250°C and at pressures from 300 to 1000 psia. Heat fluxes of 10,000 to over 500,000 Btu/hr·ft^2 were obtained with electrical currents up to 225 amp ac at about 10 v.

The results of the heat-transfer measurements are illustrated in Figs. 11.1 through 11.4. In each of these figures the heat flux, q/A, in Btu/hr·ft^2 is plotted versus the wall temperature of the stainless steel capillary tube. The wall temperature on a linear scale was plotted rather than the more conventional Δt on a logarithmic scale since it is of interest to show the actual value of the wall temperature at each condition, particularly in the uranyl sulfate solution where a second-liquid or solid phase could form at the higher wall temperatures. The heat flux was determined from the electrical a-c input power. The outside wall temperature of the capillary was calculated from the internal temperature by means of standard heat-transfer equations for volume-heated cylindrical tubes.[3] In Fig. 11.1 heat transfer from the stainless steel capillary to gas-free H_2O and D_2O at about 200°C is illustrated. Each curve is a typical heat-transfer curve and illustrates that the apparatus gives results in general agreement with those of previous investigators.[4] The lower leg of each curve represents convective heat transfer, and the upper, steeper portion represents the nucleate-boiling region. The correlation between the saturation temperature (t_{sat}) based on the total system pressure was in good agreement with the appearance of bubbles on the metal surface. The increase in wall temperature in the nucleate-boiling region with increasing total pressure

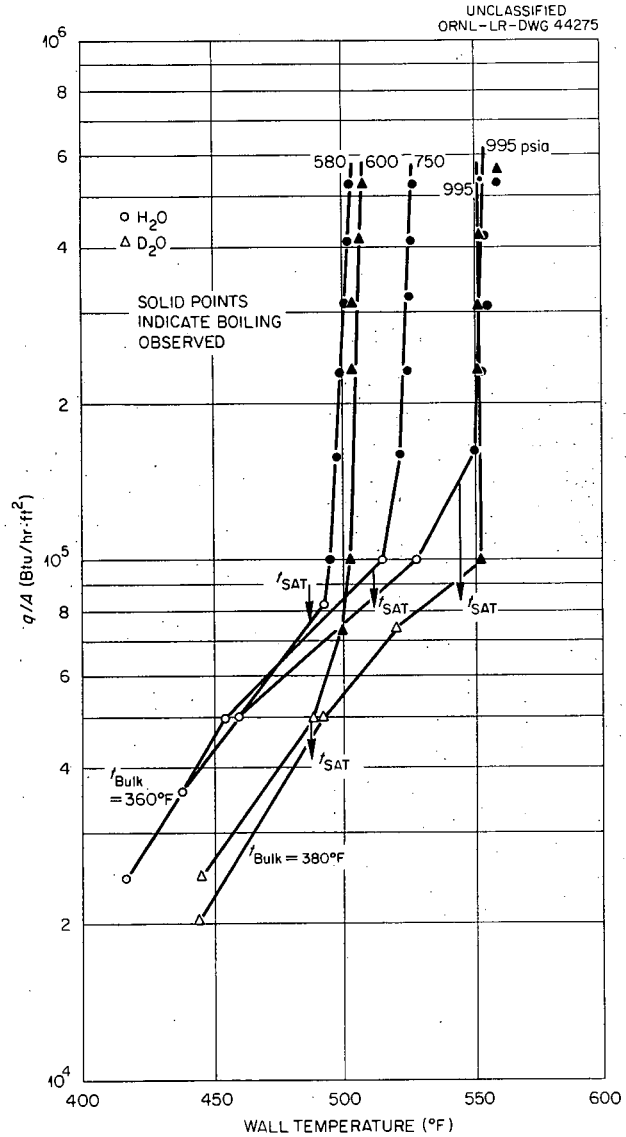

Fig. 11.1. Heat Transfer From Stainless Steel to Gas-Free H_2O and D_2O at ~ 380°F.

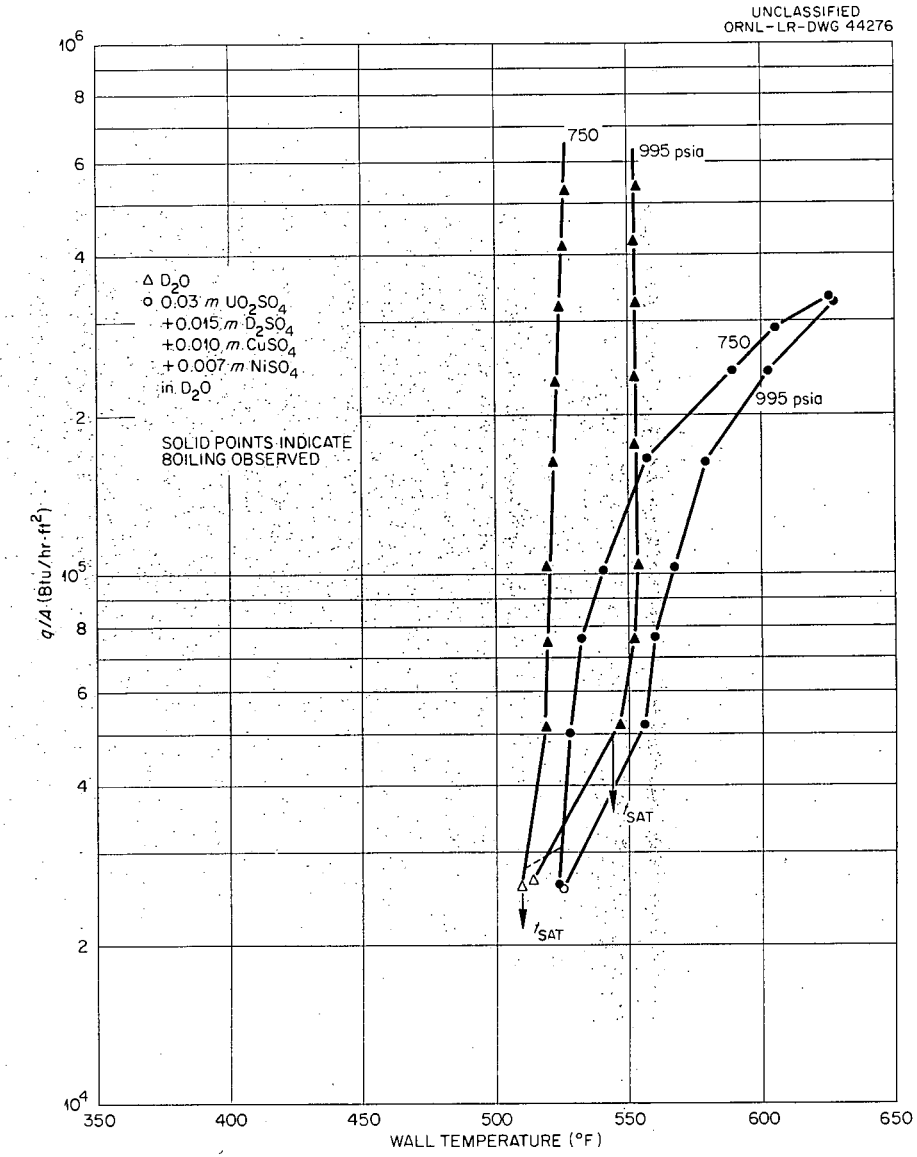

Fig. 11.2. Heat Transfer from Stainless Steel to Gas-Free D_2O and Uranyl Sulfate Solution at ~ 480°F.

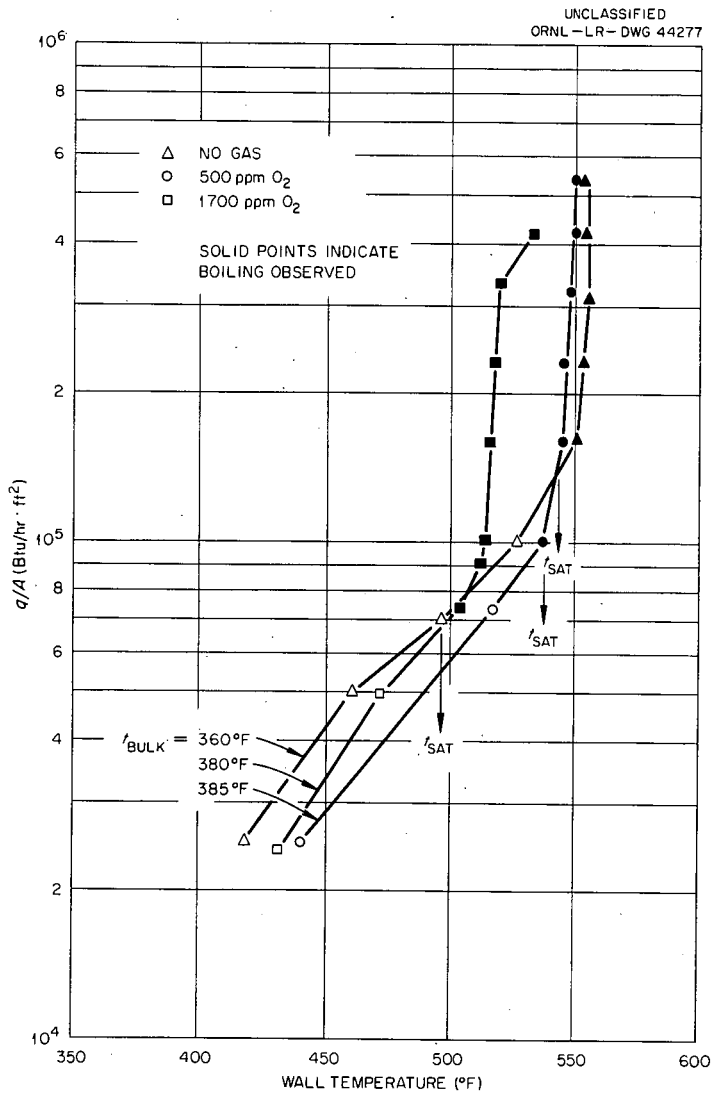

Fig. 11.3. Heat Transfer from Stainless Steel to Oxygenated H_2O at ~380°F and 990 psia.

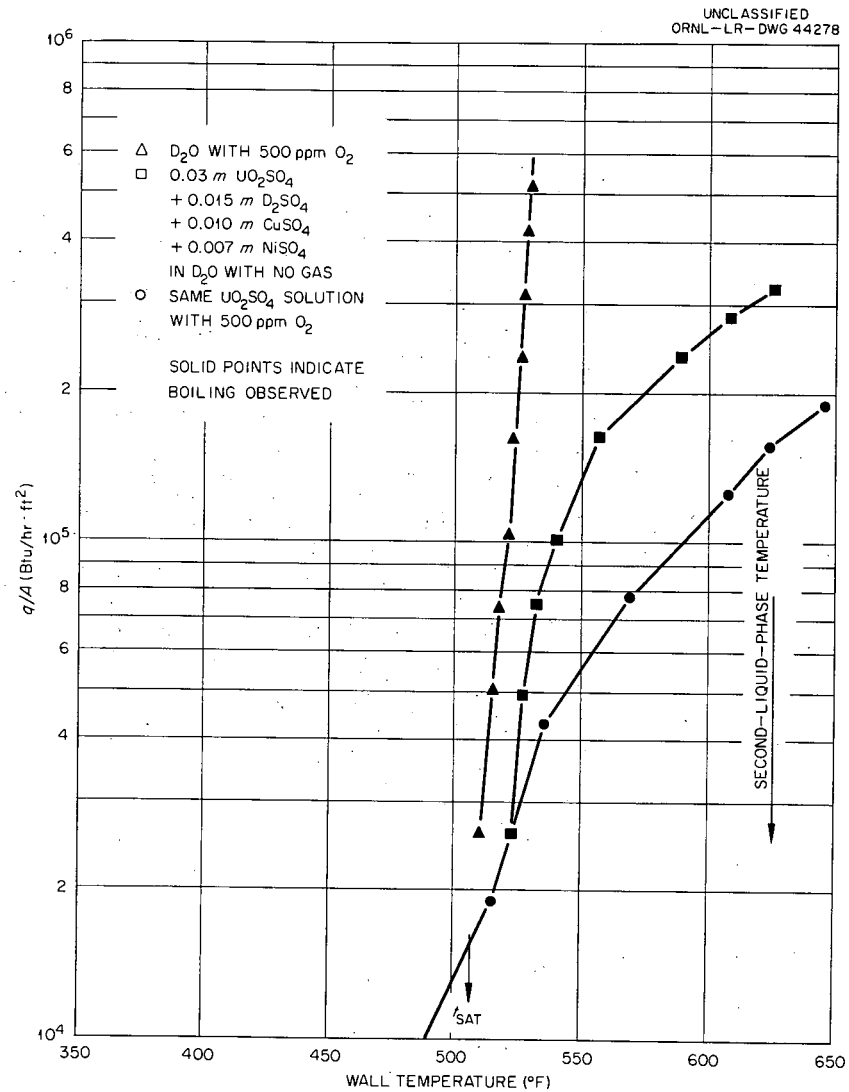

Fig. 11.4. Heat Transfer to Stainless Steel from Oxygenated D_2O and Uranyl Sulfate Solutions at ~480°F and 750 psia.

on the system is the result of the increase in saturation temperature with pressure. It can be seen that there was essentially no difference between the results for light water and for heavy water. The apparent difference between H_2O and D_2O in the convective region at the lower heat fluxes was due to the difference in bulk-solution temperature; namely, 182°C (360°F) for the light water and 193°C (380°F) for the heavy water. Curves similar to those shown in Fig. 11.1 were obtained for light and heavy water at 150 and 250°C.

With the loop circulating heavy water at about 250°C, sufficient concentrated solution was added via a pulse pump to give concentrations in the circulating stream of 0.03 *m* UO_2SO_4, 0.015 *m* D_2SO_4, 0.010 *m* $CuSO_4$, and 0.007 *m* $NiSO_4$. Heat transfer from the stainless steel capillary to the nearly gas-free solution at two different system pressures is shown in Fig. 11.2 and is compared with the heat transfer to gas-free heavy water. It can be seen that at the higher heat fluxes the transfer of heat was much poorer in the uranyl sulfate solution than in the heavy water. However, it was noticed that during the tests with the solution a heavy, black film was formed on the heated stainless steel surface. This scale was later shown to contain about 10% uranium and 5% copper and evidently represented an electrolysis product. Also, after the run the stainless steel capillary tube was found to be severely etched and pitted. This was also presumably due to electrolytic action. Furthermore, since the solution was a better conductor than the water, presumably a significant fraction of the electrical current passed through the solution and not through the capillary tube. Therefore, although the latter factor would decrease even further the observed heat fluxes, it cannot be concluded from Fig. 11.2 that heat transfer in uranyl sulfate solution is necessarily worse than in heavy water. Further experiments will be aimed at decreasing the effect of the electrolytic action.

Figure 11.3 illustrates the effect of oxygen on the heat transfer in light water at 200°C and 990 psia. The differences in the points in the convective heat-transfer region at the bottom of the graph were due to slight differences in bulk-solution temperature, as noted on the graph. However, the differences in the nucleate-boiling region must be attributed to the presence of the oxygen gas. Wall temperatures were decreased markedly in this region by the addition of the gas. However, in the run with 1700 ppm oxygen, at the upper portion of the nucleate-boiling region the curve bent over, indicating possibly the approach of film boiling and burnout at lower heat fluxes than in gas-free water.

The saturation temperatures for the tests with oxygen were determined as follows: The partial pressure of oxygen was calculated from the analytically determined oxygen solubility and Henry's law constant[5] for each value of the metal-wall temperature obtained. To this pressure was added the steam pressure at that temperature, and the sum was plotted against the metal-wall temperature. The wall temperature at which the sum of the oxygen and steam pressures was equal to the hydraulic pressure on the system was obtained by interpolation from the graph and was taken as the saturation temperature. It can be seen in Fig. 11.3 that boiling began very close to the saturation temperature so calculated. Therefore the decrease in wall temperature at constant heat flux in the nucleate-boiling region upon the addition of oxygen is due to the decrease in saturation temperature caused by the oxygen partial pressure. An additional factor evident in Fig. 11.3 is that the heat-transfer coefficient, i.e., the slope of the line, in the nucleate-boiling region was decreased upon the addition of oxygen.

In Fig. 11.4 is illustrated the effect of gas on heat transfer in uranyl sulfate solution. Again, very likely, electrolytic effects obscured the true transfer of heat. Probably the main reason for the higher wall temperatures in the solution containing 500 ppm oxygen, compared with the temperatures in the solution containing no gas, is that the oxygen-containing solution was run a day later and the capillary tube had considerable film already built up on it. The capillary tube was carried to as high a temperature as possible in order to get the surface above the second-liquid-phase temperature. However, no heavy phase could be observed on the tube; instead, the tube seemed to foam with very tiny bubbles originating at cracks in the oxide scale on the tube surface, obscuring the surface and any possible heavy phase gathered there.

The heat-transfer tests have thus shown that there is no significant difference in the heat-transfer characteristics of light and heavy water, and that the saturation temperature of oxygen-containing water can be calculated from known Henry's law constants and measured solubilities. Furthermore, the effect of oxygen in decreasing the nucleate-boiling heat-transfer coefficient was observed. On the other hand, heat transfer in uranyl sulfate solution was obscured by electrolytic effects.

REFERENCES

1. Research participant, University of Kentucky.

2. J. C. Griess *et al.*, HRP Quar. Prog. Rep. Jan. 31, 1959, ORNL-2696, p 81, J. C. Griess *et al.*, HRP Quar. Prog. Rep. Apr. 30, 1959, ORNL-2743, p 103.

3. W. H. McAdams, Heat Transmission, p 19, Eqs.(2)-(14d), 3d ed., McGraw-Hill, New York, 1954.

4. *Ibid.*, p 370.

5. E. F. Stephan *et al.*, The Solubility of Gases. . ., BMI-1067 (Jan. 23, 1956).

Part III

SOLUTION FUELS

12. REACTIONS IN AQUEOUS SOLUTIONS

M. J. Kelly

L. O. Gilpatrick H. H. Stone
M. D. Silverman G. M. Watson

12.1 RATE OF OXIDATION OF DISSOLVED H_2 OR D_2 CATALYZED BY $Cu(ClO_4)_2$ IN LIGHT AND HEAVY WATER

The study of the mechanism of the oxidation of dissolved hydrogen by dissolved cupric salts has continued. During the past six months the specific reaction-rate constants for the homogeneously catalyzed activation of molecular hydrogen and deuterium by cupric ion were determined at 100, 120, and 130°C for the systems:

20 atm H_2, H_2O, 0.1 M $Cu(ClO_4)_2$, 0.01 and 1.0 M $HClO_4$

20 atm D_2, H_2O, 0.1 M $Cu(ClO_4)_2$, 0.01 and 1.0 M $HClO_4$

20 atm H_2, D_2O, 0.1 M $Cu(ClO_4)_2$, 0.01 and 1.0 M $DClO_4$

20 atm D_2, D_2O, 0.1 M $Cu(ClO_4)_2$, 0.01 and 1.0 M $DClO_4$

The experimental data, combined with the results obtained at 110°C previously reported,[1] are presented in Figs. 12.1 and 12.2.

Activation energy for each system was calculated and found to be independent of the choice of solute gas (hydrogen or deuterium) or solvent (D_2O or H_2O). However, as the hydrogen (or deuterium) ion concentration, that is to say, the acidity, was increased from 0.01 to 1.0 M the energy of activation decreased from 27.0 ± 0.5 kcal/mole to 24.0 ± 0.5 kcal/mole.

The observed reaction rate constants were lower at higher acidities for each system. The reaction rate constants were lower for D_2 than for H_2 in similar systems.

All the results reported were based on the assumption that the solubilities of H_2 and D_2 are equal and do not change over the temperature range studied. Thus they may be subject to correction when better solubility information becomes available. Experimental work is in progress to determine these solubilities in the systems reported above.

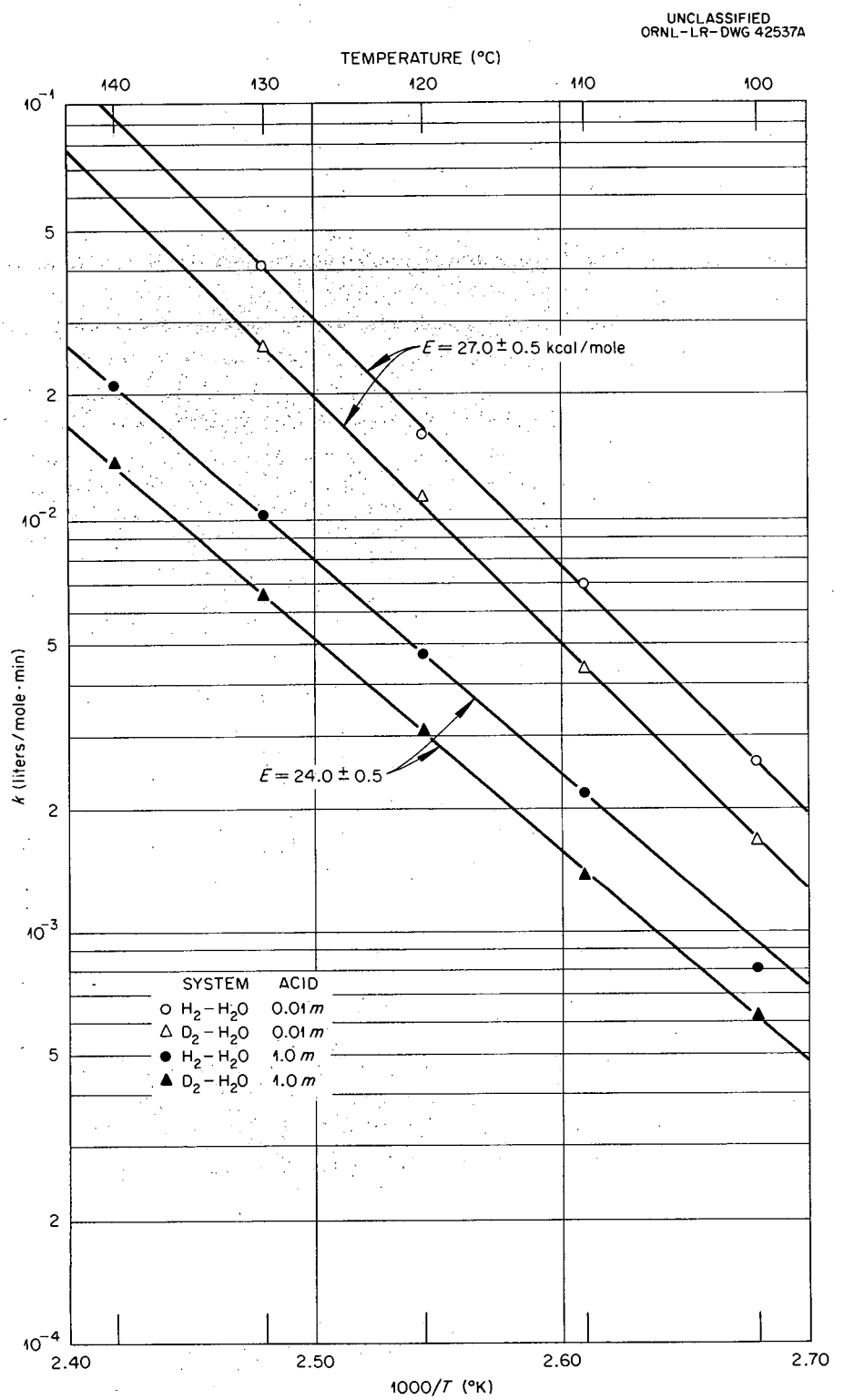

Fig. 12. 1. Effect of Temperature on Specific Reaction Rate Constant; H_2O Systems.

UNCLASSIFIED
ORNL-LR-DWG 42538A

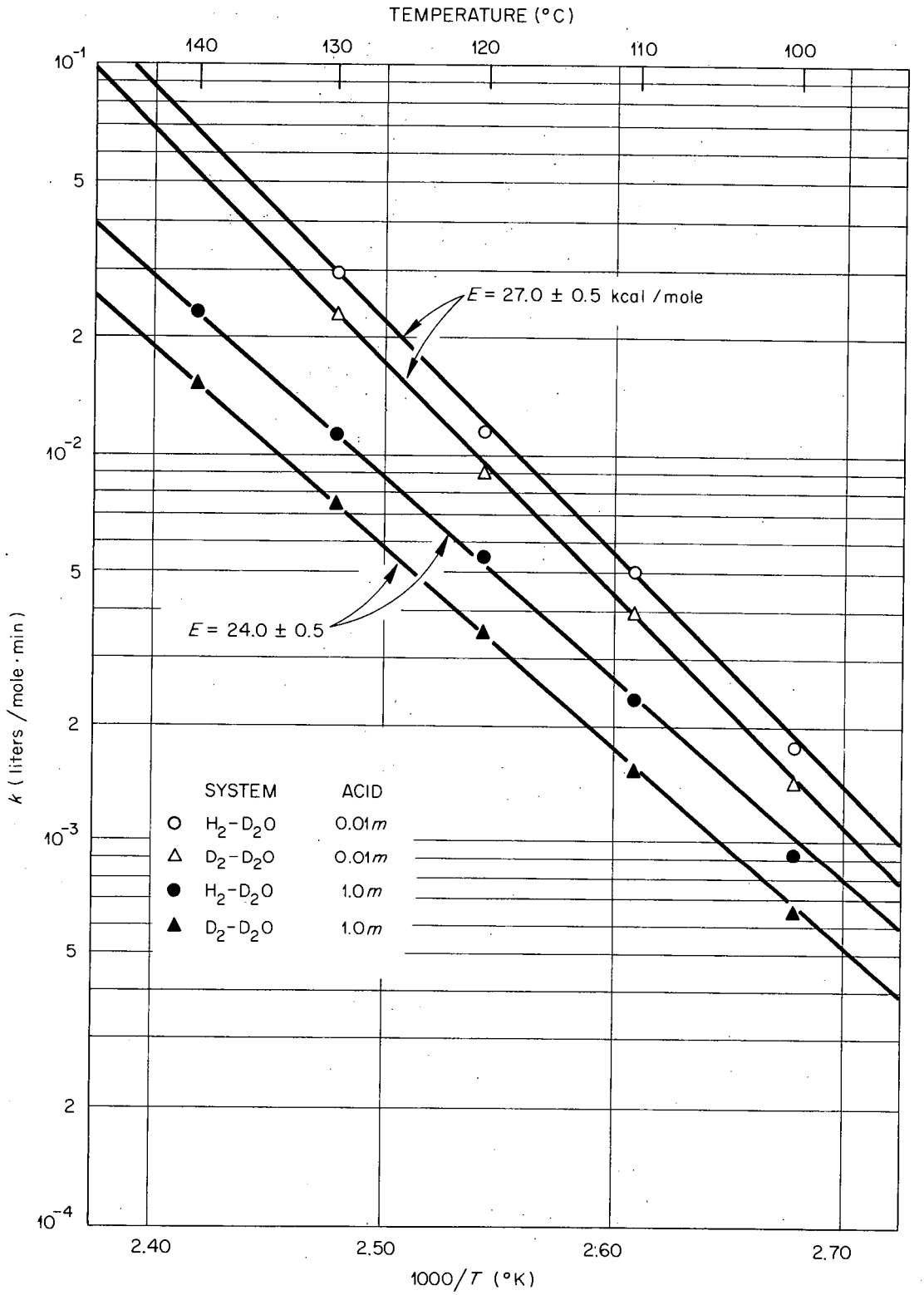

Fig. 12.2. Effect of Temperature on Specific Reaction Rate Constant; D_2O Systems.

12.2 CUPRIC ION AS A HOMOGENEOUS CATALYST IN THE UO_3-HNO_3-H_2O SYSTEM

The system UO_3-HNO_3-H_2O has been suggested as an alternative fuel for homogeneous reactor operations.[2] A series of experiments was carried out to determine the effectiveness of cupric nitrate as a recombination catalyst in the proposed nitrate system.

In order to facilitate obtaining results useful as criteria for further investigations, data were not obtained by the methods previously employed, where oxygen and hydrogen were actually recombined,[3] but the determination of k_{Cu} was accomplished by using the technique described by Peters and Halpern.[4] The rate of reaction of dissolved H_2 in the presence of cupric ion was calculated from the measured rate of reduction of $Cr_2O_7^{=}$, using the known stoichiometry of the reaction:

$$Cr_2O_7^{=} + 3H_2 + 8H^+ \longrightarrow 2Cr^{+++} + 7H_2O \qquad (1)$$

The rate expression, which is zero order with respect to oxidant, has the form:

$$\text{Rate} = k_{Cu} \left[Cu^{++}\right] \left[H_2\right] \left[OX\right]^0 \qquad (2)$$

and the oxidant is now $Cr_2O_7^{=}$ rather than O_2.

The disappearance of the $Cr_2O_7^{=}$ with time was followed with a spectrophotometer, using samples drawn from the reaction vessel and a calibration curve. The H_2 pressure within the reaction vessel was maintained constant, and therefore the H_2 concentration in the liquid phase remained constant as did the Cu^{++} concentration. Therefore, at any two times, t_1 and t_2:

$$k_{Cu} = \frac{3\left\{\left[Cr_2O_7^{=}\right]_1 - \left[Cr_2O_7\right]_2\right\}}{\left[Cu^{++}\right]\left[H_2\right]\left[t_2 - t_1\right]} \qquad (3)$$

The 3 appears in the numerator because of the stoichiometry of the reaction. The values for the concentration of H_2 in solution were calculated from values of its solubility in water at temperature, as had been done previously.[3]

The results obtained for the nitrate system are shown on Fig. 12.3 and can be represented by the expression:

$$k_{Cu} = (6.56 \times 10^{14})\ e^{-27000/RT}\left[\text{liter}\cdot\text{mole}^{-1}\cdot\text{hr}^{-1}\right]. \qquad (4)$$

Since some question might arise concerning the use of an oxidant other than oxygen, several k_{Cu} values at various temperatures were determined for simulated sulfate reactor fuel. These values were found to agree very well with values previously determined by the hydrogen-oxygen recombination method. These data are also plotted on Fig. 12.3.

Figure 12.3 shows the activation energy to be approximately the same for both sulfate and nitrate systems. The catalytic efficiency of cupric ion in the nitrate system is not so good as it is in the sulfate system. The value of k_{Cu} in the sulfate system is about 2.2 to 2.5 times greater than the value at the same temperature in the nitrate system.

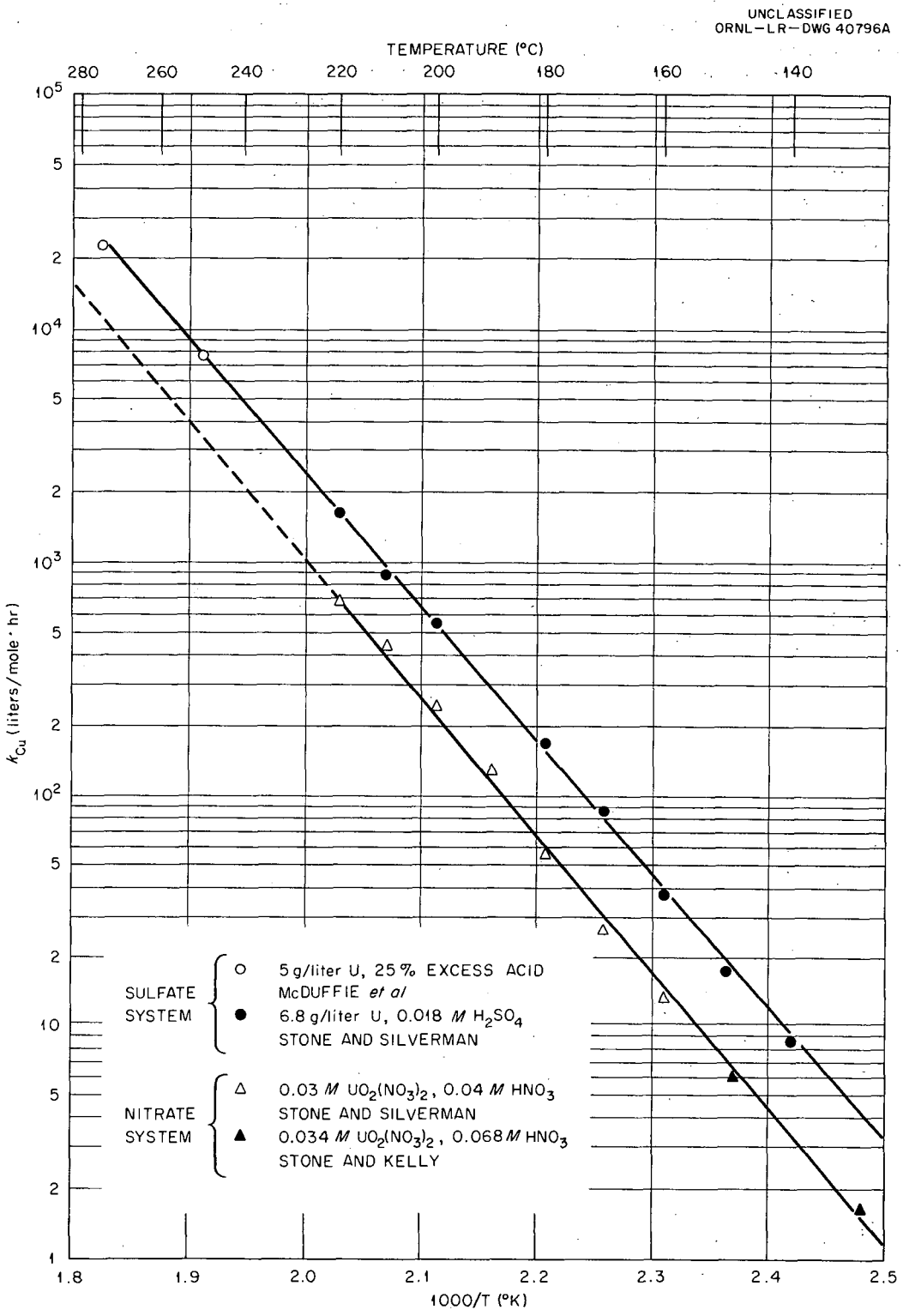

Fig. 12.3. Effect of Temperature on Recombination Rate; Comparison of Sulfate and Nitrate Systems.

For the same recombination efficiency, the reactor fuel would have to contain 2.2 to 2.5 times more cupric ion, or the operating temperature of the reactor would have to be increased about 15°C. Since the most desirable feature of the proposed nitrate system appears to be the possibility of raising the operating temperature without encountering second-liquid-phase difficulties, it would seem logical to raise the temperature rather than the cupric ion concentration.

Assuming a pressurizer pressure of 1432 psia and 100 psi of excess oxygen pressure, calculated maximum power densities, without hydrolytic gas evolution, are listed in Table 12.1 as a function of the nuclear average temperature.

Table 12.1. Maximum Power Density, Without Hydrolytic Gas Evolution

Solution: 0.02 m $Cu(NO_3)_2$, 0.04 m $UO_4(NO_3)_2$, 0.08 m HNO_3

Nuclear Average Temperature (°C)	Power Density (watts/cc)
280	21.5
260	12.3
220	1.4

These values indicate that from the standpoint of radiolytic gas recombination, the proposed fuel should be satisfactory.

REFERENCES

1. M. J. Kelly et al., HRP Quar. Prog. Rep. Apr. 30, 1959, ORNL-2743, p 240.

2. W. L. Marshall to H. F. McDuffie, Consideration of $UO_2(NO_3)_2$-HNO_3-$H_2O(D_2O)$ as a High Temperature Homogeneous Reactor Fuel, ORNL CF-59-6-100 (May 26, 1959).

3. H. F. McDuffie et al., "Catalysis of the Reaction Between Hydrogen and Oxygen," J. Phys. Chem., 62, 1030 (1958).

4. E. Peters and J. Halpern, "Homogeneous Catalytic Activation of Molecular Hydrogen by Cupric Perchlorate," J. Phys. Chem., 59, 793 (1955).

13. HETEROGENEOUS EQUILIBRIA IN AQUEOUS SYSTEMS

W. L. Marshall

C. J. Barton
J. S. Gill
G. M. Hebert
E. V. Jones
R. E. Moore
R. Slusher

13.1 TWO-LIQUID-PHASE-BOUNDARY TEMPERATURES FOR THE HRT FUEL SOLUTION AND ITS CONCENTRATES

Study of the boundaries of the liquid-liquid immiscibility region of the HRT fuel-solution system may help to explain some of the peculiarities of HRT operation.

It was shown in laboratory tests that when a synthetic HRT fuel solution was concentrated by evaporation of D_2O, the temperature for appearance of a second liquid phase fell to a minimum value of about 305°C at an eightfold concentration and rose slowly as the concentration was further increased.[1] At about the same time operation of the HRT revealed that the power-dependent loss of circulating-uranium inventory was aggravated by raising the reactor pressure but was practically eliminated by reducing the reactor pressure (see Chap. 1).* It was suggested that the minimum two-liquid-phase temperature of 305°C was important for reactor operation in that, when the reactor pressurizer temperature was higher than this, the temperature of local boiling would also be higher and the solution, if concentrated sufficiently, could reach the two-liquid-phase boundary; at this point the hundredfold increase in uranium concentration in the heavy-liquid phase and the concomitant hundredfold increase in fission power density would tend to aggravate the situation further until the second-liquid phase was heated to the decomposition point and converted into metal oxides or vaporized. If, on the other hand, the pressurizer temperature were maintained below 305°C, then local boiling would maintain the temperature of the fuel solution at or below this value; no amount of boiling concentration could, at these temperatures, cause the appearance of the concentrated second-liquid phase.

The second-liquid-phase temperatures were known to be elevated by the addition of acid to uranyl sulfate solutions. The minimum second-liquid-phase

*The total reactor pressure is nominally established by maintaining a given temperature in the pressurizer, where pure D_2O is kept in contact with its saturated vapor. This pressure is transmitted to the reactor circulating fuel system in the form of a hydraulic pressure acting through the agency of the condensed liquid in the pipe connecting the pressurizer to the fuel system. Fixing the pressurizer temperature thus fixes the reactor pressure, and it is convenient to discuss the situation in these terms.

temperature, which might be obtained upon concentrating such solutions, should likewise be raised upon the addition of acid. Liquid-liquid immiscibility boundary limits for synthetic HRT fuel solutions containing several different amounts of excess acid and for a number of concentrates of these solutions have now been determined by the procedure described previously.[1] The concentration factor is a number which, when multiplied by the molar concentration of a component in the original solution, gives the concentration of that component in the concentrate.

The concentrations of the metals, expressed as sulfates, in the original solutions based on analytical results were as follows:

$$UO_2SO_4 = 0.0257\ \underline{M}\ (25°C)$$
$$CuSO_4 = 0.0127\ \underline{M}$$
$$NiSO_4 = 0.0057\ \underline{M}$$
$$MnSO_4 = 0.0005\ \underline{M}$$

The two-liquid-phase temperature limits and concentration factors are plotted in Fig. 13.1. The minimum values are 305, 322, 330, and 342°C for excess acid concentrations of 0.0166, 0.0234, 0.0308, and 0.0413 M.

From the information obtained in these laboratory tests it might be expected that:

1. The present HRT fuel (0.0166 M excess acid) should become unstable in the presence of local hot spots if the pressurizer temperature is maintained at or above 305°C (1353 psia reactor total pressure).

2. A fuel containing 0.0234 M excess acid should become unstable with a pressurizer temperature maintained at or above 322°C (1706 psia total pressure).

3. A fuel containing 0.0308 M excess acid should become unstable with a pressurizer temperature maintained at or above 330°C (1895 psia total pressure).

If misoperation of the reactor should permit large quantities of solutes to be separated (and perhaps decomposed to oxides in the process), the composition of the remaining solution would be affected by this separation, and ultimately a steady state could be reached in which the increasing acidity of the solution would raise the minimum two-liquid-phase separation temperature until it reached that of the pressurizer; thereafter, no further separation should occur.

13.2 TWO-LIQUID-PHASE STUDIES*

It is of interest to know both the temperature of formation and the compositions of the two liquid phases which are formed in HRT fuels. Due to the small volume of heavy phase obtained from the dilute solutions the compositions of the phases in quartz-tube tests[2] were determined only on solutions having the uranium concentrated by a factor of 50 over HRT run 20 core solution.[3]

*This section contributed by J. C. Griess, H. C. Savage, R. S. Greeley, and S. E. Bolt of the Solution Corrosion Group, Chap. 14.

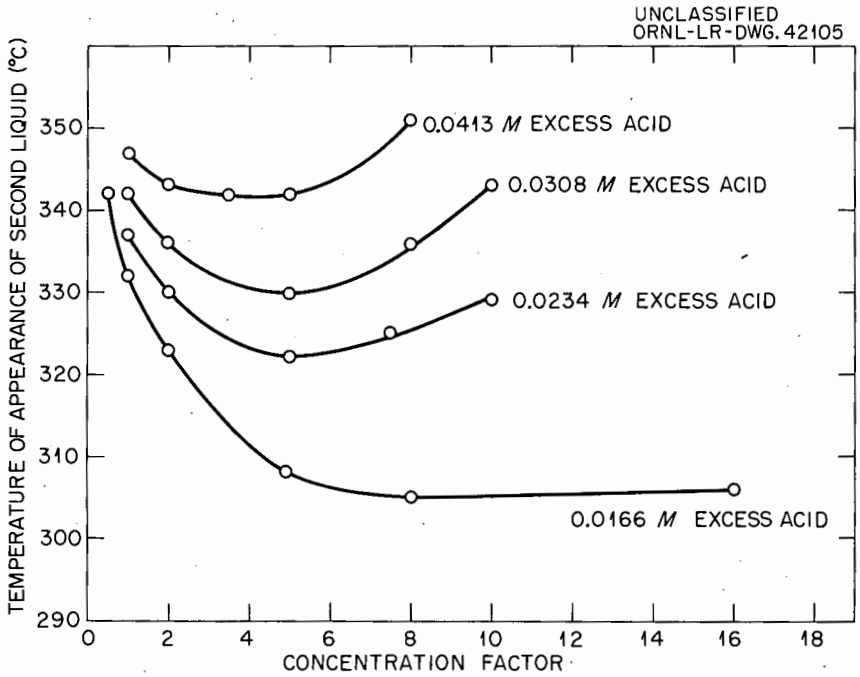

Fig. 13.1. Temperature of Appearance of the Second-Liquid Phase as a Function of Dilution and Concentration of HRT Fuel Containing Various Amounts of Excess Acid.

To check the quartz-tube data in an actual engineering system and to obtain large enough quantities of the heavy phase of the unconcentrated solution for analysis, several runs were made in a titanium loop. A titanium hydroclone and underflow pot in which the heavy phase could be collected were part of the system.

The procedure was as follows: The loop was loaded with the solution of interest and brought to about 300°C. From this point on, the temperature was raised slowly, and samples were withdrawn from the main circulating stream at approximately 2-degree intervals and analyzed spectrophotometrically. At the first indication of a loss of uranium the loop temperature was leveled off, and the separation of heavy phase was allowed to go to completion. Finally the hydroclone underflow pot was sampled in order to obtain a sample of the heavy phase. Unfortunately the geometry of the underflow pot was such that the heavy-phase samples contained some light phase.

Runs were made with solutions initially 1.25, 2.5, 5, and 10 times as concentrated as the core solution in HRT run 20 (viz., 0.030 m UO_2SO_4, 0.015 m $CuSO_4$, 0.007 m $NiSO_4$, and 0.018 m D_2SO_4 in D_2O). Solutions five times as concentrated as HRT core solution except containing 0.024 and 0.030 m D_2SO_4 (prior to concentration) were also run. Figure 13.2 is a plot of the second-phase temperature observed with these solutions versus the concentration factor of the solution. Due to temperature variations around the loop, the observed second-phase temperatures are accurate to only about 5°C. The curves drawn through the points in Fig. 13.2 were taken from data given by Marshall.[4] It can be seen that the loop data and the quartz-tube data are in fair agreement. The effect of acid in raising the two-liquid-phase temperature is evident from Fig. 13.2 and is also in agreement with the data of Marshall.

The U/SO_4, Cu/SO_4, Ni/SO_4, and free-acid/SO_4 ratios were calculated for each of the samples of heavy and light phase obtained during the runs. It was interesting to note that the Cu/SO_4 and Ni/SO_4 ratios in the light and heavy phases were about the same, whereas the U/SO_4 ratio was greater in the heavy phase than in the light phase. Unfortunately, because of the mixing of the light and heavy phases in the hydroclone underflow-pot samples, it was not possible to determine the exact heavy-phase composition. However, it was possible to make a material balance and to show that at least 80 to 90% of the heavy phase was separated from the light phase by the hydroclone and was collected in the underflow pot.

13.3 PHASE STABILITY OF RADIOACTIVE HRT FUEL SOLUTIONS

Liquid-liquid immiscibility temperatures of two samples of HRT fuel solution were determined by visual observation of phase separation in sealed silica tubes approximately three weeks after the samples were removed from the reactor during power operation. These tests were performed to check the validity of the assumption that the phase behavior of the actual reactor fuel solution is the same as that of the synthetic fuel solutions which were used in the stability tests. A detailed report of these tests has been prepared.[5] The immiscibility temperatures were determined to be 325 ± 1°C for one sample and 326 ± 0.5°C for the other. These values are slightly lower than the values predicted by experiments with synthetic fuel solutions (329.5 ± 0.5°C), but the discrepancies are small enough so that they could be accounted for by minor differences in composition between the synthetic and the reactor fuel solutions. There appears to be little reason to believe that the high radiation level which the fuel solution was exposed to in the reactor had a significant effect on its phase

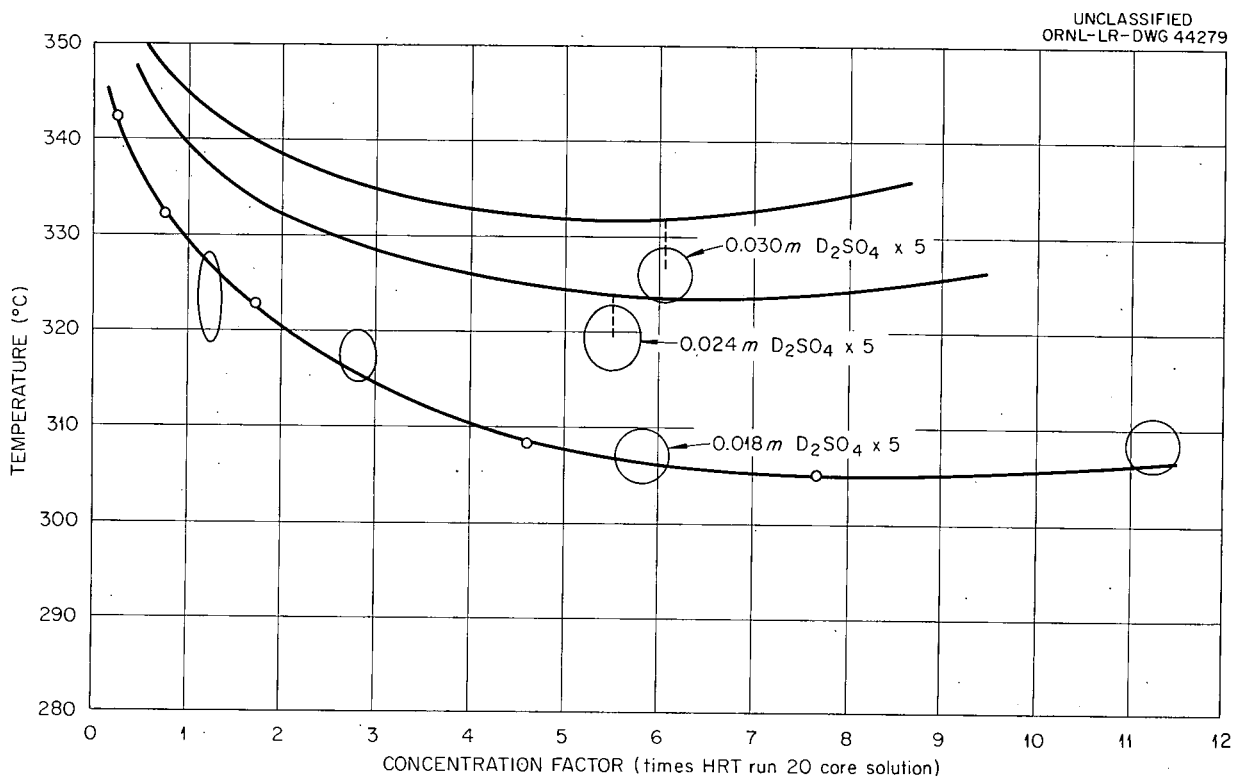

Fig. 13.2 Second-Liquid-Phase Temperatures for Concentrates of HRT Run 20 Fuel Solution.

behavior, at least after it had cooled to 2 r/ml. Dilution of fuel solution with 8 vol % H_2O_2 (which decomposed to produce a small desired oxygen overpressure), or with the same amount of H_2O, increased the immiscibility temperature about 2°C, but increasing the free D_2SO_4 concentration from about 0.017 to 0.04 m raised the immiscibility temperature from 326 to 345°C.

13.4 BEHAVIOR OF SYNTHETIC HRT FUEL SOLUTION IN THE PRESENCE OF METAL OXIDES*

The behavior of synthetic HRT fuel solutions in uncontaminated environment in quartz tubes has failed to explain completely the operational anomalies observed in the HRT; i.e., loss of uranium with increased power, power surges, power decreases, and effect of reduced pressure on operation. Using a rocking metal bomb, the behavior of synthetic HRT fuel solution in the presence of metal oxides has been investigated by determining the uranium content of solution samples removed from the bomb at temperature.[6] Results, using a synthetic fuel solution of 0.04 M UO_2SO_4, 0.02 M H_2SO_4, 0.005 M $CuSO_4$, Ni = 3 μg/ml, and pH = 1.7, with iron oxide (taken from building drain pipe and fired at 450°C) and zirconium oxide (prepared by firing $Zr(OH)_4$ at 650°C), are shown in Fig. 13.3.

The results suggest that the presence of metal oxide surfaces strongly influences the behavior of synthetic HRT fuel solution, with sorption of uranium from fuel solution steadily increasing with temperature. It will be noted that in one run with ZrO_2, samples were taken in irregular order with respect to temperature, showing that the uranium sorption is reversible. The coefficient (g of U per g of solid)/(g of U per kg of solution), shown as a function of temperature in Fig. 13.4, was calculated from results presented in Fig. 13.3, making allowance for depletion of the solution by sampling. Although quantitative deductions cannot be made, these results suggest that sorption of uranium on corrosion oxide may account for some of the anomalies observed in HRT behavior.[6]

13.5 TWO-LIQUID-PHASE REGIONS OF THE SYSTEMS UO_3-SO_3-H_2O AND UO_3-SO_3-D_2O

Investigation of the two-liquid-phase regions of the system UO_3-SO_3-H_2O was continued[7,8] and was extended to solutions, both in H_2O and in D_2O, containing initially up to 40 mole % of free H_2SO_4 or D_2SO_4. Comparison can now be made between the immiscibility behavior in H_2O and D_2O solutions. Experimental methods described previously are being used, in which the heavy and light immiscible liquid layers are equilibrated at temperature in Pyrex tubes contained in a rocking steel autoclave. The autoclave containing the tubes is cooled rapidly by immersion in an ice-water mixture; the heavy and light phases are separated, and each is analyzed for uranium and sulfate content.

Experimental data are presented graphically in Fig. 13.5. This method of representation, used previously,[7,8] is convenient for displaying data covering a wide range of concentration. It is evident that, as the temperature rises from 300 to 350°C, the heavy-liquid phase becomes very concentrated and the light-liquid phase becomes very dilute. As the temperature rises (see Fig. 13.5), the heavy phase approaches a molar ratio, UO_3/SO_3, of 1.0 with a very

*This section contributed by H. W. Hoffman and C. S. Morgan of the Engineering Research Section, Reactor Experimental Engineering Division.

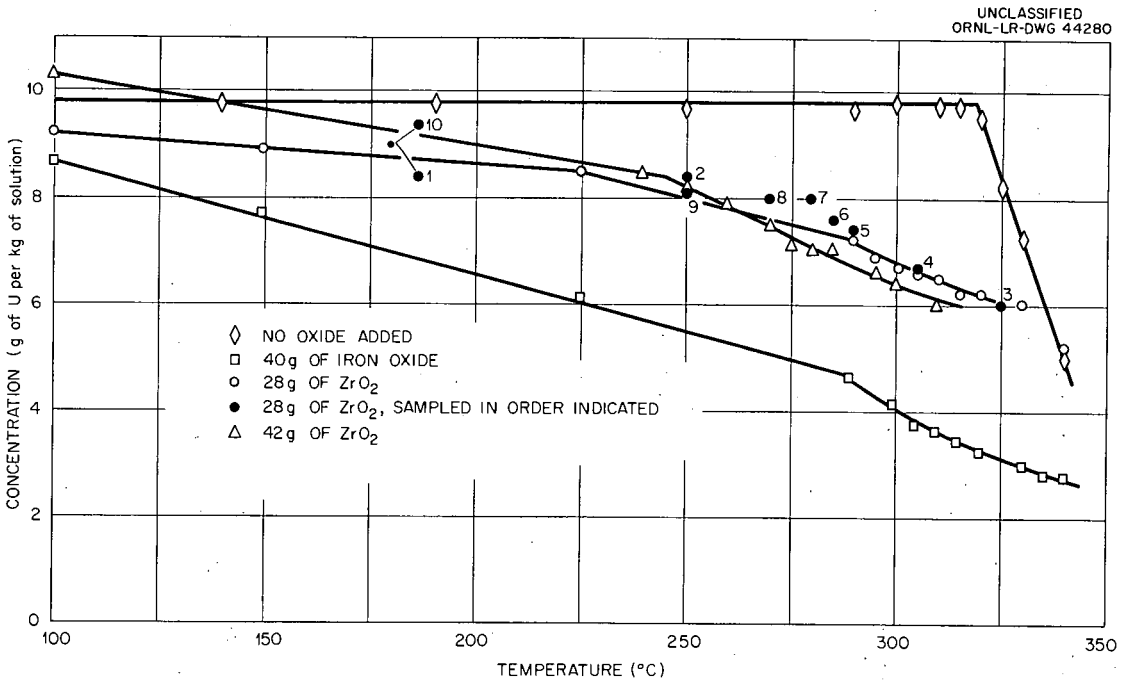

Fig. 13.3. Uranium Concentration of a Synthetic HRT Fuel Solution in the Presence of Metal Oxides.

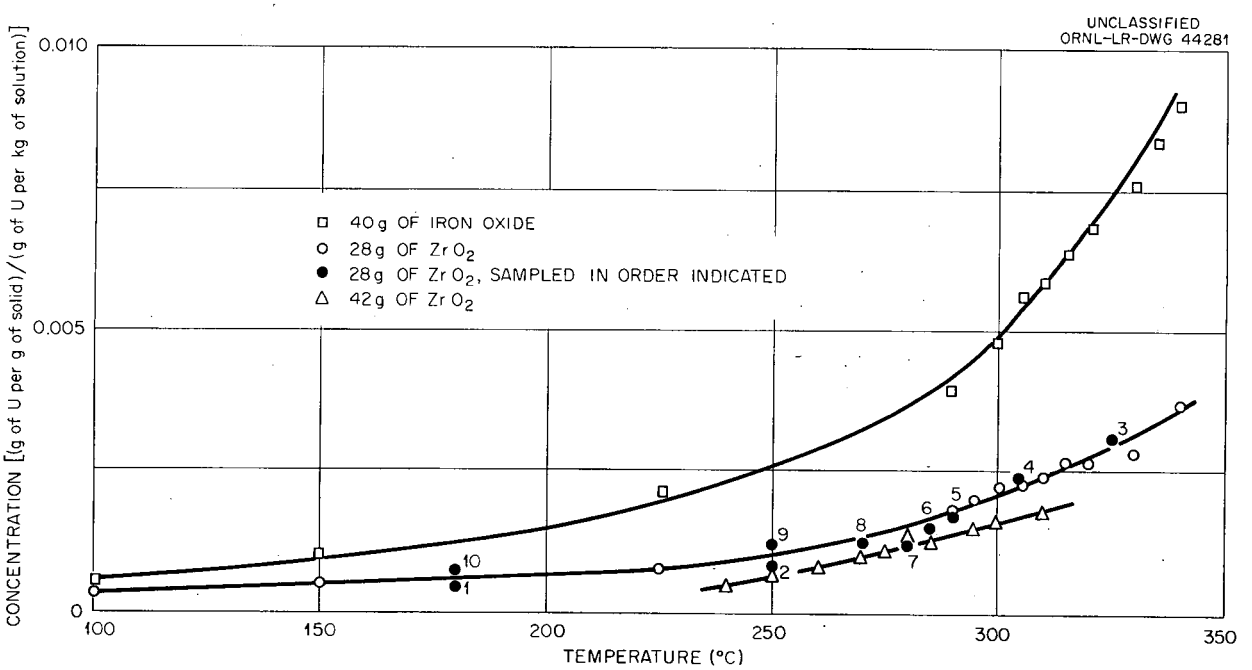

Fig. 13.4. Effect of Temperature on the Uranium Distribution Between a Synthetic HRT Fuel Solution and Metal Oxides.

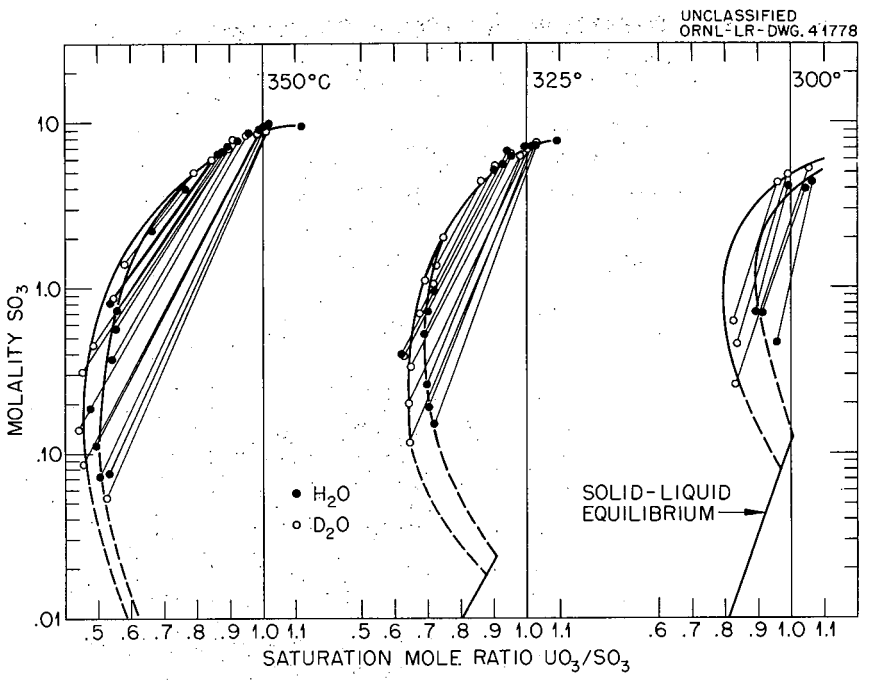

Fig. 13.5. Two-Liquid-Phase Regions; System UO_3-SO_3-$H_2O(D_2O)$.

low H_2O content, perhaps a "liquid-salt hydrate," e.g., $UO_2SO_4 \cdot 3H_2O$ or $UO_2SO_4 \cdot 4H_2O$. The equilibrium composition of the light phase, as indicated by the connecting lines, is in the range of 0.01 to 0.1 m SO_3. Since the current HRT fuel solution is in this same range, the heavy-liquid phase formed initially upon reaching the immiscibility boundary would probably be stoichiometric $UO_2SO_4 \cdot XH_2O$ which also contains $CuSO_4$ and $NiSO_4$ (see below).

Comparison of the UO_3-SO_3-H_2O and UO_3-SO_3-D_2O systems (Fig. 13.5) shows relatively little difference in solubility behavior at high concentrations of SO_3. However, at low concentrations of SO_3, the saturation molar ratios, UO_3/SO_3, are lower for the D_2O than for the H_2O system.

Since the homogeneous reactor fuel contains copper and nickel, preliminary investigations were made of the relative distribution of these two components between the light- and heavy-liquid phases of the system UO_3-SO_3-$H_2O(D_2O)$. Some of the experimental data for the multicomponent system UO_3-CuO-NiO-SO_3-H_2O are shown in Fig. 13.6. The initial systems contained 1.25 m UO_2SO_4, 0.23 m $CuSO_4$, and 0.24 m $NiSO_4$, plus 10 to 40 mole % excess H_2SO_4. The values for UO_2SO_4, $CuSO_4$, and $NiSO_4$ were held constant in order to attempt to represent approximately the data on three correlating curves, one for each cationic component.

If the saturation molar ratios, CuO/SO_3, NiO/SO_3, and UO_3/SO_3, either for the light or heavy phase at constant molality of SO_3, are added, the resulting summation ratio appears to fall on the immiscibility curve for the system UO_3-SO_3-H_2O, which does not contain the components CuO or NiO (see Fig. 13.5). This observation leads to the belief that violation of the immiscibility boundary curve by solution compositions near that of the HRT fuel will result in the separation of a heavy-liquid phase which corresponds approximately to stoichiometric UO_2SO_4, $CuSO_4$, and $NiSO_4$ plus H_2O; i.e., there will be little or no free acid in the heavy-liquid phase.

13.6 SOLID-LIQUID EQUILIBRIA: THE SYSTEM UO_3-CuO-NiO-SO_3-$H_2O(D_2O)$

Skeletal data for the system UO_3-CuO-NiO-SO_3-$H_2O(D_2O)$ at 300°C have been presented previously,[7,8] along with descriptions of experimental methods of study and the reasons for the particular approaches used. Since then, two additional binary curves for this system have been established over the concentration range from 0.02 to 0.2 m SO_3, bringing the total number of curves established in this range to: monary curves, 3; binary curves, 5; ternary curves, 1.

One of the new binary curves established the saturated solution compositions as a function of SO_3 concentration for mixtures in the system UO_3-CuO-SO_3-H_2O in which the two stable solid phases are $CuO \cdot 3UO_3$ and $UO_3 \cdot H_2O$. At 0.06 m total SO_3 a selected composition point from this binary appears in Fig. 13.7. It is very close to the solubility point for UO_3 in 0.06 m H_2SO_4. As the concentration of SO_3 is increased, saturation concentrations along the binary curve are followed until, at 0.12 m SO_3, an invariant point is found. At this point, at equilibrium, the solids present are still $CuO \cdot 3UO_3$ and $UO_3 \cdot H_2O$, but a new phase has appeared, a second-liquid phase. As the concentration of SO_3 becomes greater than 0.12 m, the $UO_3 \cdot H_2O$ solid phase disappears and the remaining phases appear to be $CuO \cdot 3UO_3$, a heavy-liquid phase, and a light-liquid phase.

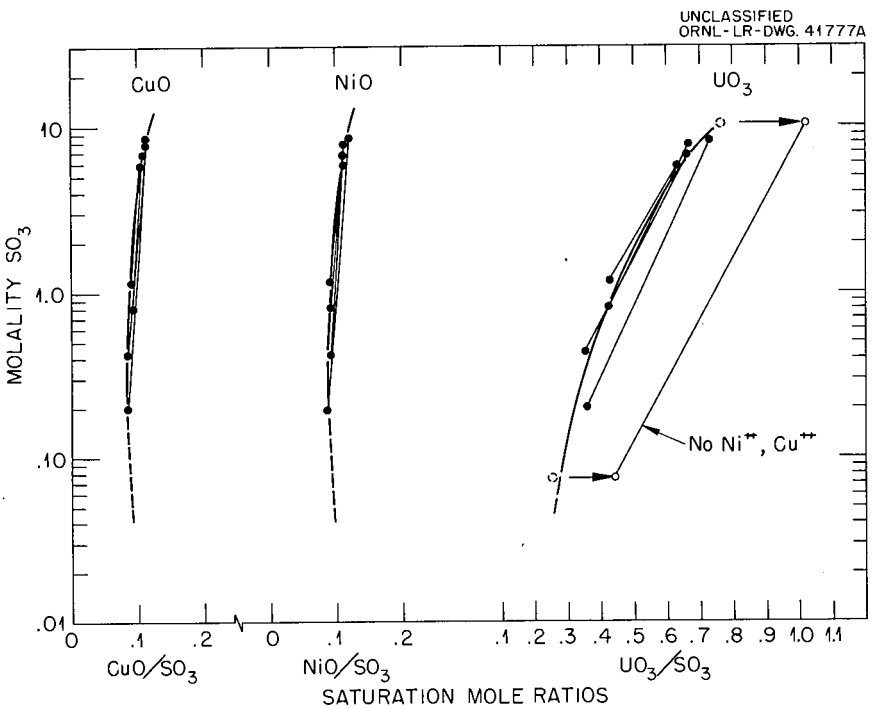

Fig. 13.6. Distribution of NiO and CuO Components in Two-Liquid-Phase Region, System UO_3-CuO-NiO-SO_3-H_2O at 350°C.

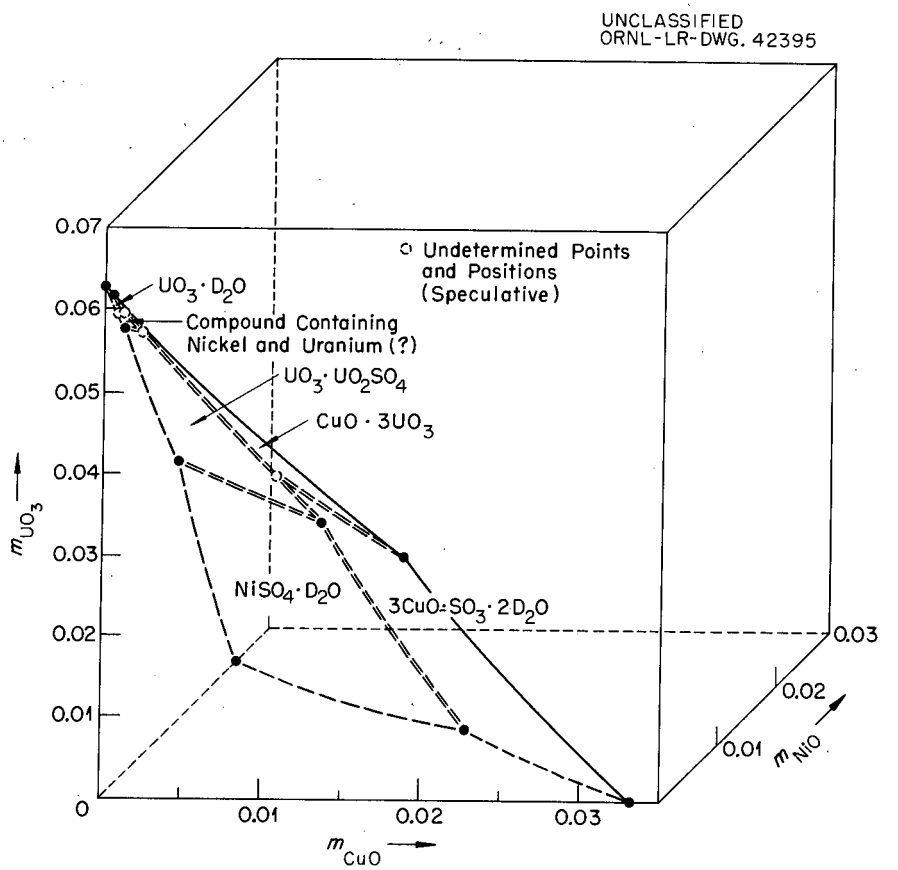

Fig. 13.7. System UO_3-CuO-NiO-SO_3-D_2O at 300°C (0.06 m SO_3).

The other new binary curve was established in the system UO_3-NiO-SO_3-H_2O over the same 0.02 to 0.2 m SO_3 concentration range. The two solids in equilibrium with the saturated solution phase are $UO_3 \cdot H_2O$, as identified by x-ray diffraction, and a compound which appears to contain nickel and uranium but is as yet unidentified. Figures 13.7 and 13.8 represent the latest over-all pictures of the multicomponent systems at 0.06 m and 0.08 m SO_3 concentrations.

Based upon two-liquid-phase data at higher temperatures and the solid-solid - liquid-liquid invariant point for these recent data, it is anticipated that at constant SO_3 concentration, liquid-liquid immiscibility will engulf considerable portions of the solid-liquid saturation region at temperatures higher than 300°C. If this is verified, solid-liquid equilibria studies at higher temperatures may become of less interest in connection with aqueous homogeneous reactor fuels than studies of liquid-liquid equilibria.

13.7 EFFECT OF UO_3/SO_3 MOLAR RATIO ON IMMISCIBILITY TEMPERATURE OF 0.10 m SULFATE SOLUTIONS

During the past six months increasing use has been made of a previously unpublished, although frequently discussed, relationship between solution composition and liquid-liquid immiscibility temperature. It appears that this temperature is a linear function of the UO_3:SO_3 molar ratio for a constant SO_3 concentration, as shown by Figs. 13.9 and 13.10. Figure 13.10 is a revised plot of information previously presented[9] for the system UO_3-SO_3-H_2O. Extrapolation of the data to low UO_3:SO_3 molar ratios suggests that the lines intersect the critical curve for the SO_3-H_2O system and that, accordingly, there must be solubility of UO_3 in the supercritical fluid of this system, confirming an observation which was experimentally established by Secoy in 1949.[10]

By analogy, it appears that the over-all molar ratio (U + Cu + Ni):SO_3 might also show a relationship with temperature which would be sufficiently close to linear to be useful, and preliminary evaluation of available data indicates that this may be the case.

Immiscibility temperatures obtained during the past six months for 0.10 m SO_3 systems having a varying UO_3/SO_3 molar ratio are shown in Fig. 13.11. The immiscibility temperature increased from 309°C for the 0.10 m UO_2SO_4 solution, i.e., $m_{UO_3}/m_{SO_3} = 1$, to 377.5°C for the 0.02 m UO_2SO_4 solution, i.e., $m_{UO_3}/m_{SO_3} = 0.2$. The critical temperature of the light-liquid phase portion of the latter solution was approximately 2°C above the immiscibility temperature. No phase separation was observed in the 0.01 m UO_2SO_4 solution, i.e., $m_{UO_3}/m_{SO_3} = 0.1$, up to the critical temperature (386°C). This observation indicates that when the UO_3/SO_3 molar ratio is less than about 0.18 for 0.10 m SO_3 solutions, UO_2SO_4 is soluble in supercritical sulfuric acid fluid.

13.8 LIQUID-LIQUID IMMISCIBILITY IN THE SYSTEM UO_3-SO_3-N_2O_5-H_2O

A fairly comprehensive study of liquid-liquid immiscibility boundary temperatures in the system UO_3-SO_3-N_2O_5-H_2O has been completed with 0.04, 0.08, and 0.16 m UO_2SO_4 solutions. A topical report on this work will be issued in the near future. The twofold purpose of this investigation was to determine whether uranyl sulfate - nitric acid solutions have significantly higher immiscibility temperatures than uranyl sulfate - sulfuric acid solutions and to

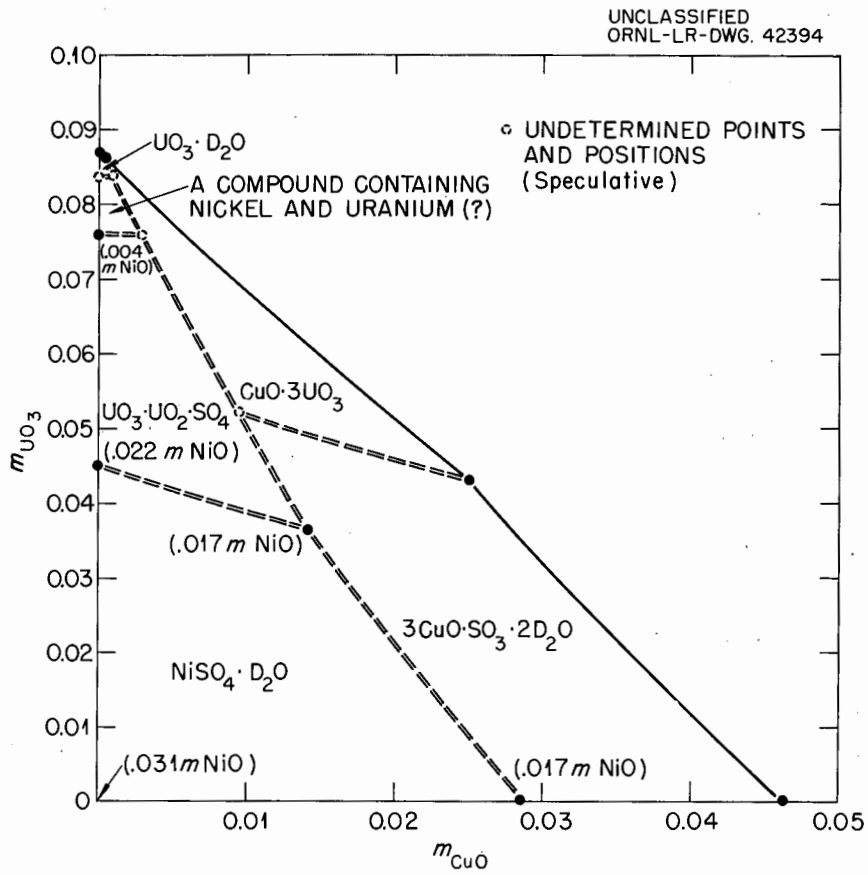

Fig. 13.8. Projection of UO_3-CuO Face of Cube Representing System UO_3-CuO-NiO-SO_3-D_2O at 300°C (0.08 m SO_3).

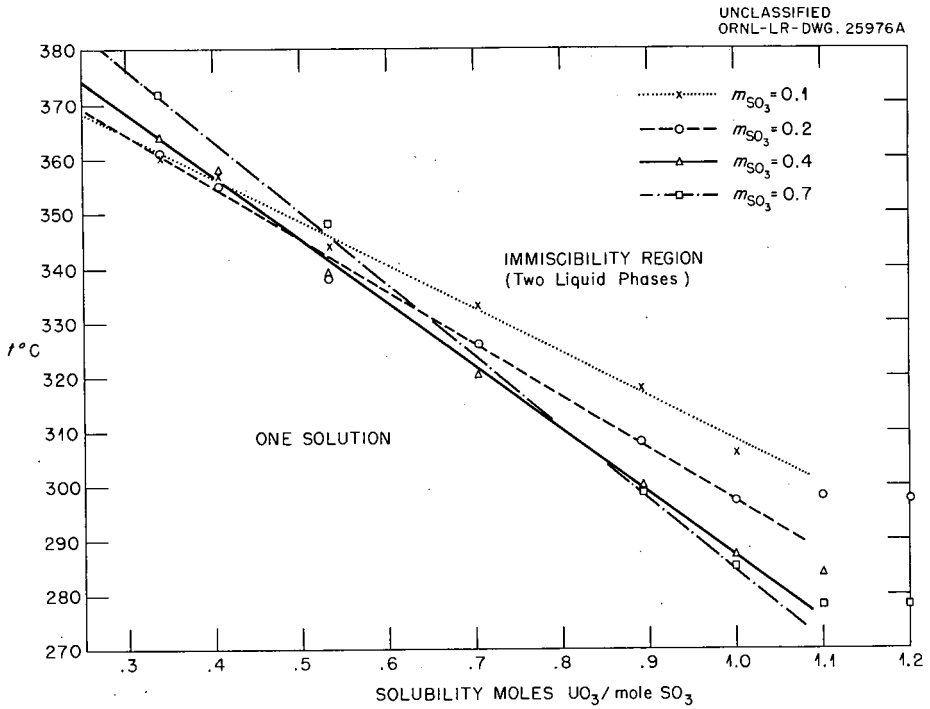

Fig. 13.9. Two-Liquid Phases, System UO_3-SO_3-H_2O.

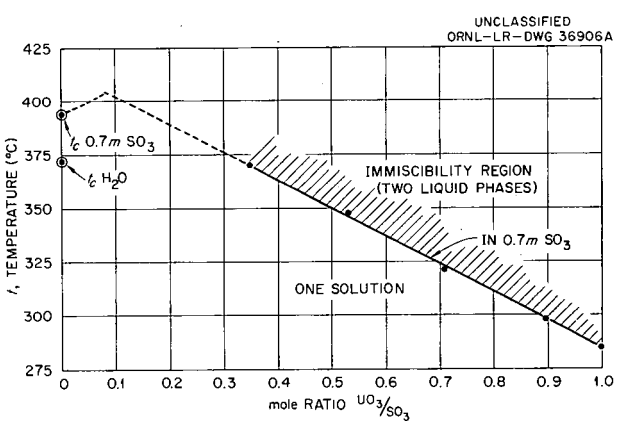

Fig. 13.10. Liquid-Liquid Immiscibility, System UO_3-SO_3-H_2O (0.7 m SO_3).

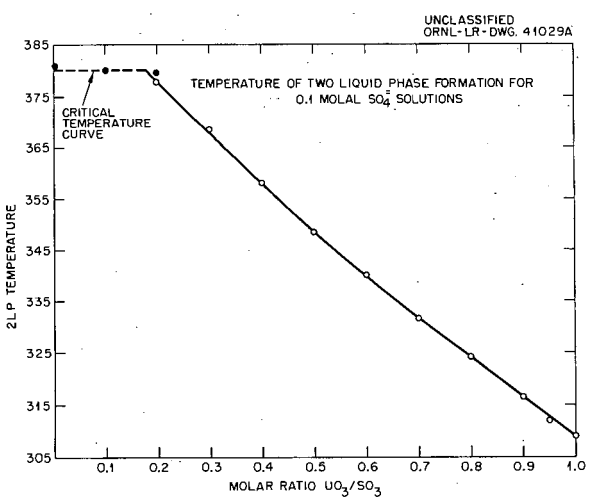

Fig. 13.11. Temperature of Two-Liquid-Phase Formation for 0.1 m SO_3^{--} Solutions.

furnish data which may help to provide a better understanding of the nature of the immiscibility phenomenon in uranyl sulfate solutions. The appearance and disappearance of a second-liquid phase was observed in small samples of solutions sealed in silica tubes suspended in a liquid nitrate bath. The metal container equipped with glass windows which was used to contain the nitrate bath is described in Sec. 13.10.1.

Comparison of the effects of nitric and sulfuric acids can be made either on the basis of the total H^+, in which sulfuric acid contains twice the H^+ as does an equimolar amount of nitric acid, or on the basis of the probable H^+ liberated by ionization. Since the second ionization constant of sulfuric acid is very low at the elevated temperatures of interest, it may be assumed that the HSO_4^- ions do not dissociate; under this assumption one mole of H_2SO_4 may be compared with one mole of HNO_3.

The data plotted in Fig. 13.12 reveal that sulfuric acid is initially more effective than nitric acid in raising the two-liquid-phase temperature if it is considered to be a monobasic acid, but less if it is considered a dibasic acid. The nitric acid and sulfuric acid curves for all three UO_2^{++} concentrations show "crossover" points at temperatures ranging from 353°C for 0.04 m UO_2^{++} solutions to 347°C for 0.16 m UO_2^{++} solutions. The molar ratios, UO_2^{++}/added H^+, at the "crossover" points were found to be relatively constant (0.455, 0.426, and 0.470, respectively, for 0.04, 0.08, and 0.16 m UO_2^{++} solutions). The significance of this constancy has not been established.

Data from Fig. 13.12, with additional data obtained by using mixtures of uranyl sulfate and uranyl nitrate as well as uranyl sulfate - sulfuric acid - nitric acid solutions, are plotted in Figs. 13.13, 13.14, and 13.15 vs the molar ratio, $NO_3^-/(NO_3^- + SO_4^=)$, in order to show the effect of substituting NO_3^- for $SO_4^=$ ions at different levels of added acid (assuming two moles of H^+ for each mole of H_2SO_4 added). It is apparent that, for solutions containing a low concentration of added acid, substitution of nitrate for sulfate raises the two-liquid-phase temperature, but for solutions of higher acid concentrations the substitution of nitrate for sulfate lowers immiscibility temperature through a minimum as the molar ratio, $NO_3^-/(NO_3^- + SO_4^=)$, is increased. Since the immiscibility temperature increases with increasing over-all acidity, it was first thought that this decrease might be due to increased transfer of nitrate from liquid to vapor phase with increasing temperatures. In order to determine the magnitude of this effect, immiscibility temperatures were determined for several 0.04 m uranyl sulfate solutions as a function of the fractional filling of the sample container at the separation temperature. The data plotted in Fig. 13.16 show that there is an approximately linear relationship between immiscibility temperature and volume fraction of liquid in the tube. Extrapolation of the lines to zero vapor volume gave the immiscibility temperature value marked "full tube" in Fig. 13.13. The data show that the dip in the curves at higher acidities is reduced but not completely removed by eliminating the vapor phase.

An interesting observation, made during the course of the volume-filling experiments, was that a solution containing 0.04 m UO_2SO_4, 0.02 m H_2SO_4, and 0.06 m HNO_3 ("full tube" immiscibility temperature 352.6°C) did not show a phase separation at temperatures up to 360°C, the maximum temperature to which it was heated, in a tube that was completely full at 351.5°C. This indicates that the immiscibility temperature may be raised significantly by the application of high pressures.

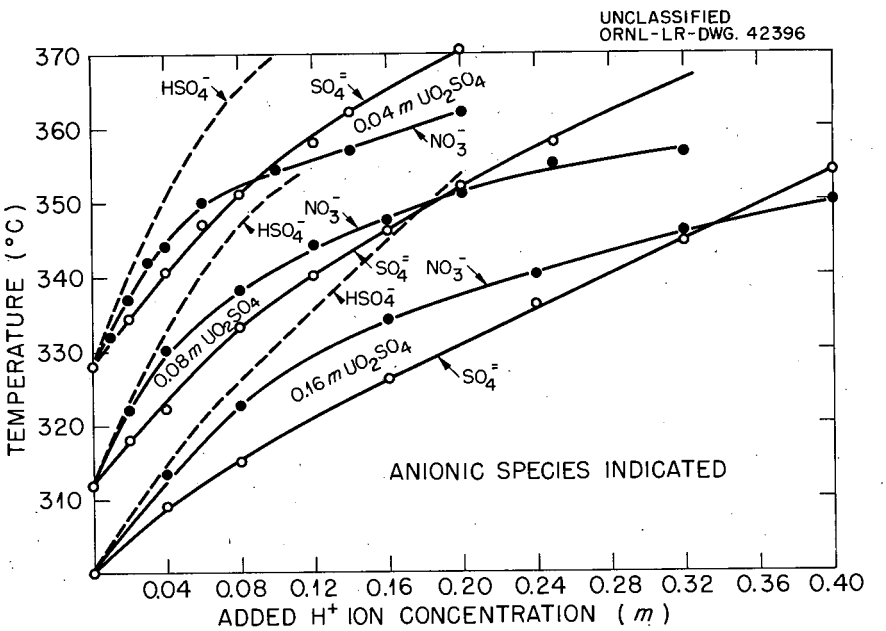

Fig. 13.12. Effect of HNO_3 and H_2SO_4 on Liquid-Liquid Immiscibility Temperature of UO_2SO_4 Solutions.

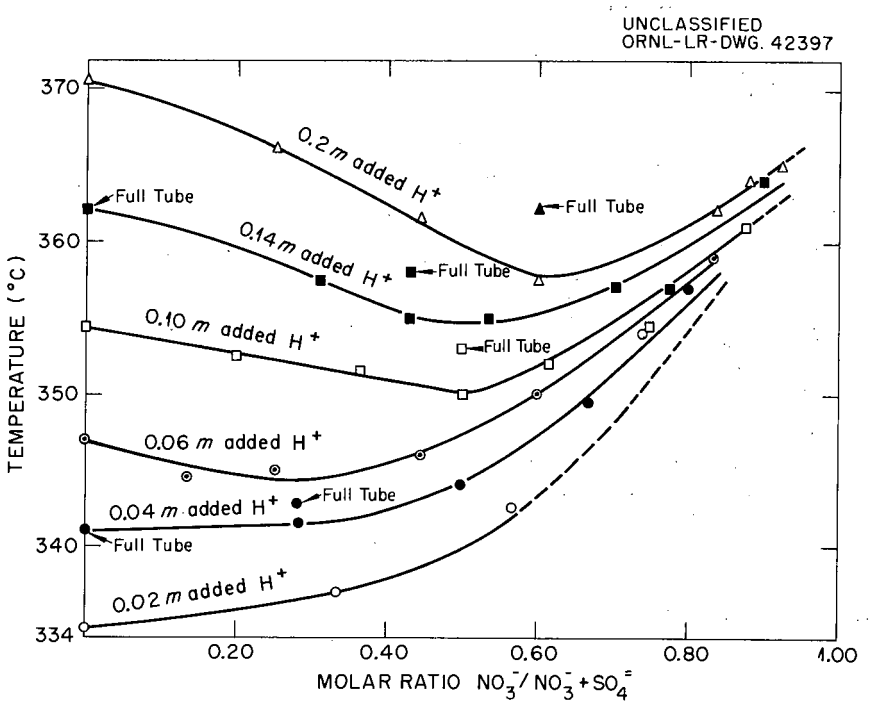

Fig. 13.13. Temperature of Separation of Heavy-Liquid Phase from 0.04 *m* UO_2^{++} Solutions as a Function of Acidity and Mole Ratio $NO_3^-/NO_3^- + SO_4^{--}$.

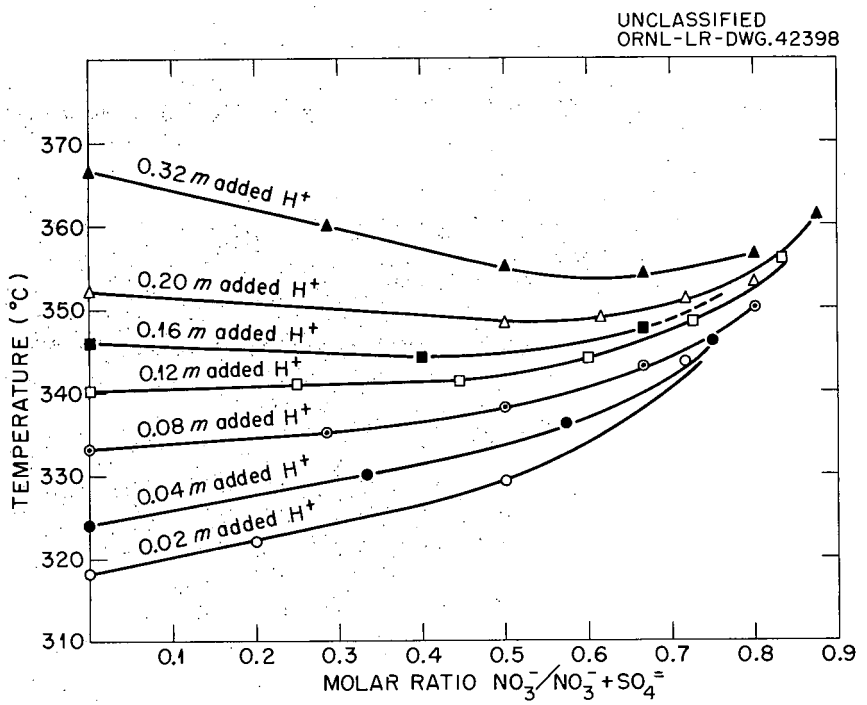

Fig. 13.14. Temperature of Separation of Heavy-Liquid Phase from 0.08 *m* UO_2^{++} Solutions as a Function of Acidity and Mole Ratio $NO_3^-/NO_3^- + SO_4^{--}$.

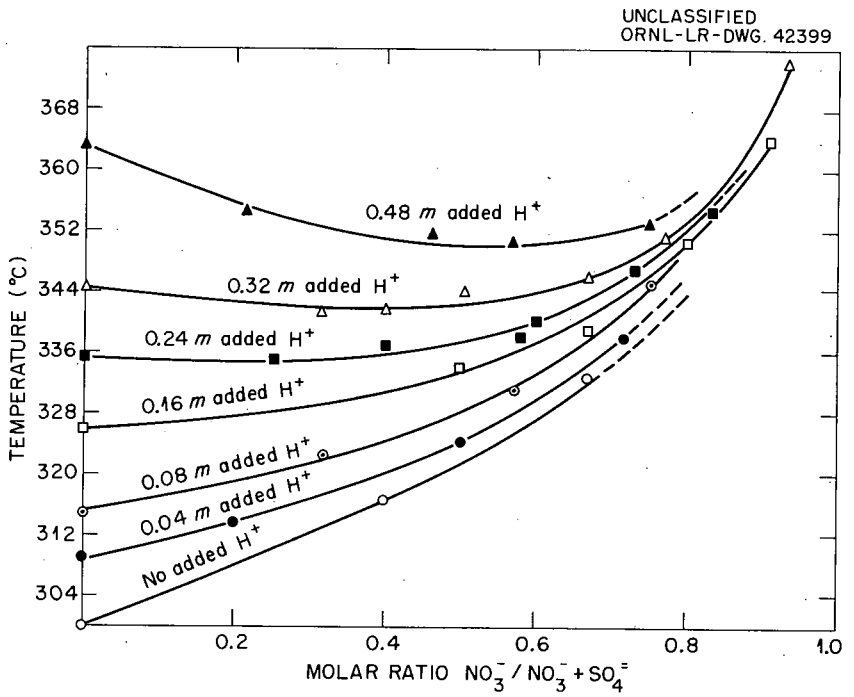

Fig. 13.15. Temperature of Separation of Heavy-Liquid Phase from 0.16 *m* UO_2^{++} Solutions as a Function of Acidity and Molar Ratio $NO_3^-/NO_3^- + SO_4^{++}$.

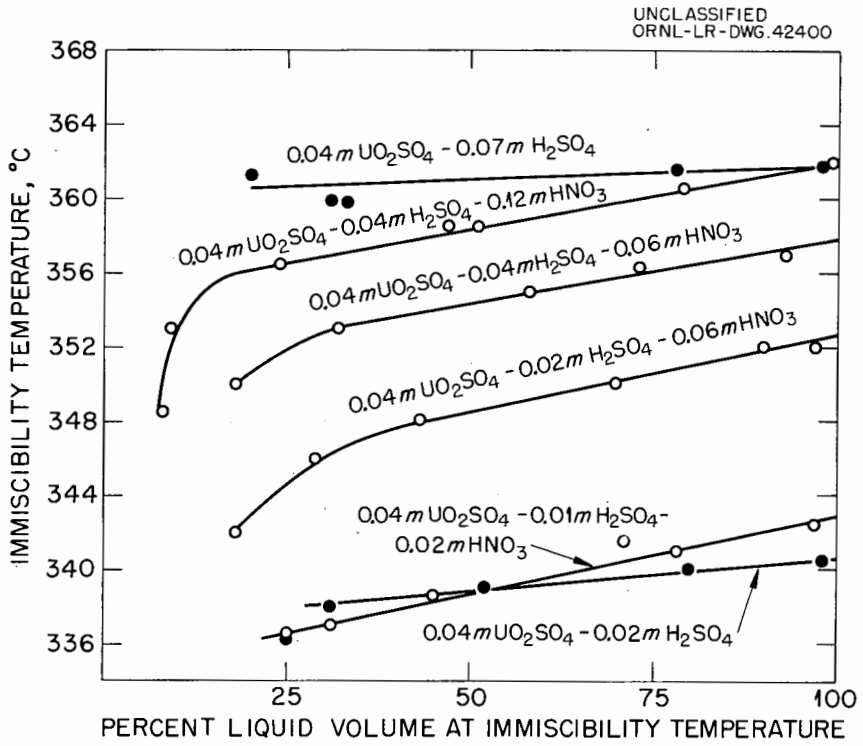

Fig. 13.16. Variation of Immiscibility Temperature with Volume Per Cent of Liquid in Sample Container.

From the standpoint of possible application to homogeneous reactors, the data obtained indicate that there is probably little advantage in using mixed nitrate-sulfate anions in uranyl solutions, as compared to UO_2SO_4-H_2SO_4 solutions, for the purpose of raising liquid-liquid immiscibility temperatures of aqueous homogeneous reactor fuels. The theoretical significance of the data is not clear at this time, but an interdependent relationship in this system between acidity and complexing of the uranyl ion seems to be indicated.

13.9 SYSTEMS BASED ON NITRATE

13.9.1 The System UO_3-N_2O_5-H_2O at 150-300°C

The investigation of the system UO_3-N_2O_5-H_2O from 150 to 300°C was continued in order to expand the range of study to lower and higher concentrations of HNO_3. Details concerning past data and experimental procedure were presented in the last progress report.[7] Since then, two memoranda were written to emphasize potential advantages and disadvantages of nitrate- compared to sulfate-based fuel systems.[11] Briefly, these pointed to absence of a liquid-liquid immiscibility region, oxides instead of salts as the stable solid phases, possible low or no radiolytic production of free N_2 gas, possible corrosion benefits, and potential economies in fuel processing. It was recalled that earlier experimental investigations at high temperature had been undertaken on concentrated nitrate solutions and that these current phase studies were the first to be undertaken in the low-concentration range. In addition to gaining an insight into the over-all phase behavior of uranyl nitrate solutions for use as homogeneous reactor fuels, precise and accurate measurements are being obtained to glean further information on the general behavior of uranium salts at elevated temperature in aqueous media. Information of this general type can be applied to the further understanding of the behavior of sulfate systems.

The best experimental data to date are shown in Fig. 13.17. In essence, the solubility curves are extended down to 5×10^{-4} $\underline{m}$ total NO_3^- and up to 5 $\underline{m}$ total NO_3^-. The apparent reversal of curvature in the 10^{-2} to 10^{-4} $\underline{m}$ NO_3^- range may be real, as evidenced by repeated agreement of data. In fact, as the NO_3^- concentration approaches zero, the saturation mole ratio, UO_3/NO_3^-, must approach infinity since there is a finite solubility of UO_3 in pure H_2O.

The data from 10^{-2} to 10^{-4} $\underline{m}$ NO_3^- were obtained by a new method. When the pH values at 25°C for pure HNO_3-H_2O solutions and for several HNO_3-H_2O solutions containing dissolved UO_3 were plotted against the logarithm of the calculated "free acid" concentration for each solution, i.e., (total $\underline{m}_{NO_3^-}$) - $2(\underline{m}_{UO_2(NO_3)_2})$, then all values fell approximately on the same curve (Fig. 13.18). Therefore, the pH at 25°C of an experimental sample, saturated at high temperature with UO_3, was measured; reference to the curve of Fig. 13.18 gave the "free acid" concentration required for this pH. Uranium was analyzed by the coulometric-titration method. From these two values the molar ratio, UO_3/NO_3^-, was obtained at very low concentrations, where the direct titration of HNO_3 is very difficult due to the low total concentration of NO_3^- and the small volume of the sample (5 ml).

The solubility data obtained to date give further evidence of the thermal phase stability of the nitrate system. There is, however, some uncertainty concerning NO_2-HNO_3-N_2O_5 equilibria in the vapor and liquid phases and the effect of oxygen overpressure on this system. Also, the solubility relationships must be known to temperatures higher than 300°C.

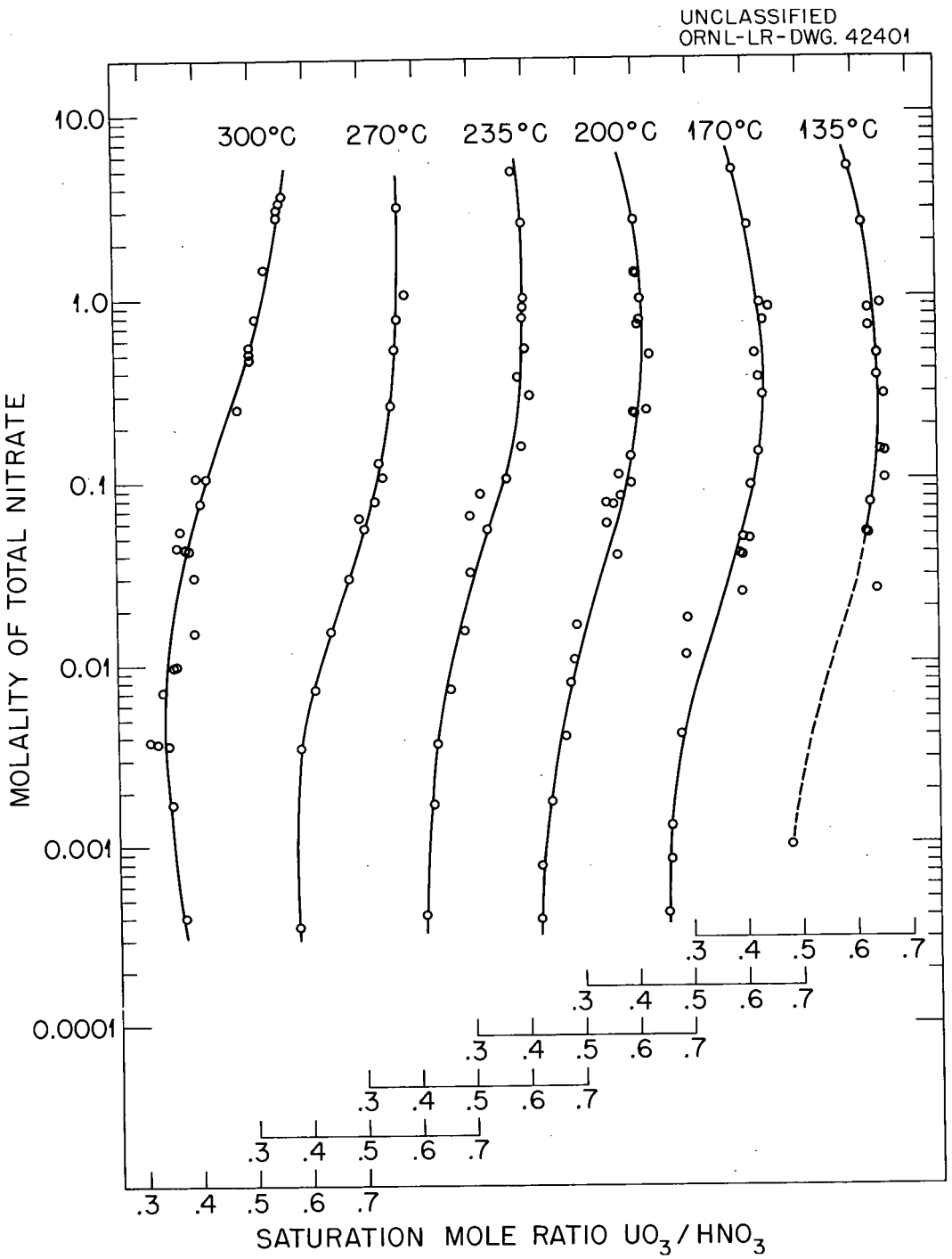

Fig. 13.17. The Solubility of $UO_3 \cdot H_2O$ in HNO_3-H_2O Solutions.

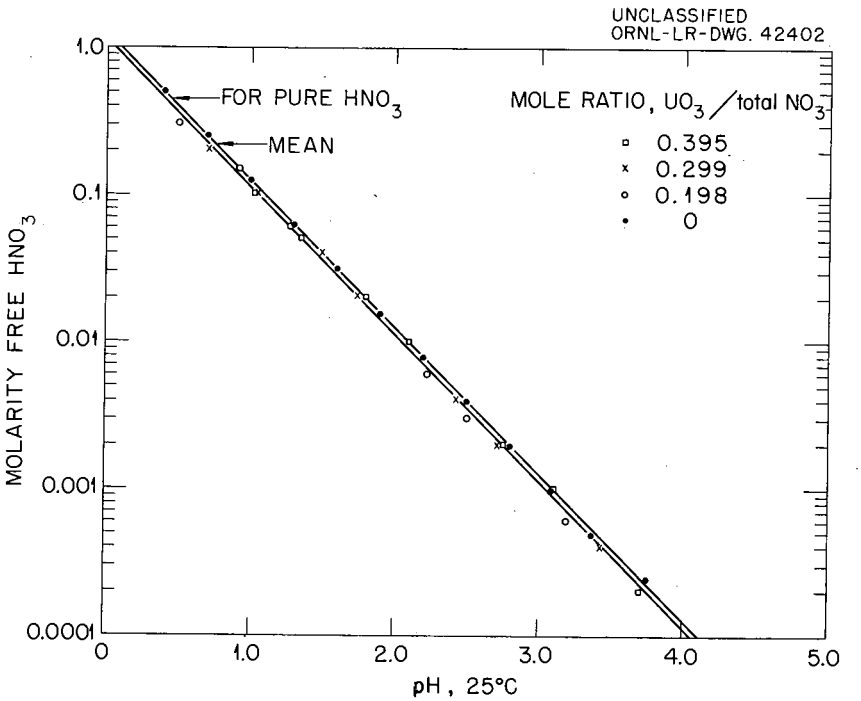

Fig. 13.18. The pH at 25°C of $HNO_3 \cdot H_2O$ and UO_3-HNO_3-H_2O Solutions.

13.9.2 The Multicomponent System UO_3-CuO-NiO-N_2O_5-$H_2O(D_2O)$ and Its Relation to Homogeneous Reactors

The encouraging results of the preliminary investigation of the system UO_3-N_2O_5-H_2O called for further consideration of nitrate-based homogeneous reactor fuels[11] in order to be assured that no phase-stability difficulties might arise with fuels containing copper and nickel in addition to uranium. In particular, it was considered important to establish the general nature of the solid phases and to ascertain whether there would be any regions of very low solubility.

The preliminary experimental approach was the same as that used for the over-all study of solid-liquid equilibria in the multicomponent sulfate system. Briefly, excess amounts of particular solids were added to HNO_3-H_2O solutions of 0.02, 0.06, 0.2, and 0.6 $\underline{m}$ HNO_3 in pressure vessels. The solution-solid mixtures were equilibrated successively at two different temperatures, 200 and 300°C; at each temperature liquid samples were withdrawn for analysis.

After a run the vessels were cooled rapidly to low temperature, and the solids were removed and submitted for x-ray diffraction analysis. The starting compositions were so chosen as to give the maximum number of solid phases at constant temperature, saturation pressure, and variable N_2O_5 concentration, thus producing monary, binary, and ternary curves for the five-component system.

The results showed no apparent significant decreases in solubility in the region from 0.02 to 0.6 $\underline{m}$ total NO_3^-. From these preliminary data, compositions having summation mole ratios, $(\underline{m}_{UO_3} + \underline{m}_{CuO} + \underline{m}_{NiO})/\underline{m}_{NO_3^-}$, of less than 0.3 to 0.4 appear to be phase stable at 300°C for this system. The solid phases identified were all oxides, CuO, NiO, and $UO_3 \cdot H_2O$, as had been expected for the nitrate system. One unidentified oxide, presumably a double oxide of Ni and U, was found. The oxide $CuO \cdot 3UO_3$ was also identified. Based on the preliminary evaluation, the system UO_3-CuO-NiO-N_2O_5-H_2O appears to present no thermal phase-stability problem in the concentration ranges of specific homogeneous reactor interest at least to 300°C. It is anticipated that the analogous D_2O system will show no marked deviation from the H_2O system although this proposition will be checked experimentally.

13.10 APPARATUS DEVELOPMENT FOR HIGH TEMPERATURE AQUEOUS STUDIES

13.10.1 Liquid-Salt Bath

In the synthetic method for the determination of phase equilibria, known mixtures of components are placed in containers and are heated or cooled. The temperature at which a phase transition occurs is noted by some means; this defines a saturation limit for the particular synthetic mixture. The usual procedure for aqueous systems at high temperature involves sealing a known mixture in a glass tube and visually observing the phase-transition temperature. The equipment originally consisted of cylindrical aluminum block containing a slit for observation.[12] These blocks were heated with spiral-wound resistance wire. Later, stirred liquid-salt baths in glass containers were used in order to minimize the effects of temperature gradients.[13] These baths, however, constituted a potential hazard since, upon the explosion of a tube, liquid salt was sprayed up and out of the bath and, usually, the all-glass container would break.

In order to remedy these difficulties metal units have been developed to contain the liquid salt, and these are now in use. Figure 13.19 shows such a unit. The container units have heavy-duty glass windows on the back and front faces. The top is covered with a metal plate, and the whole unit is placed in a wooden box with front and back windows. A light is placed in back of the box and a short-focal-length telescope is used for observation of phase transitions. A constant amount of heat is supplied by a hot plate beneath the unit, and a variable amount is furnished by a bent Inconel-covered Calrod heater immersed in the bath and connected through a variable transformer. The capillary tubes containing the compositions being tested are agitated periodically, while they are heated or cooled in the bath, by means of a Vibro-tool connected to an interval timer in the manner previously described.[12,14] This equipment was used for the determination of liquid-liquid immiscibility boundaries by the synthetic method for the systems UO_3-SO_3-N_2O_5-H_2O, UO_3-CuO-NiO-SO_3-D_2O, and UO_3-SO_3-H_2O discussed in this chapter.

13.10.2 Pressure Vessels for Use from 100 to 500°C

An all-titanium pressure vessel of 50-ml capacity was developed for routine use from 100 to 500°C. The pressure vessel was tested up to 500°C and to pressures of the order of 5000 psi. Following some further modification in the high-pressure seal, the unit is believed to be ready for use. Additional vessels, together with temperature control equipment, are to be constructed in order to study solid-liquid equilibria above 325°C, the approximate upper limit for sampling operations at present.

A similar steel pressure vessel, which contains an all-platinum liner, top, and capillary sampling tube, is approaching satisfactory completion. After final modification and acceptance, additional platinum-lined vessels will be constructed for the study above 300°C of solutions which are considerably corrosive to other materials of construction.

REFERENCES

1. W. L. Marshall, J. S. Gill, and R. E. Moore, Two-Liquid-Phase Temperature Limits for the Homogeneous Reactor Fuel Solution and Its Concentrates; Comments on Solid-Liquid Equilibria, ORNL CF-59-8-41 (Aug. 11, 1959).

2. C. J. Barton et al., Phase Stability of Homogeneous Reactor Hot Fuel Solutions, ORNL CF-59-8-72 (Aug. 18, 1959) and W. L. Marshall et al., Two-Liquid-Phase Temperature Limits for the Homogeneous Reactor Fuel Solution and Its Concentrates, ORNL CF-59-8-41 (Aug. 11, 1959).

3. W. L. Marshall et al., HRP Quar. Prog. Rep. Apr. 30, 1959, ORNL-2743, p 230.

4. W. L. Marshall, paper presented at HRP monthly information meeting, Oct. 1, 1959.

5. C. J. Barton et al., Phase Stability of Homogeneous Reactor Hot Fuel Solutions, ORNL CF-59-8-72 (Aug. 18, 1959).

6. R. N. Lyon and C. S. Morgan, An Explanation of Pips and Poops in the HRT, HRP No. 59-191 (Oct. 22, 1959).

7. W. L. Marshall et al., HRP Quar. Prog. Rep. Apr. 30, 1959, ORNL-2743, pp 227-238.

8. W. L. Marshall et al., HRP Quar. Prog. Rep. Jan. 31, 1959, ORNL-2696, pp 205-214.

9. H. W. Wright and W. L. Marshall, HRP Quar. Prog. Rep. Oct. 1, 1952, ORNL-1424, p 108.

10. C. H. Secoy, Chemistry Division Quar. Prog. Rep., Dec. 31, 1949, ORNL-607, pp 33-38.

11. W. L. Marshall to H. F. McDuffie, Consideration of $UO_2(NO_3)_2$-HNO_3-$H_2O(D_2O)$ as a High-Temperature Homogeneous Reactor Fuel, ORNL CF-59-5-100 (May 26, 1959) and ORNL CF-59-8-27 (Aug. 5, 1959).

12. W. L. Marshall et al., J. Chem. Educ., 31, 34 (1954).

13. F. E. Clark et al., J. Chem. and Eng. Data, 4, 12-15 (1959).

14. J. S. Gill and W. L. Marshall, The Compound $CuO \cdot 3UO_3$, ORNL CF-59-8-95 (Aug. 25, 1959).

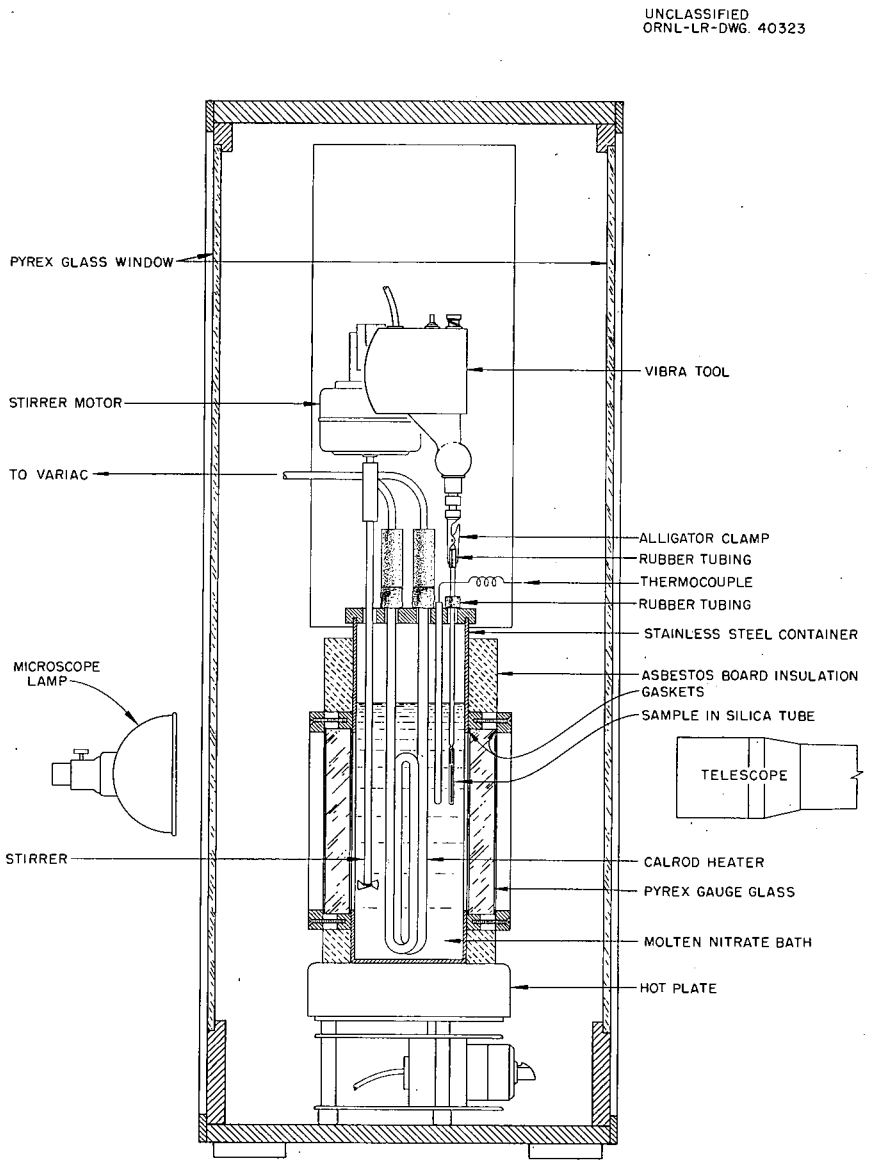

Fig. 13.19. Equipment for Solubility Studies at Elevated Temperatures.

14. SOLUTION CORROSION

J. C. Griess H. C. Savage

S. E. Bolt D. N. Hess
J. L. English P. D. Neumann
R. S. Greeley W. C. Ulrich

14.1 DYNAMIC SOLUTION CORROSION

14.1.1 Corrosion in Uranyl Nitrate Solution

Recently it has been suggested that uranyl nitrate solutions be considered as homogeneous reactor fuels.[1] Some corrosion data had been obtained for 0.17 *m* $UO_2(NO_3)_2$,[2] but no runs had been made in the 100A loops with more dilute solutions and with solutions containing copper nitrate. Therefore two runs were made with a solution containing 0.03 *m* $UO_2(NO_3)_2$, 0.02 *m* $Cu(NO_3)_2$, and 0.10 *m* DNO_3 in heavy water.[3] Type 347 stainless steel coupons and a variety of alloys as pin-type specimens were exposed in these runs.

In the previous runs with 0.17 *m* $UO_2(NO_3)_2$, it was found that in the presence of about 1000 ppm oxygen, Cr(VI) concentrations increased rapidly and affected the corrosion results (viz., corrosion was inhibited by the Cr(VI)).[2] However, in the complete absence of oxygen, corrosion of stainless steel was much greater, corrosion rates of 40 to 300 mpy being observed. Therefore in the present runs it was decided to use as low an oxygen concentration as possible in order to minimize the buildup of Cr(VI) and yet prevent the rapid corrosion of stainless steel. In the first run, 10 psi of oxygen was added initially, and this was consumed by corrosion during the run. The Cr(VI) concentration was less than 10 ppm in the last half of the run, and extensive crevice corrosion occurred. Stainless steel clamping bands holding the specimen holders together were corroded entirely through. In the second run, 25 psi of oxygen was added initially. This was sufficient to maintain oxygen in the solution throughout the run. There was no significant crevice corrosion, but in this case the Cr(VI) concentration increased to 200 ppm. It has been found in the sulfate system that this amount of Cr(VI) affects the results,[4] and therefore future runs will have to be made in a titanium system where the buildup of Cr(VI) from oxidation of the stainless steel loop does not occur.

Table 14.1 is a list of the corrosion results obtained with the various alloys at low and at high velocities in the run with 25 psi oxygen and also indicates for type 347 stainless steel the critical velocity observed. The rates and critical velocity compare favorably with those observed in uranyl sulfate solutions similar to that used in HRT run 20. These rates should be considered preliminary prior to confirmation in runs in the titanium loop. One alloy of interest is the 304 stainless steel containing 0.5% Pt. Corrosion rates at both

low and high velocities were considerably lower than for the other stainless steels tested. Greater corrosion resistance of this alloy has been observed previously in the sulfate system at low velocity.[5]

Table 14.1. Corrosion Rates of Alloys Exposed to 0.03 *m* $UO_2(NO_3)_2$ + 0.02 *m* $Cu(NO_3)_2$ + 0.10 *m* DNO_3 in D_2O for 200 hr at 250°C

Alloy	Corrosion Rate 17 fps (mpy)	Corrosion Rate 70 fps (mpy)	Critical Velocity (fps)
Carpenter 20Cb	32	580	
CD4MCu (rolled)	9	290	
Incoloy	30	440	
304 stainless steel	10	300	
304 SS + 0.1% Pt	4	300	
304 SS + 0.5% Pt	1.6	14	
304 SS + 1.2% Cu	7	340	
347 stainless steel	27	290	20-30
Titanium RC-55	0.1	0.3	
Titanium - 6% Al, 4% V	0.0	0.3	
Titanium - 4% Al, 4% Mn	0.0	0.3	
Zircaloy-2	+*	+*	

*Gained about 1 mg/cm^2.

It was of interest to determine the content of oxides of nitrogen in the vapor phase resulting from the thermal decomposition of uranyl nitrate at 250°C. Vapor-phase samples were withdrawn and analyzed for total oxides of nitrogen. Assuming that these oxides were solely from the equilibrium HNO_3 (solution) $\rightleftarrows$ HNO_3 (vapor), it was found that at 250°C with a vapor-to-liquid volume ratio of 0.25, approximately 1% of the nitric acid originally in solution was in the vapor phase. This percentage could, of course, be decreased by decreasing the vapor-to-liquid volume ratio further.

In the first run, the nickel concentration in solution increased markedly due to the corrosion of the stainless steel clamping bands, and a small amount of uranium appeared to be lost from solution. However, in the second run the solution was chemically stable except for the loss of nitric acid to the vapor phase discussed above.

14.1.2 Loop Descaling with Deoxidine-170

In the previous report it was observed that Deoxidine-170, a proprietary compound containing inhibited phosphoric acid, was a satisfactory solvent for corrosion-product scale in stainless steel loops.[6] One difficulty mentioned, however, was that the corrosion rate of titanium specimens was 600 mpy. In order to determine whether decreasing the concentration of Deoxidine-170 would decrease the corrosion rate on titanium and still descale loops effectively, runs were made at several dilution levels. Each run with Deoxidine-170 was preceded by a run with 0.17 *m* UO_2SO_4 at 250°C to film over the loop and corrosion specimens.

The corrosion rate of titanium RC-55 specimens decreased from 600 mpy to 250, 34, and 5 mpy as the Deoxidine was diluted from 100% to 75, 50, and 25%, respectively. Essentially all of the scale put on the corrosion specimens by the pretreatment was removed with the 100, 75, and 50% Deoxidine solutions within 36 hr (viz., 2 to 4 mg/cm^2). However, in the 25% Deoxidine solution only about 0.5 mg/cm^2 was removed. Therefore the 50% Deoxidine solution appeared to be optimum from the standpoint of a low titanium corrosion rate and complete scale removal.

Titanium-6% Al, 4% V specimens were also exposed in the runs. These specimens had considerably greater corrosion rates than the commercially pure titanium RC-55; e.g., about 260 mpy in the 50% solution. However, this represents a weight loss of only about 10 mg/cm^2 in the 36 hr required to complete the scale dissolution.

Analysis of the defilming solution after circulation showed that the uranium associated with the scale was dissolved but that only about 20% of the chromium associated with the scale was soluble.

14.2 LABORATORY CORROSION STUDIES

14.2.1 Stress-Corrosion Cracking of Cast Austenitic Stainless Steels

Additional tests with cast type 347 stainless steel from several different heats have confirmed previously reported data;[7] that is, stress-corrosion cracking in either chloride-containing water or boiling 42% $MgCl_2$ was observed only when the specimens were stressed to permanent deformation or when the surface of the metal had been cold-worked. Simple-beam type specimens stressed as high as 30,000 psi (with strain gauges) have not cracked in boiling 42% $MgCl_2$ during exposure periods as long as 100 hr. Under the same conditions wrought stainless steel cracks in 5 hr or less. Similarly, cracking was not observed in chloride-containing water during test periods that lasted as long as 2500 hr so long as the cast material was not permanently deformed. Wrought materials almost always crack under the same conditions in 500 hr or less.

Other cast austenitic stainless steels have been exposed in water containing 100 ppm chloride at a pH of 2.8 at 200°C. In these tests four strips of each alloy were machined from cast bars and then stressed to permanent deformation in a twin-strip assembly. The alloys tested and the observed results are shown in Table 14.2. Based on the few tests that were run, type 316 stainless steel was more resistant than the other alloys, and type 309SCb appeared to be next best. The fact that all the others cracked may not be significant in view of the fact that all were permanently deformed, a condition under which type 347 stainless steel would be expected to crack also. Further testing of these alloys stressed within the elastic range remains to be completed.

Metallographic examination of cast specimens that have cracked generally show few (usually only one) cracks which do not tend to branch as do those in wrought stainless steel. The reason for this and for the fact that cracking is usually associated with deformed metal is not known. Answers to these questions should shed light on the mechanism of stress-corrosion cracking.

The high resistance of the cast alloys to cracking in chloride environments combined with the advantage of lower fabrication costs make the cast austenitic stainless steels attractive materials for future large-scale reactors.

Table 14.2. Stress-Corrosion Cracking of Certain Cast Stainless Steels in Chloride-Containing Water at 200°C

Chloride concentration = 100 ppm
pH = 2.8

Alloy Type	Remarks*
304L	Cracks in all four specimens in less than 500 hr
309SCb	Cracks in two specimens in 100 hr; other two specimens, no cracks in 500 hr
316	No cracks in 1000 hr
330	Cracks in four specimens in 200 hr
Misco C**	Cracks in all specimens in 100 hr

*Two twin-strip assemblies (four specimens) permanently deformed.
**Composition: 28.5% Cr, 10% Ni, 0.22% C, balance Fe.

REFERENCES

1. W. L. Marshall et al., HRP Quar. Prog. Rep. April 30, 1959, ORNL-2743, p 233.

2. J. C. Griess et al., Quar. Rep. of the Solution Corrosion Group for the Period Ending Oct. 31, 1957, ORNL CF-57-10-80, p 20.

3. The composition of this solution was suggested by W. L. Marshall and found by him to be phase-stable to above 300°C in a quartz tube except for loss of nitric acid to the vapor phase.

4. J. C. Griess et al., HRP Quar. Prog. Rep. July 31, 1956, ORNL-2148, p 79.

5. J. C. Griess et al., HRP Quar. Prog. Rep. April 30, 1959, ORNL-2743, p 112.

6. Ibid., p 108.

7. Ibid., p 117.

15. RADIATION CORROSION

G. H. Jenks H. C. Savage

A. L. Bacarella
J. E. Baker
J. M. Baker
J. C. Banter
S. E. Bolt
R. J. Davis
V. A. DeCarlo
D. T. Jones
R. A. Lorenz
T. H. Mauney
A. R. Olsen
A. J. Shor
M. D. Silverman
W. C. Ulrich
K. S. Warren
S. H. Wheeler

15.1 IN-PILE LOOPS

15.1.1 Development, Construction, and Operation

(a) Loop Operation in Beam Hole HN-1 of the ORR.--The first ORR in-pile loop,[1] 0-1-25, was inserted in beam hole HN-1 of the ORR on May 18, 1959. The loop operated continuously at a mainstream temperature of 280°C until a scheduled removal on Sept. 8, 1959. During this period 2741 hr of loop operation and 36,895 Mwhr of reactor energy were accumulated. The loop was fully inserted during 30,159 Mwhr, fully retracted during 6100 Mwhr, and partially retracted during 636 Mwhr. The effect of reactor radiation on the over-all corrosion rate of the loop components was continuously monitored by measurement of the oxygen consumed and by frequent removal of solution samples for chemical analyses. The chemical stability of the fuel solution was also determined by means of these samples. The loop also contained a number of corrosion specimens which are currently being removed from the loop for examination.

Preliminary Cs^{137} analyses of solution samples from the loop during the first 800 hr show a fission power of about 650 w in the loop solution, with the reactor at 20 Mw and the loop in the fully inserted position. This indicated loop power is about 30% greater than that found for similar solutions in LITR HB-2 loops at a LITR power of 3 Mw. No Zircaloy-2 activation analyses are available as yet, but a flux map of the ORR facility made within a mockup core shows that the decrease in flux with increasing distance from the reactor lattice is greater than that in the LITR, so that the expected difference between maximum power density in the LITR and ORR facilities is greater than the difference in average power density as indicated by cesium analyses.

The loop package is shown in Fig. 15.1 and is similar to the loops previously operated in beam holes HB-2 and HB-4 of the LITR.[2] Notable differences are: (1) increased cooling capacity (16 kw) and heating capacity (8 kw) through the use of combination heater-cooler units,[3] (2) the addition of a core cooler capable of removing 4 kw of gamma heat from the core vessel wall,[4] (3) a double-pass core[5] for increased fluid velocity to improve heat removal from the core,

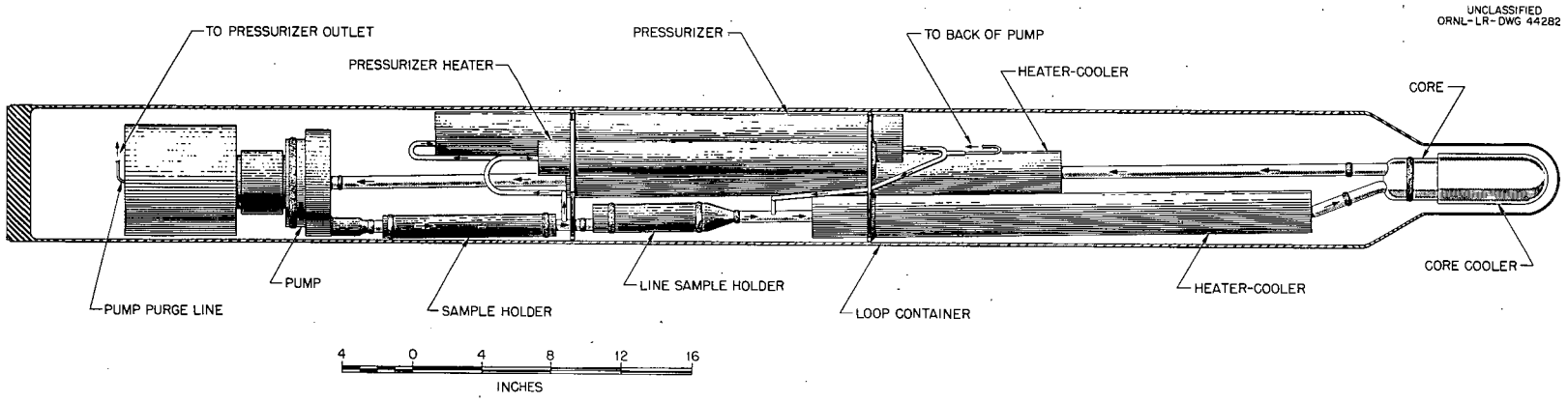

Fig. 15.1. ORR In-Pile Loop.

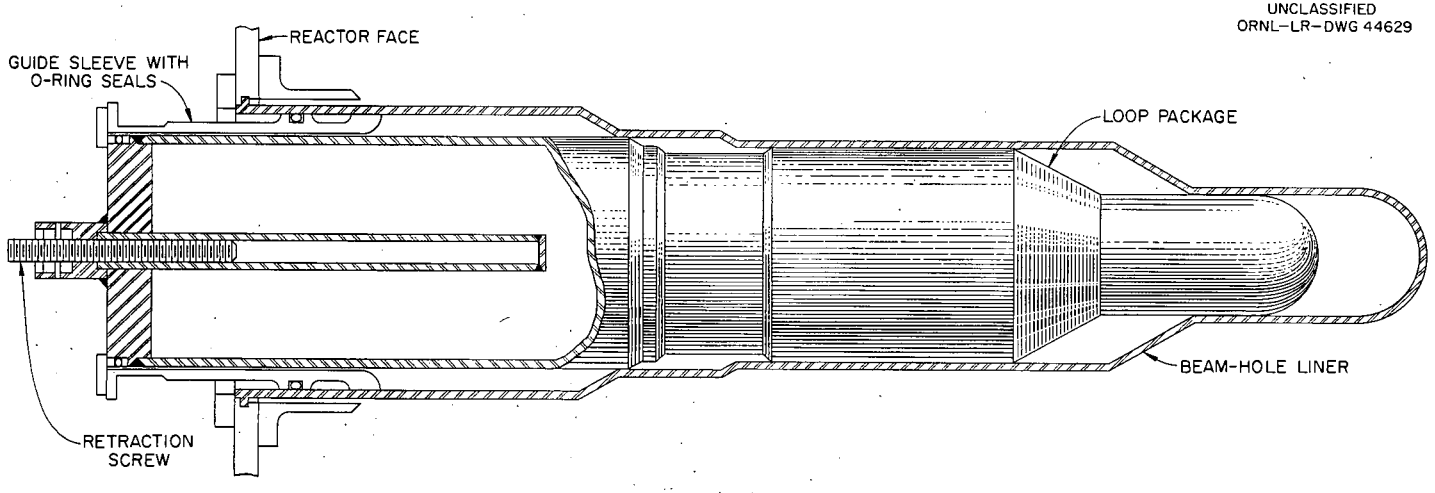

Fig. 15.2. Retraction Mechanism, ORR In-Pile Loop.

(4) a retraction mechanism as shown in Fig. 15.2, and (5) a pump purge line by which ~1 cc/sec of solution from the pressurizer is cooled from ~300° to 70°C and is fed to the pump-rotor cavity. The purge stream controls the solution residence time in the pump-rotor cavity and thus helps to minimize the possibility of uranyl peroxide precipitation. Also, the stream is low in radiolytic gas concentration and thus helps to maintain a low gas concentration in the pump. The retraction mechanism is designed to withdraw the loop approximately 18 in. from the fully inserted position so that the loop can be operated at lower neutron flux levels without a reactor setback or shutdown.

(b) Performance of Loop and Auxiliary Equipment.--A summary of the performance of various loop components and auxiliary equipment is as follows:

(1) Pump.--The 5-gpm canned-rotor circulating pump[6] incorporated in the loop contained aluminum oxide bearings and journal bushings. The stator winding was three-phase, 220 v, with class H insulation. Pumps originally used in the LITR loops had a single-phase, capacitor start, 110-v winding, with class A insulation. No operating difficulties of any kind were encountered with the pump.

(2) Retraction Mechanism.--One of the most useful features of this loop was the retraction mechanism. By being able to retract the loop, pertinent data could be obtained, and minor repairs of mechanical and electrical breakdowns could be made without a reactor shutdown. The loop was retracted a total of 28 times during the run, with no difficulty. Although the mechanism is designed to allow the loop to be retracted 18 in., the loop could only be retracted 13 in., due to a misalignment between the retraction screw and the small equipment chamber. It was found, however, that the fission and gamma heat was reduced by a factor of 10 when the loop was retracted 13 in.

(3) Valves.--There are 66 valves used in the loop experiment to perform operations such as fuel sampling, fuel and gas addition, and final draining and transfer of fuel and gas. These valves must remain leaktight throughout the run. All valves in the ORR HN-1 loop facility were of a nonrotating-stem type with type 340 stainless steel bodies and seats, and the majority were equipped with type 17-4 PH stainless steel (partially hardened) stems. Not a single valve failure was encountered during the run even though three valves, exposed to fuel and/or vapor, were opened and closed more than 600 times each, seven valves were operated more than 400 times, thirteen valves were used more than 200 times, and a total of twenty-two valves were used in excess of 100 times each.

(4) Core Cooler.--The coolant medium for the core cooler is a mixture of air and water. The cooler was adjusted to remove ~1 kw of gamma heat from the core metal wall. After 345 hr of operation, partial loss of coolant flow indicated a plugging in the line. In spite of back-flushing and the use of filters in the feed-water line, the cooler line plugged completely after 1024 hr of in-pile operation. Since the fission and gamma heat in this loop was not excessive, the run was continued without use of the core cooler.

(5) Pump Purge Flow.--After 290 hr of operation, the temperature of the pump purge line[7] (295°C) started to decrease. The temperature decline accelerated gradually until 2100 hr of operation, at which time the temperature leveled off at 182°C, indicating that the pump purge line had plugged. The run was continued, since the fission product activity in the loop fuel solution was considered low enough to preclude uranyl peroxide precipitation in the pump. The reason for plugging is unknown but is under investigation.

(6) Loop Removal.--Some difficulty was encountered with the removal of the loop from the HN-1 beam hole. The difficulty arose because: (1) the clearance between the loop and carrier was small, necessitating the removal of four 1/8-in.-thick brass skids on the shielding plug; and (2) the front shielding of the small equipment chamber projected 1/8-in. into the path of the loop, thus causing misalignment of the loop and carrier. One 8-hr shift was required to remove the loop package and separate the loop from its shield plug.

(7) Instrument and Control Panel.--The performance of all instruments in maintaining and indicating loop operating conditions was excellent. No major difficulties were encountered except with one secondary instrument which was used to contain additional microswitches for alarm, setback, and scram. For reasons still unexplained, this instrument would periodically drive upscale, tripping all alarms. Because the difficulty persisted, the scram-alarm points were moved to the master controller; this move corrected the problem.

(8) Reactor Setback and Scram Signals.--The HN-1 experiment gave the ORR a total of 12 fast setbacks and 2 scram alarms during 2741 hr of operation, all of which were due to instrument malfunction.

(9) Solution Samples.--The loop was sampled 41 times. Although a sample consists of one purge (6.8 ml), a total of five purges (34.0 ml) is taken for each sample for the flushing of lines, etc. Each sample is followed with a 34-ml fuel addition to replace the solution removed. No difficulties were encountered.

(10) Oxygen Additions.--A total of 13,804 cc (STP) of oxygen gas was added to the loop in eight additions throughout the course of the run, without incident.

(11) Major Fuel Changes.--In addition to the fuel solution removed in sampling, 1120 ml was removed from the loop and replaced with fresh fuel during the run in order to make changes in the chemical composition of the fuel. This necessitated taking 165 purges, followed by 30 fuel expansions, made with the loop operating at temperature and pressure. In addition, the loop was completely drained and refilled once (1100 ml).

(12) Radiation.--Radiation exposure of personnel during the entire run and loop removal was negligible.

15.1.2 <u>In-Pile Loop Experiment L-2-22</u>

(a) <u>Introduction and General Aspects of Experiment</u>.--LITR loop experiment L-2-22 was designed with the primary objective of determining the effect of Li_2SO_4-H_2SO_4 additives in a 0.04 m UO_2SO_4 solution on the Zircaloy-2 radiation-induced corrosion at 280°C, in comparison with the corrosion observed in a previous experiment, L-2-10,[8] which employed a solution of similar UO_2SO_4 concentration but low concentrations of additives (0.02 m H_2SO_4 and 0.008 m $CuSO_4$).

Results obtained in a previous in-pile loop experiment at 280°C showed that the addition of 0.2 m Li_2SO_4 and 0.1 m H_2SO_4 to a 0.17 m UO_2SO_4 solution produced a beneficial effect on the radiation-induced corrosion of Zircaloy-2. At a given fission power density in the solution, the corrosion rate in this solution was less by a factor of up to two than that observed in a solution which was 0.17 m in UO_2SO_4 but only 0.03 m in H_2SO_4 and 0.015 m in $CuSO_4$.[9] A similar beneficial effect of 0.4 m H_2SO_4 and 0.15 m $CuSO_4$ in a 0.15 m UO_2SO_4 solution was observed in another 280°C loop experiment,[10] L-2-14. A beneficial effect due to a Li_2SO_4 addition to 0.17 m UO_2SO_4 solutions has also been observed in autoclave experiments.[11] However, no effect of Li_2SO_4 addition was apparent in an autoclave experiment which employed UO_2SO_4 at a concentration of 0.04 m.[12]

It has been tentatively concluded that the beneficial action of the additives is due to a reduction or elimination of uranium sorption on Zircaloy-2 surfaces during exposure.[13] If this conclusion is correct, the effect can be expected to be more pronounced for the 0.04 m UO_2SO_4 solutions than for the more concentrated uranium solution, since the fraction of the observed radiation-induced corrosion which can be ascribed to sorbed uranium is greater in the more dilute solutions. The results of the autoclave experiment which showed no effect due to the additive do not support this conclusion, but it is considered possible that some factor in the experiment, such as the heavy scales which adhere to autoclave surfaces or the low power density which prevailed, may have influenced the results adversely.[14]

Because of the indicated importance of sorbed uranium in the understanding, prediction, and control of the radiation-induced corrosion of Zircaloy-2, an in-pile loop determination of the effects of additives to dilute UO_2SO_4 solution was considered necessary. Heavy scales of the type found in autoclaves are not found on in-pile-loop core specimens. In addition, the maximum neutron flux in the HB-2 loop facility is greater than that at the autoclave exposure facilities.

In addition to the above-mentioned primary objective, the experiment was also designed to gain information on the radiation-induced corrosion of some other materials and of the effects on Zircaloy-2 corrosion produced by different types of heat treatment and chemical polishing of the specimen surfaces.

Toward achieving the main objective of the experiment, Zircaloy-2 specimens of commercially annealed material with as-machined surfaces, similar to those employed in L-2-10 were included in the core. The solution initially charged and used during a major portion of the in-pile exposure was 0.18 m in Li_2SO_4 and 0.09 m in H_2SO_4 in D_2O as shown in Table 15.1, solution 1a. (H_2O rather than D_2O was employed in L-2-10.) The test with this solution was interrupted when a laboratory power failure led to conditions which required that the solution be drained. The replacement solution, No. 1, (No. 1 later became solution No. 2, upon the addition of H_2SO_4) was of a composition similar to that employed in the previous L-2-10 experiment. This replacement solution was in turn replaced after 836 Mwhr with solution No. 3, which was similar in composition to the initial solution. Solution No. 3 was employed during the final 588 Mwhr of the test. Experiments to study the deposition of uranium in the core under conditions of low solution-flow rate and low overpressure were carried out during the periods of operation with solutions 1, 2, and 3, as reported previously.[15] Thus, the over-all experiment was not a straight-forward test of Zircaloy-2 corrosion in the additive solution. However, as discussed later, some deductions concerning possible effects of the additive can be drawn from the results.

The experiment is complete except for the results of qualitative and metallographic inspection of loop components and specimens. This report covers only the results of specimen weight measurements and those results of other measurements which are considered pertinent to the interpretation of the weight results.

The various solutions and exposure times for this experiment are listed in Table 15.1. A tabulation of the corrosion specimens employed is given in Table 15.2. Normal operating conditions in- and out-of-pile included main-stream and pressurizer temperatures of 280 and 295°C, respectively, and a pump frequency of 60 cps. The solution fission power densities estimated from the results of Zircaloy-2 induced activity measurements ranged from 4.2 to 0.9 w/ml at the locations of the front and rear core channel coupons, respectively, with the

Table 15.1. Test Solutions and Operating Times at 280°C Employed in Loop L-2-22

Test Solution Identification	Solution Composition (m)[a]				Total Time (hr)	Time Under Irradiation (3 Mwhr LITR energy)
	UO_2SO_4	$CuSO_4$	Li_2SO_4	H_2SO_4		
Out-of-pile with H_2O					83[b]	
Out-of-pile with D_2O					399[b]	
Out-of-pile	~0.036	~0.002	~0.18	~0.09	365[b]	
In-pile, 1a	0.036	0.002	0.18	0.09	1947	1653
In-pile, 1 and 2	0.036	0.006		0.015-0.027	415	279
In-pile, 3	0.036	0.0014	0.18	0.09	266	196
			Total Time		3476	2128

[a] All UO_2SO_4 solutions were in D_2O and were oxygenated.

[b] Several different tests were made with these solution compositions; the value listed for total time was accumulated in the several tests.

Table 15.2. Corrosion Specimens Contained in Experiment L-2-22

Material	Material Number	Preparation	Number of Coupon Specimens					
			Core Channel	In-Line Channel	Core Annulus	In-Line Annulus	Pressurizer (liquid phase)	Pressurizer (vapor phase)
Type 347 SS	1149	Machined	4	4	6	3	4	4
Niobium		Machined	2	2	2	1	1	1
Crystal-bar zirconium	1242	Machined and Pickled	2	2	2	1		
Crystal-bar zirconium	1242	Machined	3	3	2	1		
Zircaloy-2 (g)	1241	Machined	5	5	3	1	1	1
Zircaloy-2 (g)	1241	Machined and Pickled	3	3				
Zircaloy-2 (g)	62	Machined and Pickled			4	2		
Zircaloy-2 (s)	62	Machined and Pickled			2	1		
Zircaloy-2 (r)	62	Machined and Pickled			2	1		
Zircaloy-2 (h)	62	Machined and Pickled			2	1		
Zircaloy-2 (g)	60	Machined and Pickled					2	2
Zirconium-15% Nb (a)	Zr No. 189	Machined and Pickled			2	1		
Zirconium-15% Nb	Ingot No. 189	Machined	3	3				
Zirconium-5% Sn	Lot No. 1	Machined	2	2	1	1		
Zirconium-15% Nb-5% Mo(a)	Zr-191	Machined and Pickled			3	1		
Zirconium-15% Nb-2% Mo(a)	Zr-190	Machined and Pickled			1	1		

Note: 1. Suffixes attached to the zirconium alloys refer to the following heat treatments:
(a) 900°C for 3 hr, water quenched
(g) commercially annealed
(h) 1000°C for 30 minutes, water quenched
(r) 1000°C for 30 minutes, air cooled
(s) commercially annealed, 50% cold worked

2. Zircaloy-2 coupons fabricated from material that was rolled for random orientation.
3. Zr-15% Ng-X alloy specimens prepared from stock which was hot rolled and then water quenched from 900°C.
4. Material from which the niobium specimens were fabricated was cold rolled from 0.125 to 0.100 in. and vacuum annealed at 1100°C for 1 hr.
5. Polished specimens were first finish machined and ground to 0.065-in. thickness, numbered, and polished to 0.060-in. thickness.
6. Polishing of Zircaloy-2 specimens was done in a mixture of HNO_3, lactic acid, H_2O, and HF (5:5:1:1).
7. Polishing of other zirconium alloy specimens was done in a mixture of HNO_3, H_2O, HCl, and HF (5:5:1:1).

LITR at 3 Mw. The procedures, measurements, and inspections carried out, with the exception of the boiling experiments, were similar to those employed and described for previous loop experiments.[16]

(b) Results.--(1) Scale on Core Specimens.--The results of quantitative analyses of films and scales on various specimen surfaces showed that the core and other zirconium-alloy coupons retained scale, even after defilming, in amounts which must be taken into consideration in accurate evaluations of the zirconium-alloy corrosion rates from specimen-weight data. Consequently, the analytical data were used in the estimation of the total amount of oxide on each of the core specimens. Thus estimated, the amount of oxide on a core specimen, as recovered from the loop, was about 2 mg/cm^2, regardless of material or location. For zirconium-alloy specimens exposed in in-line positions, and for stainless steel specimens exposed in core and in-line positions, the amounts of scale estimated in the above manner could be checked by comparison with the amounts more reliably indicated by weight-gain data (difference between original and as-removed weights) or by weight loss upon defilming, in the case of the steel. The comparisons indicate that the weights determined from analytical data are somewhat less than the true values but that the analytically determined values are probably sufficiently accurate for use in estimating corrosion penetration according to specimen-weight data.

The amount of uranium found on the core specimens was less than 1% of the oxide weight except in the case of the two niobium specimens, for which the indicated weight contents were 3.5 and 6.5%, respectively.

(2) Corrosion During Boiling Tests.--Based on oxygen consumption data, over-all stainless steel corrosion rates in the loop during radiation exposure were in the range of 0.5 to 3 mpy during normal operation. When uranium was deposited in the core during the boiling experiments, the over-all rates were greater. In the extreme case, the rate was about 30 mpy. There is evidence in the appearance of the core wall for an unusually severe attack of the wall, and it is likely that the increased corrosion during the boil tests was concentrated on the core wall. There is no evidence that any part of the increased over-all rate was a result of increased rates of attack of the core specimens. In general, relative rates observed for specimens exposed at different solution power densities and flow velocities appear to be about as expected from the results of previous experiments. The rates for Zircaloy-2 specimens near the rear of the channel (low power density) are high in relation to the rates for the forward specimens (high power density) as may be seen in Fig. 15.3. However, a similar relationship was observed between the rates for channel specimens in L-2-10, so that the effect is probably not related to solute deposition. The explanation for this effect is unknown but is probably related to velocity effects and/or excessive corrosion on the portion (36%) of the specimens which are covered in clamping or by adjoining specimens. It may be noted that a similar effect was observed for the channel specimens of crystal-bar zirconium in this loop.

(3) Results of Weight Measurements of As-Machined Core Specimens of Commercially Annealed Zircaloy-2.--Corrosion rates for these specimens, calculated from total radiation exposure time and from penetration values derived from weight data corrected for scale, are shown in plots of the reciprocal of the corrosion rate vs the reciprocal of the solution power density in Figs. 15.3 and 15.4 for channel and annulus specimens, respectively. Corrosion rates observed with similar specimens in L-2-10 are plotted for comparison. The rates in this experiment are substantially less than those in L-2-10.

UNCLASSIFIED
ORNL-LR-DWG 44283

Experiment	Temperature (°C)	Solution Composition (m)			
		UO_2SO_4	$CuSO_4$	H_2SO_4	Li_2SO_4
L-2-19	280	0.17	0.02	0.1	0.2
L-2-22	280	0.04	0.0023	0.1	0.2
L-2-22	280	0.04	0.0067	0.02	–
L-2-22	280	0.04	0.0014	0.1	0.2
L-2-10	280	0.04	0.0075	0.02	–

■ Specimens Machined (Corrosion Rates Corrected For Retained Scale And For Operation Without Li_2SO_4)
▲ Specimens Polished (Corrosion Rates Corrected For Retained Scale And For Operation Without Li_2SO_4)
● Corrosion Rates Corrected For Retained Scale – Based On Total Radiation Time
X Coupon Not Defilmed; Submitted For Gross Scale Analyses
XX Coupon Defilmed Before Submitting For Analyses

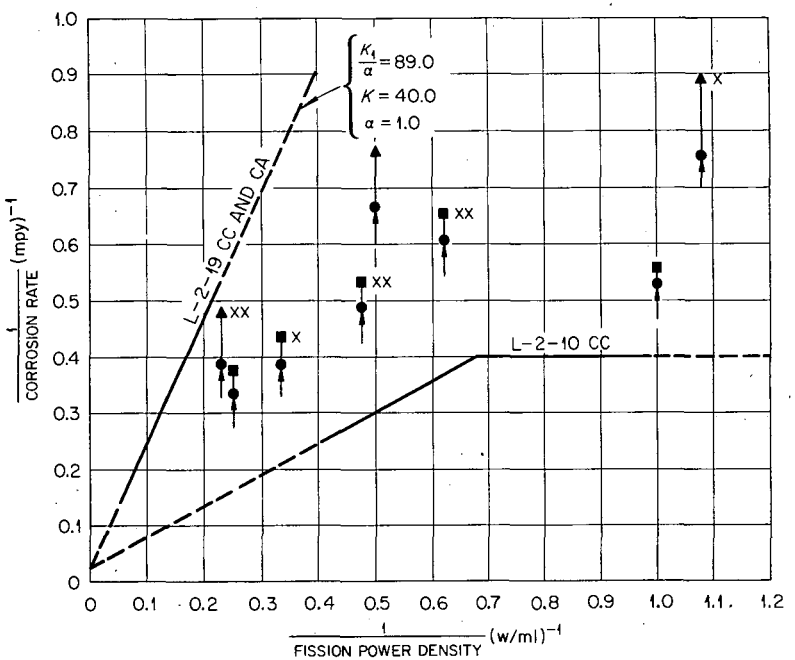

Fig. 15.3. Zircaloy-2 Corrosion Rates in Core Channel, Loop L-2-22.

UNCLASSIFIED
ORNL-LR-DWG 44284

Experiment	Temperature (°C)	Solution Composition (m)			
		UO_2SO_4	$CuSO_4$	H_2SO_4	Li_2SO_4
L-2-19	280	0.17	0.02	0.1	0.2
L-2-22	280	0.04	0.0023	0.1	0.2
L-2-22	280	0.04	0.0067	0.02	–
L-2-22	280	0.04	0.0014	0.1	0.2
L-2-10	280	0.04	0.0075	0.02	–

■ Specimens Machined (Corrosion Rates Corrected For Retained Scale And For Operation Without Li_2SO_4)
▲ Specimens Polished (Corrosion Rates Corrected For Retained Scale And For Operation Without Li_2SO_4)
● Corrosion Rates Corrected For Retained Scale – Based On Total Radiation Time
X Coupon Not Defilmed; Submitted For Gross Scale Analyses
XX Coupon Defilmed Before Submitting For Analyses

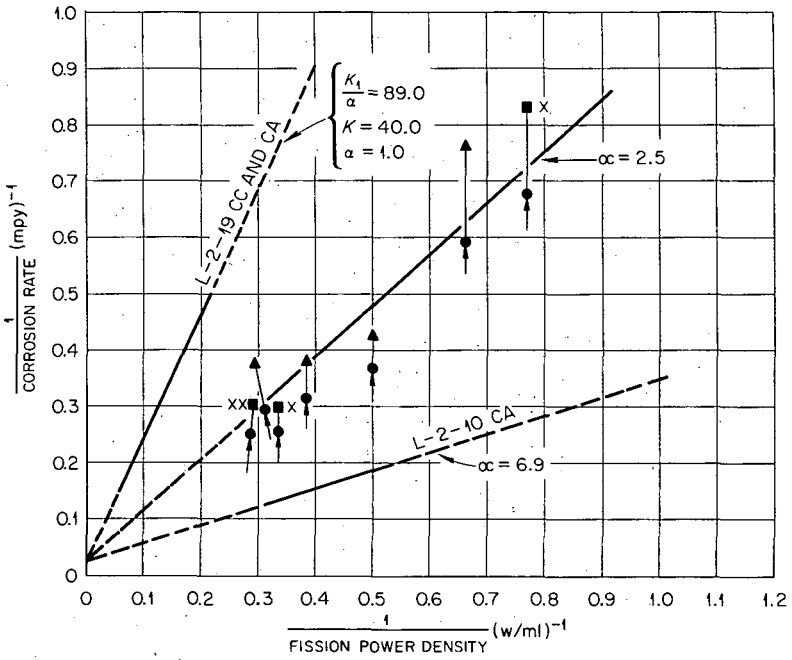

Fig. 15.4. Zircaloy-2 Corrosion Rates in Core Annulus, Loop L-2-22.

In order to arrive at estimates of the radiation corrosion of Zircaloy-2 in the lithium-additive solution, it was necessary to make estimates of the amount of corrosion which occurred during exposure to the solution which did not contain lithium. These estimates were made by assuming that corrosion in the lithium-free solution proceeded at the same rate as observed for similar coupons exposed at the same power densities in loop L-2-10, which employed a similar lithium-free solution. The corrosion penetration during the operation with the lithium-bearing solution was then taken as the difference between the total penetration and that estimated for the operation employing the lithium-free solution. The rate values calculated from the resulting values for penetration and from the time of exposure in the additive solutions are included in Figs. 15.3 and 15.4.

(4) Results of Weight Measurements of Chemically Polished Core Specimens of Commercially Annealed Zircaloy-2.--Corrosion rates calculated for these specimens by the two different methods outlined above are included in Figs. 15.3 and 15.4 for channel and annulus specimens, respectively. In general, the rates for the polished specimens are less than those for the machined specimens.

(5) Weight Results for Zircaloy-2 Prepared According to Several Different Heat Treatments.--The corrosion rates of specimens of these materials are about the same as those for similarly prepared and located specimens of commercially annealed Zircaloy-2, and, hence, no effects due to the different heat treatments listed in Table 15.2 are apparent in the results.

(6) Weight Results for Core Specimens of Crystal-Bar Zirconium, Zr-5% Sn, Zr-15% Nb, Zr-15% Nb-5% Mo, Zr-15% Nb-2% Mo, and Nb.--Weight results obtained with specimens of these materials were used to estimate values of corrosion penetration for each specimen. These values were then compared with those obtained with similarly prepared and located specimens of commercially annealed Zircaloy-2. With four exceptions, the corrosion penetration of these specimens were from 1.4 to 2.5 times greater than those for the Zircaloy-2. For two of the exceptions, the similarly determined factors were 1.0 and 4.3, respectively, for two specimens of crystal bar zirconium. The penetration values for the two niobium specimens were about 20 times greater than those for Zircaloy-2.

(7) Weight Results for Core Specimens of Type 347 Stainless Steel.--Corrosion rates of the four channel specimens, based on defilmed weight loss, exposed specimen area, and total radiation time, ranged from 1 mpy at 1.1 w/ml to 4.6 mpy at 3.6 w/ml, with no apparent effects due to velocity. The rates for the six annulus specimens ranged from 0.7 mpy at 1.5 w/ml to 2.0 mpy at 3.4 w/ml. These channel rates are somewhat greater than those determined for L-2-10 channel specimens. The annulus rates are included within the large range of rates observed with L-2-10 annulus specimens.

(8) Weight Results Obtained with In-Line and Pressurizer Specimens.--All zirconium and zirconium alloy specimens showed weight gains after defilming, with the exception of the Zr-15% Nb-5% Mo specimen which showed a weight loss of 0.2 mg/cm^2 (0.1 mpy). All niobium specimens except the one in the pressurizer vapor phase lost weight: 1.5 to 2.6 mg/cm^2 (0.3-0.5 mpy). The steel specimens showed small weight losses or gains. The average corrosion rates calculated from the weight losses range from less than 0.1 to 0.5 mpy. The higher rates were found with the in-line channel specimens.

(c) Discussion of the Effects of the Solution Additives on the Zircaloy-2 Corrosion Rates.--The Zircaloy-2 results in Figs. 15.3 and 15.4 indicate that Zircaloy-2 corrosion in this experiment was substantially less than observed in

the previous L-2-10 experiment, which employed a solution containing low concentrations of additives. This difference is in line with that expected if the additives acted to reduce uranium sorption on Zircaloy-2 surfaces during exposure, as indicated by the results of the previous loop experiment with similar additives in 0.17 m UO_2SO_4. However, the presence of appreciable amounts of scale on the specimens recovered from the core precluded direct information on the amount of uranium sorbed on the specimen surfaces and also introduced the possibility that the scale may have affected the rates during exposure by affecting the uranium sorption in effective areas. It may be noted that the amount of uranium found within the scales (1% or less, by weight), if uniformly distributed within the scale, would not appreciably alter the effective fission power density at a specimen surface from that prevailing if the scale were replaced with solution. It does not appear possible at this time to evaluate, with any degree of accuracy, the effects of the scales on the observed corrosion rates if the scales were present during most of the exposure. However, if the scales were formed in large part from materials produced in the rapid corrosion of the core walls during the "boil test," then, the scales were present during only the latter portion of the exposure, and the possibility of appreciable effects of the scales on the observed Zircaloy-2 corrosion rates would be greatly reduced.

On the basis of the correlations of Zircaloy-2 corrosion data described in the past, as well as on the basis of more recent ones, the difference between the Zircaloy-2 rates in this and in the L-2-10 loop reflect a difference between the effective power densities, for given solution power densities, at specimen surfaces during radiation exposure, regardless of the exact mechanism by which the sorption differences were brought about. The difference in effective power densities arises from differences in the amounts and/or proximity to the protective oxide of uranium sorbed on the corroding surfaces. The recently proposed model for the corrosion of Zircaloy-2 under irradiation, and the results of correlation of past 280°C Zircaloy-2 corrosion data according to the model, provide a basis for the ready estimation of the magnitude of the difference between effective power densities for annulus specimens in L-2-10 and L-2-22.[17] According to this model, the relationship between Zircaloy-2 corrosion rate and solution fission power density is given by the expression:

$$1/R = \frac{K_1}{KP\alpha} + 1/K \,, \qquad (1)$$

where R is the corrosion rate; P is the solution fission power density; α is the factor by which the effective power density at a corroding surface is greater than the solution power density (given by the sum of the solution power density and a factor proportional to the ratio of the product of the solution power density and the amount of sorbed uranium to the concentration of uranium in solution); K_1 is the ratio of constants for the thermal and radiation annealing of those radiation defects in metal or oxide which increase corrosion and is thus expected to be independent of solution composition; and K is another constant the value of which, according to the model, may change with solution composition but which in practice with the 280°C data appears to be nearly independent of solution composition. In plots of the reciprocal of corrosion rate vs the reciprocal of the solution power density, the data obtained with channel and annulus specimens in loop experiments L-2-19 and L-2-14 in which uranium sorption is believed to have been negligible fall near a straight line which extrapolates to a value of 40 mpy at infinite power density is illustrated in Figs. 15.3 and 15.4. Annulus specimens from L-2-10 fall near a straight line of different slope which also extrapolates to a value of 40 mpy at infinite power density. This different slope is ascribed to the sorption of appreciable amounts of uranium on the L-2-10 specimens. The points for channel specimens taken from L-2-10 lie

above those for the annulus specimens but deviate from a straight line. This behavior is ascribed to a decrease in the amounts of sorbed uranium on Zircaloy-2 surfaces as the solution velocity increases. Interpretation of the results for channel specimens is also complicated by the fact that 36% of the area of a specimen is covered by the specimen holder or by adjacent specimens and is thus exposed to a nearly stagnant solution. The results from other 280°C loop experiments and from autoclave experiments may be interpreted in a similar manner.

According to the recent model and Eq.(1), the annulus results in this experiment show that the effect of sorbed uranium was appreciably less than in L-2-10. If an α value of one is taken for the L-2-19 and L-2-14 results, the value of α for the L-2-10 annulus specimens is 6.9. The value of α which corresponds to the line drawn through the points for the Li_2SO_4-solution operation in L-2-22 and through a value of 40 mpy on the ordinate is 2.5, a factor of 2.8 less than that for L-2-10 specimens. The factor in the value of α which represents the effect of sorbed uranium is proportional to α-1 and is equal to 5.9 for the L-2-10 and 1.5 for the L-2-22 data, almost a fourfold difference. No attempt has been made to determine a value of α for the channel-specimen data shown in Fig. 15.3, but it may be noted that, with the exception of the lowest power density points, the data points fall above the line for the annulus data. This indicates a beneficial effect of increased velocity on the value of α and is regarded as additional evidence that, for a large part of the exposure, uranium was sorbed on Zircaloy-2 surfaces, at least in the low-velocity regions, in amounts sufficient to influence corrosion adversely, although, as shown above, the amount sorbed was appreciably less than in the previous experiment.

15.2 IN-PILE SOLUTION ROCKING-AUTOCLAVE TESTS, LITR

15.2.1 Development, Construction, and Operation

A new rocking-autoclave experiment assembly has been designed that will permit an experiment to be operated in either beam hole HB-2, HB-5, or HB-6 of the LITR. Figure 15.5 shows the complete assembly. There are several advantages of this experiment assembly over those previously used in the LITR.[18] These are: (1) the experiment is completely enclosed for containment in the event of autoclave rupture or leak; (2) an experiment can be inserted into one of several beam holes; (3) the rocking mechanism is of a more reliable design and permits 24-in. retraction of the experiment; (4) increased angle of rock, thus more agitation; and (5) the autoclave is in a plane parallel to the reactor lattice to minimize the neutron flux gradient in the autoclave.

The new, type IV autoclave, Fig. 15.6 is similar to those used in the three-hole HB-5 facility.[19] Five coupon-type corrosion specimens can be installed in the experiment. The autoclave volume is approximately 8.5 cc. Thermocouples for temperature measurement and control are located in a thermowell inside the autoclave, in the autoclave wall, and in the heater-cooler unit. The heater-cooler maintains the solution at the desired operating temperature, and results indicate that fission and gamma heat loads to 1000 w can be handled. It is anticipated that future in-pile autoclave experiments will be of the type IV design described above.

The first experiment, L5Z-140, of the type IV design has been assembled, pretreated, and is ready for insertion into beam hole HB-5. It is a Zircaloy-2 autoclave and contains five Zircaloy-2 corrosion specimens. The fuel solution is 0.04 m $UO_2(NO_3)_2$, 0.01 m $Cu(NO_3)_2$, 0.10 m HNO_3, with D_2O as the solvent. The purpose of the test is to explore problems that might be associated with the use of uranyl nitrate solutions as an AHR (aqueous homogeneous reactor) fuel.

UNCLASSIFIED
ORNL-LR-DWG 44285

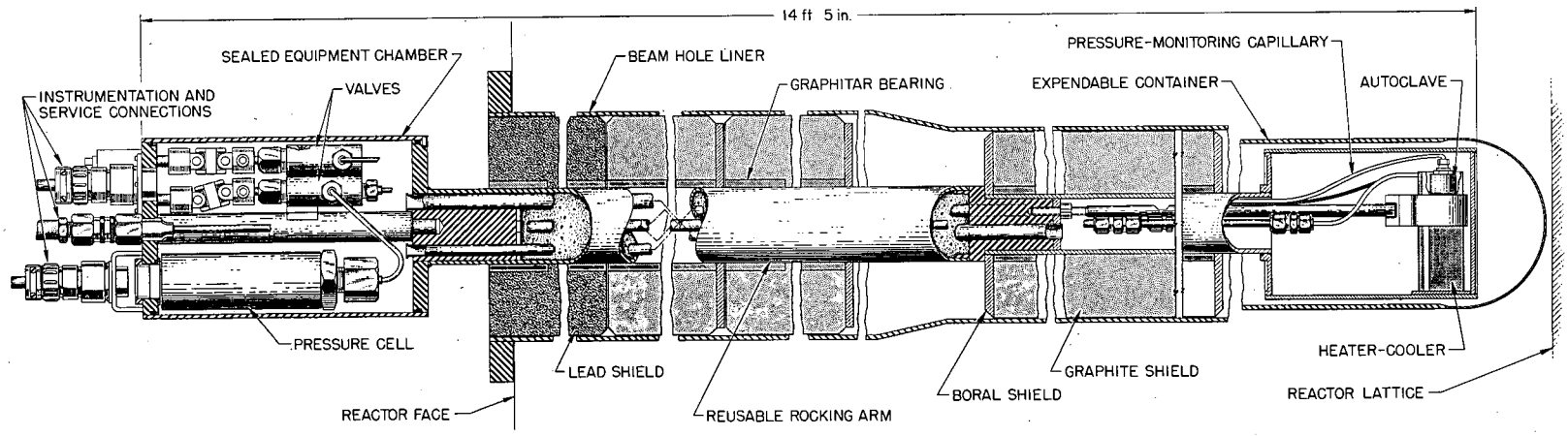

Fig. 15.5. In-Pile Rocking-Autoclave Experiment Assembly.

UNCLASSIFIED
ORNL-LR-DWG 44286

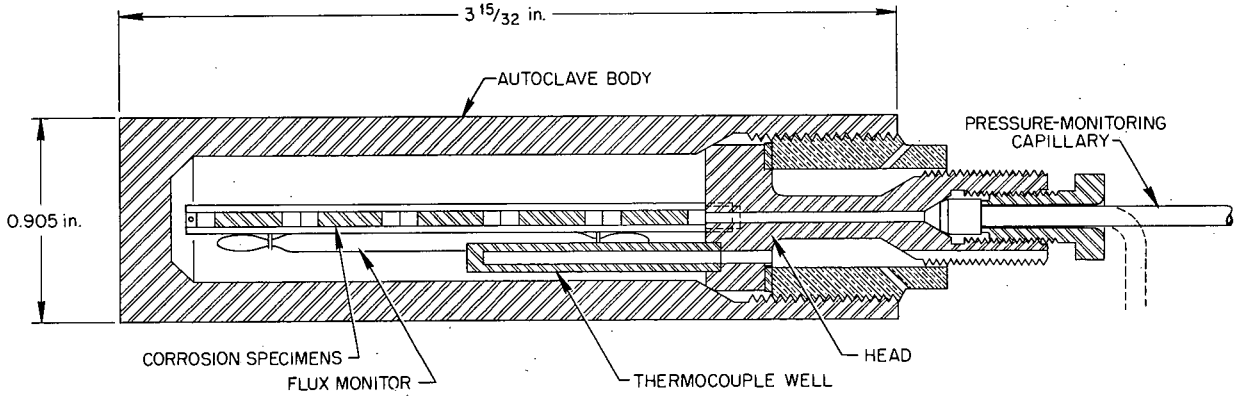

Fig. 15.6. In-Pile Rocking Autoclave, Type IV.

15.2.2 Results of In-Pile Autoclave Experiments

There have been no solution autoclaves exposed in the reactor during the past quarter. However there are a few autoclave tests which were exposed some time ago for which postirradiation examinations have been recently completed. Three autoclave experiments are reported below. Tabulation of data, in some cases preliminary data, from all rocking autoclaves exposed in the reactor to date are given elsewhere.[20,21]

15.2.3 A Comparison of the Radiation Corrosion of a Zr - 1% Cr Alloy with That of Zircaloy-2: Experiment L6Z-139

(a) Introduction.--Recently reported data illustrated that a Zr - 1% Cr alloy, heat treated at 800°C for 1 hr, then furnace cooled, possesses greater corrosion resistance to 900°F steam than does Zircaloy-2.[22] A test to determine if this alloy possesses similarly improved corrosion resistance to UO_2SO_4 solutions under irradiation was considered worthwhile and was carried out.

(b) Method and Procedure.--It has often been demonstrated that surface accumulation of uranium in in-pile corrosion tests can drastically alter the effective surface power density and, hence, the observed corrosion rates at given solution power densities.[23] Differences in tendency to sorb uranium could easily render a comparison of two alloys uncertain or even misleading. To help avoid such difficulty, a test solution was chosen which in past exposures with Zircaloy-2 has always given corrosion results which indicate that no surface uranium accumulated during radiation exposure. More precisely, the solution proposed contained 300 g of uranium per liter (as UO_2SO_4) in D_2O with the usual additives (0.04 m $CuSO_4$ and 0.04 m D_2SO_4.)[24] Another advantage of this highly concentrated uranium solution is that it makes possible relatively high power densities which tend to magnify differences in susceptibility to radiation corrosion and make the differences more easily measured. Consideration of temperature control problems and neutron shadowing effects at high concentrations of U^{235} led to the selection of 66%-enriched uranium for the solution. The resulting solution power density was 36 w/ml. The exposure was made at 275°C, rather than 280°C in order to reduce the possibility of encountering the two-liquid-phase temperature, which was found to be 287-288°C in quartz-tube tests. The experiment was exposed for 159.3 hr, with the LITR at the 3-Mwhr energy level.

(c) Results.--The average corrosion penetration of Zircaloy-2 shown by specimen weight results was 0.217 mil and that for the Zr - 1% Cr was 0.224 mil. These penetration values correspond to average corrosion rates of 12.0 and 12.4 mpy, respectively, at the solution power density of 36 w/ml. The oxygen consumption measurements indicated a generally linear average corrosion rate but a lower rate than that indicated by the specimens. This is in qualitative agreement with the expectation that the specimens, being near the axis of the autoclave, were at the temperature indicated and controlled by a well thermocouple, while the walls ran at significantly lower temperatures to remove the heat generated in solution. Only the specimen weight loss data are considered in the comparison of the alloys.

The postirradiation observation of the specimens showed a heavy deposit of a pale yellow-green material with an underlying scale which exhibited a more normal brassy appearance. During the time the specimens were immersed in distilled water for visual examination, most of the heavy deposit sloughed off. About 6 mg of uranium with approximately a stoichiometrically equivalent amount of sulfate were found to have dissolved in the water in which the specimens and

rack were immersed, and another milligram of uranium, but no sulfate, was found in the insoluble material which sloughed off the specimens and rack. These amounts of uranium are small, indeed almost insignificant, compared with that found in a small volume of the original solution. For instance, if only 0.02 ml of the solution which contained 300 g of uranium per liter had escaped the gentle rinse prior to immersion in water and inspection, then the above mentioned 7 mg of uranium would be accounted for. Subsequent to the visual inspection, about 0.5 mg/cm^2 of scale was removed from the specimens of each material by drying. The scale removed from the Zircaloy-2 specimens was nearly free of uranium. The scale sample removed from the Zr - 1% Cr on drying was spilled before analysis. Two specimens, one of each material, were defilmed cathodically, and only minor losses in weight were observed. One specimen of each material, not cathodically treated, was submitted for surface analysis. The results of these analyses showed that 4 and 8 $\mu g/cm^2$ of uranium were adsorbed on the analyzed specimens of the Zr - 1% Cr and Zircaloy-2 alloys, respectively.

(d) Discussion.--As mentioned, the relative amounts and proximity of uranium sorbed or otherwise accumulated on the two alloys to be compared is an important factor to consider along with the comparison of the corrosion rates. The results considered most directly pertinent to the question of uranium sorption are those concerning surface uranium. Since a 30-μ thick layer (the estimated range of fission fragments) of a solution containing 300 g of uranium per liter represents 900 μg of uranium per cm^2, the 4 and 8 $\mu g/cm^2$ found on samples pickled from specimen surfaces are probably negligible. One can also compare the Zircaloy-2 corrosion in this test with results from other tests, such as loop L-2-19,[25] where no uranium adsorption occurred, and infer from the comparison the extent of uranium sorption on Zircaloy-2. From these previous results, the predicted Zircaloy-2 corrosion penetration in this test, presuming no uranium adsorption, is 0.20 mil; the observed penetration was 0.22 mils. This is good agreement and is taken as further evidence that no accumulation of uranium occurred on the Zircaloy-2.

It is concluded that the experiment was probably a valid comparison of Zircaloy-2 with Zr - 1% Cr on an equal effective-power-density basis and that there is no significant difference between the radiation-induced corrosion of these two alloys.

15.2.4 A Qualitative Test of Possible Cr(III) $\rightleftharpoons$ Cr(VI) Equilibria in Fuel Solution Under Irradiation: Experiment L6Z-142

(a) Introduction.--In general, little or no chromium is found in samples of uranyl sulfate solutions which have been exposed to reactor radiations. It is likely that this insolubility results, in part at least, from a reduction by radiation products of soluble Cr(VI) to the subsequently insoluble Cr(III), although other factors, such as the adsorption of Cr(VI) on products of corrosion of the test containers and oxidation-reduction reactions which proceed after the sample is taken, may appreciably influence the apparent Cr(VI) solubility.[26]

It has been shown that ruthenium strongly catalyzes the oxidation of Cr(III) to Cr(VI) in fuel solutions out-of-pile,[27-29] suggesting that the inclusion of ruthenium in a solution under irradiation might stabilize a significant concentration of Cr(VI). If Cr(VI) can be stabilized to some extent under irradiation, then some retardation of stainless steel and Zircaloy-2 corrosion might be effected in those portions of a homogeneous reactor fuel system which are not exposed to fission fragment irradiation and for which the mechanisms of steel corrosion are apparently similar to those prevailing out-of-radiation. The

presence of the ion in solution may also beneficially affect the radiation-induced corrosion of Zircaloy-2.[30]

In an attempt to gain information on the effect of ruthenium on the rate of Cr(VI) formation in uranyl sulfate solution under irradiation, an autoclave experiment utilizing a solution containing added ruthenium was carried out.

(b) Method and Procedure.--The autoclave and four of the corrosion specimens were of Zircaloy-2. The two other corrosion specimens were of type 347 stainless steel. Evidence for the effects of ruthenium and/or Cr(VI) was sought in the results of Zircaloy-2 and stainless steel corrosion in comparison with the results of previous experiments and in the results of observed pressure changes within the autoclave which might be attributed to oxidation or reduction of chromium. In connection with the use of steel corrosion specimens in this experiment, it may be noted that the mechanism of the corrosion of steel under conditions in which the metal is in direct contact with fissioning uranyl sulfate solutions, as in autoclave experiments, has not been established, therefore the effect of ruthenium and/or Cr(VI) on the steel corrosion in this experiment could not be predicted.

The solution was 0.17 m in UO_2SO_4, 0.03 m in $CuSO_4$, and 0.03 m in H_2SO_4, in H_2O. Both ruthenium (100 ppm) as soluble $(RuNO)_2(SO_4)_3$ and chromium (200 ppm) as CrO_3 were added. The Cr(VI) addition was to ensure a supply of this material from the start. Except for the additives, the solution was the same as that used in one previous test, L6Z-104,[31] and similar to three other experiments.[32-34]

The experiment was operated (after a 6.5-hr, 310°C pressure test with water) for about two days at 280°C out of pile, about $4\frac{1}{2}$ days under irradiation at 280°C, and for an additional one-day period at 280°C after the irradiation was stopped. The solution power density during irradiation was 6 w/ml.

(c) Results.--The pressure in the system underwent a series of changes as follows: After the initial insertion of the experiment into the high flux, the pressure increased rapidly by a few psi and slowly over several hours by about 60 psi. During the remainder of the exposure, the pressure declined at a linear rate of about 5.5 psi/hr. Only small pressure changes occurred during the two retracted periods of about 1 hr each which were provided during the course of the exposure. On cessation of radiation, the pressure dropped rapidly by 36 psi then slowly and approximately linearly by 46 psi during the 24 hr, postirradiation, 280°C run. The pressure data indicate that some 27.5 cc (STP) of oxygen were consumed during the experiment.

Weight loss measurements indicated average corrosion rates of 9.2 mpy for the Zircaloy-2 and 11.0 mpy for the type 347 stainless steel specimens at the solution power density of 6 w/ml.

The analytical data indicate that at the time the autoclave was opened there was no chromium in solution. Similarly, no chromium was detected in the loose scales recovered from specimens of either material. The results of analyses of material held on the surface of Zircaloy-2 specimens after removal of the scale by drying show chromium in an amount which, if representative of the average amount on all Zircaloy-2 surfaces, would account for 1.2 mg out of the estimated 3 mg of chromium in the system. Chromium retention on the surface of steel specimens was not determined. The Zircaloy-2 scale was heavily ladened (11%) with uranium, but the retained film contained only 9 μg of uranium per cm^2. The type 347 stainless steel scale was nearly free of uranium, but 25 μg of uranium per cm^2 were found in the retained film.

(d) Discussion.--The pressure data and the analytical data for chromium are interpreted as indicating the following behavior of chromium in the experiment, although some of the pressure changes at the initiation of radiation and during the two retracted periods have not been quantitatively explained: The Cr(VI) loaded into the system at the start was reduced to Cr(III) during the first 5 hr of irradiation. The soluble chromium resulting from steel oxidation during the exposure also went to Cr(III). All the chromium was catalytically oxidized to Cr(VI) by the ruthenium during the 24 hr following irradiation. This Cr(VI) was adsorbed on Zircaloy-2, and possibly on stainless steel surfaces, at some unknown time prior to the opening of the autoclave. In connection with the adsorption on Zircaloy-2, it may be noted that Cr(VI) is known to adsorb strongly on hydrous zirconia, therefore, the adsorption of the chromium in this test is consistent with the existence of the Cr(VI) oxidation state at the time the autoclave was opened.[31]

The observed corrosion rate of Zircaloy-2 in this experiment is greater than that observed in the previous experiment, L6Z-104,[32] which contained no added ruthenium or chromium but was otherwise similar. The high uranium content of the heavy Zircaloy-2 scale in this experiment was probably responsible for most of this difference and might have masked any beneficial effects due to Cr(VI), if present. The type 347 stainless steel corrosion rate was somewhat higher than the 9.6 mpy at 10.1 w/ml observed in the comparable test, L6Z-104, even though the power density in the present test was lower. It is possible that the higher rate is a result of the presence of ruthenium in the autoclave, although the spread of values observed for stainless steel in other previous experiments includes the present value.[32-34] No firm conclusions can be drawn from the steel results, either, regarding the presence of Cr(VI).

15.2.5 Corrosion of a Heated Zircaloy-2 Surface Under Irradiation: Experiment L52T-145

(a) Introduction.--The possibility of rapid corrosion and other phenomena resulting from heating in core walls is of concern in the interpretation of past operations and in the design of future homogeneous reactor operations. Deposition of uranium and other solutes on heated surfaces under boiling conditions has been demonstrated both in out-of-pile[35,36] and in in-pile loop tests.[37] This autoclave experiment was undertaken in an attempt to determine if similar phenomena occur on heated surfaces exposed to reactor radiations under the pressure and other conditions which prevail in autoclaves (little or no overpressure and very low solution velocity).

For this experiment, a heated Zircaloy-2 corrosion specimen was included with other, unheated Zircaloy-2 corrosion specimens in a titanium autoclave. In other respects, the experiment was similar to some other in-pile autoclave experiments which have been described previously.[38] The specimen corrosion data obtained at the end of the radiation exposure as well as the pressure data obtained during exposure were examined for evidence of deposition of solutes from the uranyl sulfate - copper sulfate test solution. Deposition of solutes on the heated surface would be expected to result in an increased radiation intensity and, hence, in an increased rate of corrosion of the surface. Deposition might also affect the steady-state pressure of radiolytic gas through effects on the rate of production and/or of recombination of the gas. Unfortunately, the autoclave system which was employed was one in which the autoclave is agitated by rotation about a horizontal axis. In this type of autoclave, the interpretation of the results of pressure measurements obtained while the autoclave is at high temperature and, especially, while exposed to radiation, are open to question

because, mixing within the autoclave is poor, and temperature gradients may exist which lead to stratification of gas and vapor.[39]

(b) Materials and Procedure.--The heated Zircaloy-2 specimen surface was provided in the form of a hollow pin filled with partially enriched UO_2. Two coupon-type control specimens were mounted, one at either end of the heated pin specimen, in a type III, axially oriented titanium autoclave. The solution was 0.026 m in UO_2SO_4, 0.020 m in $CuSO_4$, and 0.016 m in D_2SO_4, in D_2O, and resembled that in HRE-2. The initial oxygen pressure was about 600 psi at 250°C, and sufficient solution was loaded into the autoclave to ensure complete submersion of the heated pin at all times.

The experiment was exposed to radiation in HB-5 for 36 hr, with the solution temperature controlled at 250°C. The experiment was next cooled and removed from the reactor for about two weeks because of mechanical problems associated with the rocking device. Later, the experiment was reinstalled and exposed at 280°C for 312 hr, then at 300°C for 140 hr, and finally at 320°C for 235 hr.

Postirradiation treatment included visual inspection, analysis of the solution, weighing of specimens after drying, again after cathodic defilming, and analysis of scales removed from the two coupons and from the hot pin on drying.

(c) Results.--The neutron fluxes in the experiment, determined from Zircaloy-2 induced activity measurements, gave rise to power densities at the two control specimens of 0.7 and 1.5 w/ml, respectively, and 0.8 to 1.3 w/ml at the low- and high-flux ends of the pins, respectively. The calculated heat flux through the pin ranged from 3.5 to 5.7 w/cm^2 from one end to the other.

The results of oxygen pressure measurements at 25°C showed more scatter than usual, with an exceptionally high rate of oxygen consumption during the 250°C portion of the experiment and an exceptionally low rate during the 280°C portion. Comparison of oxygen consumption data with the Zircaloy-2 specimen weight losses indicates that only about one-third of the total oxygen consumed went toward oxidation of specimens and the remaining two-thirds toward corrosion of the titanium autoclave and specimen rack. The pressure data can therefore be expected to be dominated by titanium corrosion and are of limited use in the interpretation of the Zircaloy-2 specimen behavior. The changes in pressure observed upon the initiation or termination of radiation indicated average values for radiolytic gas pressures of 89 psi at 250°C, 24 psi at 280°C, 13 psi at 300°C, and 33 psi at 320°C. The indicated radiolytic gas pressures at 300°C and below are close to those expected from results with previous experiments. The 320°C value is well above the expected value.

Postirradiation visual inspection showed that, on removal, the heated pin was in good condition, with no evidence of excessive corrosion. The pin was described as grayish-brown with a gold-colored scale over most of the surface. The coupons appeared metallic blue-gray, with no apparent scale accumulation. On treating the control specimens with acetone and drying, it was found that, as often happens, all heavy scale came off; no additional weight change occurred on cathodic defilming. The heated pin was apparently covered by a more tenacious material, since considerable scale (3 mg/cm^2) remained intact during the acetone treatment and drying, and was only removed on cathodic defilming in dilute acid.

Specimen weight losses indicated average corrosion penetrations of 0.43 and 0.22 mil for the two control specimens and 0.30 mil for the heated pin.

Analysis of the irradiated solution showed only minor changes from the original concentrations. The heavy scales from pin and from coupons contained very little uranium.

(d) Discussion.--It can be estimated that in the absence of boiling, the surface temperature of the heated pin at the high flux end would have been about 30°C above that of the bulk solution.[40] Consideration of the sums of the partial pressures due to oxygen, radiolytic gas, and D_2O vapor at the appropriate temperatures show that it is likely that boiling occurred on the hot pin in this experiment at all times during exposure to radiation.

There is no evidence in the specimen weight data for a greater than usual accumulation of uranium on the hot pin during exposure. Interpolation of the control specimen data to the intermediate solution power density witnessed by the hot pin indicates that the pin corroded about 20% less than would have been predicted for an unheated control coupon at the location of the pin. However, it should be noted that the results of scale examinations showed that the pin was coated with about 3 mg/cm^2 of scale which was not removed during the drying. This weight of scale corresponds to about 1/3 to 1/2 of the estimated range of fission fragments in the scale. If this amount of scale was present during exposure, the corrosive effects of uranium deposited on the scale surface would be greatly reduced by absorption of fission recoil energy in the scale and by geometry effects due to the scale.

The radiolytic gas pressure data show no effects which can be ascribed to deposition of solutes with the possible exception of the indicated high pressure at the 320°C test temperature. However, as noted previously, little weight can be given to the results of the gas pressure measurements because of the possibility of stratification of gas in the horizontal autoclave.

In summary, it appears likely that boiling occurred on the heated pin surface at all times during the exposure. The total corrosion suffered by the heated surface was less than the average of the control specimens and it is considered probable that there was no effect on corrosion in this test resulting from the boiling. However it is possible that a short period of high corrosion rate on the heated pin occurred during the initial 250°C exposure and that during or after this corrosion a heavy tenacious scale developed and retarded further corrosion.

15.3 SUPPORTING RESEARCH

15.3.1 Adsorption of Uranium on Hydrous Zirconium Oxide from UO_2SO_4 Solutions

The studies of the adsorption of uranium on hydrous zirconium oxide from UO_2SO_4 solutions at 250°C have continued with goals of characterizing the adsorption capacity of the oxide as a function of the uranium concentration and eliminating the inconsistencies in the data previously reported.[41] In addition, some measurements of the variation of surface area and water content of the oxide with firing under varying conditions were made in order to see if these variables might explain some of the variations noted in the adsorption capacities.

Several runs were made at 250°C, and one run was made at room temperature with the high-temperature ion-exchange apparatus, using solutions containing 5 and 25 g of uranium per liter which were all 0.02 m in H_2SO_4. Another run, 0.02 m in HNO_3 in addition to the other constituents, was also made (the uranium concentration was 5 g/liter). In all runs but the one at room temperature the oxide was preheated overnight at temperature, either in the solution used in

the run or in water. Three different preparations of oxide were used. Two of these were essentially the same in all respects, while the third had a much lower surface area than the other two. A sample of one oxide was heated in air at 250°C for $12\frac{1}{2}$ hr, two samples of another were fired in platinum crucibles over Meeker burners (~600-700°C) for 1 hr, and a sample of the low-surface-area oxide was heated in air at 250°C for 5 hr. Surface areas and water contents of these oxides were determined before and after firing.

The preheating treatment given the oxide improved the reliability of the results considerably. A comparison of the results at room temperature with those at 250°C shows that uranium adsorption is definitely enhanced at elevated temperatures. The expected trend of higher capacity with solutions of higher concentrations was also evident. In general the capacity of the oxide for sulfate is higher than its capacity for uranium, on a molar basis. This is particularly true at room temperature. The capacity of the oxide for nitrate adsorption is very high, as indicated by the removal of practically all the nitrate from the solution which contained HNO_3. Firing the oxide over the Meeker burner caused a 90% decrease in surface area, whereas firing in air at 250°C for a longer period decreased the surface area by only 18%. Corresponding water losses of 18% and 15% by weight of the oxide were noted. The low-surface-area oxide lost 16% of its surface area as a result of firing in air at 250°C. No water loss was determined in this case.

In several of the present runs, the ratio of adsorbed sulfate to adsorbed uranium is sufficiently high to indicate the possibility of its adsorption in the form $UO_2(SO_4)_2^{=}$, as proposed by Kraus and Nelson[42] in their work with organic ion exchange resins. In others, however, the ratio is too low to substantiate this ion as the adsorbed species. The very high ratio found at room temperature is probably merely an indication of the preferential adsorption of sulfate over the uranium species, whatever its form may be. The strong adsorption of nitrate by the oxide is not so surprising, since it is well known that basic ion exchangers have a strong affinity for nitrate ions.[43] The loss of sulfate and nitrate from solution was accompanied by a decrease in the free acid. If most of this acid were lost from the first few ml passing through the column, some of the uranium could have precipitated hydrolytically. Permanent retention of some of this uranium might account for some of the results indicating extremely high uranium adsorption. Two properties of the oxide, surface area and water content, appear to be quite important in determining its adsorption capacity. Decrease in surface area would, of course, decrease the area available for adsorption; and loss of water would be particularly important if it were held in a form which would create active adsorption sites.

15.3.2 Electrochemical Studies of Zircaloy-2 Corrosion

A previous report[44] includes a discussion of the electrochemical method used for the measurement of corrosion rates for Zircaloy-2 in oxygenated 0.05 m H_2SO_4 at 208°C and the results of a series of experiments performed on rod specimens of Zircaloy-2 taken from one stock of material. Similar experiments have been carried out with rod specimens from another stock, and the results show that the corrosion characteristics of this material differ substantially from those of the previous material. The rods used in the latter measurements were from a stock of material obtained from Westinghouse several years ago, while those used in the former measurements were taken from stock obtained within the past few years from Firth-Sterling. Rods of both stocks were used as-received, with no pretreatments other than repeated washing in soap and water followed by rinsing in acetone and water. The exact histories of these materials are unknown,

but it is known that different fabrication procedures were used in the manufacturing, with the Firth-Sterling material fabricated to give random crystal orientations[45] and finished by centerless grinding.

The corrosion rate data obtained in the one 48-hr run with the Westinghouse material are shown in Fig. 15.7 in a log R vs time plot. The results obtained in one experiment with the Firth-Sterling material, which is representative of the several experiments carried out, are included for comparison. A comparison of the potential as a function of time for the two Zircaloy-2 stocks is shown in Fig. 15.8. A difference between the two stocks is apparent in both the rate and potential results. The source of this difference is being studied further.

Rate data obtained in the initial 100 min of exposure of the Firth-Sterling material fall near a straight line in a plot of the reciprocal of the rate vs time.[44] The same is true for the data obtained during the initial 40 min with the Westinghouse material in run 16, as shown in Fig. 15.9. The data for Westinghouse material for times between 1 and 48 hr also fall near a second straight line, the slope of which is somewhat greater than that of the first line, but which can be and is drawn through the intercept established by the first line. The results of two other short-duration experiments with the Westinghouse stock are in agreement with the short-term results illustrated.

It is worth recalling here that the fact that the rate data can be represented by an equation of the form

$$1/R = C + Bt \ , \qquad (2)$$

where R = corrosion rate, t = time, and B and C are constants,

as shown in Fig. 15.9, signifies that an exponential relationship exists between the corrosion rate of the metal and the thickness of protective oxide. There are several formulations of exponential relationships between rate and thickness of film which are consistent with the hyperbolic rate-time relations.[46-48]

Values of B in Eq.(2), determined from the data, are included in Fig. 15.9 in units of cm^2 per μg of oxygen as well as in units of $cm^2.amp^{-1}.min^{-1}$. A previous report[44] stated the value for B in Eq.(2) as being 0.8 $cm^2/\mu g$ of oxygen for the Firth-Sterling data covering the first hour of corrosion. The value is obtained originally in units of $cm^2.amp^{-1}.min^{-1}$ and converted to $cm^2/\mu g$ of oxygen. The conversion factor previously used was incorrect, and a corrected value obtained for the first linear portion is 0.29 $cm^2/\mu g$ of oxygen.

Another experiment was performed with a Westinghouse Zircaloy-2 specimen, at a higher temperature, 267°C ± 7°C, in the same oxygenated aqueous acid environment. Attempts to perform polarizability measurements were frustrated by periodic potential oscillations and by failure of the equipment through expulsion of the electrical leads under the high pressure. The oscillations are shown in Fig. 15.10. It is to be observed that the oscillations occurred at essentially the same potential each time, about 672 mv below platinum as reference in the same environment, that the amplitude of the oscillations increased from 258 to 329 mv over a 13-min interval, that the potential excursion was approximately 12-15 sec in duration and, finally, that there were a variety of approaches to the "passivation" potential (-672 mv below platinum). Such oscillations in potential are not uncommon for metals in corrosion environments,[49] and they are interpreted as representing alternating activation-passivation phenomena.

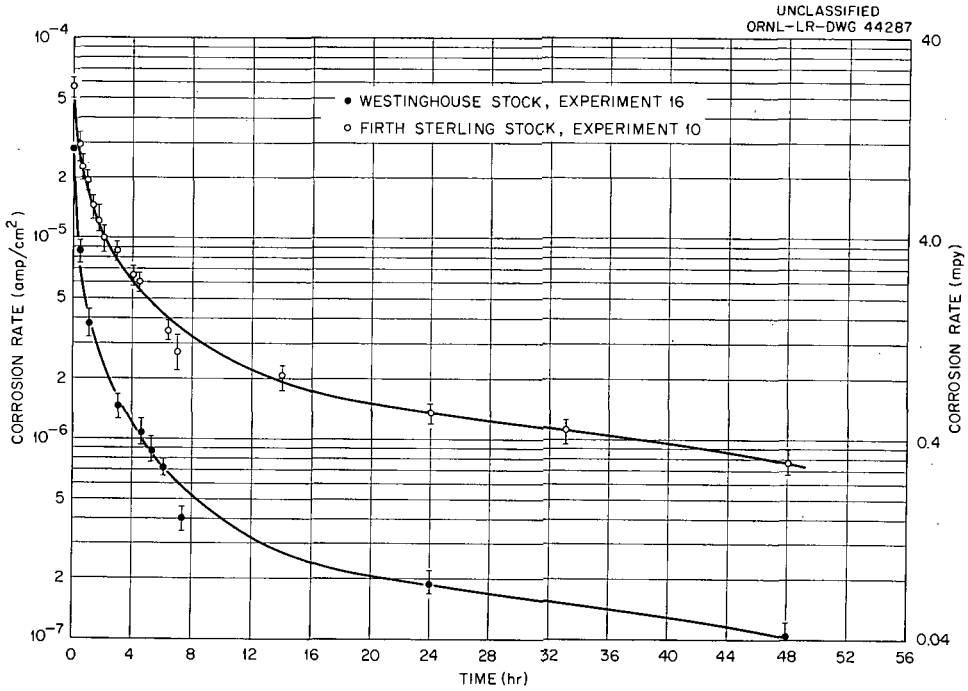

Fig. 15.7. Rate-Time Plot, Zircaloy-2 in 0.05 m H_2SO_4, 600 ppm O_2, at 210°C.

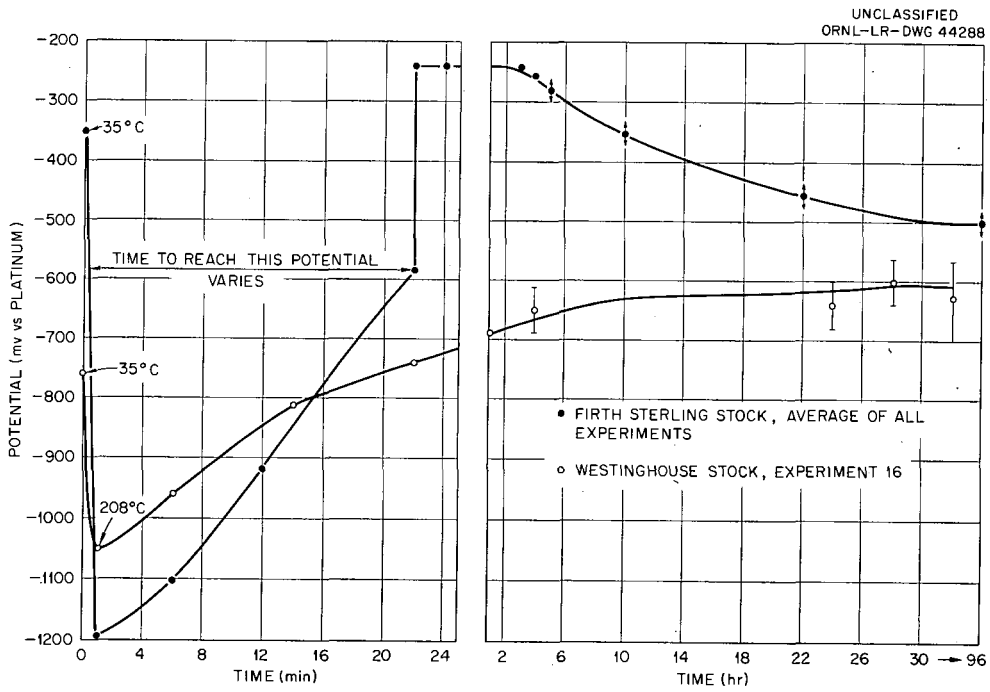

Fig. 15.8. Potential-Time Plot, Zircaloy-2 in 0.05 m H_2SO_4, 600 ppm O_2, at 210°C.

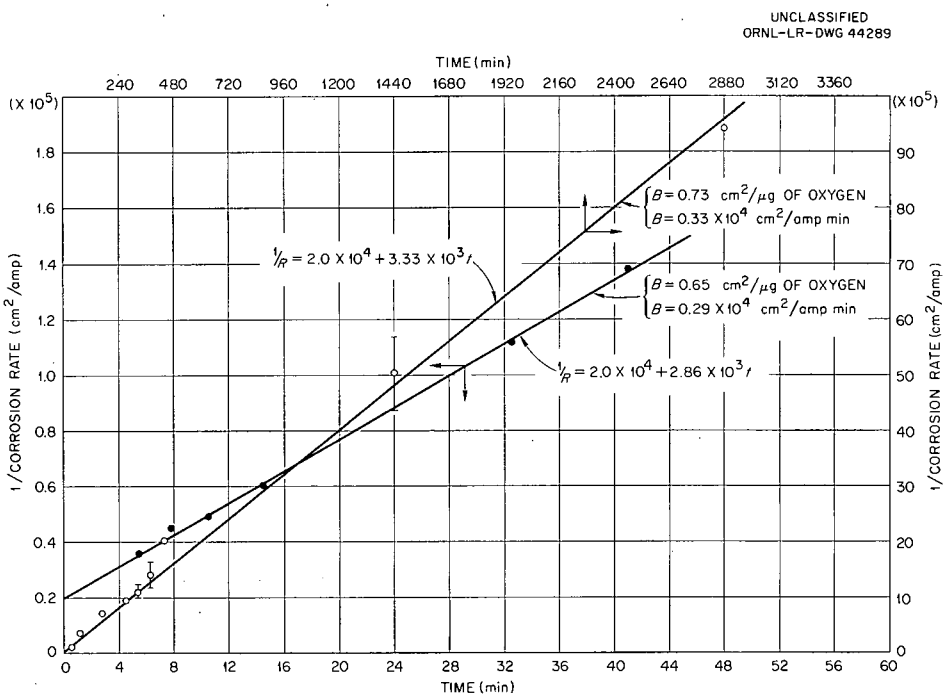

Fig. 15.9. Reciprocal Rate-vs-Time Plot for Zircaloy-2 in 0.05 m H_2SO_4, 600 ppm O_2, at 210°C.

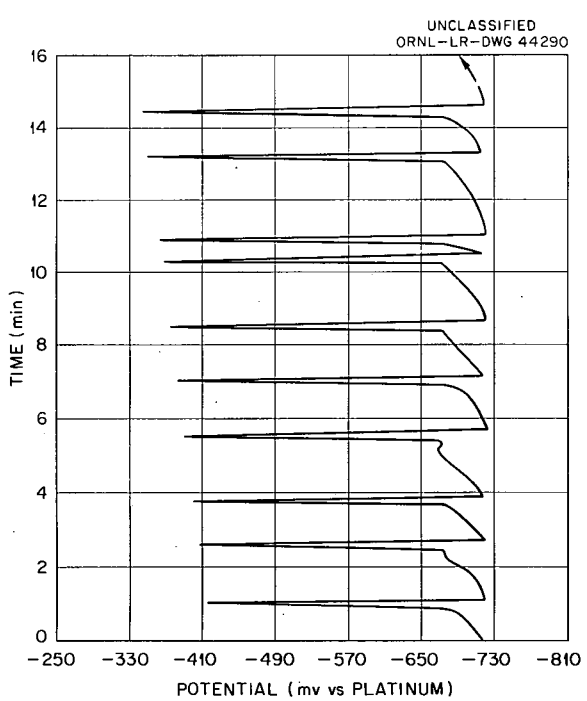

Fig. 15.10. Potential-Time Plot, Zircaloy-2 in 0.05 m H_2SO_4, 600 ppm O_2, at 267°C.

REFERENCES

1. H. C. Savage, G. H. Jenks, HRP Quar. Prog. Rep. for Period Ending April 30, 1957, ORNL-2331, p 112-113 and Fig. 13.1.

2. H. C. Savage, G. H. Jenks, HRP Quar. Prog. Rep. for Period Ending April 30, 1956, ORNL-2095, p 9-92 and Fig. 13.1.

3. T. H. Mauney and H. C. Savage, Test Results on a Heater-Cooler Unit for the ORR In-Pile Loop, ORNL CF-57-6-66 (June 28, 1957).

4. R. A. Lorenz and D. T. Jones, Laboratory Test of a Core Cooler for ORR Loop HN-1, ORNL CF-56-12-65 (Dec. 18, 1956).

5. H. C. Savage et al., HRP Quar. Prog. Rep. Oct. 31, 1958, ORNL-2654, p 164, Fig. 15.5.

6. A. Weitzberg and H. C. Savage, Performance Test of 220-V Three-Phase Stator for Use with 5-gpm In-Pile Loop Pump, ORNL CF-57-10-24 (Oct. 4, 1957).

7. H. C. Savage et al., HRP Quar. Prog. Rep. for Periods Ending April 30 and July 31, 1958, ORNL-2561, p 202.

8. G. H. Jenks et al., HRP Quar. Prog. Rep. Jan. 31, 1957, ORNL-2272, p 107.

9. G. H. Jenks et al., HRP Quar. Prog. Rep. April 30 and July 31, 1958, ORNL-2561, p 223.

10. G. H. Jenks et al., HRP Quar. Prog. Rep. Oct. 31, 1957, ORNL-2432, p 117.

11. G. H. Jenks et al., HRP Quar. Prog. Rep. Jan. 31, 1958, ORNL-2493, p 138.

12. G. H. Jenks et al., HRP Quar. Prog. Rep. Jan. 31, 1958, ORNL-2493, p 138.

13. G. H. Jenks et al., HRP Quar. Prog. Rep. April 30 and July 31, 1958, ORNL-2561, p 223.

14. R. J. Davis, K. S. Warren, and G. H. Jenks, Summary Report of HRP In-Pile Corrosion Test Autoclave L53T-132 (in press).

15. G. H. Jenks et al., HRP Quar. Prog. Rep. Jan. 31, 1959, ORNL-2696, p 133.

16. G. H. Jenks et al., HRP Quar. Prog. Rep. Oct. 31, 1958, ORNL-2654, p 142-164.

17. G. H. Jenks (paper in preparation).

18. K. S. Warren and R. J. Davis, In-Reactor Autoclave Corrosion Studies, LITR I. Outline of Methods and Procedures, ORNL CF-57-5-110 (May 22, 1957).

19. H. C. Savage et al., HRP Quar. Prog. Rep. Jan. 31, 1957, ORNL-2272, p 110 and Figs. 13.1-13.3.

20. R. J. Davis, Tabular Summary of Zircaloy-2 In-Pile Rocking Autoclave Corrosion Data, ORNL CF-58-6-92 (June 18, 1958).

21. R. J. Davis, Tabular Summary of In-Pile Rocking Autoclave Solution Corrosion Data, ORNL CF-59-9-75 (Sept. 24, 1959).

22. J. Paul Pemsler, The Corrosion of Zirconium Alloys in 900°F Steam, NMI-1208 (Aug. 18, 1958).

23. G. H. Jenks et al., HRP Quar. Prog. Rep. Oct. 31, 1957, ORNL-2432, p 120-126.

24. G. H. Jenks et al., HRP Quar. Prog. Rep. April 30, 1957, ORNL-2331, p 120-123.

25. G. H. Jenks et al., HRP Quar. Prog. Rep. April 30 and July 31, 1958, ORNL-2561, p 223.

26. J. C. Banter, J. E. Baker, and R. J. Davis, Analysis of the Status of Chromium in Solution Under In-Pile Conditions, ORNL CF-58-7-63 (July 15, 1958).

27. J. C. Griess et al., Quar. Rep. of The Solution Corrosion Group for the Period Ending April 30, 1958, ORNL CF-58-4-131, p 28-30 (April 30, 1958).

28. J. C. Griess et al., Quar. Rep. of The Solution Corrosion Group for the Period Ending July 31, 1958, ORNL CF-58-7-132, p 21-23 (July 31, 1958).

29. J. C. Griess et al., Quar. Rep. of The Solution Corrosion Group for the Period Ending Oct. 31, 1958, ORNL CF-58-10-95, p 41-47 (Oct. 31, 1958).

30. K. S. Warren, R. J. Davis, and G. H. Jenks, In-Reactor Autoclave Corrosion Studies, II. Autoclave Z-18, ORNL CF-57-3-112, p 16-20 (March 22, 1957).

31. K. A. Kraus et al., Proceedings of the International Uses of Atomic Energy, Geneva, 1958, P/1832, Vol. 28, p 3, United Nations, Geneva, 1958.

32. G. H. Jenks et al., HRP Quar. Prog. Rep. Jan. 31, 1958, ORNL-2493, p 135-138.

33. G. H. Jenks et al., HRP Quar. Prog. Rep. Oct. 31, 1958, ORNL-2654, p 173-176.

34. G. H. Jenks et al., HRP Quar. Prog. Rep. April 30, 1959, ORNL-2743, p 162.

35. J. C. Griess et al., Quar. Rep. of The Solution Corrosion Group for the Period Ending Jan. 31, 1959, ORNL CF-59-1-79, p 9-19.

36. J. C. Griess et al., Quar. Rep. of The Solution Corrosion Group for the Period Ending April 30, 1959, ORNL CF-59-4-44, p 8-24.

37. G. H. Jenks et al., HRP Quar. Prog. Rep. Jan. 31, 1959, ORNL-2696, p 133-143.

38. G. H. Jenks et al., HRP Quar. Prog. Rep. April 30, 1959, ORNL-2743, p 153-160.

39. G. H. Jenks et al., HRP Quar. Prog. Rep. April 30 and July 31, 1958, ORNL-2561, p 228.

40. G. H. Jenks et al., HRP Quar. Prog. Rep. Jan. 31, 1955, ORNL-1853, p 119.

41. G. H. Jenks et al., HRP Quar. Prog. Rep. April 30, 1959, ORNL-2743, p 163-167.

42. K. A. Kraus and F. Nelson, Am. Soc. Testing Materials, Spec. Tech. Pub. No. 195, p 27-57 (1958).

43. J. E. Salmon and D. K. Hale, Ion Exchange, Butterworth, London, 1959.

44. G. H. Jenks et al., HRP Quar. Prog. Rep. Jan. 31, 1959, ORNL-2696, p 146.

45. M. L. Picklesimer, (private communication).

46. K. Hauffe, Oxydation von Metallen and Metalegierungen, Springer-Verlag, 1956.

47. U. R. Evans, Trans. Electrochem. Soc. 91, 547 (1947).

48. R. E. Meyer, J. Electrochem. Soc. 106, 930 (1959).

49. U. F. Franck, Z. Elektrochem. 55, 154 (1951).

Part IV

SLURRY FUELS

16. ENGINEERING RESEARCH

H. W. Hoffman

C. S. Morgan D. G. Thomas

16.1 RHEOLOGY OF AQUEOUS THORIUM OXIDE SUSPENSIONS

Previous studies[1] have demonstrated the applicability of the Bingham-plastic model to the interpretation of the laminar-flow data obtained with thorium oxide suspensions. In the Bingham-plastic model, the yield stress, τ_y, and the coefficient of rigidity, η, are the characteristic parameters. The current object of rheologic studies is to extend this model by relating other factors such as slurry concentration, particle size, and method of oxide preparation to the suspension yield stress.

An attempt was made by use of a least-squares analysis to apply an equation for yield stress,

$$\tau_y = A \frac{\phi^n}{D_p{}^a} , \tag{1}$$

to data obtained in laminar-flow experiments with a range of particle size, D_p, from 1/4 to 12 μ and a range of volume fraction solids, ϕ, from 0.03 to 0.15. The value of the exponent n was found to vary from 1.86 to 4.26. A log-log plot, shown in Fig. 16.1, indicates that n is proportional to the 0.8 power of σ, the standard deviation[2] of the particle size, and leads to the empirical relationship:

$$n = (1.4 \pm 0.25)\ \sigma^{0.8} . \tag{2}$$

Application of Eq. (2) using a standard deviation of 2.6, typical of the slurries tested, gives

$$n = 3.00 \pm 0.54 , \tag{3}$$

and in the remainder of the analysis n was assumed to be 3.0.

The exponent a is found to have a value of 1.42, as shown in Fig. 16.2, but the coefficient A varies between 90 and 420 with a most probable value, as indicated by the analysis, of 180.

The calcining temperature and the previous pumping history of the slurry do not appear to have a consistent bearing on the yield stress except as reflected

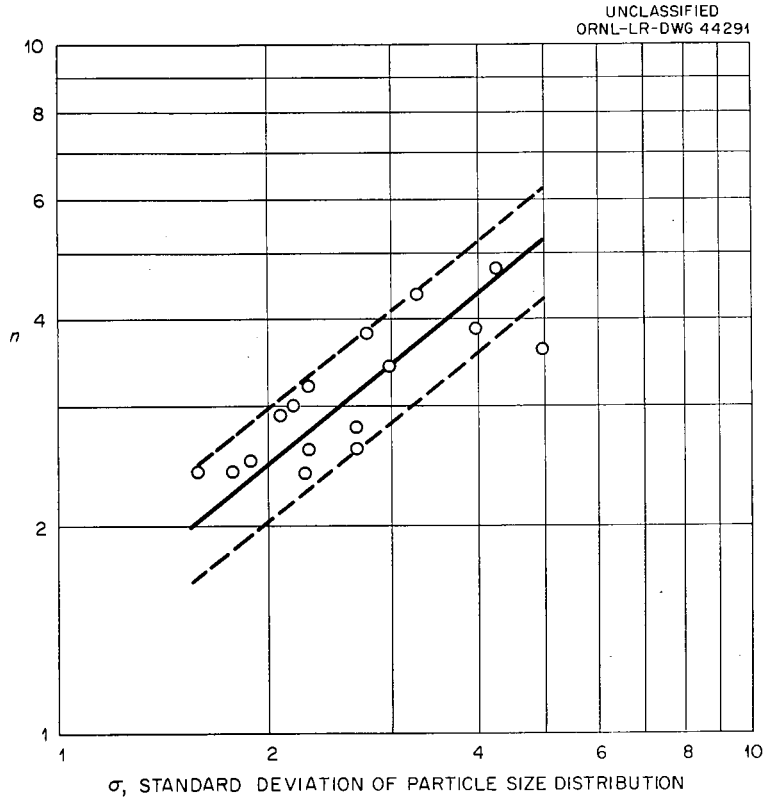

Fig. 16.1. Effect of Distribution of Particle Sizes on n in Relation $\tau_y \sim \phi^n$.

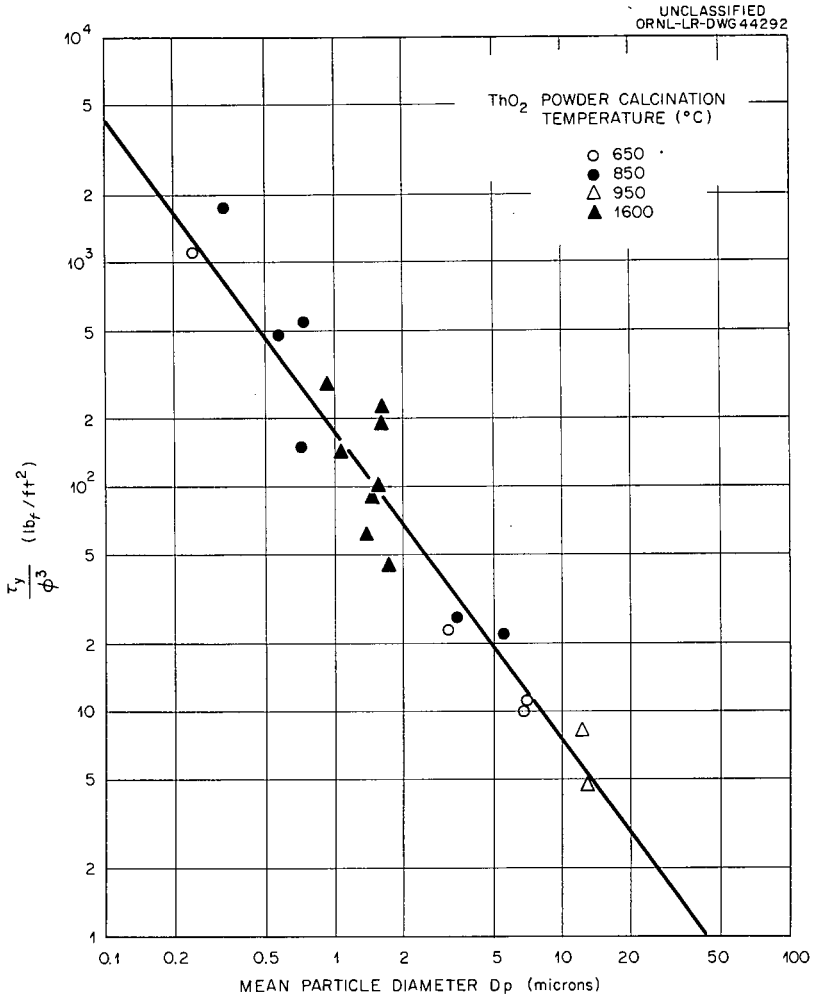

Fig. 16.2. Effect of Particle Diameter and ThO_2 Powder Calcination Temperature on Slurry Yield Stress.

in D_p and σ. However, the range in A implies the importance of factors not considered in Eq. (1), such as particle shape and ionic environment, or the possibility of more accurate expressions involving concentration, particle size, and particle size distribution.

16.2 SLURRY RESUSPENSION AND DROPOUT STUDIES

Previous studies[3] of the minimum mean stream velocity required for suspension transport showed that two regions of flow must be considered. In the first region the suspension is sufficiently concentrated to be in the compaction zone and hence has an extremely slow settling rate. The second region is observed with more dilute suspensions which are in the hindered-settling region and settle about 10 to 100 times faster than slurries which are in compaction. It was shown[3] that a critical wall shear velocity for suspension transport, $(u_{*w})_c$, existed which was a function of the particular slurry but was essentially independent of concentration, provided that the slurry was not in compaction. Dimensional considerations suggest that a correlation of the form

$$\frac{U_t}{(u_{*w})_c} = \psi\left(\frac{D_p(u_{*w})_c}{\nu}\right), \tag{4}$$

where U_t = settling velocity, ft/sec,

$(u_{*w})_c$ = wall shear velocity for minimum suspension transport velocity, ft/sec,

D_p = particle diameter, ft,

ν = kinematic viscosity, ft^2/sec,

might generalize the data for the noncompaction region. This was tested using data from the literature[4,5] for glass beads, steel shot, sand, and lead shot as well as the present data for ThO_2 suspensions. For flocculated suspensions, the particle diameter was taken as the floc diameter from hindered-settling measurements and the terminal settling velocity was assumed to be that of the floc at infinite dilution. For unflocculated suspensions, the mean particle diameter and single-particle settling rates were used. The results are given in Fig. 16.3. Although the data cover a wide range of particle diameters, settling rates, and particle densities, as well as pipes from 3/4 to 30 in. in diameter, they appear to be correlated by a single curve; however, additional data using both flocculated and unflocculated suspensions are required for verification.

16.3 THORIA CAKING STUDIES

16.3.1 Tests with Electrolyte Additives

Cake formation in ThO_2 slurry circulation systems has been prevented[6] by the addition of small quantities of materials which form electrolytes in water (e.g., CrO_3, MoO_3, and UO_3) to the fresh ThO_2. The surface-active effect of the electrolyte is believed to alter the degradation of oxide particles. Slurry circulation tests are being made in the 30-gpm loop to determine whether cake formation can be prevented by adding an electrolyte after the ThO_2 particles are degraded to small particles in the cake-forming size range. Such tests are of interest

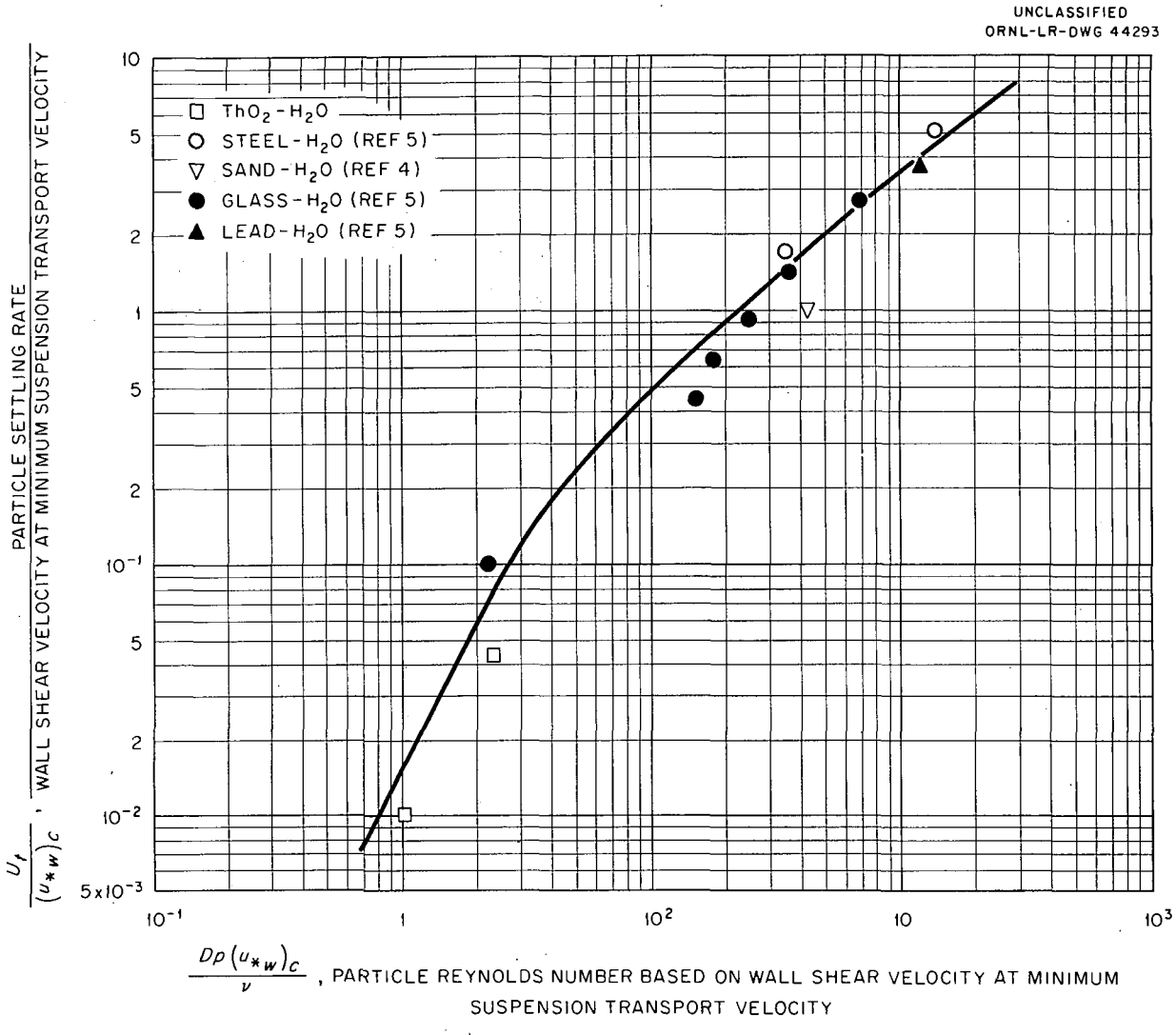

Fig. 16.3. Correlation for Minimum Sediment Transport Velocity.

since oxide particles which resist degradation in out-of-pile tests may degrade on long in-pile circulation, and it would be desirable to prevent caking by an addition of electrolyte at that time.

Thoria spheres that are produced during loop circulation of certain ThO_2 batches are agglomerates of caking-size particles. During circulation particles wearing off the spheres can reagglomerate on metal surfaces to form cakes. A slurry of such spheres was circulated in the 30-gpm loop at 275°C with additions of CrO_3 to concentrations of 500, 1500, 3500, and 10,000 ppm, based on ThO_2. Results did not give a definitive answer as to whether CrO_3 could prevent cake formation when added after particle degradation had occurred. With 500, 1500, and 3500 ppm CrO_3, cake formation occurred as would have been expected in the absence of electrolyte additions. With 10,000 ppm CrO_3, there was no cake in the pump impeller and only a thin film in the 5-fps section of the multidiameter sample barrel. However, before the CrO_3 concentration was raised to 10,000 ppm, the spheres had been partially dispersed as evidenced by fines in the slurry. The cumulative effect of circulation in the presence of CrO_3, rather than the high chromic acid concentration, may have reduced the caking tendency of the slurry. A run with fresh ThO_2 spheres and 10,000 ppm CrO_3 resulted in cake formation. Further slurry circulation tests are being made with $NaAlO_2$, which strongly influences slurry properties at room temperature, and even at elevated temperatures, as evidenced by a reduction of slurry yield stress by about 50% during loop circulation at 280°C.

16.3.2 Low-Concentration Slurry

A slurry circulation test with ThO_2 batch LO-20 (normally a cake former) at concentrations from 11 to 52 g of Th per kg of H_2O resulted in cake and sphere formation. This indicates that the solids concentration is not an important factor in cake formation and that degradation due to particle-particle interaction is of secondary importance.

16.3.3 Detection of ThO_2 Cake Formation

A heat-transfer disc was placed in the 30-gpm loop circuit to test for cake formation. The disc, made of copper, is similar to the disc installed in the 200B loop[7] except that it is heated instead of cooled. A heater placed around the disc causes the inner surface temperature to be approximately 12°C above the slurry stream temperature when there is no ThO_2 deposit. The heat-transfer coefficient, which is calculated from readings of thermocouples placed at different depths in the disc, proved sensitive to ThO_2 films. There was a decisive difference for films approximately 2 mils and 1 mil thick. Deposits of ThO_2 on the disc were similar to those in the 5-fps section of the multidiameter sample barrel which has the same diameter, evidencing no effect on caking of different metal surface or of the thermal difference.

In one run in which ThO_2 deposition occurred, the loop was put through four thermal cycles between room temperature and 275°C. Cake deposits were damaged by the thermal cycling as evidenced by striations and layers of different thickness on the copper disc and in the multidiameter sample barrel.

16.4 SURFACE CHEMISTRY OF ThO_2*

Water-vapor adsorption isotherms on ThO_2 prepared by oxalate precipitation followed by calcination at 800°C evidenced definite chemisorption.[8] Kelvin pore-size distributions computed from desorption isotherms exhibited a relatively sharp pore distribution at a radius of about 10 Å, as well as a very broad spectrum of pores in the range of 10 to 200 Å. Thorium oxide from oxalate which had undergone long digestion in the supernatant had reduced pore capacity.

High-resolution electron micrographs, Fig. 16.4, show that particles of ThO_2 calcined at 800°C consist of aggregates of minute crystals whose predominant morphology is that of octahedrons, with no indication of a platelet structure.[8] Electron micrographs, Figs. 16.5 and 16.6, show that sharp edges of ThO_2 particles calcined at 1600°C are rounded during loop circulation.

REFERENCES

1. D. G. Thomas, Solids Dispersed in Liquids, ORNL CF-56-10-35 Revision 1, (Oct. 15, 1958).

2. J. M. Dallavalle, Micromeritics, 2d ed., p 57, Pitman Publishing Co., New York, 1948.

3. D. G. Thomas, Use of Thorium Oxide Suspensions in Aqueous Homogeneous Nuclear Reactors, paper presented at AEC Symposium on "Particle-Fluid Interactions," New York, May 4 and 5, 1959; see also HRP Quar. Prog. Rep., April 30, 1959, ORNL-2743, p 63-65.

4. N. S. Blatch, Trans. Am. Soc. Civil Eng. 57, 307-363 (1906).

5. G. Murphy, D. F. Young, and R. J. Burian, Progress Report on Friction Loss of Slurries in Straight Tubes, ISC-474 (April 1, 1954).

6. R. B. Korsmeyer et al., HRP Quar. Prog. Rep., April 30 and July 31, 1958, ORNL-2591, p 109.

7. R. B. Korsmeyer et al., HRP Quar. Prog. Rep., Jan. 31, 1959, ORNL-2696, p 61.

8. A. L. Draper and W. O. Milligan, Structure and Surface Chemistry of Thorium Oxide, summary report from Rice Institute, Huston, Texas (Sept. 1, 1959).

*This work was carried out at the Rice Institute under subcontract No. 1201.

UNCLASSIFIED
PHOTO 48785

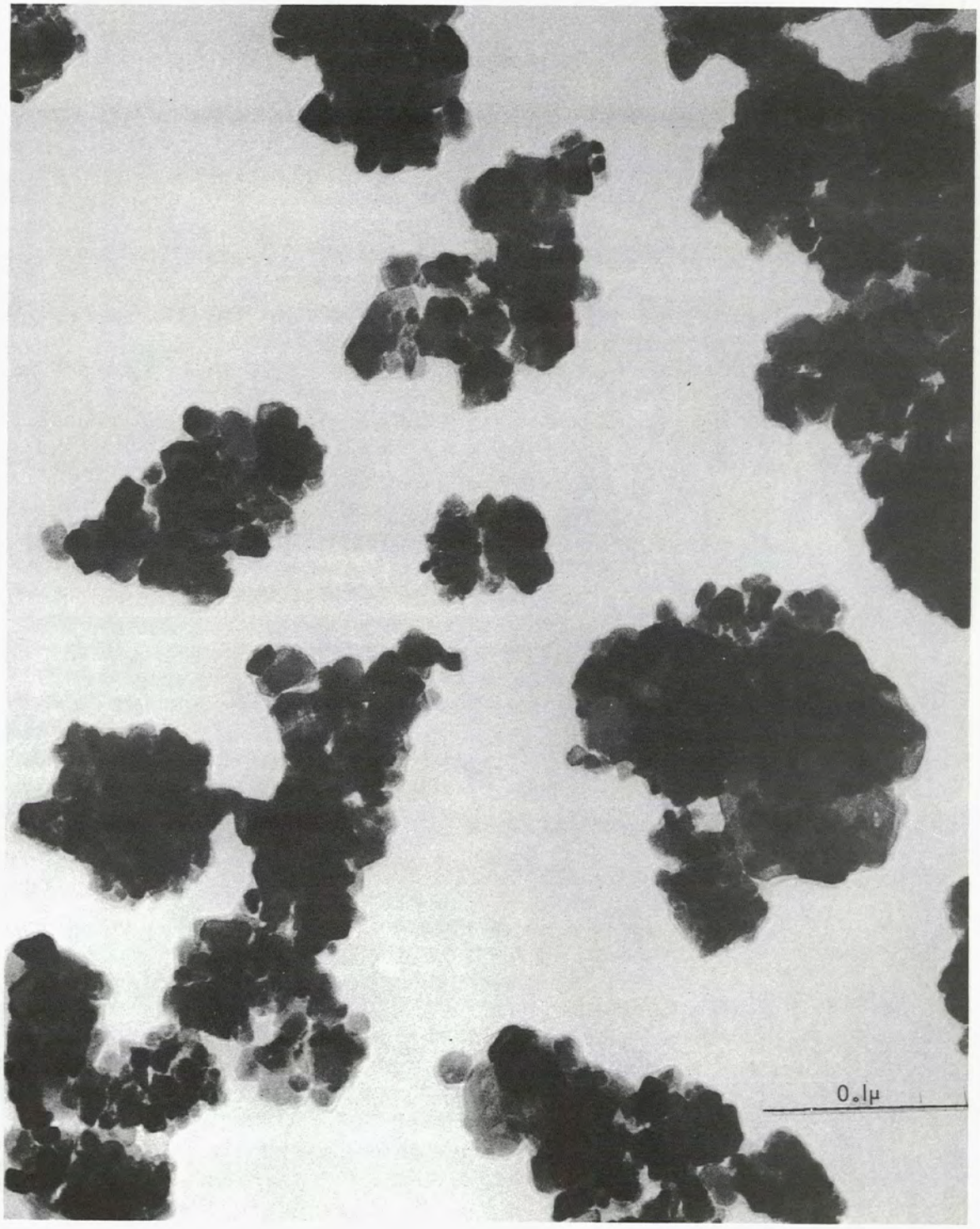

Fig. 16.4. Electron Micrograph of 800°C-Calcined ThO_2. 400,000X.

UNCLASSIFIED
PHOTO 48786

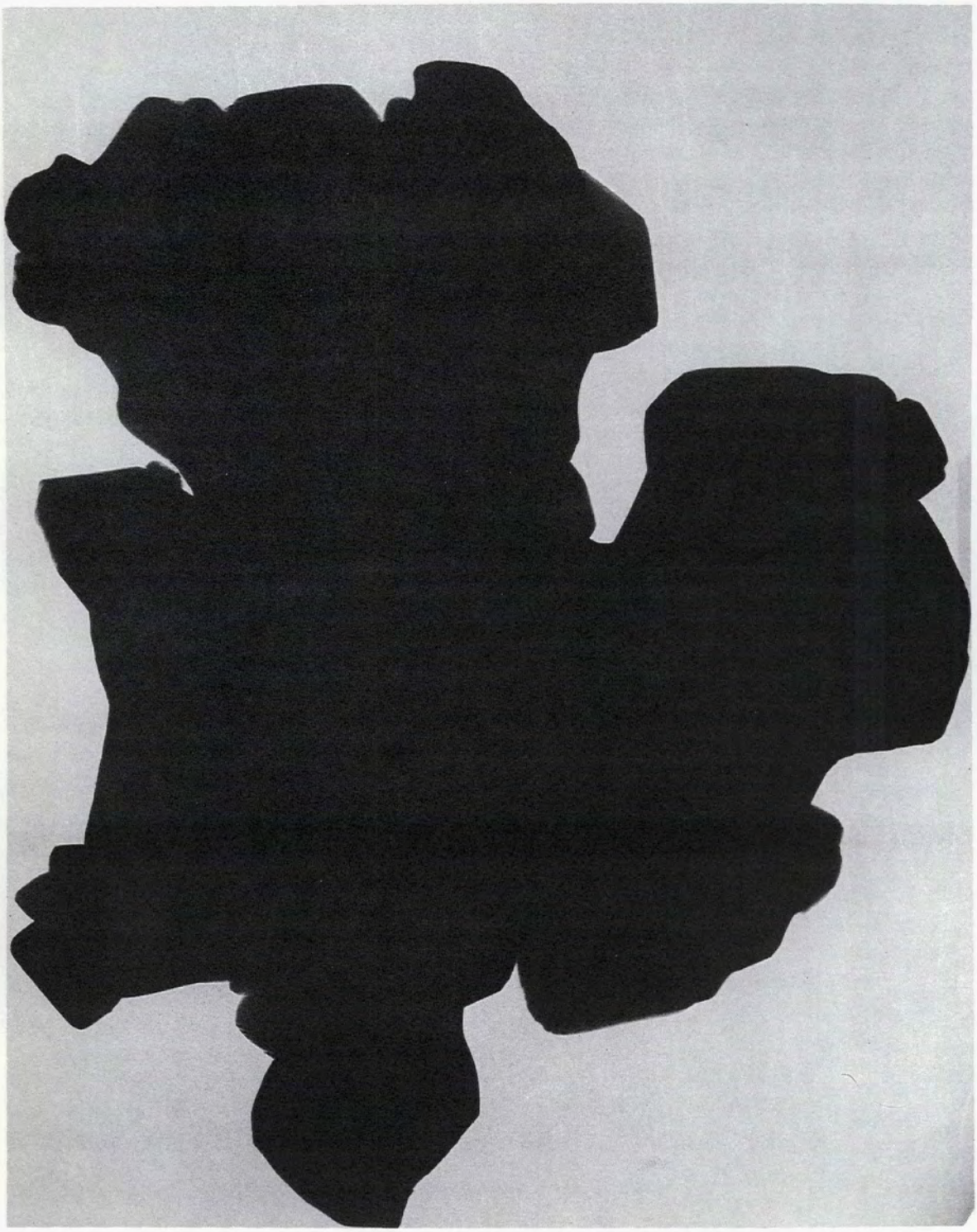

Fig. 16.5. Electron Micrograph of 1600°C-Calcined ThO_2 Before Circulation. 100,000X.

UNCLASSIFIED
PHOTO 48784

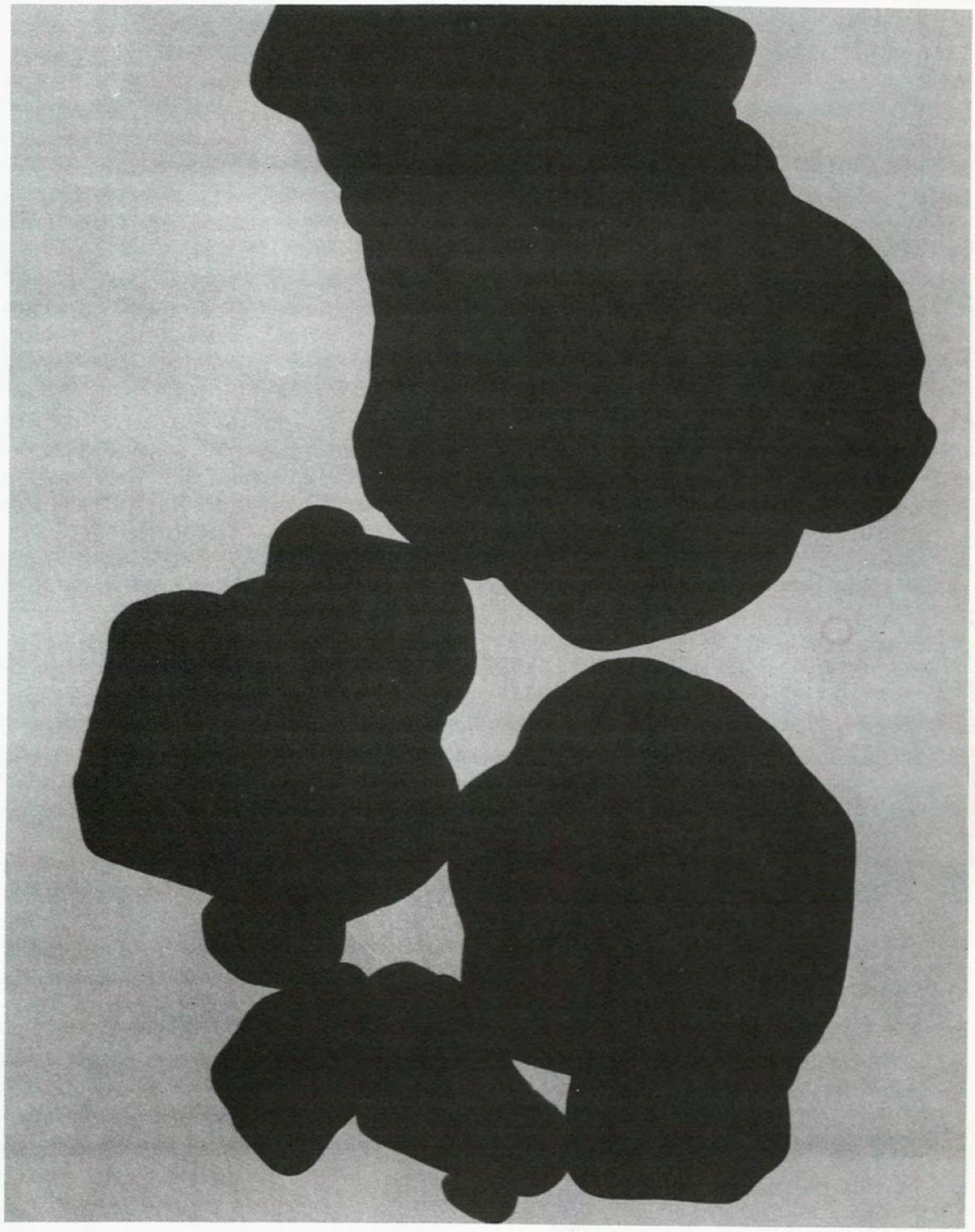

Fig. 16.6. Electron Micrograph of 1600°C-Calcined ThO_2 After Circulation. 100,000X.

17. SLURRY IRRADIATION STUDIES

J. P. McBride N. A. Krohn

17.1 SLURRY IRRADIATIONS IN THE LITR

A slurry (500 g of Th per kg of D_2O) of thorium oxide containing 8% natural uranium prepared by adsorption from ammonium uranyl carbonate and fired at 1050°C was irradiated in the LITR for 370 hr (LITR-55). The experiment was operated initially at 300°C, with the temperature being reduced gradually to 230°C over the period of the test. It was expected from previous tests in the Graphite Reactor, with a slurry of thorium, that small pressures of radiolytic gas would be generated, but none was observed. The discrepancy might be caused by the higher gamma flux in the LITR or by a higher catalytic activity of the 8%-uranium material.

17.2 POSTIRRADIATION EXAMINATION

All the irradiated slurries (LITR-53, 54 (ref 1), and 55) were recovered and examined. The first was a slurry of 650°C-fired thoria from Westinghouse to which 0.5% U^{235}, as the oxide, and 144 ppm of palladium (deposited on thoria) were added before irradiation under oxygen for 242 hr at 290°C. The recovered slurry was yellowish brown and settled slowly, leaving a turbid supernatant which could not be clarified. This resulted in high thorium, uranium, and fission product contaminations of the supernatant (Table 17.1). Corrosion product pickup was low, as expected from a low-fired oxide (Table 17.2).

Table 17.1. Distribution of Fission Products in Irradiated Slurries

	Amount in Supernatant (%)									
Experiment	Gross β	Gross γ	Sr	Zr	Cs	Ru	RE	Nb	I	Pa
LITR-53*	11.9	11.9	2.0	16.3	47.7	25.3	16.2	10.1	16.4	10.9
LITR-54**	1.8	1.7	1.9	1.8	56.7	9.1	1.6	1.0	3.9	1.3
LITR-55**	0.9	2.2	9.9	0.2	47.0	25.0	21.8	0.5	33.4	0.3

* 650°C-calcined Westinghouse ThO_2; 19.2% of thorium in supernatant.

**1050°C-calcined ThO_2-8% natural uranium oxide.

Table 17.2. Corrosion Products in Irradiated Slurries

Experiment	Atmosphere	Time Stirred (hr)	Time Irradiated (hr)	Corrosion Products (g/kg Th)		
				Fe	Ni	Cr
LITR-53	Oxygen	242	242	5	2	0.5
LITR-54	Air	360	335	76	6	3
LITR-55	Air	408	370	43	10	8

The second slurry recovered was of a thorium oxide containing 8% natural uranium, prepared by the adsorption method and then fired at 1050°C. It was irradiated 335 hr under air at temperatures from 265 to 300°C. The recovered slurry was black and showed the usual distribution of fission and corrosion products.[1]

The third slurry, described above, was dry when recovered, apparently having lost its water during the cooling period. The solids, which were brown, were washed out of the autoclave with 12 ml of water and subsequently separated and analyzed in the usual way.

17.3 IN-PILE GAS PRODUCTION AND RECOMBINATION STUDIES

Three irradiation experiments in the ORNL Graphite Reactor were made for the purpose of measuring radiolytic gas production and recombination rates in slurries under an initial atmosphere of oxygen (250-320 psi at 25°C). Two slurries were D_2O suspensions of thorium oxide containing 2.8% U^{235} prepared by calcining coprecipitated thorium-uranous oxalate at 650°C. The third was ThO_2-3% U^{235} prepared by adsorption and fired to 1000°C. In the first irradiation the concentration was 500 g of Th per kg of D_2O and in the other two, 250 g of Th per kg of D_2O. Production rates of deuterium at 200°C were 3.9×10^{-4}, 1.9×10^{-4}, and 2.0×10^{-4} mole/hr, respectively, corresponding to a G value of ~0.8. No equilibrium pressure data were obtained in the first test because of early failure of the stirrer-drive coils.

The second irradiation ran 1530 hr, and equilibrium pressures were reproducibly measured from 200 to 290°C. Radiolytic gas pressures were calculated from the total pressures with the aid of a pressure-temperature calibration curve obtained prior to reactor startup (Fig. 17.1). First-order recombination rate constants calculated from equilibrium measurements and measured during reactor shutdowns agreed well with each other and with previous results (Fig. 17.2).

The third irradiation was for 2016 hr. Equilibrium radiolytic gas pressures in excess of steam and added oxygen were not reproducible, and from measurements at low temperatures with the reactor down it became apparent that the oxygen added initially was being rapidly consumed, probably as a result of the increased abrasiveness of the 1000°C-fired oxide. At some time near 1000 hr, the oxygen apparently was completely used up, and a deuterium atmosphere was accumulated, resulting in very low gas-production rates for the remainder of the run.

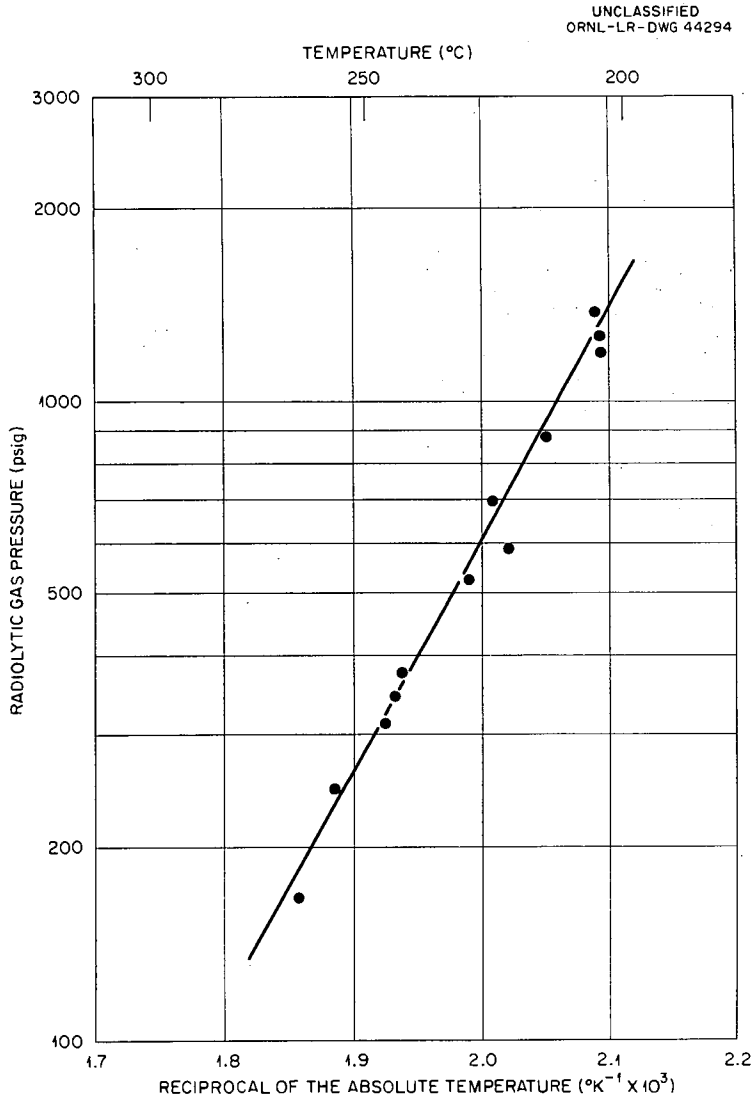

Fig. 17.1. Equilibrium Radiolytic-Gas Pressures over a Slurry of Thorium-Uranium Oxide in the Presence of Excess Oxygen.

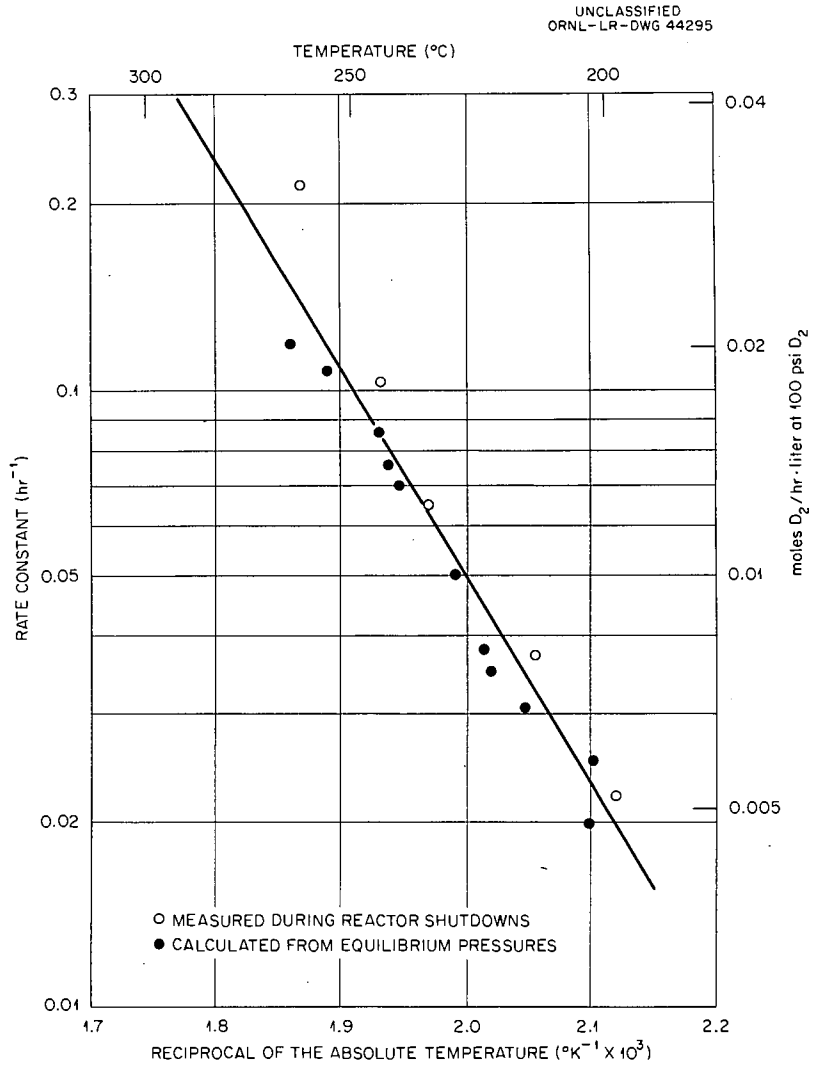

Fig. 17.2. Reaction Rate Constants for Recombination of Radiolytic Gas over a Slurry of Thorium-Uranium Oxide in the Presence of Excess Oxygen.

17.4 HYDROGEN SOLUBILITY IN AQUEOUS SLURRIES

The solubility of hydrogen in water was determined by the method proposed for determining the solubility of gases in slurries.[2] The isotherms are shown in Fig. 17.3a. A cross plot of the data from isotherms was made to give the isobars shown in Fig. 17.3b. Henry's law constants calculated from the isotherms are given in Table 17.3 together with data obtained by a direct sampling technique.[3] Agreement with Battelle Memorial Institute (BMI) data was good except at 150 and 200°C.

REFERENCES

1. J. P. McBride et al., HRP Quar. Prog. Rep. Apr. 30, 1959, ORNL-2743, p 204-223.

2. H. F. Soard, Solubility of Oxygen, Hydrogen, and Iodine in Thorium Oxide Slurries, ORNL CF-59-2-97, (Feb. 2, 1959).

3. H. A. Pray, C. E. Schweichert, and B. H. Minnich, The Solubility of Hydrogen, Oxygen, Nitrogen, and Helium in Water at Elevated Temperatures, BMI-T-25, p 15 (May 1950).

Table 17.3. Henry's Law Constants* for Hydrogen in Water

Temperature (°C)	From BMI Data**	From ORNL Data
27	11.0	11.0
100		10.4
150	9.30	5.0
200	6.98	4.3
250	2.90 (260°C)	2.6
300	1.86 (316°C)	1.7

*$K = P_A/N_A$, where P_A = partial pressure of gas in psi and N_A = mole fraction of gas in solution.

**See ref 3.

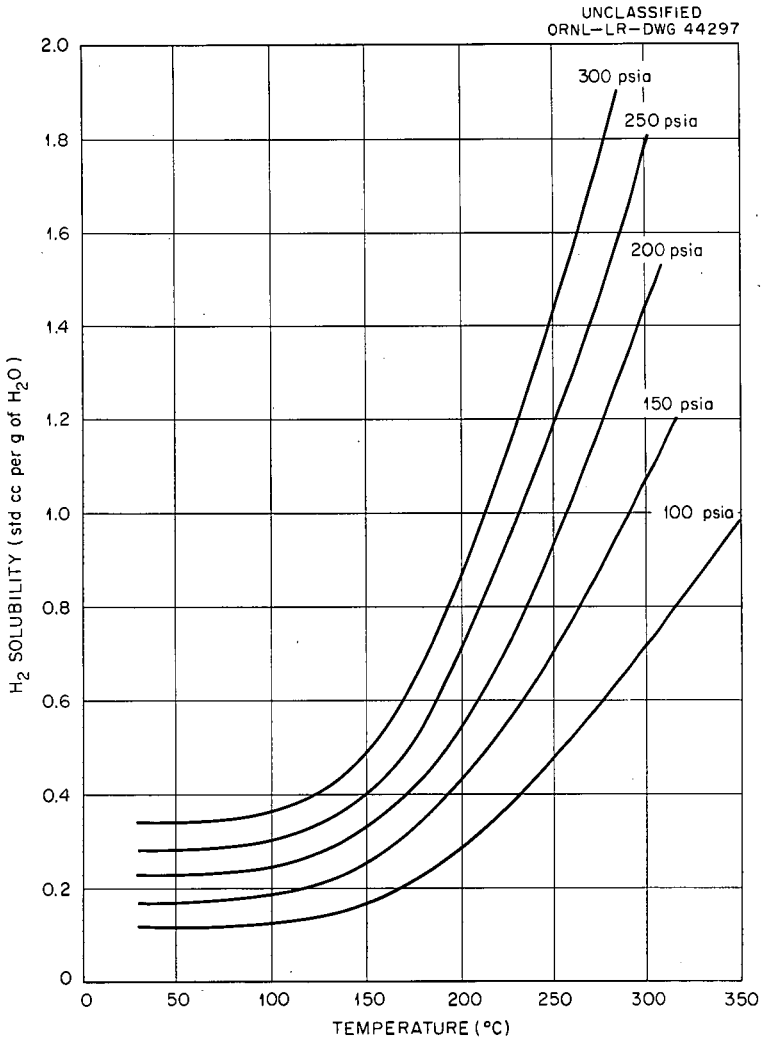

Fig. 17.3a. Solubility Isotherms for Hydrogen in Water.

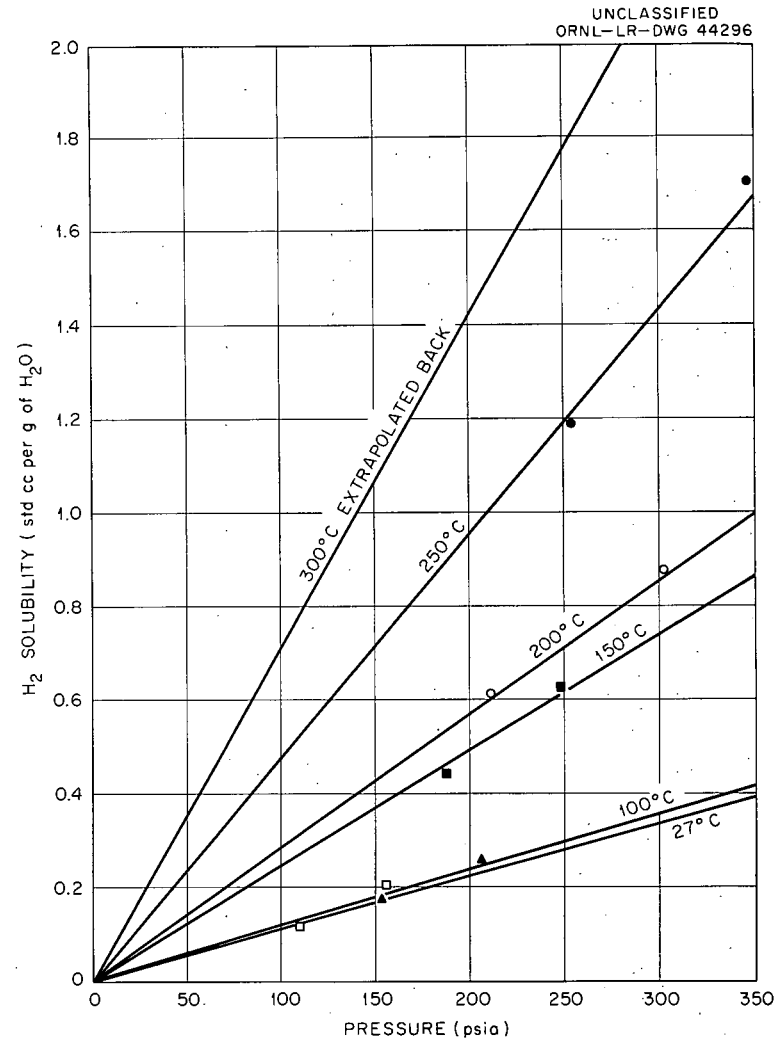

Fig. 17.3b. Solubility Isobars for Hydrogen in Water.

18. DEVELOPMENT OF GAS-RECOMBINATION CATALYSTS

J. P. McBride L. E. Morse

Development of a catalyst for the internal recombination of radiolytic gas in thorium and thorium-uranium oxide slurries continued with studies concerning the effect of pumping on the natural catalytic activity of a thorium-uranium oxide slurry containing no added catalyst and further studies on the preparation and use of palladium catalysts. A new gas-injection apparatus for carrying out the gas recombination measurements was also developed. In previous work and in some of the recent studies, gas-recombination measurements were made by adding the hydrogen and oxygen to a slurry in an autoclave, bringing the autoclave to temperature, and following the recombination by measuring the decrease in pressure with time. The new method permits adding measured quantities of the gases to the autoclave at high temperature, eliminating the explosion hazard encountered frequently in the previous method, permitting data to be obtained at high temperatures with very active catalytic systems, and greatly increasing the number of experiments that can be performed in a given time.

The activity of catalytic systems was expressed in two ways: by the reaction rate in moles of H_2 (D_2) consumed per liter per hour at a given temperature and 100 psi H_2 (D_2) partial pressure, and by a catalyst performance index, CPI,[1] which is equal to the catalyst activity as defined above divided by 0.38 times the G value for gas production, which was taken as 0.6. It was convenient also to correlate the CPI on the basis of a 1 millimolal catalyst concentration. The CPI is equal to the power density in w/ml that can be supported by a given catalytic system at a steady-state H_2 (D_2) partial pressure of 100 psi.

18.1 EFFECT OF PUMPING ON CATALYSIS IN THORIUM-URANIUM OXIDE SLURRY

The catalytic activity of a 1050°C-fired thorium - 8% uranium oxide slurry in D_2O (containing no catalyst) that was pumped at 200°C in a D_2 atmosphere [REED run BS-26 (ref 2)] was followed by determining gas recombination rates of stoichiometric D_2-O_2 mixtures in slurry samples taken at various time intervals. The recombination rates at 280°C were comparatively low, varying from about 0.005 mole D_2/liter-hr for the sample pumped 22 hr to 0.06 mole D_2/liter-hr for the 654-hr sample, both measurements at 100 psi D_2 partial pressure. Rates were somewhat higher in the intermediate temperature regions and increased with pumping time (see Table 18.1). These are probably associated with reduced uranium or corrosion-product species that are oxidized and hence deactivated by heating under stoichiometric gas.[3]

Table 18.1. Catalytic Activity of a Th-8% Uranium Oxide Slurry in D_2O Pumped in a D_2 Atmosphere*

Pumping Time (hr)	U(IV) (%)	Reaction Temperature (°C)	Recombination Rate, P_{D_2} = 100 psi (moles D_2/liter-hr)
22	57	280	0.005
142	74	174	0.49
		279	0.03
339	86	204	0.36
		279	0.07
654	93	167	1.33
		204	0.34
		281	0.06

*REED run BS-26 (ref 2).

18.2 PALLADIUM AS A CATALYST

The activity of the palladium used as a catalyst in thorium oxide slurries depends on its method of preparation. Several methods of preparing the palladium catalyst were investigated. The "Westinghouse method"[2] consisted in reducing palladium onto thorium oxide suspended in an acetone-alcohol solution of palladium nitrate and recovering the resulting solid. In the second method (the dispersion method), thoria fired at 650 to 1600°C was refluxed in a palladium nitrate solution at a palladium concentration of 7000 ppm or less (based on thorium) to produce a dispersed system, and then reduced with H_2 to give a flocculated suspension whose solids were dried to a readily slurriable powder. Studies were carried out with these preparations. The Westinghouse preparation was the least active, with a CPI of 1.4-4.8 w/ml per 100 psi D_2 per millimolal concentration of palladium; that from the dispersed system was 10 to 20 times more active.

18.2.1 Westinghouse Type of Preparation

Work on the Westinghouse type of preparation was carried out primarily in support of the REED radiation-corrosion studies being made with slurries in the LITR. Two slurries were investigated: a 125 g of Th per kg of D_2O slurry of Th - 5% uranium oxide containing 125 ppm of palladium based on thorium, and, in an effort to obtain higher power densities, a 111-g/kg slurry of Th - 8% uranium oxide containing 1983 ppm of palladium, based on thorium. Since the in-pile experiments are conducted under excess oxygen (i.e., in excess of $O_2/D_2 = 0.5$), these slurries were heated at 280°C in the presence of O_2 (300 psi at 25°C) prior to their use in recombination experiments. Reaction rates in the former slurry were 0.10 to 0.16 mole D_2/liter-hr at 280°C and 100 psi D_2 partial pressure, and in the latter 0.6 to 1.5 mole D_2/liter-hr under the same conditions. These rates correspond to over-all catalyst performance indexes

[catalyst activity/(0.38)(0.6) = (w/ml)/100 psi D_2] of 0.4 to 0.7 in the former and 3 to 7 in the latter. On the basis of a 1 millimolal concentration of palladium, the Westinghouse preparation would support between 1.4 and 4.8 w/ml at 100 psi D_2 partial pressure per millimole of palladium.

The catalyst preparation added to the above slurries contained 0.026 g of palladium per gram of ThO_2. After reduction of the palladium onto the 650°C-fired thoria in the acetone-alcohol mixture in the preparation step, the recovered solid was dried at 150°C. In addition, for the slurry containing the higher palladium concentration, the solid was heated in O_2 and then in H_2 (each for 0.5 hr) at 450°C.

18.2.2 Dispersion Preparation Method

Experiments with the slurry system prepared from palladium catalyst preparations made by the dispersion method were carried out with the new gas-injection apparatus (Sec. 18.3). The dispersion-prepared material (P-16) was obtained by refluxing 1600°C-fired ThO_2 in an aqueous palladium nitrate solution, treating the mixture with H_2 to reduce the palladium, and calcining the resulting solid at 800°C. The palladium concentration was 230 ppm, based on thorium. An aqueous slurry was prepared from this material. It contained 100 g of Th per kg of H_2O and was heated in water overnight at 280°C in the presence of O_2 (300 psi at 25°C). To preserve this "oxidized" state, the slurry was maintained in an O_2 overpressure when not in use, and the order of injecting gases was: O_2 before H_2. The reaction rates in near-stoichiometric gas mixtures in the slurry were equivalent to a catalyst performance index of 5.8 to 17.5 w/ml per 100 psi H_2 (Table 18.2). For a 1 millimolal palladium concentration the CPI would be 27 to 81 w/ml per 100 psi H_2 per millimolal concentration of palladium. Treatment of the slurry at 280°C for 65 hr with an H_2 overpressure (500 psi at 25°C) resulted in similar rates for near-stoichiometric quantities of H_2 and O_2 (H_2/O_2 ratios between 1.5 and 2.5). At large excesses of either H_2 (H_2/O_2 = 2.4 to 6) or O_2 ($H_2/O_2 \leq 0.54$) above the stoichiometric, rates were too fast to measure. The slurry-catalyst system in either the "oxidized" or "reduced" forms showed no decrease in activity with repeated experimentation. The total time the slurry was at 280°C under both oxidizing and reducing conditions was approximately 15 days.

18.3 GAS-INJECTION APPARATUS FOR CATALYST STUDIES*

An apparatus that permits the injection of measured quantities of hydrogen and oxygen into an autoclave containing slurry at reaction temperature is shown in Fig. 18.1. The gases are drawn into calibrated pipettes at known pressure by retracting the piston of capstan-operated high-pressure generators and then, by appropriate valving and reversing of the piston, forcing the gases into the slurry autoclave. The pressure-transmitting fluid is water.

The apparatus is now in routine use in laboratory gas-recombination studies. Calibration of the equipment permits an accurate measure of gas addition and hence control over the proportions of H_2 and O_2 added. Addition of the gases at temperature makes it unnecessary to cool the bomb between experiments to charge gas and the quantity of gas required for each experiment is markedly decreased, less than 0.1 ml of water being added during any one experiment. Addition of the gases at temperature has also eliminated the

*Designed by J. C. Suddath, Process Design Section, Chemical Technology Division.

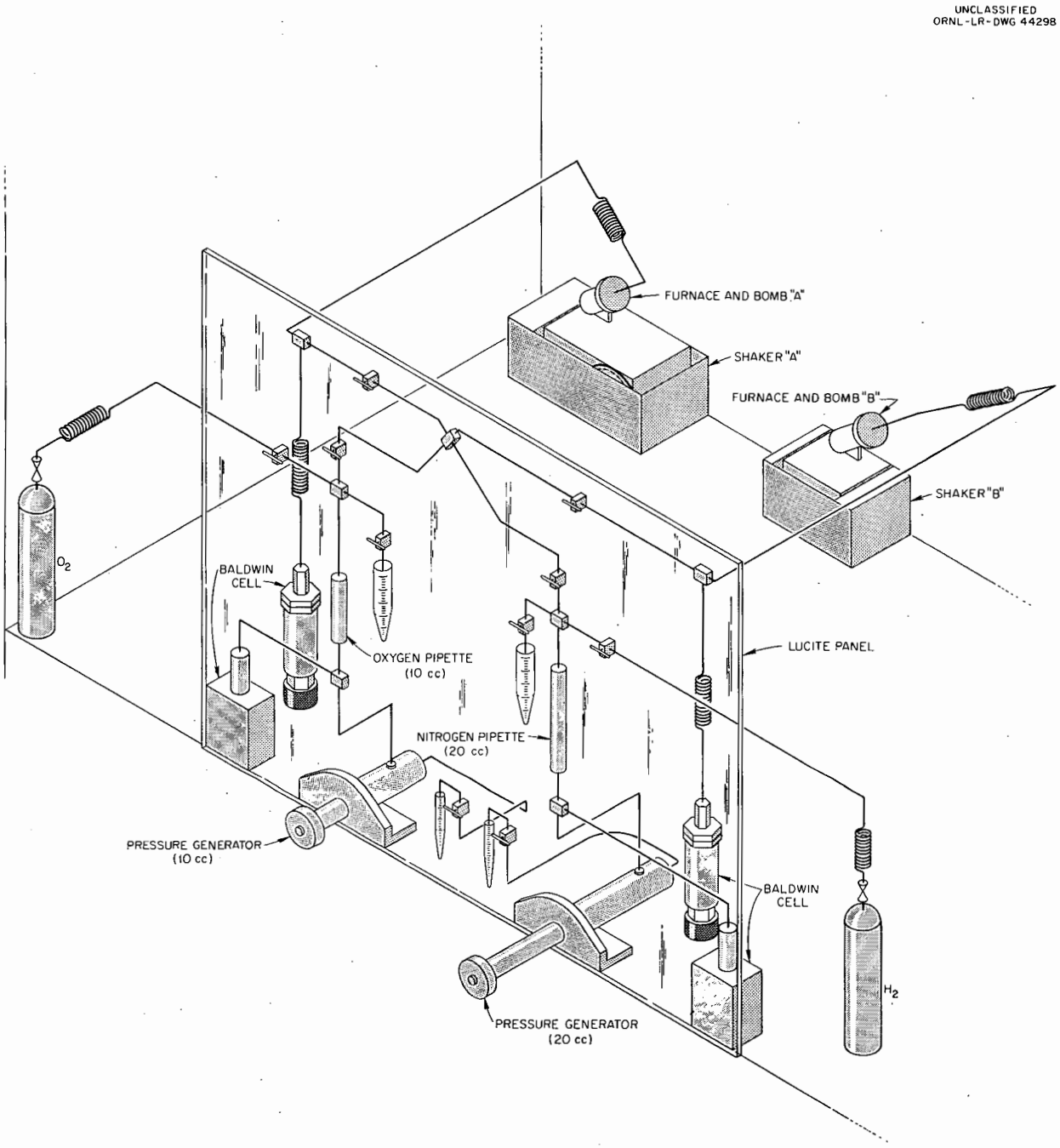

Fig. 18.1. Gas Injection Apparatus for Gas-Recombination Studies.

Table 18.2. Reaction of H_2-O_2 Mixtures in Aqueous Thorium Oxide Slurries Containing Palladium Catalyst; Dispersion Preparation Method, P-16 (230 ppm Palladium, Based on Thorium)

100 g of Th per kg of H_2O, 1600°C-fired ThO_2
Slurry pretreated with O_2 at 280°C for 16 hr
Reaction temperature, 280°C

H_2/O_2 Ratio	Reaction Rate P_{H_2} = 100 psi (moles H_2/liter-hr)	Catalyst Performance Index (w/ml per 100 psi H_2)	
		Based on Wt of Pd given	Based on 1 millimolal Pd
2.3	1.8	8.1	37
2.1	3.9	17.1	79
1.9	4.0	17.5	81
1.8	1.3	5.8	27

explosion hazard encountered when gases were charged at room temperature and heated to reaction temperature. The arrangement of the apparatus permits the removal from the slurry, without dismantling the autoclave, of the water added as a result of the combination of the added hydrogen and oxygen. Essentially 100% material balance was demonstrated after a series of more than 90 recombination experiments, water being removed after every 30 or so experiments.

18.4 DEVELOPMENT OF CONTINUOUS GAS PRODUCTION-RECOMBINATION APPARATUS

An apparatus to study the properties of slurry-catalyst systems under steady-state operating conditions is under development (Fig. 18.2). The apparatus uses an electrolysis cell to produce hydrogen and oxygen, a separate recombiner vessel, and a connection for the return of the condensed recombined gases to the electrolysis cell. Continuous operation has been demonstrated for periods of 26 and 99 hr, the former without and the latter with the condensate return connected. Recombination rates compared favorably with those in batch tests. It is planned to control the rate of condensate return and hence the level of liquid in the electrolysis cell by means of an automatic leveling device which has been constructed and is being tested. The major operating difficulty has been detonation of electrolytic gas in the electrolysis cell. No propagation of the explosions occurred through the 0.020-in.-ID tubing which connects the gas phases to the recombiner.

The generator vessel is made of nickel and has a central, insulated anode immersed in 25 wt % KOH solution. The generator is operated 90% full, with a 10-ml gas space at the top. This gas space contains Teflon de-entrainment devices which serve also as electrical insulation. The vessel serves as the cathode. The recombiner autoclave is made of type 347 stainless steel and has two sections connected by an axial internal draft tube and baffle. The bottom section contains 10 cc of the catalyst preparation heated by an external furnace. The top section contains a small condenser coil and a condensate reservoir. This section protrudes from the top of the heating furnace and is not insulated against heat loss. The axial draft tube is under constant reflux

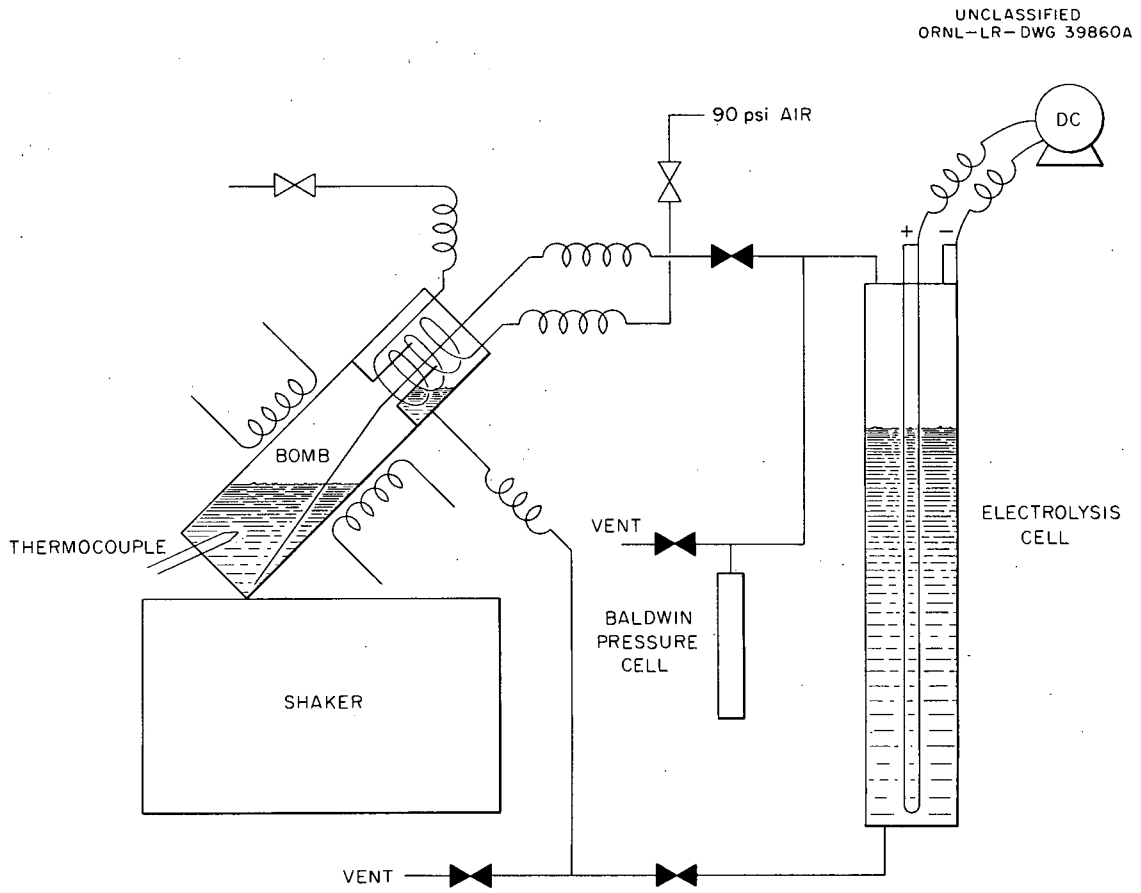

Fig. 18.2. Continuous Gas Production-Recombination Apparatus.

conditions, allowing steam and some gases to pass into the condenser and the overflow of the condensate reservoir to return to the bottom section of the recombiner autoclave. From the lowest point of the condensate reservoir a capillary tube returns condensate to the bottom of the generator vessel at a rate that is dependent on the hydraulic head loss between the condensate liquid level and the potassium hydroxide electrolyte liquid level. Condensate return is controlled by raising or lowering the electrolytic generator.

The total pressure of the gas phases of the system is measured and recorded by a Baldwin gage whose output potential is continuously recorded on a Brown potentiometer as a function of time. The temperature of the reacting catalyst preparation is measured by a thermocouple inserted into a thermowell which projects from the top of the recombiner into the heated slurry. The data consist of a simultaneous record of temperature, total pressure, and electrolytic cell current.

REFERENCES

1. E. L. Compere et al., HRP Quar. Prog. Rep. Apr. 30, 1959, ORNL-2743, p 140.

2. W. D. Fletcher, Westinghouse Electric Corporation, personal communication.

3. J. P. McBride et al., HRP Quar. Prog. Rep. Apr. 30, 1959, ORNL-2743, p 204-223.

19. SLURRY CORROSION

E. L. Compere H. C. Savage

J. M. Baker D. T. Jones S. A. Reed
S. J. Ball R. A. Lorenz L. Rice
S. E. Bolt R. E. McDonald A. J. Shor
V. A. DeCarlo A. R. Olsen W. C. Ulrich
R. B. Gallaher L. F. Woo

19.1 PUMP LOOPS

19.1.1 Introduction to Pump-Loop Tests; Circulation of Thorium-Uranium Oxide Fuel Slurries

A series of six 100A-pump-loop tests was executed during the report period to evaluate the chemical and circulating properties and the corrosion-erosion attack of heavy-water slurries of two experimental Th-U oxide preparations which were representative of possible fuels for a proposed single-region reactor.[1] The mixed oxides, which contained 8.8% U/Th (batch MO-39) and 15% U/Th (batch MO-54), were prepared by the Chemical Technology Division by the adsorption of uranium from ammonium-uranyl carbonate solutions on thoria[2] with subsequent calcination at 1050°C. The batches were then classified to mean particle sizes of 2.4 and 2.3 μ, respectively. The concentration of uranium in thoria of the proposed slurry reactor fuel was regarded as being within or below the range of the test batches.

Five of the runs in the test series were made at 200°C, the proposed operating temperature of the experimental reactor. The sixth run of the series was made at 280°C, principally to determine the stability of uranium at the higher operating temperature.

The operating conditions and pertinent results of the test series are summarized in Table 19.1.

19.1.2 Loop Operating Characteristics

In addition to observing the corrosion-erosion attack of heavy-water slurries of the two Th-U oxide preparations, it was of interest to determine the chemical stability, i.e., solubility and redox, of uranium during circulation using atmospheres of oxygen and of deuterium in the test loops. It had been reported[3] that uranium had been leached from the slurry solids in previous loop runs using oxygenated slurries of similar oxide preparations. Therefore the CS-loop run series was made using oxygenated slurries with the test loop operated under steam pressurization to provide a semistatic liquid column in the

Table 19.1. Summary of 100A-Loop Tests with Slurries of Th-U Oxides

Run Number	BS-26		BS-27*		CS-48		CS-49		BS-28		CS-50	
Operating temperature, °C	200		200		200		280		200		200	
Slurry circulating hours	723.9		406.9		806.7		680.6		591.0		527.1	
Atmosphere, (std) cc/liter	D_2, 494		O_2, 546		O_2, 720		O_2, 376		D_2, 253		O_2, 503	
Batch No., g U/kg Th	MO-39, 88		MO-39, 88		MO-39, 88		MO-39, 88		MO-54, 150		MO-54, 150	
Concentrations, g Th/kg D_2O												
Avg. inventory	418		232		317		389		386		377	
Avg. circulating (max.-min.)	398 (555-82)		197 (292-125)		298 (345-198)		380 (457-281)		284 (411-186)		364 (411-331)	
	Pre	Post	Pre	Post	Pre	Post	Pre	Post	Pre	Post	Pre	Post
Crystallite size, Å	1478	1083	352**	800	1478	500	1478	900	1088	756	1088	675
Surface area (N_2), m^2/g	1.4	1.7	1.6	1.8	1.4	2.6	1.4	1.7	1.3	1.3	1.3	1.5
$\bar{d}$, μ	2.5	2.8	2.8	2.3	2.5	1.2	2.5	2.1	2.3	2.3	2.3	2.0
σ	1.32	1.58	1.58	1.36	1.32	1.64	1.32	1.41	1.34	1.36	1.34	1.45
$U^{+4}/\Sigma U$ (± 5%)	0.38	0.80	0.80	0.28	0.38	0.38	0.38	0.33	0.37	0.68	0.37	0.35
Range of slurry pH	8.2-10.0		5.9-6.5		5.1-6.6		3.8-6.6		6.2-8.7		5.3-6.6	
Uranium, *m*	0.15		0.08		0.12		0.15		0.23		0.22	
Attack rates, mpy												
Impeller (cast Zircaloy-2)	Nil		Nil		2.2		1.7		Nil		Nil	
Loop piping (SS), 6 fps, initial, final	7.7, 1.4		<0.1, <0.1		3.6, 0.8		5.3, 1.0		67, 0.7		6.1, 0.3	
Pin specimens:												
Velocity, fps	23	50	21	44	23	40	23	40	22	45	20	36
Austenitic stainless steel	0.3	81	WG	<0.1	0.3	2.0	0.1	3.3	0.3	16	0.1	0.3
Martensitic stainless steel	4.0	63	0.4	0.3	0.4	1.2	0.2	1.8	1.3	43	0.1	0.3
Ferritic stainless steel	0.8	42	WG	0.3	0.5	3.0	0.3	2.9	0.8	14	0.1	0.4
Incoloy	0.1	23	WG	1.1	0.4	3.5	0.2	6.5	0.1	64	0.1	0.8
Croloy 5	34	112	3.2	4.0	4.8	10	0.3	1.0	2.0	59	0.2	0.5
Croloy 2 1/4	45	142	7.2	6.8	6.5	13	1.4	1.9	1.7	30	0.7	1.5
Inconel	0.1	4.8	2.5	3.2	1.3	5.7	5.7	14	<0.1	2.2	0.2	1.2
Invar	47	76	0.6	1.3	1.7	4.0	-	-	-	-	-	-
Titanium	WG	1.9	WG	<0.1	WG	0.8	<0.1	0.4	WG	WG	0.1	0.1
Zircaloy-2	0.1	0.3	WG	WG	WG	0.2	WG	WG	WG	WG	WG	0.1
Gold	0.2	6.8	<0.1	7.3	0.1	2.8	0.3	5.3	0.1	2.8	0.2	6.6
Platinum	0.1	3.3	WG	1.6	<0.1	2.4	0.3	6.7	<0.1	1.3	0.1	0.8

*Prepumped slurry from run BS-26.
**Sample after 6 hr pumping gave crystallite size of 916 Å, consistent with subsequent values.

vertical loop pressurizer in which soluble uranium and/or corrosion-product ions (Cr^{+6}) could collect. In this manner soluble ions in the slurry supernatant could be isolated from the solids for analysis.

Loop BS was operated with a dynamic, downflow pressurizer using gas pressurization in order to provide optimum inventory control for slurry dropout and resuspension tests.

In each run the test loops were brought to the desired operating temperature and gas concentration before the solids were added. Injections of Th-U oxides were made as rapidly as practical (~3 hr) to facilitate following the oxidation state of uranium. Slurry samples were withdrawn periodically during each test and analyzed for soluble uranium,[4] U^{+4}, and U^{+6}, in addition to the other analyses normally performed on the samples.

19.1.3 Uranium Redox and Solubility

The initial $U^{+4}/\Sigma U$ ratios of batches MO-39 (8.8% U/Th) and MO-54 (15% U/Th) were 0.38 and 0.37, respectively (Table 19.1). During circulation at 200°C under deuterium atmosphere, the respective ratios increased to 0.80 (run BS-26) and 0.68 (run BS-28). The degree of reduction, plotted as a function of circulating time for the respective runs, is shown in Fig. 19.1. With both preparations most of the reduction took place during the first 200 hr of circulation.

In contrast, when the two preparations were circulated in comparable tests (runs CS-48 and CS-50) using oxygen atmospheres, little (if any) oxidation of the uranium was detected. Similarly in run CS-49, which was conducted at 280°C using a slurry of batch MO-39, the variation in $U^{+4}/\Sigma U$ ratio ranged within limits of the analytical measurements.

In the sixth test of the series (run BS-27) the slurry which was removed from run BS-26 after 724 hr of circulation in a deuterium atmosphere was recirculated at 200°C as an oxygenated slurry to determine if the reduced fraction of the uranium in the MO-39 oxide could be readily reoxidized. The $U^{+4}/\Sigma U$ ratio changed from 0.80 to 0.28 in about the first 45 hr of circulation. Chemical analytical data indicated that approximately 10% more uranium was in the hexavalent state after recirculation in run BS-27 than was detected initially in the original unpumped MO-39 preparation; however, a greater variation also occurred in the chemical analyses during this run.

Only trace amounts of uranium were detected in the slurry supernatant liquids and in the liquid samples withdrawn from the loop CS semistatic pressurizer. A maximum uranium concentration of 16 ppm was detected in one sample of the pressurizer liquid during run CS-50. However, the sample displayed a Tyndall effect which indicated the presence of finely divided solids in suspension. No soluble uranium was detected (<2 ppm) in the sample after it was centrifuged.

19.1.4 Slurry Circulation Properties

The handling and circulating properties of oxygenated slurries of the two mixed-oxide preparations compared favorably with slurries of pure thoria of similar particle size and specifications.[5] The properties of batch MO-54, 15% U/Th, were also satisfactory during circulation in deuterium atmosphere.

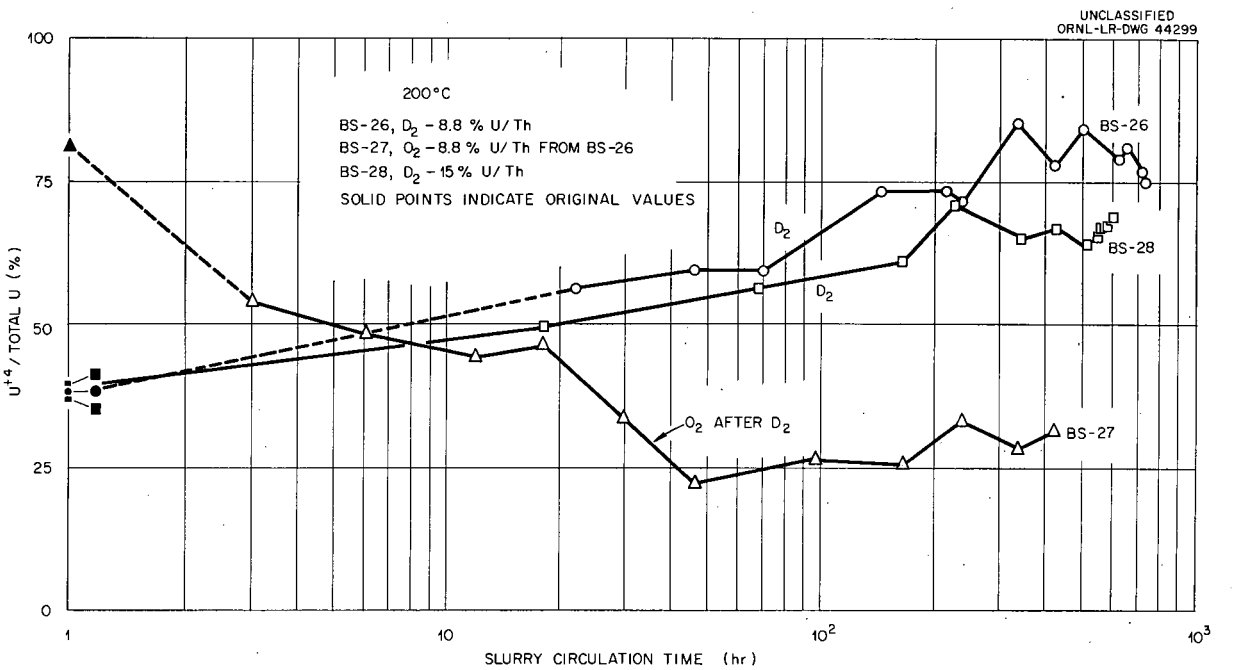

Fig. 19.1. Uranium Redox of Th-U Oxide Slurries During Circulation in 100A-Loop Tests.

However, the slurry of the 8% U/Th preparation which was used in run BS-26 with a deuterium atmosphere behaved erratically during circulation. In the first 200-hr operational period of the run, with a loop pipeline velocity of 6 fps, the circulating concentration decreased gradually from 433 to 394 g of Th per kg of D_2O. After 200 hr, the system inventory concentration was reduced to 387 g of Th per kg of D_2O by injecting additional D_2O into the system. Using the same flow velocity (6 fps), the circulating concentration at 200°C remained steady at 387 g of Th per kg of D_2O until circulation hour 406. Between circulation hours 406 and 478, the circulating concentration suddenly dropped from 387 to 82 g of Th per kg of D_2O.

A substantial accumulation of solids in the loop pressurizer, interpreted to be a combination of solids deposition and a stable foam, accompanied the concentration change. The observed changes were coincident with the time at which the steady conversion of the U^{+6} content of the slurry to U^{+4} reached its final limit as indicated by chemical analyses.

As a result of boiling in the pressurizer after an unscheduled circulation stoppage due to burnout of the pump power lead, the solids became resuspended; thereafter, a steady circulating concentration was maintained at the target conditions.

The apparent crystallite sizes (as determined by x-ray line broadening) of both preparations generally decreased during circulation in the six runs (Table 19.1). Both preparations also underwent some degradation during circulation as oxygenated slurries. In runs CS-48 and -49, which utilized slurries of batch MO-39, degradation was evidenced by sedimentation particle-size distribution particle-size distribution data for samples taken after about 50 hr of circulation. At the conclusion of run CS-49 (680 hr) the $\bar{d}$ (average diameter) of the solids had diminished from 2.5 to 2.1 μ. A similar particle-size reduction rate was noted during the same period of circulation during run CS-48; however, during the last 120 hr of the test the degradation rate increased. At the end of the test (806 hr) the $\bar{d}$ had decreased to 1.2 μ. In a like manner, in run CS-50 the $\bar{d}$ of batch MO-54 was reduced from 2.3 to 2.0 μ during the first 50 hr of circulation. Values dropped to as low as 1.8 μ during the subsequent portion of the test, but the distribution analysis of the final sample taken after 527 hr of circulation indicated a $\bar{d}$ of 2.0 μ.

Particle-size distribution analyses of samples taken during BS-27, in which prepumped batch MO-39 was recirculated, indicated a mild degradation from $\bar{d}$ 2.8 to 2.3 μ. However, a particle-size growth was indicated ($\bar{d}$, 2.5 to 2.8) during run BS-26 using a deuterium atmosphere (Table 19.1). When such an apparent growth was observed[6] in previous tests with slurries circulated under reducing atmospheres, the growth was ascribed to interference of reduced corrosion products in the particle-size analysis scheme.

At the conclusion of each test, slurry solids were removed from the loops (at operating temperature and pressure) using 0.4-in. hydroclones employing induced underflow.[7] From 74 to 92% of the solids inventories in the systems were recovered in this manner during 30-min periods of hydrocloning. Additional material was recovered from the loops by circulating-water rinses made at room temperature. Total recoveries of solids ranged from 94 to 99.5%. Material losses varied from 0.025 to 0.6 kg out of 4.8- to 10.6-kg charges in the six tests.

19.1.5 Slurry Rheological Properties

The slurries displayed favorable rheological properties which were little affected by circulation in either atmosphere (Table 19.2). The values of yield stress and of the modulus of rigidity of the slurries closely approximated those of slurries of pure thoria[8] and were generally lower than those of slurries of admixed ThO_2-UO_3 used in comparable tests.[9]

Table 19.2. Room-Temperature Rheological Properties of D_2O Slurries of Th-U Oxides

Slurry concentration: 500 g Th-U/kg D_2O

Batch Number and Concentration	Yield Stress[a] (lb/ft^2)	Modulus of Rigidity[a] (centipoises)
Batch MO-39, 8.8% U/Th		
Unpumped	0.02	1.42
After run BS-26, D_2 atmosphere[b]	0.02	1.14
After run BS-27, O_2 atmosphere	<0.02	1.35
After run CS-48, O_2 atmosphere	<0.02	1.29
After run CS-49, O_2 atmosphere	<0.02	1.46
Batch MO-54, 15% U/Th		
Unpumped	0.02	1.08
After run BS-28, D_2 atmosphere	0.02	1.49
After run CS-50, O_2 atmosphere	<0.02	1.79

[a]Determined at room temperature using a capillary-tube viscometer.

[b]Precirculated in run BS-26.

19.1.6 Corrosion-Erosion

Attack data for the test-loop components and pin-corrosion specimens exposed in the test series are presented in Table 19.1. Attack of loop components was mild in all tests. The most aggressive attack of the austenitic stainless steel loop piping occurred in the first 5 to 20 hr of circulation during runs BS-26 and BS-28 in which deuterium atmospheres were used. However, the rates diminished rapidly and leveled out at 1.4 and 0.7 mpy, respectively. Such a pattern of attack is normal for tests using reducing atmospheres. In the tests with oxygenated slurries the average attack rates of the systems ranged from <0.1 to 1 mpy. The highest rate occurred in run CS-49, which was made at 280°C.

Cast Zircaloy-2 impellers were used in the circulating pumps of both loops. The impeller in loop BS, which had been in service for over a year, was not detectably attacked. Attack on the new impeller used in loop CS was localized on the front hub adjacent to the wear rings. A normal "wearing-in" was noted during the first two tests in which it was used. In the third run, attack was not detectable.

Attack rates of pin specimens exposed in the six tests were in excellent agreement with rates observed in previous runs made at similar conditions. In general, normal effects of atmosphere, velocity, and slurry concentration were manifested in the test series.

As an aid in comparing these effects on corrosion-erosion, the specimen attack data given in Table 19.1 were examined by the ratio-analysis method.[10] The results of the examination are presented in Table 19.3. Because of the similar slopes of the curves which resulted from plotting the logarithms of the attack rates of the individual specimens versus the flow velocities to which they were exposed in the various tests, the actual rates were extrapolated, where necessary, to median low and high velocities, i.e., 20 and 45 fps, respectively, to simplify the comparisons.

In general, the effect of increasing the uranium content of the mixed oxides from 8.8 to 15% U/Th was to lower the attack rates by an average factor of 0.4. At the lower velocity, 20 fps, the average effect of changing the operating atmosphere from oxygen to deuterium was to increase the attack rates by a factor of 1.4; at 45 fps the atmosphere change increased the rates by an average factor of 3.5.

It will be noted that the effect of atmosphere was most pronounced at the higher velocity. In that regard the materials may be arranged into three general groups as shown in Table 19.3. At 45 fps the noble metals and Inconel displayed lower rates in deuterium atmosphere than in oxygen atmosphere, whereas attack of titanium, Zircaloy-2, and Incoloy was little affected by changing atmosphere. In contrast, attack rates of stainless and alloy steels were markedly increased in deuterium atmosphere, and the attack was highly localized.

19.2 TOROIDS

19.2.1 Introduction

Toroid tests reported below were concerned with the continued evaluation of thoria-urania slurries and with an exploratory study of the hydriding of zirconium alloys. The studies on thoria-urania dealt with preparations calcined at 1050°C; this temperature was regarded as giving good particle-integrity properties.

19.2.2 Tests with Slurries of Thorium-Uranium Oxides

Potential slurry reactor fuels would likely contain urania included in thoria particles. Such inclusion might significantly affect the corrosion-erosion, handling, and particle-integrity properties of circulating aqueous slurries. Such effects might also depend on operating conditions, such as atmosphere. Adequate delineation of the effects of inclusion of urania in thoria was desirable to assist in the judicious specification of conditions yielding a satisfactory slurry fuel. It was desirable to explore in toroids the effects of comparatively wide ranges of such variables as oxide composition, calcination conditions, operating atmosphere, etc., to assist in this study. Since the uranium was introduced by adsorption onto the thoria particles and was caused to enter the particles by calcination, the condition of firing would be expected to affect strongly the character of its association with the particles.

Table 19.3. Relative Effects of Velocity, Atmosphere, and Uranium on Attack of Materials by Circulating Slurries of Th-U Oxides

Effects expressed as ratios relative to rate in reference condition (normalized to 8.8% U/Th, O_2 atmosphere) at given velocity.

Material	20 fps			45 fps		
	Reference Rate (mpy)	Effect of Uranium 15%/8.8%	Effect of Atmosphere D_2/O_2	Reference Rate (mpy)	Effect of Uranium 15%/8.8%	Effect of Atmosphere D_2/O_2
Austenitic stainless steels	0.14	1.0	1.1	2	0.3	21
Ferritic stainless steels	0.2	0.7	3	3	0.3	11
Martensitic stainless steels	0.3	0.4	8	1	0.5	52
Croloy 5	4	0.05	7	7	0.2	25
Croloy 2 1/4	8	0.06	3	13	0.2	11
Zircaloy-2	0.1	1.0	1.0	0.2	0.4	1.0
Titanium	0.06	0.2	1.0	1.2	0.08	1.0
Incoloy	0.6	0.07	0.7	4	0.4	3
Inconel	0.6	0.5	0.1	6	0.5	0.6
Gold	0.07	1.6	0.9	9	2	0.3
Platinum	0.1	1.0	1.0	4	0.5	0.6

Results of the initial phase of toroid tests using D_2O slurries of a group of experimental Th-U oxide preparations were reported earlier.[11] The initial part of the test series was concerned with slurries of four preparations which contained from 5 to 33% U/Th that had been calcined at 650°C in air.

Recently a second phase of the test series was completed using the same four preparations after recalcination for 4 hr at 1050°C (a) in air and (b) in hydrogen. Slurries containing 500 g of Th-U per kg of D_2O were circulated in 300-hr tests at 26 fps using atmospheres of oxygen and of deuterium at various overpressures. The operating temperature was 280°C except for one group of four tests conducted at 200°C. Pertinent data for the series are given in Table 19.4.

No degradation of the oxide particles was noted in this test series, indicating (within the ability of toroid tests) that good particle integrity may be associated with oxides so manufactured. Some uranium was detected in the supernatant from various tests, although no distinction was attempted between soluble and colloidally suspended uranium. Somewhat higher values were noted for tests under oxygen atmosphere than were found under deuterium atmosphere. In the case of hydrogen-calcined thoria-uranias containing 8.7 or higher percentage U/Th, substantial quantities of uranium were detected in the supernatant from oxygenated slurries, with the highest value (1668 ppm) associated with the highest U/Th ratio in the slurry.

Chromate ion was also detected in the supernatant from tests under oxygen atmosphere (but not deuterium atmosphere) with highest values noted for the tests at 280°C, 115 psi O_2, in which hydrogen-calcined thoria-uranias were used.

The attack data were examined by use of ratio analysis[10] (Table 19.5), which permitted the separation of the effects of major variables into multiplicative factors. The reference condition was taken as 280°C, 115 psi atmosphere, air-calcined 8.7% U/Th (a representative fuel slurry). The normalized reference rate for type 347 stainless steel was 9 mpy, an average value compared with results obtained with pure thoria.

The dominant variables in the attack appeared to be type of metal and atmosphere. Under oxygen, titanium-75A and Zircaloy-2 were negligibly attacked, but they were appreciably attacked when under deuterium atmosphere. Furthermore, for three out of four of the tests at 15 psi D_2, Zircaloy-2 underwent hydriding (Sec. 19.2.3). Inconel was the most severely attacked under oxygen atmosphere and the least severely attacked under deuterium atmosphere. Stainless steel pins and toroids were attacked a factor of 2 more severely under D_2 atmosphere. With the exception of the Zircaloy hydriding, these effects were consistent with results normally obtained with similar slurries of pure thoria.

Generally, calcination of the various oxides under hydrogen appeared to result in diminished attack rates under oxygen atmosphere, as did operation under lower (50 vs 115 psi) pressure. Under deuterium atmosphere, use of hydrogen-calcined oxides did not display a consistent effect for all metals; but frequently more severe attack was noted. Lower pressures of deuterium atmosphere, tested on air-fired materials, mostly gave higher attack rates.

The effect of the uranium content of the thoria was less pronounced than in the previously reported test series.[12] In general the attack was less severe with increasing uranium content, particularly so for the 33% U/Th oxide.

Table 19.4. Results of Toroid Tests with Slurries of Thorium-Uranium Oxides

Time: 300 hr
Velocity: 26 fps
Concentration: 500 g Th-U/kg D_2O
Temperature: 280°C
Calcination temperature: 1050°C

Oxide Preparation (% U/Th)	Atmosphere and psia (Room Temperature)		Atmosphere of Final Calcination	Attack Rate[a] (mpy) Toroid (347 SS)	347 SS	Ti-75A	Inconel	Zr-2	Slurry pH, Postrun	Concentration of Ions in Supernatant Liquid (ppm) Cr^{+6}	U
5.3	O_2	50	Air[b]	0.2	1.5	WG	2.1	WG	5.6	36	16
	O_2	50	Air	1.7	6.6	0.1	11.0	WG	c	c	c
	O_2	115	Air	2.1	9.0	WG	d	WG	6.6	94	10
	O_2	115	H_2	1.0	6.3	0.8	13.0	0.1	5.5	181	<2
	D_2	115	Air	7.4	14	16.0	1.6	1.8	12.0	<1	21
	D_2	115	H_2	6.6	33	0.9	2.6	4.5	10.1	<1	<2
	D_2	15	Air	11.0	73	135	8.8	4.4[e]	10.2	<1	7
	D_2	15	Air	11.0	60	64	10	4.5[e]	10.3	<1	14
8.7	O_2	50	Air[b]	0.4	4.2	WG	4.0	0	c	44	<15
	O_2	50	Air	2.1	8.8	WG	21.0	WG	c	c	c
	O_2	115	Air	2.1	7.9	0.1	d	WG	5.2	75	18
	O_2	115	H_2	1.5	5.6	0.1	9.5	WG	5.0	247	319
	D_2	115	Air	4.2	20.0	19.0	2.0	2.7	14	<1	6
	D_2	115	H_2	17	41	0	4.5	4.6	9.6	<1	<2
	D_2	15	Air	4.8	47	100	7.9	0.2[e]	10.1	<1	7
	D_2	15	Air	5.4	41	74	7.8	6.6[e]	10.2	<1	12
11	O_2	50	Air[b]	0.3	2.0	WG	3.2	WG	5.8	15	45
	O_2	50	Air	0	6.6	0.1	15	WG	c	c	c
	O_2	115	Air	3.2	10	0.1	d	WG	4.8	94	29
	O_2	115	H_2	1.9	4.0	0.8	7.3	0	c	246	207
	D_2	115	Air	5.9	16	19	1.6	2.4	14.8	<1	26
	D_2	115	H_2	9.7	44	9.1	6.2	9.0	c	c	23
	D_2	15	Air	8.9	83	44	7.8	9.2[e]	10.4	<1	6
	D_2	15	Air	11.0	53	55	11	5.8[e]	9.3	<1	6
33	O_2	50	Air[b]	0.1	3.3	WG	1.6	WG	6.0	15	50
	O_2	50	Air	0.4	2.8	WG	8.7	WG	c	c	58
	O_2	115	Air	0.9	5.6	WG	d	WG	5.2	180	31
	O_2	115	H_2	2.4	4.9[f]	0.5	WG[f]	0	c	189	1668
	D_2	115	Air	3.1	15	20	0.9	2.7	13.0	<1	17
	D_2	115	H_2	6.4	31	17	5.1	3.6	c	c	15
	D_2	15	Air	0.3	4.1	0.2	1.1	0.4	7.0	<1	5
	D_2	15	Air	0.4	4.9	WG	2.5	WG	7.7	<1	2

(a) Corrected for slug flow.
(b) Operating temperature, 200°C.
(c) Insufficient sample.
(d) Subsurface attack.
(e) Hydriding of Zircaloy-2 produced fissures.
(f) Crystalline deposit.
WG = Weight gain. Attack rate not computed.

Table 19.5. Effect of Variables in Attack by Thoria-Urania Slurries

Expressed as multiplicative factors obtained by ratio analysis from data of Table 19.4.

Atmosphere:	Oxygen					Deuterium				
Metal (pins):	347 SS	Toroid (347 SS)	Ti-75A	Inconel[a]	Zr-2[b]	347 SS	Toroid (347 SS)	Ti-75A	Inconel	Zr-2
Reference rate,[c] mpy:	9	3	<0.1	18	<0.1	17	6	7	2	3
Average effects of variables expressed as ratio to reference rate										
Oxide effects: 5.3% U/Th	1.0	0.8	b	0.9	b	1.0	1.2	2	0.9	1.4
8.7% U/Th[c]	1	1	1	1	1	1	1	1	1	1
11% U/Th	0.9	0.5	b	0.7	b	1.1	1.2	3	1.1	1
33% U/Th	0.6	0.5	b	0.5[d]	b	0.7	0.3	0.7	0.5	2
Calcination under H_2	0.6	0.3	b	0.07[d]	b	2	0.8	1.5	4	0.7
Atmosphere effects: 115 psi[c]	1	1	1	1	1	1	1	1	1	1
Lower pressure	0.7[e]	0.9	(4)	1	b	3	2	0.3	3	2[f]
Temperature effects (200/280°C): 50 psi O_2	0.5	0.5	b	0.2	b	-	-	-	-	-

(a) Reference rate based on lower pressure; no weight data obtained at 115 psi O_2 due to subsurface attack.
(b) Ratio not evaluated as pin-weight change was negligible, or there was a weight gain.
(c) Reference condition for given atmosphere: 8.7% U/Th, air-calcined, atmosphere pressure 115 psi, 280°C.
(d) Assuming discordant value for 33% U/Th, H_2 calcination, due to error or interaction of (0.02X).
(e) Assuming discordant value for 33% U/Th, lower pressure, due to error or interaction of (0.11X).
(f) Substantial Zircaloy hydriding observed (3 out of 4 oxides in 15 psi D_2).

In the tests at 200°C under oxygen atmosphere, the attack was generally lower than at 280°C (50% for stainless steel). In the test using 33% U/Th under deuterium atmosphere very low values were noted; it is likely that most of the deuterium was consumed in reducing the hexavalent uranium in the preparation during the 300-hr test. This was substantiated by the observation that the pH values were neutral instead of the alkaline values frequently noted in tests under deuterium atmosphere.

19.2.3 Hydriding of Zirconium-Base Alloys

A discussion was given previously[13] of the hydriding of Zircaloy-2 observed initially in a series of toroid tests concerned with the evaluation of Th-U oxide fuel slurries. An exploratory test program was initiated to identify the major factors which contributed to the hydriding. In this program over 90 toroid tests have been completed to investigate the effects of (1) thoria or thoria-urania preparation variables, (2) zirconium alloy effects, (3) operating atmosphere, and (4) amount of gas overpressure. Also a number of tests were completed to investigate the influence of circulation time on hydriding. (The phenomenon will be referred to as hydriding in the discussion below, although deuterium was commonly the hydrogen isotope involved.)

All the runs were made using slurries of 500 g of Th or Th-U per kg of D_2O at a relative flow velocity of 26 fps and at an operating temperature of 280°C. Eighteen different oxide preparations were used in the series. Slurries of pure ThO_2 with mean particle sizes from 2.1 to 60 μ which had been calcined from 650 to 1600°C and admixtures of thoria and $UO_3 \cdot H_2O$ were tested. Adsorbed and coprecipitated preparations of Th-U oxides that contained 5 to 33% U/Th which were calcined in air and in hydrogen atmosphere were used in many of the tests (Sec. 19.2.1), and one test employed a flame-calcined, 5.8% U/Th preparation.[14]

Slurries of the various preparations were circulated in atmospheres of oxygen, deuterium, argon, and deuterium-argon mixtures. Total pressures of 15 to 250 psi (at room temperature) of gas were charged to the toroids.

Specimens of five zirconium alloys were exposed in the tests. These included three items of Zircaloy-2 and one each of Zircaloy-3A (0.25% Sn, 0.22% Fe, low Cr, Ni) and a zirconium - 15% niobium experimental alloy.

Detailed pre- and postrun examinations of the test specimens, including hydrogen analyses, were performed by the HRP Metallurgy Section.[15] In many instances gross hydriding was observable by visual or macroscopic examination. On about half of the 108 specimens, however, more precise metallurgical examinations were required to establish the absence or presence and degree of hydriding.

It was not within the scope of the investigation to determine quantitatively the extent of hydride formation as a result of changing the test conditions. Data are presented in Table 19.6 to show the effect of major variables on the frequency of hydriding. In addition to frequency, however, the severity and qualitative nature of the observed hydriding under various circumstances is of interest and will be discussed below.

Pin specimens exposed in toroids underwent distinct patterns of attack arising from slug flow and erosion by the circulating slurry. Various degrees of hydriding of such specimens are shown in Fig. 19.2. The pin section was electroanodized after polishing, causing hydride to appear as darkened areas.

Table 19.6. Hydriding Frequency of Zirconium Alloys in Slurry Toroid Experiments Under Various Atmospheres

500 g (Th + U)/kg D_2O, 280°C, 26 fps

Alloy:		Zircaloy-2			Zircaloy-3	Zr-15% Nb
Item No.:		569	593	1210	546	58
Number of hydrided specimens/total specimens exposed:						
Oxygen Atmosphere						
psig	Slurry					
115	Pure thoria	0/ 1	-	-	-	-
	<9% U/Th	1/ 7	-	0/1	0/1	1/1
	>9% U/Th	0/ 2	-	-	-	-
65	Pure thoria	-	-	0/2	-	-
	<9% U/Th	0/ 2	-	-	-	-
25	<9% U/Th	2/ 3	-	-	-	-
15	Pure thoria	-	-	2/2	-	-
Deuterium Atmosphere						
250	<9% U/Th	1/ 1	-	1/1	-	-
115	Pure thoria	9/ 9	-	-	-	-
	<9% U/Th	11/11	-	5/5	2/5	0/3
	>9% U/Th	10/10	-	-	-	-
65	<9% U/Th	4/ 4	-	1/1	2/2	0/1
25	<9% U/Th	7/ 7	1/1	1/1	1/1	-
	>9% U/Th	2/ 2	-	-	-	-
25 + 90 psi Ar	<9% U/Th	5/ 5	4/4	-	-	-
15	Pure thoria	-	-	1/4	-	-
	<9% U/Th	3/ 3	1/1	1/1	1/1	-
115 Ar	Pure thoria	2/ 2	-	-	-	-

SUMMARY

Alloy	Item	O_2	D_2 or Ar
Zircaloy-2	569	3/15	54/54
Zircaloy-2	593	0/ 0	6/ 6
Zircaloy-2	1210	2/ 5	10/13
Zircaloy-3A	546	0/ 1	6/ 9
Zr-15% Nb	58	1/ 1	0/ 4
Total		6/22	76/86
Pressure, psig			
250		-	2/ 2
115		2/13	37/43
65		0/ 4	7/ 8
25		2/ 3	12/12
25 + 90 psi Ar		-	9/ 9
15		2/ 2	7/10
115 Ar		-	2/ 2
Total		6/22	76/86
Slurry			
Pure thoria		2/ 5	12/15
<9% U/Th		4/15	52/59
>9% U/Th		0/ 2	12/12
Total		6/22	76/86

UNCLASSIFIED
PHOTO 48806

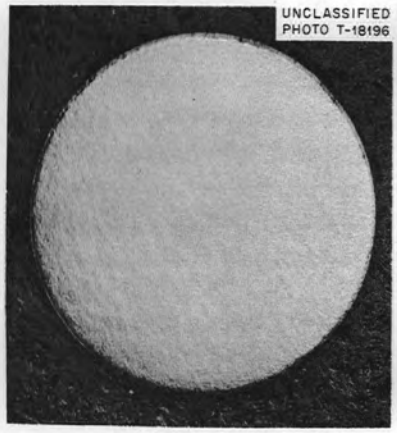

311 hr
100 psi Ar
PURE ThO_2 - 650°C
26 X

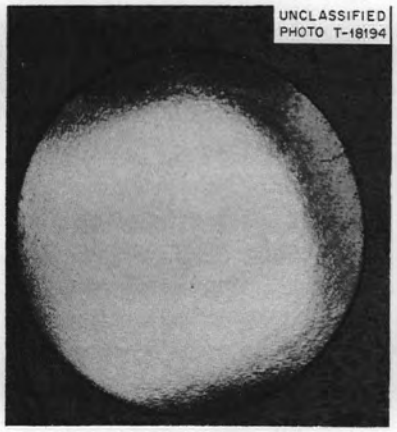

345 hr
15 psi D_2
(Th-9% U) O_2 - 1125°C
26 X

742 hr
15 psi D_2, 100 psi Ar
(Th-9% U) O_2 - 1050°C
26 X

311 hr
100 psi D_2
(Th-9% U) O_2 - 1050°C
26 X

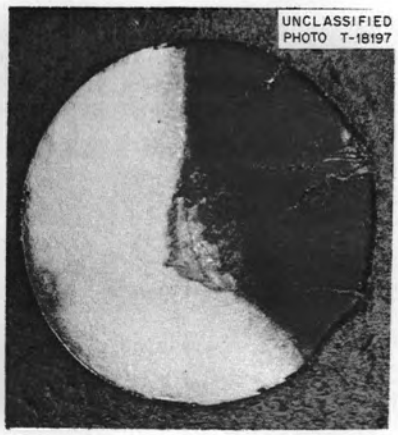

767 hr
15 psi D_2
(Th-9% U) O_2 - 1050°C
26 X

UNCLASSIFIED
PHOTO T-17282

SAME AS ABOVE
SIDE VIEW
10 X

Fig. 19.2. Degrees of Zircaloy-2 Hydriding in Toroid Tests at 280°C, 26 fps, 500 g Th-U/kg D_2O (Item 569).

The hydriding attack appeared to be concentrated in the upstream and downstream regions where erosion was greatest and was not pronounced on the side of the specimens. A normal erosion pattern was always observed, and a slight groove eroded on the upstream surface.

Zirconium hydride needles, random or more concentrated, represented the least appearance of the material. Small areas of hydride, perhaps completely around the pin, were noted in circumstances of mild hydride formation. If formation was more pronounced, regions of apparently complete conversion to hydride appeared to penetrate inward from regions of erosion. Where substantial gross hydriding was noted, cracks were observed extending from the pin surface inward, almost through the hydride layer. In the runs of longest duration (~750 hr) almost complete conversion of the 0.1-in. pin to hydride was found, with extensive cracking.

Deuterium pickup, as evidenced by vacuum-fusion analyses and subsequent isotopic assay to distinguish from hydrogen associated with the manufacturing process, was often in excess of 1000 ppm.

The most important effects were associated with the nature and overpressure of the atmosphere, and with duration of exposure. The frequency and severity of hydriding under deuterium atmosphere were generally high. Above a threshold pressure the attack appeared to be more severe at higher pressures and cracking resulted. Some indication of a threshold pressure was obtained; it appeared to be lower as time of exposure increased, and as the per cent uranium in the oxide became higher.

The addition of argon to deuterium did not reduce the attack severity. Furthermore, tests in an atmosphere originally only argon, in which sufficient corrosion-erosion ensued to have generated 55 psi deuterium, also gave substantial hydriding, indicating that corrosion hydrogen may be a factor.

Under oxygen atmosphere, particularly at the higher pressures and shorter times, both the severity and frequency of hydride needle formation were sharply inhibited, and no gross hydriding was reported.

The effects of time appeared in two ways. In tests under the higher D_2 atmospheres, hydriding advanced steadily with time, a few specimens becoming essentially completely converted into hydride, with extensive cracking (Fig. 19.2). Under low oxygen or hydrogen pressures the effect of time is interpreted in terms of the cumulative effect of corrosion-erosion of all materials in the toroid on the gaseous atmosphere. More extensive attack would reduce the oxygen pressure or build up deuterium to a greater extent and thus affect the apparent threshold pressures.

Over a wide range the qualitative severity of erosion did not appear to affect the attack. Usual quantitative weight-loss measurements on defilmed specimens were not made since the electrolytic procedures might introduce hydrogen; careful qualitative examination was felt to be more important in this phase of the investigation. However with minimum erosion, minimum (or no) hydriding was noted, and in cases of severe erosion (e.g., a run in which oversize thoria particles, "clinkers," were used) hydriding appeared to be reduced in the areas under direct attack.

The nature of the thoria or thoria-urania preparation did not appear to affect hydriding very much; however as the per cent uranium in the oxide increased, hydriding was indicated at lower pressures.

Zircaloy-2 was the most susceptible of the alloys tested, three separate batches showing high frequency under deuterium atmosphere. Zircaloy-3A appeared to be about the same, although a somewhat lower percentage frequency was noted, with fewer specimens tested. Zirconium - 15% niobium alloy, in five tests, showed hydride needle formation only in the one test under oxygen atmosphere.

The effects of a number of possibly important variables were not considered. These include flow velocity, system geometry, and operating temperature. In addition the slug-flow characteristic of toroid experiments may be quite important, as specimens are alternately exposed to impinging slurry and to the gaseous phase. Specimens of zirconium alloys exposed in dynamic pump loops for periods up to 500 hr using slurries of several of the same thoria preparations under atmospheres of deuterium and of oxygen have shown only slight localized areas of hydride needles on a few specimens.

19.3 IN-PILE AUTOCLAVE SLURRY CORROSION TESTS

19.3.1 Introduction

The study of the radiation corrosion of reactor materials by thoria-urania slurries in in-pile autoclave experiments involved work in several different fields. In order to obtain a direct estimate of the effect of in-pile exposure on corrosion, an out-of-pile control experiment is compared below with its associated in-pile experiment, previously reported.[16] Results of the postexposure examination of specimens and slurry from these and other in-pile experiment are compared. Procedures for the reduction of data from specimen activation were developed, permitting improved estimates of experiment flux dose and power density. A correlation of data from various in-pile slurry corrosion experiments was developed, relating the instantaneous corrosion rate to fission power density and to the duration of exposure. In addition, the operation of an in-pile slurry-corrosion experiment in a stainless steel autoclave was completed.

Autoclave experiment L6S-151S was removed from beam hole HB-6 of the LITR on October 13, after 1110 hr of operation at temperature. The experiment consisted of a type 347 stainless steel autoclave with pin-type corrosion specimens of type 347 stainless steel, Zircaloy-2, and titanium. It was loaded with thorium oxide containing 5 wt % enriched uranium, based on thorium, dispersed in D_2O at a nominal concentration of 1100 g of Th per kg of D_2O. A Pd-ThO_2 catalyst was added to recombine radiolytic gas during in-pile operation. Data from this experiment will be reported at a later date.

19.3.2 Out-of-Pile Control Experiment

Autoclave experiment Y6Z-128S, an out-of-pile control for in-pile experiment L6Z-127S, has been completed. Loading and operation of experiment Y6Z-128S was performed to duplicate as nearly as possible that of experiment L6Z-127S. The Zircaloy-2 autoclave contained slurry at a concentration of 410 g of Th per kg of D_2O, with 5.1 wt % enriched uranium based on thorium, 0.011 *m* MoO_3, and an excess oxygen atmosphere. The autoclave was operated at 280°C.

The corrosion results of the two experiments are presented in Fig. 19.3. Since some scatter in the oxygen-pressure data was observed in experiment Y6Z-128S, a smoothed line was drawn through the results. Initially the corrosion was relatively rapid, but the rate soon decreased, so that after 100 hr

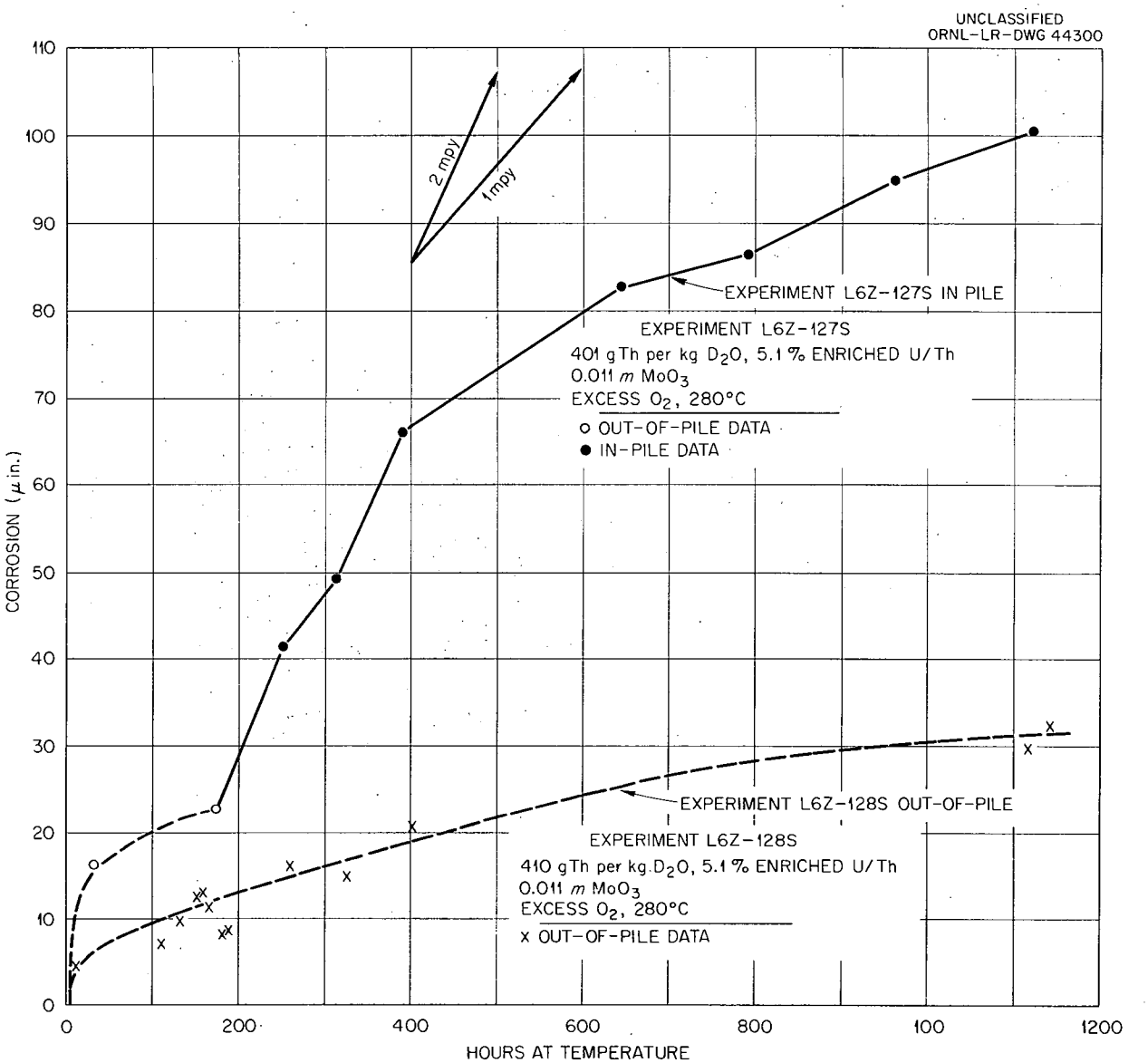

Fig. 19.3. Effect of In-Pile Irradiation on the Corrosion of a Zircaloy-2 Autoclave by Thoria-Enriched Urania.

a corrosion rate of 0.3 mpy was observed. This rate continued to decrease to a final value of less than 0.1 mpy. The corrosion results of experiment L6Z-127S have been reported previously.[16] Prior to insertion in the HB-6 facility of the LITR, the autoclave had been operated out-of-pile for 174 hr to insure integrity of the equipment. The initial corrosion rate had appeared to be higher than that in experiment Y6Z-128S, but it had soon decreased to approximately the same rate as that of experiment Y6Z-128S. At the onset of irradiation the corrosion rate in experiment L6Z-127S had increased markedly, with total corrosion in experiment L6Z-127S after 1100 hr being a factor of 3 greater than that in experiment Y6Z-128S. The corrosion rate appeared to be increased by in-pile radiation and diminished by time at temperature.[17]

19.3.3 Post-Experiment Examinations

Autoclaves from control experiment Y6Z-128S and radiation experiment L6Z-129S, which was reported previously,[18] have been opened, and the analyses of the slurry and the examination of the pin-corrosion specimens have been completed. The analyses of the slurry before and after irradiation are presented in Table 19.7 along with comparison results from experiment L6Z-127S. The ratio of uranium to thorium in the bulk of the slurry did not change significantly during the course of experiments Y6Z-128S and L6Z-129S, indicating no apparent separation of the uranium from the thorium. In experiment L6Z-127S a low value of uranium, relative to thorium, was reported. However, no perceptible deposits or regions in which uranium was concentrated were noted, and insufficient sample was available for a check analysis. In experiment Y6Z-128S the zirconium in the bulk of the slurry represented 29% of the calculated zirconium consumed by corrosion, while in in-pile experiments L6Z-127S and L6Z-129S the zirconium found in the slurry represented only 5 and 3%, respectively, of the zirconium involved in the corrosion process.

In experiment Y6Z-128S the smaller slurry particles appeared to grow larger, with particles in the diameter ranges 0.5 to 1.0 μ and 1.0 to 1.5 μ increasing 8 and 28%, respectively. In the two in-pile experiments the indicated increase in particle size was even greater as obtained by the activation analysis sedimentation method, provided that no bias existed as a result of the extended irradiation.

The corrosion results of pin specimens in experiment Y6Z-128S and L6Z-129S are presented in Tables 19.7 and 19.8 along with comparison results[16] from experiment L6Z-127S. The Zircaloy-2 and type 347 stainless steel pin specimens exhibited a uniform attack. The Inconel pin in both experiments (Y6Z-128S and L6Z-129S) showed a heavily etched and pitted surface. This corrosion appeared not to be a radiation attack, since in out-of-pile experiment Y6Z-128S the corrosion of the Inconel was at least an order of magnitude greater than that of the other alloys, while in in-pile experiment L6Z-129S the extent of corrosion of the Inconel was similar to that in experiment Y6Z-128S. The lack of response of the corrosion of the Inconel to in-pile irradiation is in contrast to the corrosion of the Zircaloy-2 specimens which increased upon exposure of the specimens to in-pile irradiation. Near one end of the Croloy 2 1/4 pin specimen in experiment L6Z-129S some deep pits were observed.

In experiments Y6Z-128S and L6Z-127S the average value for the corrosion of the Zircaloy-2 pins was considerably lower than the corrected value for the corrosion of the Zircaloy-2 surfaces based on oxygen data. However the pin-weight changes involved were quite small (~0.5 mg), and undue weight should not be attached to the discrepancy.

Table 19.7. Analyses of Thoria-Urania from Autoclave Experiments

Conditions	Experiment Number								
	Y6Z-128S (Out-of-Pile Control)			L6Z-127S (Irradiated)			L6Z-129S (Irradiated)		
	Original[a]		Postrun	Original		Postrun	Original[a]		Postrun
Volume of supernatant, ml			2.1			0.4			
pH of supernatant			6.5						
Th inventory, g	1.548		0.805	1.547		0.070	3.936		0.192[b]
U, mg per g Th	51		56	51		5.4[d]	49		54
Zr, μg per g Th	NA[c]		2650	NA		2790	NA		909
Mo, μg per g Th	2500[e]		NA	2540[e]		NA			
Pd, μg per g Th							156[e]		NA
Particle size and distribution, by sedimentation analysis									
Average diameter, μ	0.9[f]	0.7[g]	0.9[g]	0.9[f]	0.7[g]	6.2[g]	0.9[f]	0.7[g]	4.8[g]
Weight per cent									
>3 μ	17	7	3	17	7	64	17	7	60
1.5 to 3 μ	2	0	2	2	0	12	2	0	9
1.0 to 1.5 μ	17	0	28	17	0	7	17	0	7
0.5 to 1.0 μ	59	58	66	59	58	7	59	58	14
<0.5 μ	5	34	2	5	34	10	5	34	10

[a]The thoria-urania in the original material was a special preparation of the Chemical Technology Division by coprecipitation of enriched uranium with thorium as the oxalate and firing at 1000°C.
[b]No D_2O in autoclave when it was opened; most likely the clamp on the cut capillary not tight enough to prevent loss of D_2O.
[c]NA, not analyzed.
[d]Insufficient sample available for redetermination.
[e]Calculated from load.
[f]Centrifugal sedimentation pipette method.
[g]Activation analysis sedimentation method, 0.001 *M* $Na_4P_2O_7$ in H_2O.

Table 19.8. Corrosion of Pin Specimens by Thoria-Urania Slurries in Irradiated and Unirradiated Zircaloy-2 Autoclaves Under Excess Oxygen Atmosphere

Conditions	Experiment Number		
	Y6Z-128S (Out-of-Pile Control)	L6Z-127S (Irradiated)	L6Z-129S (Irradiated)
Temperature, °C	280	280	240 to 320 gen. at 280°C
Concentration of slurry, g Th per kg D_2O	410	400	1086
Wt %, U/Th	5.1	5.1	4.9
Concentration of catalyst	0.011 *m* MoO_3	0.011 *m* MoO_3	0.002 *m* Pd
Hours at temperature, out-of-pile	1140	174	188
Total hours at temperature	1140	1122	1660
Hours irradiated	0	732	1260
Effective fraction of full irradiation time, fully inserted flux	0	0.179[a]	0.445
Flux from specimen activation, neutrons·cm^{-2}·sec^{-1} (corrected to fully inserted position)	0	8.3×10^{12}[a]	5.6×10^{12}
Average power density while irradiated, w/ml at 280°C	0	0.8[a]	3.2
Autoclave generalized corrosion,[b] μin.			
Out-of-pile	33	22	40
Total	33	100	175
Corrected corrosion[c] of Zircaloy-2 surfaces, μin.	19	105	190
Pin specimen corrosion,[d] μin.			
Zircaloy-2	3, 6	31, 104	153
Inconel	217	54	164
Type 347 stainless steel	27, 12	32, 39	5, 5
Croloy 2 1/4			95

[a]Tentative values.
[b]Based on total decrease in oxygen pressure.
[c]Based on decrease in oxygen pressure, accounting for the corrosion of the alloys other than Zircaloy-2 in the autoclave as observed by specimen weight changes.
[d]Zircaloy-2 pin corrosion in experiment L6Z-127S and L6Z-129S based on weight gain; all other pin corrosion based on weight loss.

19.3.4 Computation of Experiment Flux from Specimen Activation

Substantial and frequent variations in the flux exposure of in-pile experiments because of experiment retraction and to changes in reactor power level have made it necessary to modify the usual computational procedures for the determination of experiment flux and dose by measurement of the activation of corrosion specimens.[19] Such a specimen is counted (after cleaning) along with a specimen of the identical material activated in a known flux. In the case of Zircaloy-2 the decay chain[20] of interest is:

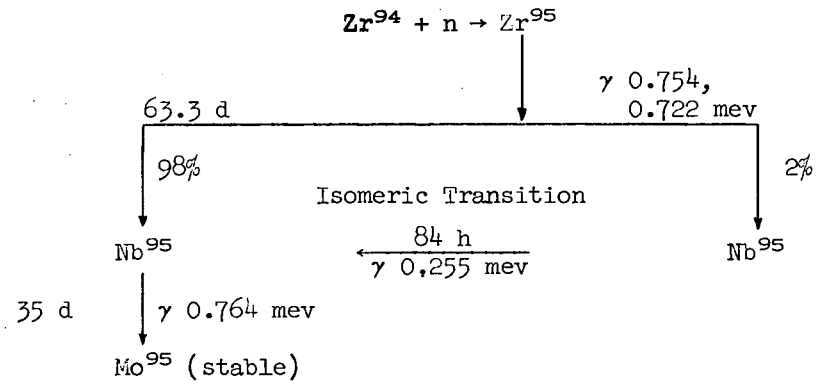

The gamma activities of both Zr^{95} and Nb^{95} are of approximately the same energy, and both are counted. It is possible to neglect, without appreciable error, the isomeric Nb^{95} nuclide produced to the extent of 2%, although more refined calculations could take it into account.

Values of the reactor power lower than full power are expressed as fractions p of full power. The reduction in flux due to retraction is expressed as a fraction q of the flux in the fully inserted position. This fraction is taken as being the same as the value obtained from calibration specimens in similar positions, with the same reactor lattice array, in beam-hole calibration experiments[21] taken before and/or after the autoclave corrosion experiment in question. It is possible to show that under the above assumptions the flux ϕ at the corrosion specimen, with the reactor at full power and with the experiment fully inserted, may be calculated from the equation:

$$\phi = \frac{A_s \, \phi_c \, f(t_c, d_c)}{A_c \, \Sigma_i \, p_i \, q_i \, f(t_i, d_i)} ,$$

where

$$f(t,d) = \frac{1}{\lambda_2 - \lambda_1} \left[\left(2\lambda_2 - \lambda_1\right)\left(1 - e^{-\lambda_1 t}\right)\left(e^{-\lambda_1 d}\right) - \lambda_1 \left(1 - e^{-\lambda_2 t}\right)\left(e^{-\lambda_2 d}\right) \right] ,$$

and where λ = decay constant for parent (1) and daughter (2) isotopes,
t = continuous irradiation time during period i of constant flux,
d = decay time from end of period i to time of counting,
A = activity per gram of specimen or control at time of counting,
s = specimen, and
c = control.

Except for the introduction of the intensity factors p and q and summation over consecutive intervals i of exposure, the above expressions correspond to the classical treatment.[19]

The above equations have been programmed for the general-case solution on the IBM-704 computer by the Service Group of the Oak Ridge Central Data Processing Facility at K-25.

Decay constants, counting data, and flux-map calibration are entered into the machine, followed by chronological tabulation of reactor power level and experiment position. The machine computes t_i, d_i, p_i, q_i, $f(t_i, d_i)$, $\Sigma_{o}^{i} t_i$, $\Sigma_{o}^{i} p_i q_i t_i$, $\Sigma_{o}^{i} p_i q_i f(t_i, d_i)$, and ϕ. From these data it is also possible to compute total and average dose or power density for any period or for the total experiment.

Values have been computed for two recent in-pile slurry-autoclave experiments, L6Z-121S and L6Z-129S.[18,22] These are given in Table 19.9 as fully inserted experiment flux, irradiation time, and full-flux hours. In the case of experiment L6Z-129S, which contained 1090 g of Th per kg of D_2O, 4.9% U/Th, 93% enrichment, the maximum experiment power density was 7.2 w/ml, and the average experiment power density was 3.2 w/ml. Experiment L6Z-121S did not contain uranium.

Table 19.9. Experiment Flux from Specimen Activation; IBM-704 Computer Results

	Symbol	L6Z-121S	L6Z-129S
Flux (fully inserted)	ϕ	0.527×10^{13}	0.563×10^{13}
Irradiation time, hr	Σt	261.5	1259.6
Full flux hours	Σpqt	260.8	560.2

19.3.5 Time Correlation of Zircaloy-2 Radiation-Corrosion Data from Slurry-Autoclave Experiments

Data from a number of in-pile autoclave corrosion experiments with high-temperature aqueous slurries are available.[23] A tabulation of these data along with control experiments and data from the literature are given in Table 19.10. The experiments were carried out at varied levels of fission power density, with averages up to 3.2 w/ml. Pure thoria and thoria-urania slurries, O_2 and D_2 atmosphere, and MoO_3 and palladium catalysts were used. The duration of experiments ranged to 1262 hr of irradiation. It may be noted that the maximum observed attack was 175 μin. and the maximum over-all rate was <1 mpy. Consequently, the effects reported below were not great under the conditions of observation.

Generally similar patterns of attack were noted. The changes in the rate of attack with time were followed by observing changes in gas pressure, while over-all corrosion effects were determined from weight-change data and physical examination after exposure. Fair over-all agreement has been observed. The

Table 19.10. In-Pile Slurry Corrosion of Zircaloy Autoclave, 280°C

Conditions	Experiment Number									
	WAPD[a] (288°C)	120	128	117	121	122	125	126	127	129
Flux,[b] 10^{12} neutrons·cm^{-2}·sec^{-1}				7	5.3	5.3[c]	5.3[c]	5.4[c]	8.3[c]	5.6
w/ml, avg.						0.57	0.44	1.6	0.8	3.2
max.						0.64	0.60	6.5	4.2	7.2
Hours irradiated				670	261	765	1044	140	732	1260
Atmosphere	None	O_2	O_2	O_2	O_2	O_2	D_2	D_2	O_2	O_2
g of Th per kg of D_2O		1000	410		1000	990	950	980	400	1090
g of U per kg of D_2O						5	5	49	20	54
Catalyst			MoO_3			MoO_3	MoO_3	MoO_3	MoO_3	Pd
Pretreatment time, hr	5040	485	1143	24	17	34	88	144	174	188
Total time >100°, hr	5040	485	1143	993	319	1074	1232	314	1122	1660
Corrosion, μin.										
Pretreatment	35	55	33	8	17	27	(10)	(12)	22	40
Total	35	55	33	40	49	105	62	53	100	175

[a]D. E. Thomas, "Corrosion of Zirconium in Water and Steam," p 663, Fig. 11.38, Metallurgy of Zirconium, NNES VII-4, ed. by B. Lustman and F. Kerze, McGraw Hill, New York, 1955.

[b]Thermal neutron flux in experiment determined from specimen activation.

[c]Tentative. More refined estimate based on methods of Sec. 19.3.4 to be used.

corrosion-time data have appeared to give the best correlations when plotted according to the classical logarithmic law.[24] Such a plot is shown in Fig. 19.4.

It has appeared that a small amount of corrosion of the order of zero to 30 μin. occurred with different values early in each experiment, attributable to various causes. In the absence of irradiation or in the periods prior to irradiation, fairly linear plots having approximately parallel slopes were obtained, indicating that the various experiments followed the logarithmic corrosion law at similar rates in the absence of radiation. The instantaneous rate was inversely proportional to the total time at temperature.

In each radiation experiment an increase in corrosion rate was noted as the irradiation began, except in the case of experiments 117 (pure D_2O) and 121 (pure thoria in D_2O), where no fission energy was generated. Generally the lines were again fairly straight. The flat parts of the line in experiments 125 and 129 were associated with periods of very low fission-power density. The slopes depended on the fission-power density of the experiment.

The effect of fission-power density on corrosion was estimated by obtaining the difference between a projection of the effects in the absence of radiation and the observed effect. In the presence of a fissioning slurry, the increase in slope above the unirradiated value could be correlated as proportional to the cube root of the fission-power density. The instantaneous rate may be estimated for either region of the curve by the expression,

$$\text{mils per year} = \frac{88 + 280 \times (\text{w/ml})^{1/3}}{\text{total hours at temperature}} .$$

The occurrence of time at temperature rather than irradiation time in the denominator has appeared to be required by the experimental data. One interpretation is that the time at temperature measures an increasing resistance to corrosion, which is independent of the over-all corrosion which has occurred. From this view, the fission-power density would act as an added driving force or potential. If the resistance to attack were to be reduced by the erosive action of flowing slurries, then corrosion rates under the combined influence of high flow velocities and high fission-power densities could rise to higher levels. However, present experiments which exhibit low corrosion rates are at trivial velocities. A sufficient basis for a satisfactory model must await experiments in in-pile slurry pump loops.

19.4 IN-PILE SLURRY LOOP

The primary objective of the initial test runs in a 5-gpm slurry loop was to evaluate the performance of the loop with regard to circulation of slurry, performance and reliability of the sintered-metal filter, adequacy of the pump purge, and over-all corrosion resistance of the system.

The loop under test is identical to the in-pile solution loops which have been used in the radiation-corrosion studies of uranyl sulfate solutions during the past five years (see Chap. 15, Radiation Corrosion). Satisfactory operation of this loop with slurries is dependent on maintaining the pressurizer free of thoria. This has been accomplished by means of a sintered-metal filter installed in the main stream of the loop, and the thoria-free filtrate is used as the

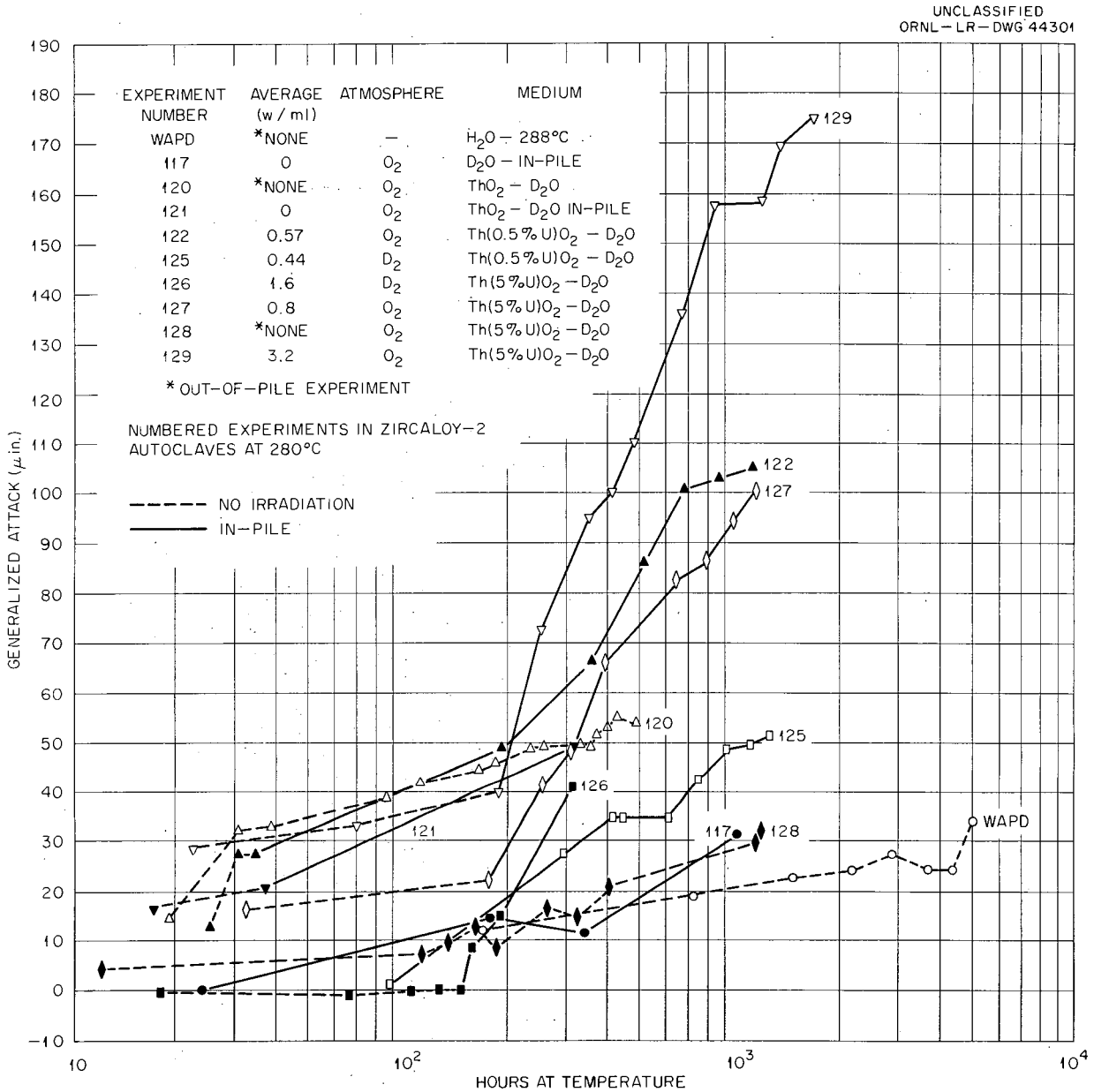

Fig. 19.4. Effect of Time and Radiation on Zircaloy Corrosion in Several Autoclave Experiments.

pressurizer feed stream. Thus the testing and evaluation of filters suitable for slurry filtration at temperatures to 300°C is an important phase of the loop development effort. Results obtained during the report period are discussed below.

19.4.1 Slurry Filtration

Slurry filtration tests have been made with nine sintered-metal filters of 18-8 stainless steel, one sintered-metal filter of nickel, and one of aluminum oxide. The mean pore sizes (diameter) of the filters have ranged from 5 to 20 μ. One type 347 stainless steel filter, No. 1, of unknown pore size performed satisfactorily at both 30 and 280°C when fitted with an inner liner to form an annular space in which a filter cake of thoria was formed as an additional filtering aid.[25] Two additional sintered-metal filters of type 347 stainless steel with mean pore sizes of 8 to 9 μ filtered satisfactorily in tests at 30°C, and one of the units (filter No. 9) was installed in loop L-2-26S and has performed satisfactorily for 600 hr at temperatures of 250 and 280°C with a thorium oxide slurry of mean particle size of 2 μ which contained 1/2 wt % uranium.

One aluminum oxide filter of 98% purity and having a mean pore size of 5 μ was satisfactory in tests at 30°C but has not been evaluated at elevated temperature.

A summary of the results with various types of sintered materials as thorium oxide slurry filters is shown in Table 19.11. This table includes some results previously reported.[26-28] These results show that a filter material in which the pore size is closely controlled in the 5- to 10-μ range will filter thorium oxide slurries at temperatures to at least 280°C and at concentrations to at least 1000 g of Th per kg of H_2O. In some cases a filter cake is required to produce thoria-free filtrate. Slurries of 2- to 3-μ mean particle size were used in these tests.

From loop tests at elevated temperature in which the slurries were circulated under an oxygen atmosphere, the filters of type 347 stainless steel have exhibited various degrees of plugging--either from corrosion products or ThO_2. However this has not precluded satisfactory loop operation for periods to 2000 hr.

19.4.2 Loop Tests at Elevated Temperature

Run 16 in test loop L-4-24S, previously reported,[29] was terminated after a 728-hr run at 250°C. The circulating slurry concentration compared favorably with book inventory throughout the run, as indicated by analyses of slurry samples. Thorium oxide can be added to the loop as desired by means of a slurry-addition system which utilizes part of the thoria-free water from the pressurizer to displace the slurry charged into an addition tank. The effect on the loop-liquid inventory is negligible. Throughout the run the sintered-metal filter produced a thoria-free filtrate at a rate of approximately 1.7 cc/sec.

Based on experience gained in the elevated-temperature slurry runs in test loop L-4-24S, a new loop, L-2-26S, was constructed which is dimensionally suitable for operation in beam hole HB-2 of the LITR. The loop is constructed of

Table 19.11. Summary of Thorium Oxide Filtration with Sintered Filters*

Filter Number	Filter Material	Mean Pore Diameter (μ)	Test Conditions Temp. (°C)	Test Conditions Time (hr)	Observations
1	347 SS wire	Unknown	30	2	ThO_2 in filtrate
			30	138	Thoria-free filtrate**
			250	2000	Thoria-free filtrate**
			250	180	Thoria-free filtrate; flow rate decreased, indicating filter plugging**
2	304 SS powder	10	30	0.5	ThO_2 in filtrate
			30	100	Thoria-free filtrate initially, then ThO_2 began to pass through in spots which later rusted
3	304 SS powder	10	30	2	ThO_2 in filtrate**
			30	300	Thoria-free filtrate until rust spots appeared and finally a crack developed at one rust spot**
4	Nickel powder	16	30	123	Thoria-free filtrate for 33 hr but passed slurry when slurry concentration was increased
			30	98	Thoria-free filtrate**
5	347 SS wire	19	30	2	ThO_2 in filtrate
			30	2	ThO_2 in filtrate**
6	347 SS wire	14	30	2	ThO_2 in filtrate
			30	2	ThO_2 in filtrate**
7	347 SS wire	11	30	20	ThO_2 in filtrate
			30	53	ThO_2 in filtrate**
8	347 SS powder	8	30	270	Thoria-free filtrate
9	347 SS powder	9.6	30	145	Thoria-free filtrate
			250-280	573	Thoria-free filtrate; flow rate decreased from 22 cc/sec to 0.6 cc/sec, then increased to 7 cc/sec and remained steady
10	347 SS wire	16	30	0.5	ThO_2 in filtrate
			30	24	ThO_2 in filtrate**
11	Al_2O_3	5	30	400	Thoria-free filtrate

*All filters in the form of a right cylinder with the following nominal dimensions: length, 8 to 12 in.; OD, 1/2 to 7/8 in.; ID, 3/8 to 5/8 in.
**Perforated inner liner was used to provide a filter cake as filtering aid.

type 347 stainless steel. In order to provide thoria-free water for the pressurizer and for purging the pump, the sintered-metal filter, with liner and filter cake, used successfully for 2000 hr in loop L-4-24S, was installed in the main stream of the loop. The filtrate flow from the filter passes through the pressurizer-heater and the pressurizer, both of which are standard in-pile solution-loop components. The core section of the loop is the double-pass type[30] incorporated in the ORR in-pile loop (see Chap. 15, Radiation Corrosion). Bulk slurry flow velocity in this core is approximately 2 fps at a flow rate of 5 gpm, and the main-stream velocity is approximately 9 fps. After a cumulative operating time of 182 hr (130 hr with ThO_2 slurry) at both 250 and 300°C, the filtrate flow rate decreased to a value too low for proper pressurizer operation (from ~2 cc/sec down to 0.1 cc/sec). Circulation of the thorium oxide slurry containing approximately 500 g of Th per kg of H_2O (from batch DT-46, 1600°C-fired, 2.4-μ particle size) was adequate, but some loss of oxide from the main circulating stream was encountered and is attributed to the loss of pump-purge flow with resultant accumulation of a small quantity of thorium oxide in the pump-rotor cavity. The over-all corrosion rate of the loop was 0.3 mpy based on iron pickup in the circulating slurry. The reason that the filter plugged during this run, after operating satisfactorily for 2000 hr in loop L-4-24S, is unknown. The filter unit was removed and replaced with a new sintered-metal filter of type 347 stainless steel which had an 8-μ mean pore size.

For run 2 the loop was charged with a thorium oxide from batch DT-18 containing 1/2 wt % U, and D_2O was used as the dispersant. Immediately upon charging the loop with slurry it was noted that thorium oxide passed through the filter, and subsequent examination showed that the filter had been damaged either during installation or as a result of elevated-temperature operation. The filter had cracked where it was joined to an end bushing. The filter unit was removed and modified by the installation of a bellows to provide mechanical flexibility.

Run 3, which followed, is still in progress. All thorium oxide charged to the loop is circulating, as indicated by slurry samples removed from the loop. A nominal slurry concentration of 500 g of Th per kg of D_2O is being maintained, and the loop operating temperature is at 280°C. The pressurizer flow rate, controlled by the restriction of the filter, began at 22 cc/sec, decreased to a low value of 0.6 cc/sec at operating hour 140 but has subsequently increased to approximately 7 cc/sec at 600 hr of slurry circulation. This thoria-free filtrate flow appears to be fairly constant at this time. The thoria slurry being circulated in the loop is considered suitable for in-pile testing because it contains uranium for fission-power generation in the loop core.

Several injections of deuterium gas in the presence of excess oxygen were made to the pressurizer. These were exploratory experiments to determine the efficacy of the particular loop system for the study of D_2 and O_2 recombination kinetics. In addition, such experiments were preparatory to testing the long-range steady-state recombination kinetics in the system for dynamic in-pile loop experiments.

It was found by observing and analyzing the decay of loop pressure with time that the system behaved as though the recombination rate was measured directly. Under the conditions of the experiment the rate of diffusion of deuterium and oxygen into the pressurizer liquid and the particular rate of circulation of the pressurizer liquid were not significant in the rate of pressure decay. Such observations confirmed previous deductions based on autoclave

experiments of the Chemical Technology Division and the analytical characteristics of a loop model (see Sec. 19.4.3). The suitability of the loop system as an experimental tool for the determination of kinetics information was thus indicated.

The over-all corrosion rate of the loop was 0.1 mpy based on the corrosion products of the type 347 stainless steel loop piping picked up by the circulating slurry.

19.4.3 Analysis of Loop Recombination Kinetics

The kinetics of recombination of radiolytic gases may be evaluated by means of steady-state or transient experiments, and both methods ultimately are to be used in the slurry in-pile loop program. The steady-state method, in which a steady input of mixed gases ($2\ D_2 + O_2$) is supplied by in-pile radiation or by out-of-pile metered feed from gas cylinders, leads to the most reliable and easily interpreted results, provided that an appropriate level of input can be developed. The analysis of transients, including the approach to this steady state, is a more flexible but more difficult process.

The determination of the recombination kinetics of radiolytic gases in the slurry in-pile loop from transient pressure-temperature measurements is complicated because mass transfer between at least three regions must be considered. These are the main slurry loop, the pressurizer-liquid region, and the pressurizer gas space. The pressurizer is at a temperature usually different from the main loop. The total pressure is determined by the amount of gas in the pressurizer gas space and the volume of this space and by the pressurizer temperature, which also fixes the steam pressure in this region. Recombination presumably occurs only in the main loop, which contains the slurry and catalyst. Clear, filtered water flows from the main loop through the pressurizer and returns to the main loop.

Several kinetic models have been analyzed for such a system in order to relate the observable time-pressure relationship to the rate of recombination in the circulating slurry. Recombination, mass transfer between pressurizer and main loop, and diffusion between pressurizer liquid and gas have been considered. The models considered the rapid injection of gas into the loop, followed by subsequent pressure decay, and also steady-state formation or injection of stoichiometric gas.

(a) Recombination.--The equations below consider only one gas (usually hydrogen) to be rate-controlling. Consequently the kinetics may be developed in terms of a single "radiolytic" gas. It is recognized that more complex cases could be required; however, such a treatment has generally been adequate in most earlier solution and slurry recombination studies, both in-pile and out-of-pile.

The following equation, which assumes immediate equilibrium between gas and liquid phases, holds for pressure of the loop if first-order recombination kinetics are controlling:

$$\left[\frac{A}{C} + \frac{1}{M_1}\right] \frac{dY}{dt} = -\frac{Ak}{c}(Y) , \qquad (1)$$

where

$$Y = \frac{P - P_e}{P_o - P_e} , \quad A = \frac{1}{mH} , \quad c = M_P A + \frac{V}{RT} ,$$

and P = pressure of stoichiometric, rate-controlling gas at time t,
P_o = initial partial pressure of rate-controlling gas,
P_e = final equilibrium partial pressure of this gas,
k = solution first-order rate constant (depends on slurry and catalyst concentration),
M_1 = mass of liquid in main-stream of loop,
M_P = mass of pressurizer liquid,
m = molecular weight of liquid,
H = Henry's Law constant at pressurizer temperature,
V = volume of pressurizer gas space,
T = pressurizer absolute temperature,
R = ideal gas constant.

With a steady generation or injection rate of Q moles of gas per unit time,

$$P_e = \frac{Q}{M_1 A k} \quad . \tag{2}$$

With no gas generation, the decay of pressure is given by

$$\frac{dP}{dt} = -k'P = -k\left[\frac{\frac{A}{C}}{\frac{A}{C} + \frac{1}{M}}\right] P \quad . \tag{3}$$

(b) Recombination and Pressurizer Flow.--When the rate of transfer of gas between pressurizer and the main-stream becomes slow relative to recombination or reduced pressurizer flow rates, the following second-order differential equation becomes necessary:

$$\frac{d^2Y}{dt^2} + \left[\frac{FA}{c} + k + \frac{F}{M_1}\right]\frac{dY}{dt} + \left[\frac{FAk}{c}\right]Y = 0 \ , \tag{4}$$

where F is the mass flow rate through the pressurizer (instantaneous gas-liquid equilibrium still assumed).

Analytical general solutions of Eq. (4) are unwieldy, but particular solutions have been obtained by using the REED Donner electronic computer under assumptions of system geometry and loading reasonable for actual or simulated in-pile operation. As the pressurizer flow rate was given lower values with a given recombination rate, the half-life of pressure decay began to deviate from the recombination half-life in an appreciable way. However, with expected pressurizer flow rates of 8 cc/sec, recombination rates up to $\sim 20\ hr^{-1} = k$ may be studied without undue interference from pressurizer flow.

(c) Diffusion Control.--Mass transfer between gas and liquid phases could become rate-controlling at relatively high levels of recombination rate and pressurizer flow rate. Third-order differential equations treating cases both of molecular and eddy diffusion have been derived, and analog solutions will be sought if experimental evidence indicates that such models must be considered.

REFERENCES

1. W. R. Gall et al., HRP Quar. Prog. Rep. for Periods Ending April 30 and July 31, 1958, ORNL-2561, p 63.

2. J. P. McBride et al., HRP Quar. Prog. Rep. Oct. 31, 1958, ORNL-2654, p 211.

3. R. L. Pearson et al., HRP Quar. Prog. Rep. Jan. 31, 1959, ORNL-2696, p 186.

4. O. Menis et al., HRP Quar. Prog. Rep. April 30, 1959, ORNL-2743, p 252.

5. E. L. Compere et al., HRP Quar. Prog. Rep. Jan. 31, 1959, ORNL-2696, p 102.

6. E. L. Compere et al., HRP Quar. Prog. Rep. for Periods Ending April 30 and July 31, 1958, ORNL-2561, p 180.

7. H. C. Savage et al., HRP Quar. Prog. Rep. Oct. 31, 1958, ORNL-2654, p 124.

8. E. L. Compere et al., HRP Quar. Prog. Rep. Jan. 31, 1959, ORNL-2696, p 104.

9. E. L. Compere et al., HRP Quar. Prog. Rep. April 30, 1959, ORNL-2743, p 122.

10. E. L. Compere, Multifactor Ratio Analysis of Corrosion Data Using Logarithmic Transformation, ORNL CF-58-9-3.

11. E. L. Compere et al., HRP Quar. Prog. Rep. Jan. 31, 1959, ORNL-2696, p 113.

12. E. L. Compere et al., HRP Quar. Prog. Rep. for Periods Ending April 30 and July 31, 1958, ORNL-2561, p 180.

13. E. L. Compere et al., HRP Quar. Prog. Rep. April 30, 1959, ORNL-2743, p 134.

14. C. C. Haws et al., HRP Quar. Prog. Rep. April 30, 1959, ORNL-2743, p 216.

15. W. J. Leonard et al., Interim Report on Metallographic Examination of Zirconium-Base Alloys for Evidence of Hydriding, HRP-MET-99.

16. E. L. Compere et al., HRP Quar. Prog. Rep. Jan. 31, 1959, ORNL-2696, pp 120-124.

17. Ibid., p 124.

18. E. L. Compere et al., HRP Quar. Prog. Rep. April 30, 1959, ORNL-2743, pp 139-145.

19. J. E. Baker, Calculation Methods for Determination of Neutron Flux and Power Density at In-Pile Loop Specimen Locations from Specimen Activity Measurements, ORNL CF-56-8-178 (Aug. 29, 1956).

20. W. H. Sullivan, Trilinear Chart of the Nuclides, ORNL, Jan. 1957 (Rev. Jan. 1959).

21. E. L. Compere et al., HRP Quar. Prog. Rep. April 30, 1959, ORNL-2743, pp 140-141.

22. E. L. Compere et al., HRP Quar. Prog. Rep. Jan. 31, 1958, ORNL-2493, pp 110-114.

23. E. L. Compere et al., HRP Quar. Prog. Rep. for Periods Ending:
(a) Jan. 31, 1958, ORNL-2493, pp 110-114.
(b) April 30 and July 31, 1958, ORNL-2561, pp 191-199.
(c) Oct. 31, 1958, ORNL-2654, pp 133-140.
(d) Jan. 31, 1959, ORNL-2696, pp 120-124, 130-131.
(e) April 30, 1959, ORNL-2743, pp 139-148.

24. U. R. Evans, Metallic Corrosion Passivity and Protection, p 135, Longmans Green and Co., New York, N. Y., 1948.

25. H. C. Savage et al., HRP Quar. Prog. Rep. Jan. 31, 1959, ORNL-2696, pp 124-126 and Fig. 12.8.

26. D. T. Jones, J. M. Baker, Thorium Oxide Slurry Filtration: Preliminary Tests of a 3-Micron Poroloy Sintered-Metal Filter; Runs 11, 12 and 13 in Loop L-4-24S, ORNL CF-59-1-49 (Jan. 9, 1959).

27. H. C. Savage et al., HRP Quar. Prog. Rep. April 30, 1959, ORNL-2743, p 145.

28. H. C. Savage et al., HRP Quar. Prog. Rep. Jan. 31, 1959, ORNL-2696, pp 124-126.

29. H. C. Savage et al., HRP Quar. Prog. Rep. April 30, 1959, ORNL-2743, p 145.

30. H. C. Savage et al., HRP Quar. Prog. Rep. Oct. 31, 1958, ORNL-2654, Fig. 15.5.

Part V

FUEL MANUFACTURE AND PROCESSING

20. URANYL SULFATE FUEL PROCESSING

P. A. Haas
E. L. Youngblood

20.1 REMOVAL OF NICKEL FROM FUEL SOLUTION BY ELECTROLYSIS

The results of runs made in an HRT-scale electrolytic cell containing a mercury cathode and a platinum-screen anode indicated that the electrolytic removal of nickel from concentrated HRT fuel solution is feasible. The system was designed[1] to process 30-gal batches of fuel solution and was tested with a solution of approximately the composition: 0.045 M $NiSO_4$, 0.27 M $CuSO_4$, 0.03 M $MnSO_4$, 0.34 M UO_2SO_4, 0.24 M H_2SO_4. The amount of nickel removed from a heavy-water fuel solution was proportional to the quantity of electricity passed through the solution (Fig. 20.1). The current efficiency for nickel removal was 1%, requiring about 220 amp-hr/liter to remove 90% of the nickel from the concentrated fuel solution.

Copper was removed from the fuel solution at a rate proportional to the quantity of copper present (Fig. 20.2). The rate for removal of copper was considerably higher than that for nickel, so that copper was essentially removed at the point at which 50% of the nickel remained.

Manganese was removed only after the copper had been removed (Fig. 20.3). Approximately 60% of the uranium was reduced from the (VI) to the (IV) valence state during the removal of 90% of the nickel.

Short-circuits in the cell due to amalgam growth from the cathode to the anode were largely eliminated by agitation of the mercury with a stream of fuel solution from a circulating-pump discharge. Stable amalgam loading up to 4.7 wt % of deposited metals (Ni + Cu + Mn) were obtained. However, there were some indications that an excessive loading retards nickel removal.

Anodic corrosion of the stainless steel components near the anode was severe for unprotected surfaces. In the last cell design, anodic corrosion was controlled by covering the stainless steel components near the anode with plastic; however, because of the instability of plastics in a high radiation field other means of protection would be required for actual processing.

Preliminary tests indicated that a 1 M HNO_3 - 1.5% H_2O_2 solution can be used to regenerate the mercury in the electrolytic cell. Copper and nickel removal rates were up to 30 g/hr, so that 80 hr would be required to regenerate amalgam from a 30-gal batch of fuel solution. This method resulted in the dissolution of up to 30% of the mercury per run. Additional testing would be required to determine if difficulties develop in successive regenerations of the cathode.

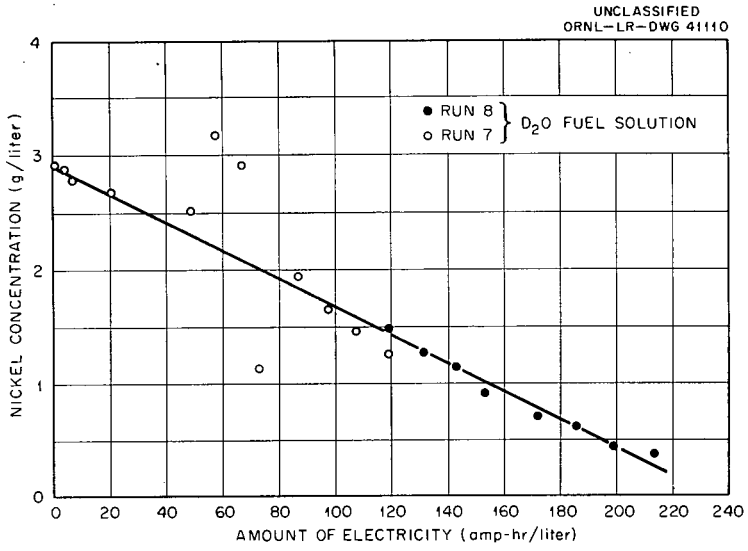

Fig. 20.1. Rate of Nickel Removal from a Heavy-Water Fuel Solution in an Electrolytic Cell.

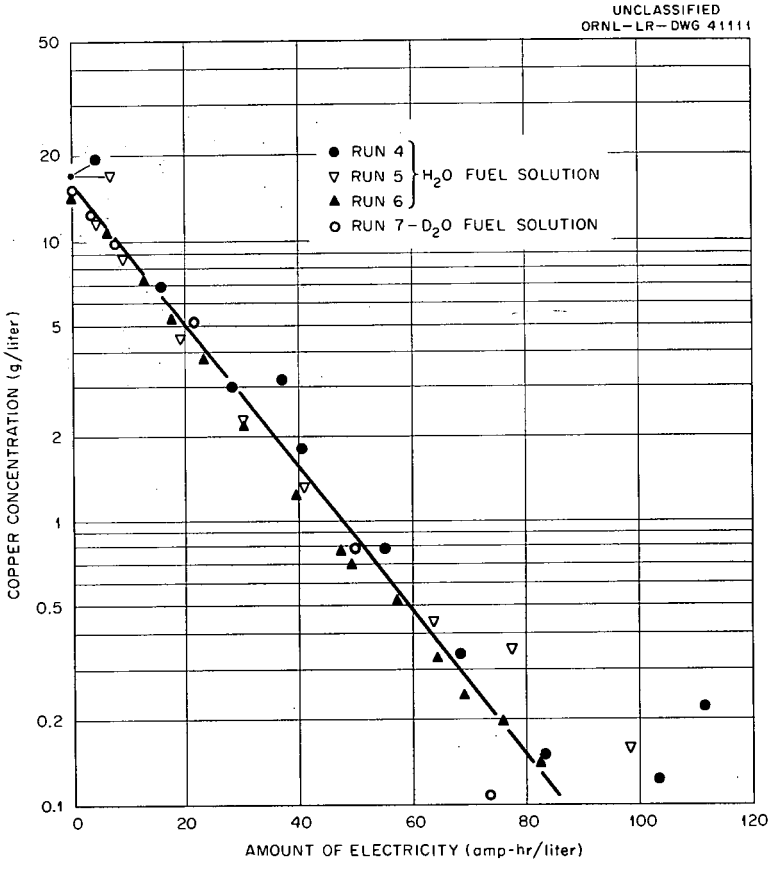

Fig. 20.2. Rate of Copper Removal from a Heavy-Water Fuel Solution in an Electrolytic Cell.

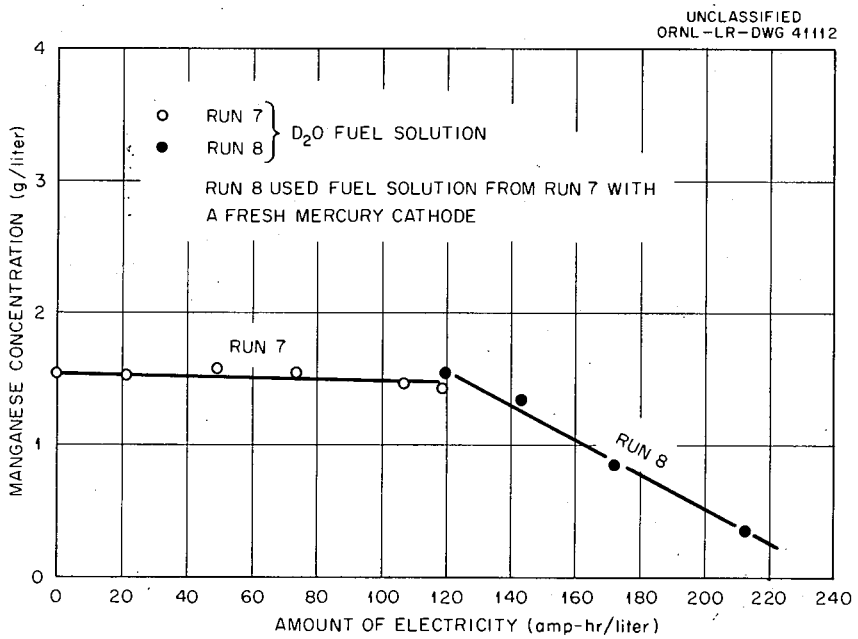

Fig. 20.3. Rate of Manganese Removal from a Heavy-Water Fuel Solution in an Electrolytic Cell.

20.2 PURIFICATION OF REACTOR FUEL SOLUTIONS BY PRECIPITATION OF URANIUM WITH HYDROGEN*

A series of runs was made in a titanium loop to demonstrate the feasibility of a method for purification of aqueous homogeneous reactor fuels from soluble fission and corrosion products, such as nickel and cesium. Briefly, the method consists in heating the impure fuel solution in a hydrogen atmosphere, thereby precipitating uranium and copper as UO_2 and metallic copper and leaving in solution those ions not reduced by hydrogen. After separation of the uranium oxide and copper by filtration or decantation, the copper and uranium oxide are dissolved in oxygenated sulfuric acid.

Figure 20.4 illustrates the precipitation of uranium and copper and the reconstitution of the fuel solution. The initial solution contained 9.9 g of uranium per liter, 0.60 g of copper per liter, 0.735 g of nickel per liter, and was 0.034 M in D_2SO_4, in D_2O. To this solution was added 50 ppm iodine as potassium iodide, 20 ppm cesium as cesium sulfate, and 100 ppm neodymium as neodymium sulfate. At room temperature, 100 psi of deuterium was added, and the system was brought to 250°C, at which temperature precipitation of the uranium and copper began. Within 7 hr the uranium concentration had decreased to 0.05 g/liter, and the copper concentration had decreased to 0.04 g/liter. In an additional 15 hr, the uranium concentration dropped to 0.024 g/liter and the copper remained at about 0.04 g/liter. Essentially all the nickel and cesium remained in solution; the neodymium concentration decreased from 100 ppm to 60 ppm and the iodine concentration decreased from 50 ppm to 6 ppm. After 22 hr of circulation, the nearly uranium-and-copper-free solution was drained from the loop. The loop was rinsed once with water at room temperature, and then a solution of 0.075 M D_2SO_4 was added to the loop with 200 psi of oxygen. Within 2 hr at 250°C the original solution was essentially reconstituted except for about 80 ppm nickel, 6 ppm iodine, and 30 ppm neodymium. No cesium was detected in the reconstituted solution. The recovery of uranium and copper was greater than 99%. It is believed that this method has some advantages for rapid processing of core fuels for homogeneous reactors.

REFERENCE

1. Chemical Technology Division, Unit Operations Section, Monthly Progress Report, March, 1959, ORNL-CF-59-3-61, p 24-25.

---

*This section contributed by J. C. Griess, H. C. Savage, R. S. Greeley, and E. S. Snavely, Jr., of the Solution Corrosion Section, Reactor Experimental Engineering Division.

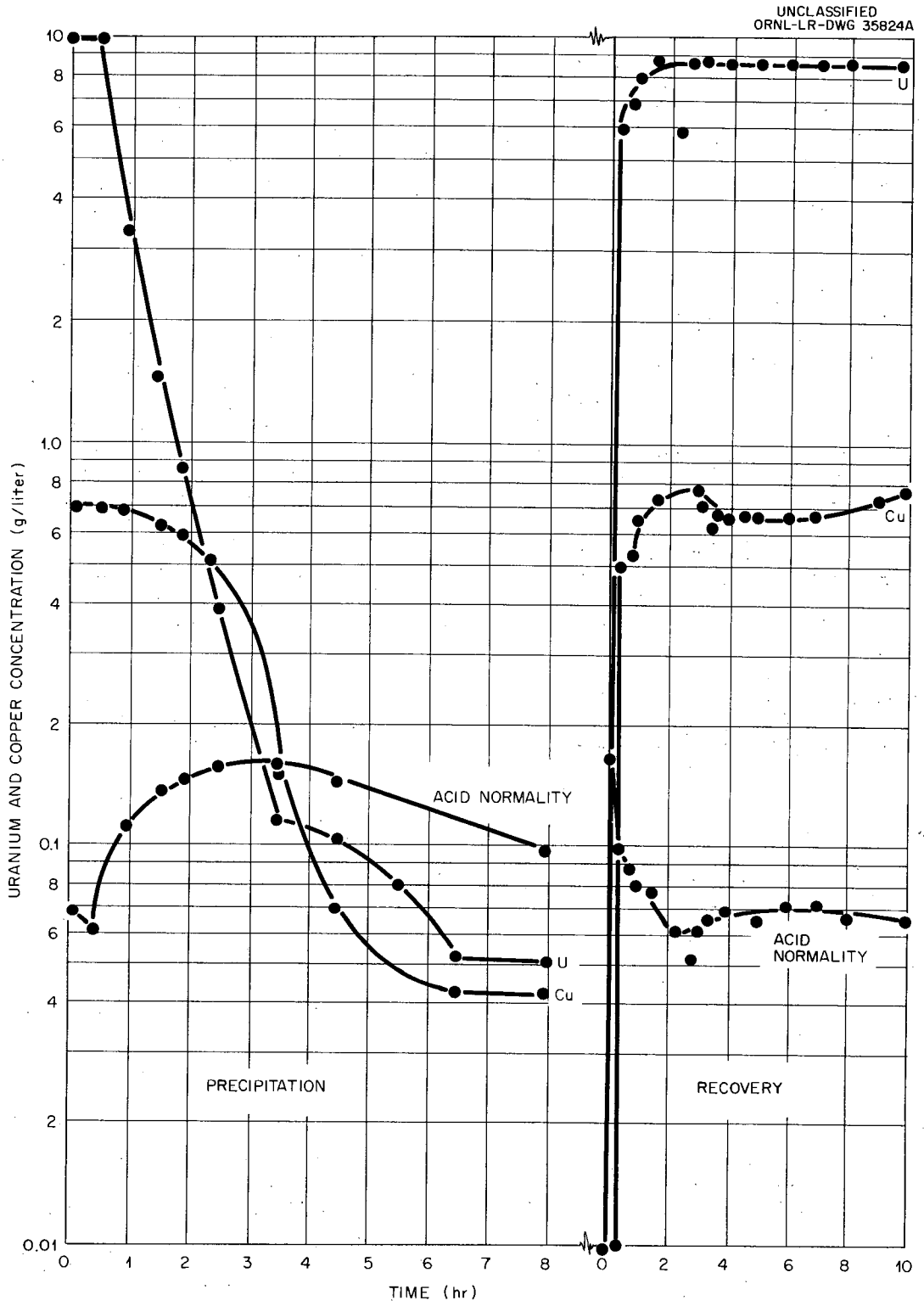

Fig. 20.4. Concentration vs Time for Major Components of UO_2SO_4 Solutions During Precipitation and Recovery of Uranium and Copper. Runs G-123, -124.

21. THORIUM OXIDE PREPARATION AND PRODUCTION

O. C. Dean C. E. Shilling

21.1 THORIUM-URANIUM OXIDE: ADSORPTION PREPARATION METHOD

Studies were carried out on the properties of thorium-uranium oxides prepared by the deposition of uranium on preformed thoria (650°C-fired) by the thermal decomposition of an ammonium uranyl carbonate solution, followed by firing at 1100°C. Principal preparation variables investigated were uranium content and firing atmosphere. The species of oxide produced by firing in oxidizing and in reducing atmospheres appeared to differ both chemically and physically. The mixed oxides fired in H_2 also appeared to be less homogeneous than those fired in air. The percentage of uranium leached by 8 N HNO_3 from the mixed oxides fired at 1100°C in air decreased with increasing uranium content and was proportional to the surface area of the mixed oxide.

21.1.1 Experimental

Thorium-uranium mixed oxides containing 0.0054, 0.029, and 0.044 molar fractions of uranium oxide were prepared by the adsorption method described previously.[1] The thorium oxide used was 650°C-fired DT-58. The mixed oxides were fired at 1100°C under various conditions: 4 hr in air, 24 hr in air, 4 hr in H_2, and 4 hr each in H_2 and then air. The 1100°C firing temperature was selected on the basis of the previous work, which had indicated this to be the highest firing temperature in air that would not cause sintering.

The mixed oxides were characterized by x-ray diffraction measurements, nitrogen-adsorption surface-area measurements, average uranium valence determinations, and by the amounts of uranium that were leachable in 8 N HNO_3. Average uranium valences were determined from chemical analyses for U(IV) and total uranium. The leaching studies were made by refluxing a 1-g sample for 1 hr in 50 ml of 8 N HNO_3 solution. Uranium contents are expressed in molar fractions of uranium oxide, x, corresponding to the formula[2] $Th_{1-x}U_xO_{2-y}$.

21.1.2 Effect of Preparation Variables on Lattice Dimensions

The lattice parameter of a solid solution prepared from crystals having cubic structures (i.e., fluorite) should be, according to Vegard's law,[3] a linear function of the composition. Lattice dimensions were calculated for the mixed-oxide products (Table 21.1) and plotted as a function of uranium content (Fig. 21.1). A theoretical line calculated from Vegard's law, using lattice dimensions of 5.5973 Å for the DT-58 ThO_2 and 5.4691 Å for pure UO_2,[4] is shown in Fig. 21.1 along with the uranium data. The mixed oxides fired in H_2 show a large deviation from the theoretical Vegard curve with increasing uranium

Table 21.1. Effect of Firing Conditions and Uranium Content on Thorium-Uranium Oxide Properties. Prepared by the Adsorption Method

Original ThO_2, DT-58-650°C
Firing Temperature, 1100°C

Firing Conditions		x,[a] Molar Fraction, Uranium Oxide	y,[a] Excess Oxygen (g atoms O/mole mixed oxide)	X-ray Data		N_2 Surface Area (m^2/g)	Amount Leached by 8 N HNO_3 (%)[b]	
Atmosphere	Time (hr)			Lattice Constant (Å)	Crystallite Size (Å)		Uranium	Thorium
Air	4	0		5.5971	928	4.9		0.21
		0.0054	0.0040	5.5961	487	8.5	30.8	0.55
		0.029	0.019	5.5936	1418	1.4	9.0	0.07
		0.044	0.025	5.5925	1407	1.3	8.4	0.08
		1.00	0.625		767	1.4	100[c]	
Air	24	0		5.5974	1453	2.6		0.10
		0.0054	0.0041	5.5968	710	5.0	17.1	0.10
		0.029	0.017	5.5938	1407	0.94	6.9	0.02
		0.044	0.024	5.5918	1255	0.94	4.5	0.04
		1.00	0.634		802	0.34	100[d]	
H_2	4	0		5.5963	722	6.3		0.35
		0.0054	0.0013	5.5967	710	5.9	4.0	0.33
		0.029	0.0025	5.5944	549	7.6	6.5	0.55
		0.044	0.0043	5.5933	547	8.0	16.5	0.44
		1.00	0.017		685	3.5	100[d]	
H_2 then air	4 each	0		5.5951	927	4.6		0.35
		0.0054	0.0035	5.5968	674	6.0	9.8	0.35
		0.029	0.014	5.5937	1358	1.5	6.5	0.07
		0.044	0.024	5.5922	1337	1.0	6.9	0.13
		1.00	0.624		724	0.41	100[c]	

[a] x and y are subscripts in the mixed-oxide formula: $Th_{1-x}U_xO_{2+y}$.
[b] 1 g of solid refluxed 1 hr in 50 ml of 8 N HNO_3.
[c] Complete dissolution in <4 min.
[d] Complete dissolution in 1-1/2 min (40°C).

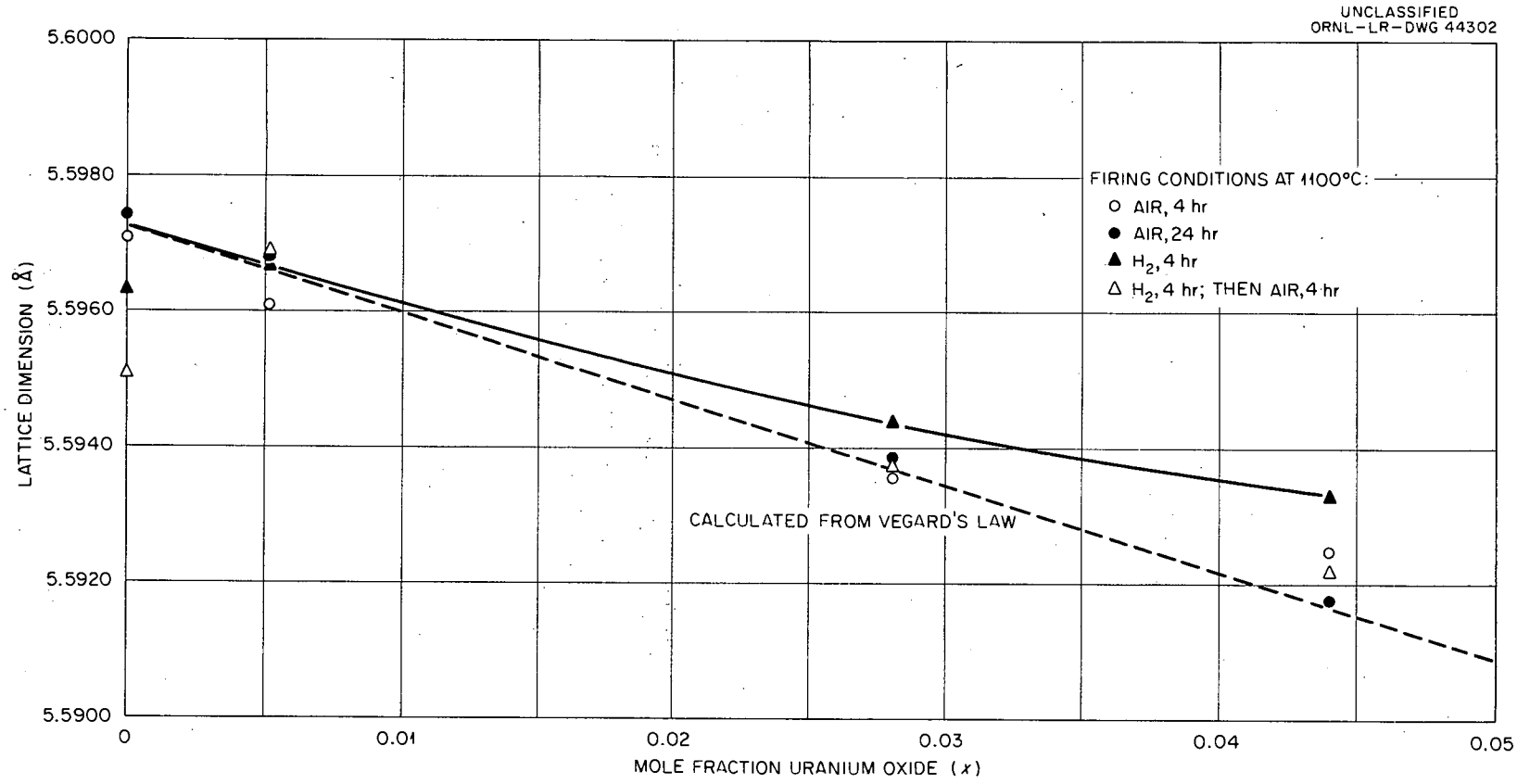

Fig. 21.1. Lattice Dimension as a Function of Uranium Content in Th-U Oxides Prepared by the Carbonate Adsorption Method.

content and, therefore, appear to be less homogeneous than the air-fired samples, whose lattice dimensions correlate well with the predicted values except at the highest uranium concentration.

21.1.3 Uranium Content, Surface Area, and Crystallite-Size Relation

For air-fired oxides the surface area decreased and the crystallite size increased as the concentration of uranium oxide was increased from a molar fraction of 0.0054 to 0.029 (Table 21.1 and Figs. 21.2 and 21.3), while for oxides fired in hydrogen the surface area increased and the crystallite size decreased slightly. In air-fired oxides, for uranium concentrations from 0 to 0.5 mole %, the surface appeared to undergo a change which results in disruption of crystallites, probably a diffusion of some uranium oxide species into ThO_2. The relatively insignificant changes in surface area and crystallite size for oxides fired in hydrogen, where UO_2 is the stable uranium species, indicate that the diffusivity of uranium dioxide is low at the 1100°C firing temperature. The increase in crystallite size of the air-fired oxides shows the effect of excess O_2 in promoting sintering in the thoria-urania species.

21.1.4 Oxygen-Uranium Relation

In Fig. 21.4 the excess oxygen, y, in the mixed oxides defined by the formula $Th_{1-x}U_xO_{2+y}$ is plotted vs the uranium content. Theoretical curves corresponding to ThO_2 plus UO_2, U_2O_5, U_3O_8, and UO_3 are also illustrated. All experimental points for the air-fired preparations lie within the composition limits corresponding to U_2O_5 and U_3O_8. Originally, those preparations fired in H_2 may have approached y = 0, or uranium as UO_2. All stood 24 to 48 hr prior to analysis and had reasonably high surface areas; so there may have been some reoxidation. In solid solutions of uranium and thorium oxides, for specified firing conditions, the excess oxygen, y, should be proportional to the uranium concentration. The nonlinearity observed for air-fired samples (Fig. 21.4) in regions of higher uranium concentration suggests an approach to saturation of the thoria-urania lattice with interstitial oxygens and a consequent lowering of the over-all oxygen/uranium ratio as more uranium diffuses into the solid.

21.1.5 Leachability of Uranium from Thorium-Uranium Oxides

For the oxides fired in air, the fraction of uranium leached in 8 N HNO_3 decreased with increasing uranium content (Table 21.1; Fig. 21.5) and was proportional to the surface area of the mixed oxide (Fig. 21.6). The oxides fired in hydrogen showed a lower specific leaching effect (Table 21.1). Refiring the mixed oxide in air after firing in hydrogen increased the leachability of the uranium and, at the higher uranium concentrations, the amounts leached from the mixed oxide fired in air or H_2 and air were about the same.

21.2 OXIDE PREPARATION DEVELOPMENT*

Work on the development of methods for preparing oxide continued, with emphasis on the production of spherical particles by the flame denitration of alcoholic solutions of nitrates and by a gel technique.

---

*This work was done by P. A. Haas, C. C. Haws, and K. O. Johnsson of the Unit Operations Section, Chemical Technology Division.

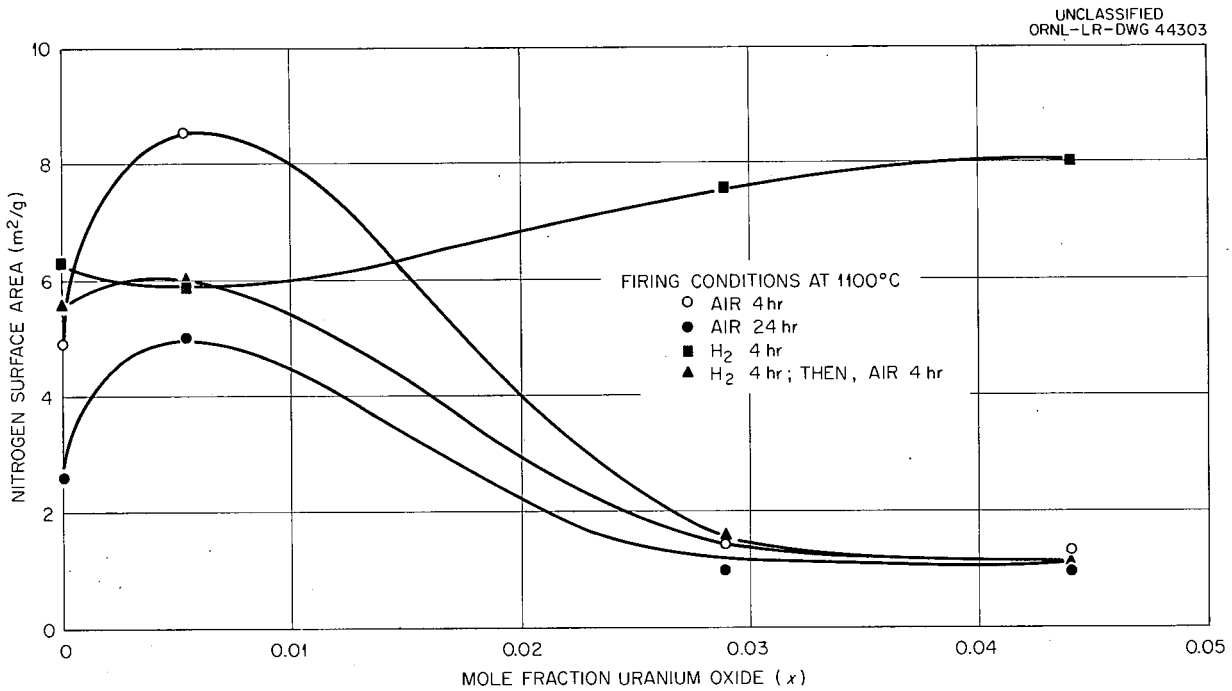

Fig. 21.2. Effect of Uranium Content on Nitrogen (BET) Surface Areas of Th-U Mixed Oxides Prepared by the Carbonate Adsorption Method.

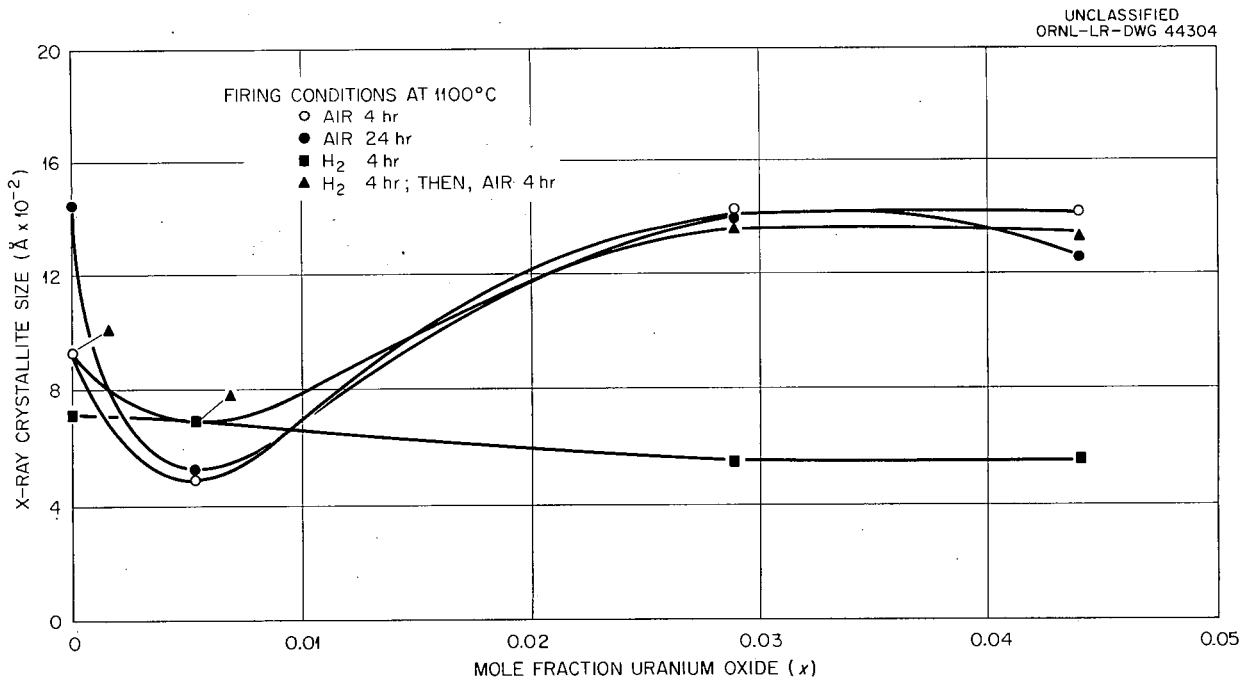

Fig. 21.3. Effect of Uranium Content on X-Ray Crystallite Size of Th-U Oxides Prepared by the Carbonate Adsorption Method.

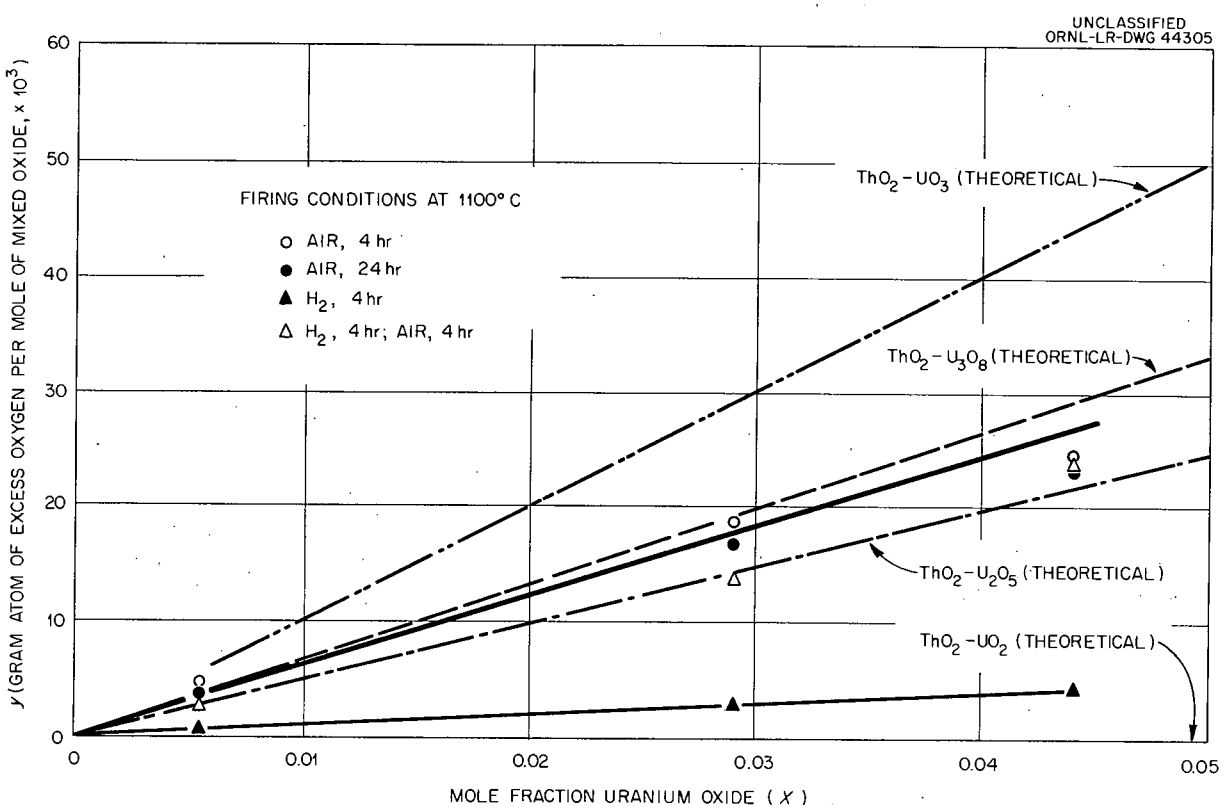

Fig. 21.4. Excess Oxygen in the System ThO_2-UO_2-O as a Function of Uranium Oxide Content and Firing Conditions: Carbonate Adsorption Method. x and y are subscripts in the mixed-oxide formula: $Th_{1-x}U_xO_{2+y}$.

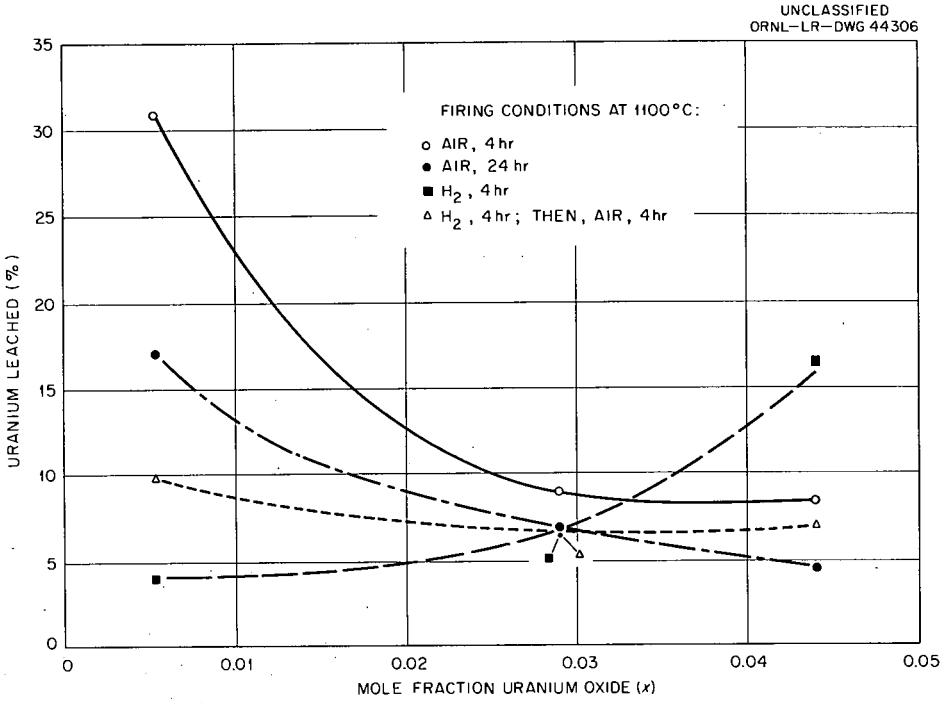

Fig. 21.5. Effect of Uranium Content on Leachability of Uranium from Th-U Oxides Prepared by the Carbonate Adsorption Method. A 1-g sample was leached for 1 hr by 50 ml of boiling 8 *N* HNO_3.

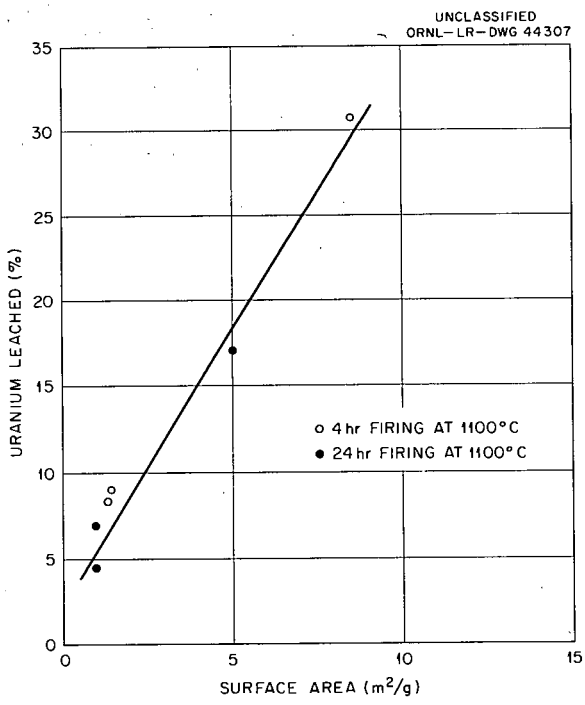

Fig. 21.6. Uranium Leachability vs Specific Surface Area for Air-Fired Mixed Oxides Prepared by the Carbonate Adsorption Method.

21.2.1 Flame Denitration

Spherical oxide particles containing 82 to 99 wt % ThO_2, 1 to 10 wt % Al_2O_3, and 0 to 8 wt % uranium oxides were prepared and calcined at up to 1800°C by flame denitration. Feed solutions of the nitrates in methyl alcohol were used with C_3H_8-O_2-air flames in MgO or ZrO_2 reflectors. With U/Th in a ratio of 0.08, a large fraction of spherical particles (Fig. 21.7) was obtained for 2.5, 5, and 10 wt % Al_2O_3; the fraction of spherical particles was much smaller for 1 wt % Al_2O_3. Low yield-stress values of 0.02 to 0.06 lb/ft^2 and low surface areas of 1.3 to 3.1 m^2/g (Table 21.2) for mean diameters of for 0.9 to 2.9 μ indicate good properties for circulating slurries. Toroid tests of these materials are being made.

Spherical particles were also obtained by flame denitration to give ThO_2 containing 5 wt % Al_2O_3 (Fig. 21.8), while similarly prepared Th-U oxides without Al_2O_3 were not spherical in shape. Flame-denitrated samples were prepared, but not yet photomicrographed, of oxide mixtures of U-Al, Th-Si, and U-Si. Since beryllium is much less of a neutron absorber than aluminum or silicon, preparation of ThO_2-BeO mixtures is planned.

A 45-lb test sample of mixed oxides (U/Th = 0.08, 2.5 wt % Al_2O_3) was prepared by using high feed flows and the other denitration conditions that gave the product shown in Fig. 21.7. Feed rates equivalent to 720 g/hr of oxides were tested (Table 21.2), and rates of 400 g/hr appear practical for present burner designs and 3-in.-ID reflectors.

21.2.2 Preparation of Spherical Particles by a Gel Technique*

Spherical thorium oxide particles in the size range 0.5 to 30 μ were prepared by the partial neutralization of thorium nitrate solution with ammonia, setting the resulting sol to a gel by mixing with isopropyl alcohol, and drying and firing the resulting solids. After being fired at 1000°C, a typical product had a surface area of 0.68 m^2/g and a pycnometric density of 6.8 g/cc.

(a) Sol and Gel Preparation.--The sol was ordinarily prepared by adding ammonium hydroxide to a well-stirred thorium nitrate solution. Efforts to obtain a reproducible sol by control of the concentration, temperature, and degree of agitation were in general unsuccessful. It was possible, however, by careful control of the ammonia addition rate to obtain a sol with a ratio of 3.8 moles of ammonia to one of thorium nitrate. Sols 1.3 to 1.5 M in thorium were more or less readily prepared and, by evaporation of such a sol, it was possible to prepare a 3 M sol which, after being dried at room temperature, had an ammonia-to-thorium mole ratio of 3.5 to 1. Higher concentrations of thoria formed stiff gels. Other methods of making reproducible sols are under investigation.

Mixing the sols prepared as above with isopropyl alcohol resulted in the formation of a two-phase system with the bulk of the thorium concentrated in one phase. The fluidity of the thorium-rich phase decreased with increasing isopropyl alcohol content in the two-phase system and, in the case of a 1.4 M sol (NH_3/Th = 3.5) mixed with 90.6 wt % isopropyl alcohol, the thorium-rich phase set to a hard gel containing >98% of the thorium. The more concentrated

*This work was done by R. L. Pearson and A. T. Kleinsteuber of the Chemical Development Section, Chemical Technology Division.

Fig. 21.7. Flame-Calcined Thorium/Uranium Oxide Containing 2.5% Al_2O_3. Conditions: U/Th mass ratio, 0.08; outside reflector temperature, 1500°C; classification, 95% <5 μ. Oxide properties: surface area, 2.4 m^2/g; yield stress, 0.02 lb/ft^2; mean particle size, 1.7 μ.

Table 21.2. Slurry Characteristics of Flame-Denitrated Thorium-Uranium Oxides Containing Alumina

Firing temperature, 1500°C (outside wall of magnesia reflector)
Volume feed rate, 50 ml/min for run 74B, 20 ml/min for all others
U/Th wt ratio, 0.08 for all samples

Run No.	Nominal Alumina Conc. (wt %)	Mean Part. Size (μ)	Yield Stress* (lb/ft^2)	Surface Area (m^2/g)	Approx. Feed Rate (g of oxides per hour)	Feed Concentration (g of nitrates per liter of solution)
62	5	1.5	< 0.02	2.0		
63	2.5	1.7	0.02	2.4		
66	1	2.0	0.026	2.6		
69	10	1.6	0.05	3.1		
68	2.5	2.9	0.02	1.6	90	188
70	5	1.4	0.02	1.4	95	204
72	5	0.9	0.02	1.7	195	408
73	5	1.1	0.06	2.1	95	204
74B**	2.5	2.8	0.02	1.3	720	600

*Yield stresses at room temperature, corrected to a slurry density of 2 g/ml.
**Run 74B lasted 0.33 hr; others 4 hr longer.

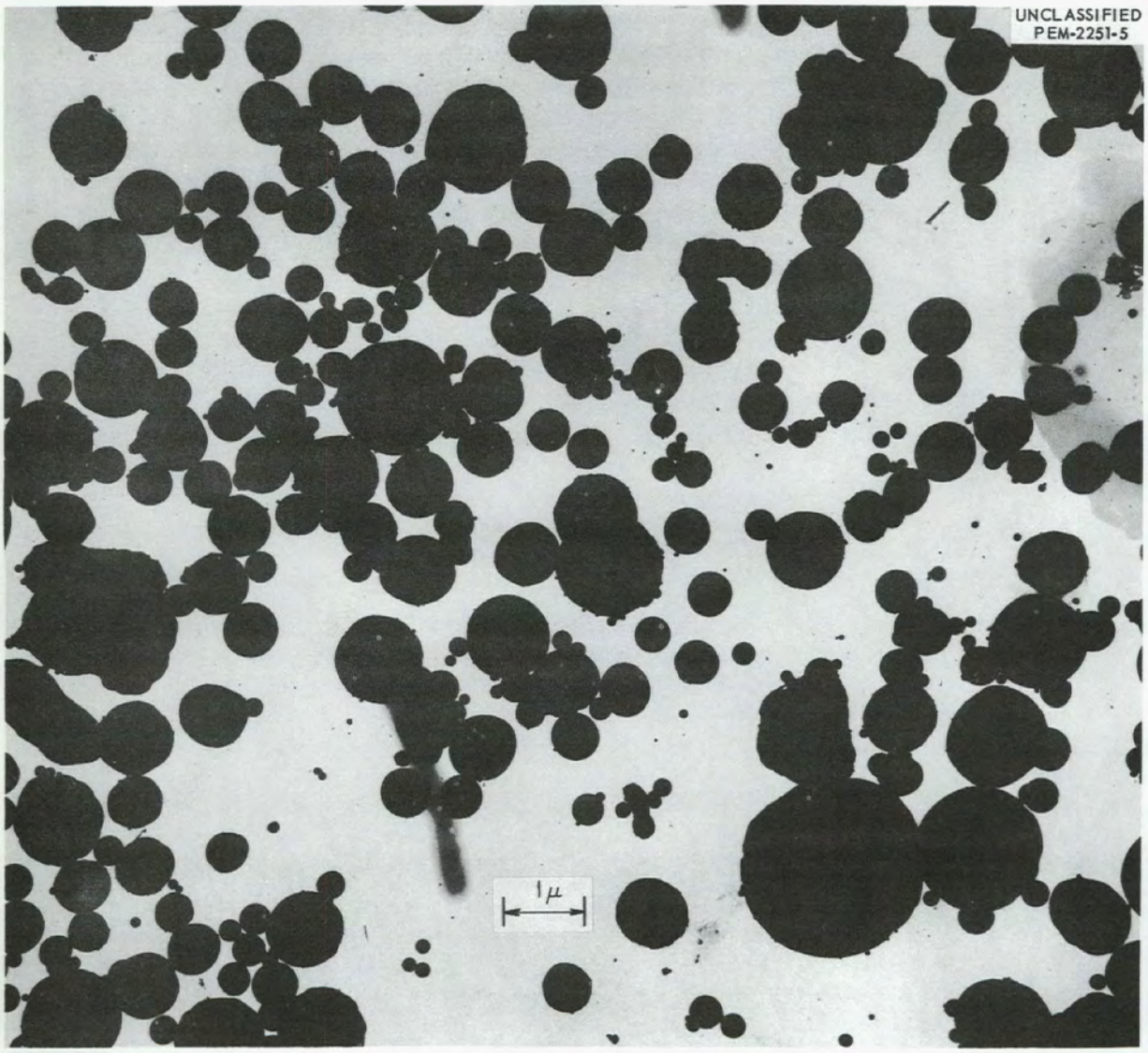

Fig. 21.8. Flame-Calcined Thorium Oxide Containing 5% Al_2O_3. Conditions: 5% Al_2O_3 by weight; 95% ThO_2 by weight; outside reflector temperature, 1500°C; estimated particle temperature, 2400°C; sample not classified, shown as collected. Oxide properties: N_2 surface area, 1.3 m^2/g; theoretical minimum surface area, 0.6 m^2/g; mean particle size, 1.0 μ; yield stress, 0.026 lb/ft^2 ($\rho = 2.0$).

the sol, the less isopropyl alcohol was necessary to produce a gel, a 1.58 M sol being set by only 43 wt % of isopropyl alcohol.

(b) Bead Formation.--Spraying the above sols onto isopropyl alcohol, or mixing the sol and isopropyl alcohol streams in an orifice, resulted in the formation of spherical particles (Fig. 21.9). The first beads produced had thin walls with hollow centers and shattered easily. Beads made from sols in which the thorium content and the NH_3/Th mole ratio were altered showed no improvement in their solidness. It was found, however, that increasing the water content of the isopropyl alcohol eliminated the holes. Five cubic centimeters of a 1.5 M Th sol having an NH_3/Th ratio of 3.50 was sprayed into 100 ml of isopropyl alcohol containing various amounts of water. The beads became solid above 12 vol % water (Table 21.1). Stirring the beads in the mother liquor improved the solidness.

(c) Washing and Firing.--The beads as formed contained about 50 wt % NH_4NO_3, which had to be removed prior to the drying and firing in order to prevent coalescence during these operations. The beads as formed also will "dissolve" in any H_2O-isopropyl alcohol mixture containing more than 25 wt % H_2O. Adding 33 vol % of concentrated ammonia to the mother liquor, equilibrating for several hours, and washing the beads a second time in a wash of one part of reagent ammonia to two parts of isopropyl alcohol decreased the nitrate content to less than 0.5 wt % and prevented coalescence during the drying and firing.

The final washing and firing procedure to produce beads of sufficient strength to resist degradation on pumping has not yet been determined. Figure 21.10 shows beads fired at 1000°C which appear to have rough edges, possibly resulting from excessive nitrate impurities in the beads prior to firing.

21.3 OXIDE PREPARATION*

The equipment for preparing oxides was moved from Building 3019 to a new site, Building 2528 (Ref. 11). In general, the old equipment was used at the new site, although several small changes were made. The outstanding improvement in the new building was in the off-gas system, which provides eight building air changes per hour at a flow rate of 3700 ft^3/min. The plant was completed on July 24, 1959, and the first thorium oxide preparation was begun on July 26, 1959. The present output of the plant is approximately 600 lb/month, operating around the clock on a five-day week, with one operator per shift.

Fifteen precipitations were made in order to prepare approximately 2150 lb of thorium oxide. Eleven of the 15 were for producing thorium-uranium mixed oxides. The eleven mixed-oxide runs were broken down as follows: three runs of 8% uranium oxide, three runs of 0.5% uranium oxide, and five runs of 3% uranium oxide. The products of the three 0.5% mixed-oxide runs are awaiting classification. The product of one of the three 3% mixed-oxide runs was classified and dried and is ready for shipment, pending analytical determinations. The products of the three 8% runs were shipped to Y-12.

*This work was done by R. H. Winget of the Pilot Plant Section, Chemical Technology Division.

Fig. 21.9. Thoria Spheres Produced by Gelling a Thoria Sol with Isopropyl Alcohol. 800X.

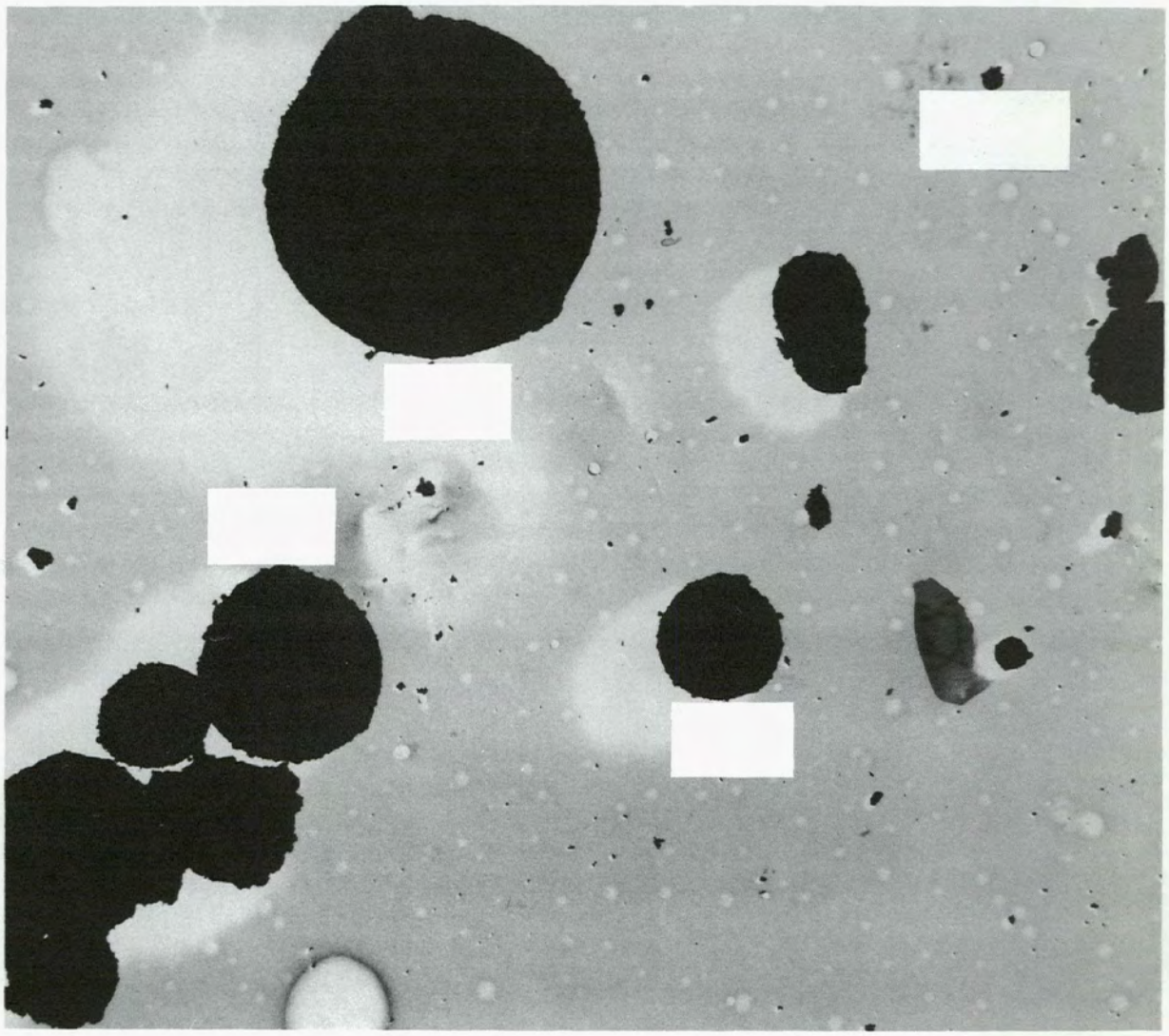

Fig. 21.10. Thoria Bead Produced by the Gel Technique; Fired at 1000°C.

A total of 1041 lb of oxide prepared in the new building was shipped to REED, 524 lb being 8% uranium mixed oxide and the remainder being thorium oxide. During May, 1095 lb of 800°C-calcined oxide that had been prepared in the old building was shipped to REED.

REFERENCES

1. J. P. McBride, et al., HRP Quar. Prog. Rep. Oct. 31, 1958, ORNL-2654, p 202-214.

2. J. S. Anderson, et al., J. Chem. Soc., 1944: p 3324.

3. L. Vegard, Z. Physik 5, 17 (1921).

4. R. E. Rundle, MDDC-1608.

5. K. O. Johnsson and R. H. Winget, Pilot Plant Preparation of Thorium and Thorium-Uranium Oxides, ORNL-2853 (in press).

Part VI

METALLURGY

22. METALLURGY

G. M. Adamson

F. W. Cooke
T. M. Kegley
W. J. Leonard
M. L. Picklesimer
P. L. Rittenhouse
R. L. Stephenson
C. H. Wodtke

22.1 HRT REPAIR AND EXAMINATION

22.1.1 Examination of Specimens Removed from the HRT after Run 17

The macro- and microexaminations of the specimen disks cut from the Zircaloy-2 diffuser screens in the HRT core tank, of the titanium specimen holder inserted in the core tank during run 17, and of the mechanical-property specimens recovered from the top screen (originally supported in the specimen holder) have been completed. With the exception discussed below, no changes in conclusions from those drawn from the preliminary examination and reported previously[1-3] have been made.

A more extensive microstructural examination of additional sections of the titanium specimen-holder (some near the holes, others midway along the station, and one from a station in the neck region of the core tank) has shown that the previously reported high deuterium content in the holder exists only in the region of the holes and burned brackets. The deuterium content decreases from approximately 2000 ppm at the burned hole or bracket to less than 200 ppm at approximately 1 in. away from the nearest burned surface and to less than 10 ppm at approximately 1-1/2 in. No deuterium was picked up by the metal in the center portion of any station, and none was picked up in any region which was not associated with a burned hole or bracket. The microstructures found in the regions having low hydrogen and deuterium contents were those expected from the fabrication history of the section. Thus it appears that the deuterium pickup was not so extensive as was previously thought.

Portions of the screen specimen cut from the HRT core tank have been melted by induction heating and by arc melting and have been dissolved in a 6 N HNO_3 electrolytic dissolution cell to determine the kind and nature of the radioactivity released. Such information was desired by the Design Section to assist them in determining the type of ventilation required during the maintenance operation. Helium and argon flowed past the specimens, carrying gaseous and particulate activity to various portions of the test system. For the melted samples, activity measurements (by G. W. Parker and W. J. Martin of the Chemistry Division) were made on the melting chamber, the tube carrying the exhaust gases to a filter unit, and on a millipore filter.

The measurements showed that Ce activity was detectable at all points and that Cs, Zr, Ru, Te, and I activity was detectable over the furnace chamber. While no identification was attempted, considerable activity was also detected on the exhaust-gas train and filter for the specimens dissolved electrolytically. Thus radioactive particles and gases were released by melting and by electrolytic dissolution.

22.1.2 Measurement of HRT Zircaloy-2 Core-Vessel Thickness*

On September 10, 1959, a survey of the thickness of the HRT core vessel was made by use of an ultrasonic technique. The measurements were made at many locations from inside the vessel, using a new rig developed by the Component Development Section of REED,[4] and employing the direct pulse-echo technique with the Immerscope. Comparative measurements were made at a few locations by the resonance technique using the Vidigage. Previous measurements were made at only one point on the outside of the core tank with the Vidigage.

A recent study revealed that the velocity of ultrasound in Zircaloy-2 varies by as much as 3%. Certain peculiarities in the Vidigage system which arise because of the use of high-order harmonic resonances can produce measurement errors as large as the percentage velocity variation multiplied by the harmonic number. The Immerscope method, although usually less precise than the Vidigage method, measures directly the length of elapsed time between successive pulse reflections across the wall. This time interval can be measured to within about ±1%, and thus the maximum error, including errors due to the difference in average and actual ultrasonic velocity in Zircaloy-2, is 4%. Since the velocity used for calculation was determined from actual pieces of core-vessel plate, the error should be much smaller.

Measurements were made at approximately 30° intervals longitudinally and at approximately 20° intervals latitudinally. In a few selected areas more measurements were taken at closer spacing. Many points were measured twice, and a few three or more times, in a manner requiring complete repositioning of the unit at various times during the measuring; in most cases the values checked within 2 mils, with 4 mils being the largest discrepancy. Many points were also checked, using the same crystal and positioning rig but measuring with the Vidigage. Except for a single point discussed below, the two sets of data again checked within about 4 mils.

Figure 22.1 is a representation of the vessel from 90 to 270° and from 270 to 90° (0° corresponding with building north), the points measured, and the thicknesses which were determined. The thickness in the central and upper portion of the vessel varies from about 0.297 to 0.313 in. (297 to 313 mils). In the lower region of the vessel, thicknesses of 262 to 310 mils were noted. Heavy scale deposits in the lower region caused difficulty and, in some instances, prevented measurement. At the areas where two numbers are shown enclosed in a bracket, it was not possible to get a definite reading, because of scale or roughly ground surfaces which tipped the crystal; excessive attenuation may also have interfered. In the few areas where this occurred and which could be checked by other means, a single reading was obtained that fell between the two limits. A single number represents one or more clear readings.

---

*These measurements were made by J. W. Allen and R. W. McClung of the Nondestructive Test Group of the Metallurgy Division.

UNCLASSIFIED
ORNL-LR-DWG 44308

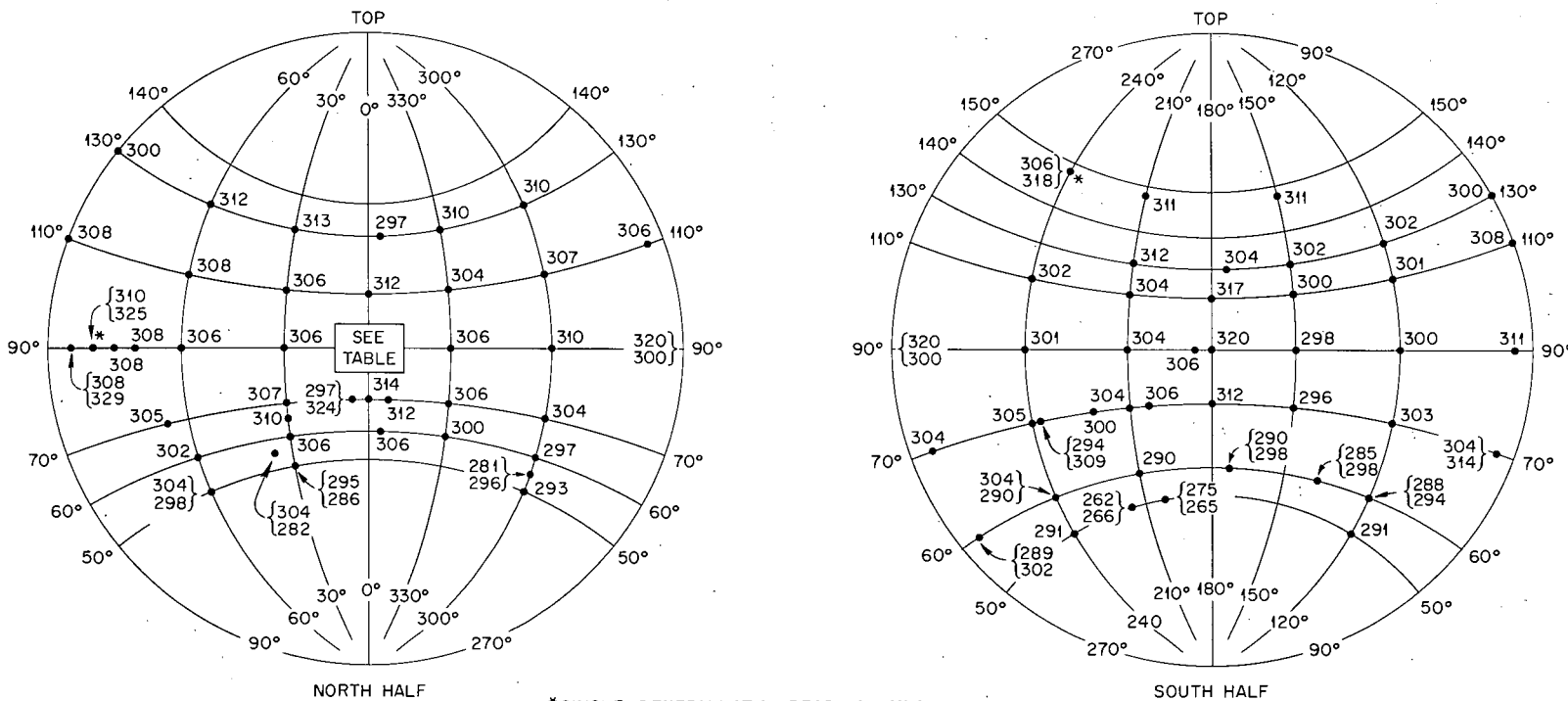

*SINGLE-DETERMINATION READING NOT DISTINCT.

Fig. 22.1. Thickness Measurements for HRT Core Vessel Measured with an Immerscope.

The original thicknesses of the vessel were measured ultrasonically at Newport News and have been reported previously.[5] These values vary from 300 to 320 mils and average 311 mils; the original plate thickness was reported as being 310 to 317 mils. While it is not possible, at this time, to obtain exact comparisons by indexing the two sets of measurements (no common reference point is now available), by making over-all comparisons it appears that in the main portion of the vessel some attack has occurred, but it has not been heavy. However, in some areas in the lower portion the attack has been more pronounced.

Exceptions to the above thickness values were noted in the immediate vicinity of the four vertical welds which were oriented approximately at 0, 90, 180, and 270°, or approximately on the building north, south, east, and west axes. These welds, which presented considerable difficulty in making the measurements, appeared to be somewhat thicker than the parent metal, with the thickness being in the range from 308 to about 330 mils. A series of measurements in this area at the equator show that small changes in position can cause variations in the indicated thickness of as much as 20 mils, Table 22.1.

The position which was measured previously from outside the core tank through the blanket access port is at 0° at the equator and is on one of the welds. Vidigage measurements prior to run 15 indicated a thickness of 315 to 325 mils. After run 17 the thickness was measured to be 278 mils, indicating a considerable loss in thickness.[6] The first Vidigage measurement in this series indicated a thickness of 269 mils; however, subsequent readings produced the data in Table 22.1. It is concluded that the measurement after run 17 was in error and that there has been little corrosion in the reference area.

Table 22.1. Variation in Core-Tank Thickness (Mils) near Reference Point

Degrees Latitude	Degrees Longitude				
	357	0	3	5	7
93	310	314	328		313
90	311	309, Vidigage 308, 310, 312	323	(325-331)*	307
87	309	(316-309)*	322		

*Single-determination reading not distinct.

22.2 ZIRCALOY-2 FABRICATION STUDY

Although a fabrication procedure has been developed[7] that will yield a Zircaloy-2 plate with reduced preferred orientation and mechanical fibering, this procedure has not been shown to yield optimum properties. A study has therefore been undertaken to evaluate the various fabrication procedures and to determine the effects of specific fabrication variables on the final state of anisotropy. The aims, experimental procedures, and variables studied have been reported previously.[8-10]

To supplement the data on the 12 schedules reported previously,[9-10] tensile and impact data have been obtained on eight additional schedules, including two commercial adaptations of the basic ORNL procedure and six new experimental schedules. The new schedules were designed to show the effects of cross rolling at various stages of fabrication and to show the effects of the degree of final reduction (25 vs 40%) on the anisotropy of the mechanical properties of Zircaloy-2 produced by the fabrication procedure developed at ORNL. The conclusions that may be drawn from these tests are:

1. Final warm working of either 25 or 40% in the last stage of the HRP commercial fabrication schedule produces similar mechanical properties. The degree of preferred orientation is, however, greater for the material reduced 40% in the final working, as shown by the greater ellipticity of cross section in the fractured tensile specimens.

2. Cross rolling with the ingot axis normal to the rolling plane (ingot slice) during ingot breakdown tends to decrease the differences in the tensile properties in the rolling and transverse directions but also decreases the contractile strain in the normal direction in comparison to its straight-rolled counterpart.

3. Cross rolling with the ingot axis in the rolling plane and in the transverse direction gives a material with much higher yield strength in the transverse than in the rolling direction. The contractile strain in the normal to the rolling plane is greater than that in the transverse direction in specimens whose tensile axis is in the rolling direction.

4. All-beta rolling before the final warm reduction produces mechanical properties which are comparable to those of material produced by the standard HRP schedule, but the contractile strain in the normal direction is smaller than for material which has had intermediate alpha rolling.

Analyses of the tensile data from all the fabrication schedules have confirmed the statement, reported previously,[8] that since all tensile values fall within ranges of only 10,000 psi, the effects of the fabrication variables on anisotropy are difficult to separate by a comparison of the tensile properties. Examination of the cross sections of fractured tensile specimens from the fracture to the shoulder has shown that the cross sections, originally circular, become elliptical wherever plastic flow has occurred and that the ellipticity varies from schedule to schedule and with specimen orientation within the schedule. A number of analyses involving the major and minor axes of the ellipse of cross section, for example, the "elliptical index,"[9] were attempted as an aid in separating the fabrication variables, but all were lacking in that they were not independent of the distance from the fracture. By eliminating the distance from the fracture as a variable and plotting each of the cross-section contractile natural strains as a function of the tensile natural strain at the same points, straight lines are obtained with slopes which are characteristic of the anisotropy of each material.

Efforts are being made to extend the relationships further so as to permit prediction by calculations of the strain characteristics of specimens pulled in the direction normal to the plate. The development of these relationships has been covered in detail in other reports.[10] Correlations are now being developed between the slopes of the strain plots and the tensile, impact, and inverse-pole-figure data. X-ray diffraction preferred orientations have been run and inverse pole figures plotted on 12 selected schedules for use in such comparisons.

22.3 FORMING OF ZIRCALOY-2

Power spinning of Zircaloy-2 has been tried as a method for fabricating future core vessels. The forming of hemispheres having 1/8-, 1/4- and 5/16-in. walls has been discussed previously.[11] While three spheres were fabricated, it required hand picking and fitting plus some machining to obtain fitups close enough for satisfactory girth welds.

During this period, the hemispheres and spheres were carefully measured by the ORNL mechanical department, using both ultrasonic and mechanical means. The new measurements show larger variations than were reported by the fabricator but would not otherwise change the previous conclusions. Variations in ellipticity and thinout will require either large (up to 100%) machining allowances or resizing by hot pressing to achieve the tolerances required for welding. While it appears to be feasible to form Zircaloy-2 hemispheres by power spinning, the problems introduced by the poor dimensional control are greater than had originally been predicted by the fabricators.

22.4 ZIRCONIUM ALLOY DEVELOPMENT

Zirconium-base alloys containing niobium have shown considerable promise for the development of a more corrosion-resistant alloy to replace Zircaloy-2 as the core-tank material for aqueous homogeneous reactors. The information necessary for the development of these alloys is being procured by basic physical metallurgical studies and in-pile corrosion tests.

Considerable data have been obtained and reported[12] on the quench-and-reheat aging transformation in Zr-15Nb-X and Zr-20Nb-X alloys. To complete the work previously done, both short-time and long-time agings were made on a number of the Zr-15Nb-X and Zr-20Nb-X alloys at several temperatures. The hardness data have been determined, but the analysis of those data is not yet complete. Recent rechecks of the kinetics data reported for the Zr-15Nb binary with two newly melted ingots have not shown the reproducibility expected. Chemical analyses are being made for variation in niobium and impurity contents.

Determinations of the transformation sequence for the Zr-15Nb binary have been made with the use of rotation, oscillation, and Weissenberg x-ray diffraction techniques.[13,14] On aging at temperatures below 525°C, the sequence has been found to be: decomposition of the body-centered-cubic (bcc) retained beta phase to a metastable hexagonal omega phase containing up to 7% niobium and a bcc beta phase which is progressively enriched in niobium with increasing aging time. After additional aging at 450°C and higher, the metastable omega phase is eventually replaced by a close-packed-hexagonal equilibrium alpha phase, which also contains approximately 5% Nb. After three weeks of aging at 400°C, samples have not shown the presence of detectable amounts of alpha phase.

A Widmanstätten martensitic phase is found in the microstructure of beta-quenched Zr-Nb alloys containing more than 12% Nb. The phase has been identified as a monoclinic structure which can be obtained by a 5° distortion of a body-centered-tetragonal structure with a c/a ratio of 1.1. The Widmanstätten phase appears only on the (100) type planes of the bcc matrix and will redissolve into the matrix without decomposition on reheating to 250°C or higher.

Similar examinations of a few of the ternary alloys have shown no effect of the ternary addition on the sequence of transformation or the nature of the products formed, but increases in the incubation times for the reactions were observed.

REFERENCES

1. G. M. Adamson et al., HRP Quar. Prog. Rep. Jan. 31, 1959, ORNL-2696, p 152.

2. G. M. Adamson et al., HRP Quar. Prog. Rep. Apr. 30, 1959, ORNL-2743, p 168.

3. G. M. Adamson et al., Met. Div. Ann. Prog. Rep. Oct. 1959, ORNL-2839, p 110.

4. I. Spiewak, HRP Quar. Prog. Rep. Jan. 31, 1959, ORNL-2696, p 28.

5. D. E. Tackett, "Fabrication History of HRT Core Tank," Appendix E, ORNL CF-58-12-6 (July 1, 1955).

6. G. M. Adamson, HRP Quar. Prog. Rep. Oct. 31, 1958, ORNL-2654, p 191.

7. M. L. Picklesimer and G. M. Adamson, Development of a Fabrication Procedure for Zircaloy-2, ORNL CF-56-11-115 (Nov. 21, 1956).

8. G. M. Adamson et al., HRP Quar. Prog. Rep. Oct. 31, 1959, ORNL-2654, pp 184-186.

9. G. M. Adamson et al., HRP Quar. Prog. Rep. Apr. 30, 1959, ORNL-2743, pp 183-191.

10. G. M. Adamson et al., Met. Div. Ann. Prog. Rep. Oct. 1959, ORNL-2839, pp 127-129.

11. G. M. Adamson et al., HRP Quar. Prog. Rep. Apr. 30, 1959, ORNL-2743, p 191.

12. G. M. Adamson et al., HRP Quar. Prog. Rep. Oct. 31, 1957, ORNL-2432, pp 131-133.

13. M. L. Picklesimer et al., Met. Div. Ann. Prog. Rep. Oct. 1958, ORNL-2632, pp 67-70 (classified).

14. H. L. Yakel, Jr., Met. Div. Ann. Prog. Rep. Oct. 1958, ORNL-2632, pp 29-33 (classified).

Part VII

ANALYTICAL CHEMISTRY

23. ANALYTICAL CHEMISTRY

O. Menis H. P. House D. L. Manning T. C. Rains

C. M. Boyd
R. G. Ball[1]
G. Goldstein
N. M. Ferguson

U. Koskela P. F. Thomason H. E. Zittel

C. P. Baker
R. E. Corcoran
S. R. Dinsmore
L. G. Farrar
A. D. Horton
F. J. Miller
J. L. Mottern[2]

23.1 DETERMINATION OF MOLYBDENUM BY DERIVATIVE POLAROGRAPHY

A derivative polarographic method was developed for the determination of small amounts of molybdenum in impure slurries of ThO_2-UO_x. The method is based on either of two reduction waves of molybdenum, which have $E_{1/2}$ values of -0.48 and -0.64 v versus the SCE in a 0.15 M nitrilotriacetic acid solution of pH 3. At either voltage, the diffusion current is directly proportional to the concentration of molybdenum. By utilizing the wave at -0.64 v versus the SCE and the standard addition technique, molybdenum in the range of 20 to 200 μg/ml can be estimated with a coefficient of variation of the order of 5%. The tolerance limits of U(VI), Cr(VI), Fe, and Ni are, respectively, 10, 10, 7, and 0.1 times the concentration of molybdenum.

23.2 PYROLYTIC SEPARATION OF FLUORIDE FROM NITRATE OR SULFATE SOLUTIONS

Pyrolysis was applied to the separation of microgram quantities of fluoride from HNO_3-$Al(NO_3)_3$ solutions and also from H_2SO_4-H_2O_2 solutions, prior to the determination of the fluoride by titration with $Th(NO_3)_4$. Procedures were devised to circumvent difficulties initially encountered due to the interference by volatile pyrolytic products of nitrate and sulfate with the fluoride titration. The nitrate or sulfate solutions are made basic and evaporated to dryness. The nitrate residue is then pyrolyzed with U_3O_8 as flux at 1000°C while the sulfate residue is overlaid with $K_2Cr_2O_7$ as flux and then pyrolyzed at 650°C. In each case, the fluoride is volatilized, liberated as HF, absorbed in dilute NaOH and, after dilution of the solution, determined volumetrically. For microgram quantities of fluoride, the coefficient of variation is 5% or less.

23.3 FLAME-PHOTOMETRIC DETERMINATION OF RARE-EARTH ELEMENTS

Additional data relative to the flame spectra of all rare-earth elements except cerium and promethium were collected for further evaluation of the applicability of flame photometry to the estimation of individual rare-earth elements, particularly in mixtures. Characteristic bands and lines of the spectra were located precisely by means of a prism and a grating spectrograph. These data were utilized in interpreting detailed flame spectra of the several rare-earth elements which were obtained by means of a recording flame photometer equipped with a mask which radically reduced the background emissivity by screening out light from the luminous inner core.

23.4 FURTHER STUDY OF THE DETERMINATION OF OSMIUM BY A COLORIMETRIC METHOD

Studies have been continued on a colorimetric method for the determination of osmium, with particular emphasis on the procedure in which the colored complex, osmium diphenylcarbazide, is developed in the aqueous phase and on an evaluation of interferences. After development of the colored complex in a perchloric-acetic acid solution at 65°C, the solution is cooled, extracted with chloroform, and the absorbancy of the organic extract is measured. Operating conditions have been established whereby a molar absorbancy index of 150,000 can be attained. For osmium in the range of 0.2 to 2 μg/ml, the coefficient of variation is 6%. Iron(III), Cu(II), Ru(III), and Au(III) interfere seriously, while Cr(VI), Ni, Mo(VI), and Ir(III) interfere only when they are present in amounts greater than 100 times that of the osmium. Chloride in concentrations exceeding 0.1 M interfere by inhibiting complete color development.

23.5 COULOMETRIC DETERMINATION OF U(IV) AND U(VI) IN ThO_2-UO_x

The application of coulometry to the determination of U(IV) and U(VI) in slurries of ThO_2-UO_x has been investigated further.[3] Limitations encountered due to the difficulty of pre-reducing the interfering ions, Fe(III) and Cr(IV), in an HCl medium have been partially overcome by the substitution of an H_3PO_4 medium. The slurry is dissolved by refluxing it under an inert (argon) atmoshere in 7 M H_3PO_4 containing a few drops of HF. The Fe(III) and Cr(VI) in an aliquot diluted until the H_3PO_4 is 2 M is coulometrically reduced at 0.0 v versus an Ag/AgCl electrode, after which the U(VI) is determined by coulometric reduction at a controlled potential of -0.3 v. As previously described,[3] total U is also determined coulometrically after oxidation of U(IV) with $HClO_4$, and U(IV) is calculated by difference. The chief difficulty in this procedure is the selection of a potential at which the interfering ions will be completely reduced without partial reduction of U(VI); the optimum prereduction potential is a function of the Fe(III)/U(VI) and Cr(VI)/U(VI) ratios. For this reason, other procedures, for example, the use of a platinum electrode to carry out the prereduction of interfering ions and also the direct coulometric oxidation of U(IV) to U(VI), are under investigation.

23.6 DETERMINATION OF FREE ACID IN THE HRT FEED SOLUTION

Throughout HRT runs 17 and 18, a potentiometric method was used to determine free acid.[4] The results, however, for both control and reactor samples were quite erratic.[5] Consequently, for run 20, a new method, suggested by McDuffie,[6]

was utilized.[7] In brief, the method is as follows: A Dowex-50 cation-exchange resin column is prepared by washing it with a 2.5 M Li_2SO_4 solution. The sample solution is then passed through this column, after which the resin is washed with 0.05 M Li_2SO_4 and the acid in the eluate is titrated photometrically with a standard solution of a base. The titration is made with an ORNL automatic titrator,[8] utilizing chlorphenol red as the indicator. In the analysis of 60 control samples, in which the acid was approximately 0.02 M, the coefficient of variation was 4%.

Consistently high results were obtained for one control sample which was found to be the only one containing significant amounts of iron. Iron is apparently hydrolyzed on the resin and, as a consequence, the results for free acid are high. The tolerance limit for iron is approximately 100 ppm. Since the concentration of iron in the "hot" samples was much less than 100 ppm, no modification of the procedure was considered to be necessary.

Currently a thermometric method[9] for the estimation of free acid is being evaluated in the High-Radiation-Level Analytical Facility.

23.7 COULOMETRIC ANALYSIS OF HOMOGENEOUS REACTOR FUEL

Copper, uranium, and nickel were determined in the fuel solution throughout run 20 of the HRT by a coulometric method previously described[10] which was modified somewhat during the run.[11] A standard calomel electrode is now used as the reference electrode because it was found to be more stable than the Ag/AgCl electrode previously used.

Iron, if present, is prereduced by electrolyzing at -0.09 v versus the SCE. Copper and uranium are determined by measuring the integrated current necessary to reduce both elements at a potential of -0.325 v versus the SCE, after which the copper is determined by coulometric oxidation of the copper at +0.150 v versus the SCE. A background current of 0.05 ma indicates complete oxidation. Uranium is computed from the difference between the integrated current for the reduction of both uranium and copper and for the oxidation of copper alone. The solution is then made alkaline with NH_4OH, degassed with nitrogen, and pretitrated at a potential of -0.8 v versus the SCE, after which the nickel is determined by electrolyzing the solution at -1.225 v versus the SCE until the background current is 0.05 ma. The integrated current during this operation is a measure of the nickel content of the sample.

An extraction procedure reported previously[10] has not been applied because there has been no holdup of expected fission-product poisons.

A summary of the precision results of the analyses of control samples is given in Table 23.1.

23.8 ANALYSIS OF HRT OFF-GAS AND SHIELD GAS BY GAS CHROMATOGRAPHY

During run 20 of the HRT, 23 samples of reactor off-gas and 18 samples of gas from the reactor shield were analyzed by means of gas chromatography on a molecular-sieve column 1.6 m long and 1/4 in. in diameter. Reactor off-gas contains principally oxygen, with the deuterium or hydrogen content varying from less than 0.1 vol % after shutdown to 15.2 vol % at peak power. The average deuterium content was 5.3 vol %. The off-gas contains carbon monoxide and

carbon dioxide, usually about equal in amount, in the range of <0.01 to 3.2 vol %. In 90% of the samples the carbon monoxide - carbon dioxide content was less than 1 vol %. Shield gas is nitrogen-enriched air in which the oxygen content ranges from 3.2 to 22 vol %, and averages 11 vol %.

Table 23.1. Precision of Test Results in the Analysis of HRT Control Samples for Period July - September, 1959

Component	Number of Determinations	Coefficient of Variation (%)
Uranium	79	1.8
Sulfate	78	1.3
Copper	81	1.4
Nickel	77	2.6

REFERENCES

1. Present address, American Cyanamid Co., New Orleans, La.

2. Present address, Davison Chemical Company, Erwin, Tenn.

3. O. Menis, et al., HRP Quar. Prog. Rep. Apr. 30, 1958, ORNL-2561, p 327-332.

4. J. L. Mottern, Anal. Chem. Ann. Prog. Rep. Dec. 31, 1957, ORNL-2453, p 56.

5. H. F. McDuffie, L. O. Gilpatrick, and H. H. Stone, HRP Quar. Prog. Rep. Oct. 31, 1958, ORNL-2654, p 226.

6. H. F. McDuffie, L. O. Gilpatrick, and H. H. Stone, HRP Quar. Prog. Rep. Jan. 31, 1959, ORNL-2696, p 216.

7. F. J. Miller and H. E. Zittel, "Evaluation of the Free-Acid Determination in Uranyl Sulfate Solutions by the Dowex-50 Resin Separation Procedure," Anal. Chem. Div. Preliminary Report FJM-13:HEZ-3 (Jan. 21, 1959).

8. E. B. Wagner, "Automatic Potentiometric Titrator, Velocity Servo, ORNL Model Q-1728," Method Nos. 1 003028 and 9 003028 (6-21-56), ORNL Master Analytical Manual; TID-7015, Sec. 1.

9. F. J. Miller and P. F. Thomason, Thermometric (Enthalpymetric) Titration of Free Acid in the Presence of Certain Hydrolyzable Ions, ORNL-2489 (June 13, 1958).

10. O. Menis, U. Koskela, et al., HRP Quar. Prog. Rep. Apr. 30 and July 31, 1958, ORNL-2561, p 330.

11. A. D. Horton, et al., Proceedings, Second Conference, Analytical Chemistry in Nuclear Reactor Technology, TID-7568 (Pt. 2) (Apr., 1959), p 96.

OAK RIDGE NATIONAL LABORATORY
HOMOGENEOUS REACTOR PROJECT

OCTOBER 1, 1959

PROGRAM DIRECTOR

R. B. BRIGGS — D
A. L. GUNNELS, SEC. — REE

PROGRAM EDITOR

W. D. REEL — TI

DESIGN AND ENGINEERING

R. N. LYON, ASSOCIATE DIRECTOR — REE
T. K. CARLSMITH,* SEC. — REE

DESIGN

W. R. GALL,** SECTION CHIEF — REE
M. I. LUNDIN,** ASSISTANT SECTION CHIEF — REE

DESIGN AND SPECIFICATIONS

R. C. ROBERTSON, GROUP LEADER — REE
C. A. BURCHSTED — REE
J. E. JONES, JR. — REE

DRAFTING

J. P. GILL,** GROUP LEADER — REE
W. B. KRICK — REE
L. E. PENTON — REE
T. E. HAYNES — REE

REACTOR ANALYSIS

P. R. KASTEN, SECTION CHIEF — REE

REACTOR PHYSICS

M. TOBIAS, GROUP LEADER — REE
D. R. VONDY — REE
H. A. MACCOLL — REE

ENGINEERING DEVELOPMENT

I. SPIEWAK, SECTION CHIEF — REE
F. N. PEEBLES, ASSISTANT SECTION CHIEF — REE

MAINTENANCE DEVELOPMENT

J. S. CULVER, GROUP LEADER — REE
R. BLUMBERG — REE
E. C. HISE* — REE
P. P. HOLZ — REE
C. JONES — REE

COMPONENT DEVELOPMENT

C. H. GABBARD, GROUP LEADER — REE
E. C. HISE* — REE
J. C. MOYERS — REE
H. R. PAYNE — REE
J. P. HURST — REE
G. A. WINDLE — REE

CORE AND BLANKET DEVELOPMENT

C. G. LAWSON, GROUP LEADER — REE
R. J. KEOL — REE
M. RICHARDSON — REE
R. P. WICHNER — REE
T. L. CASTILE — REE
B. J. YOUNG — REE

SYSTEM DEVELOPMENT

L. F. PARSLY, GROUP LEADER — REE
P. H. HARLEY — REE
R. E. CARNES — REE

LOOP OPERATIONS AND DATA ANALYSIS

D. M. EISSENBERG, GROUP LEADER — REE
H. B. PIPER — REE
A. N. SMITH — REE
J. T. DICKEY — REE
C. A. GIFFORD — REE
H. G. MOORE — REE

ENGINEERING RESEARCH

H. W. HOFFMAN,** SECTION CHIEF — REE

AQUEOUS HOMOGENEOUS REACTOR – SLURRY STUDIES

D. G. THOMAS — REE
P. H. HAYES — REE
R. M. SUMMERS — REE
C. S. MORGAN — REE
B. J. SUTTON — REE

INSTRUMENTATION AND CONTROLS

R. L. MOORE,** SECTION — I&C

REACTOR I&C SYSTEM DESIGN

J. R. BROWN,** GROUP LEADER — I&C
R. W. BORGERS** — I&C
P. E. SMITH** — I&C

HRP SUPPORTING SERVICES

H. D. WILLS, GROUP LEADER — I&C
P. G. HERNDON — I&C
R. M. BURNETT — I&C

VALVE DEVELOPMENT AND SPECIFICATIONS

A. M. BILLINGS, GROUP LEADER — I&C
B. J. JONES — I&C

INSTRUMENT DEVELOPMENT AND EVALUATION

D. G. DAVIS,** GROUP LEADER — I&C
S. J. BALL** — I&C
T. M. CATE** — I&C

REACTOR MATERIALS RESEARCH

E. G. BOHLMANN, ASSOCIATE DIRECTOR — REE
T. K. CARLSMITH,* SEC. — REE
R. E. WACKER, RECORDS — REE

SOLUTIONS

J. C. GRIESS,** SECTION CHIEF — REE
R. S. GREELEY — REE
P. D. NEUMANN** — REE
H. L. BARKER** — REE
W. H. HINDS — REE
B. L. JOHNSON** — REE

SLURRIES

E. L. COMPERE, SECTION CHIEF — REE

OUT-OF-PILE STUDIES

S. A. REED — REE
R. B. GALLAHER — REE
R. P. BENSON — REE
F. E. MCDANIEL* — REE
G. G. WARNER — REE

IN-PILE LOOPS

A. J. SHOR — REE

IN-PILE AUTOCLAVES

L. F. WOO — REE
F. E. MCDANIEL* — REE

MATERIALS EXPERIMENT ENGINEERING

H. C. SAVAGE, SECTION CHIEF — REE

OUT-OF-PILE OPERATIONS

S. E. BOLT,* GROUP LEADER — REE
T. H. MAUNEY — REE

100A LOOPS

J. F. WINESETTE — REE
C. R. BENSON — REE
C. M. BURCHELL — REE

IN-PILE EXPERIMENT FABRICATION

S. E. BOLT,* GROUP LEADER — REE
J. R. HART* — REE
R. W. RAY — REE

IN-PILE SLURRY LOOP

R. A. LORENZ,* GROUP LEADER — REE
J. M. BAKER — REE
J. R. HART* — REE

REACTOR OPERATIONS

R. A. LORENZ,* GROUP LEADER — REE
V. A. DECARLO — REE
K. G. CHANDLER — REE
E. H. GUINN — REE
J. W. MOSIER — REE
J. W. MYERS — REE
D. G. PEACH* — REE
C. E. ROBERTS — REE
R. G. ROSS — REE
A. L. SUTTON — REE
W. E. TEICHERT — REE
R. M. WALLER* — REE

RADIATION

G. H. JENKS, SECTION CHIEF — REE

IN-PILE LOOPS

J. E. BAKER — REE
S. H. WHEELER — REE

IN-PILE BOMBS

R. J. DAVIS — C
J. L. RUTHERFORD — REE

SUPPORTING RESEARCH

A. L. BACARELLA — C
J. C. BANTER — REE

METALLURGY

G. M. ADAMSON, SECTION CHIEF — M
F. W. COOKE — M
W. J. LEONARD — M
M. L. PICKLESIMER** — M
P. L. RITTENHOUSE** — M
C. H. WOOTKE — M
P. J. JONES** — M
G. C. NELSON** — M
C. M. SMITH — M

METALLOGRAPHY

R. S. CROUSE,** LEADER — M
T. M. KEGLEY, JR.** — M
B. F. DAY** — M
R. L. FITZGERALD** — M
T. J. HENSON** — M

SUBCONTRACT
UNIVERSITY OF UTAH

AC — ANALYTICAL CHEMISTRY DIVISION
C — CHEMISTRY DIVISION
CT — CHEMICAL TECHNOLOGY DIVISION
D — DIRECTOR'S DIVISION
I&C — INSTRUMENTATION AND CONTROLS DIVISION
M — METALLURGY DIVISION
RC — REACTOR CHEMISTRY DIVISION
REE — REACTOR EXPERIMENTAL ENGINEERING DIVISION
TI — TECHNICAL INFORMATION DIVISION
* — DUAL CAPACITY
** — PART TIME

INDUSTRIAL PARTICIPATION
JAPANESE ATOMIC ENERGY RESEARCH INSTITUTE

CHEMICAL TECHNOLOGY

D. E. FERGUSON,** PROBLEM LEADER — CT
I. LOOPE, SEC. — CT
J. MAYES, SEC. — CT

CHEMICAL DEVELOPMENT

D. E. FERGUSON,** SECTION CHIEF — CT

OXIDE PREPARATION

O. C. DEAN,** GROUP LEADER — CT
A. T. KLEINSTEUBER** — CT
K. H. MCCORKLE** — CT
C. E. SCHILLING** — CT
C. W. GREENE** — CT

THORIUM OXIDE STUDIES

J. P. MCBRIDE, GROUP LEADER — CT
N. A. KROHN, PROBLEM LEADER — CT
IRRADIATION STUDIES
L. E. MORSE — CT
P. P. HAYDON — CT
W. L. PATTISON — CT
H. F. SOARD — CT

SURFACE CHEMISTRY

C. H. SECOY, GROUP LEADER — CT
H. F. HOLMES — CT
F. H. SWEETON — CT

DESIGN

W. E. UNGER,** ASSISTANT SECTION CHIEF — CT

ThO_2 DEVELOPMENT DESIGN

J. C. SUDDATH** — CT

HRT-CP DESIGN SUPPORT

H. O. WEEREN** — CT

INSTRUMENTATION

C. S. LISSER** — I&C

PILOT PLANT

R. B. LINDAUER,** SECTION CHIEF — CT

THORIUM OXIDE PREPARATION

W. H. LEWIS,** GROUP LEADER — CT
R. H. WINGET, PROBLEM LEADER — CT

UNIT OPERATIONS

P. A. HAAS,** GROUP LEADER — CT

SLURRY PREPARATION DEVELOPMENT

C. C. HAWS, JR. — CT
K. O. JOHNSSON — CT
V. L. FOWLER — CT
R. D. ARTHUR — CT

CHEMICAL RESEARCH

H. F. MCDUFFIE,** ASSISTANT DIRECTOR — RC
T. F. KELLY, SEC. — RC

HETEROGENEOUS EQUILIBRIA IN AQUEOUS SYSTEMS

W. L. MARSHALL, GROUP LEADER — RC
J. S. GILL — RC
G. M. HEBERT — RC
E. V. JONES — CONSULTANT
R. E. MOORE — RC
R. SLUSHER — RC

REACTIONS IN AQUEOUS SOLUTIONS

G. M. WATSON, SUPERVISOR — RC
M. J. KELLY, GROUP LEADER — RC
D. R. CUNEO — RC
L. O. GILPATRICK — RC
M. D. SILVERMAN — RC
H. H. STONE — RC

ANALYTICAL CHEMISTRY

MYRON T. KELLEY,** DIRECTOR
C. D. SUSANO,** ASSOCIATE DIRECTOR

K. A. ODOM,** SEC. — AC
H. E. ZITTEL, COORDINATOR — AC
HRP ANALYTICAL CHEMISTRY

CORROSION ANALYTICAL LABORATORY

O. MENIS,* SECTION CHIEF — AC
H. P. HOUSE,** ASSISTANT SECTION CHIEF — AC

RESEARCH

O. MENIS,* GROUP LEADER — AC
C. M. BOYD — AC
D. L. MANNING, GROUP LEADER — AC
G. GOLDSTEIN — AC

DEVELOPMENT AND SPECIAL ANALYSES

T. C. RAINS, GROUP LEADER — AC
N. M. FERGUSON — AC

SERVICE

C. K. TALBOTT, SUPERVISOR — AC
F. L. LAYTON — AC
T. P. RACON — AC
W. D. CLAPP, JR. — AC
C. A. CLARK — AC
P. S. GOODWIN — AC
B. D. HICKS — AC
T. G. MILLER — AC
E. ONEST — AC

SPECTROCHEMICAL SERVICES

C. FELDMAN,** SUPERVISOR — AC
W. R. MUSICK** — AC
A. H. MARSHALL** — AC
J. A. MORRIS,** GROUP LEADER — AC
J. J. MUNDZAK** — AC

HRT AND IN-PILE LOOP ANALYSIS

U. KOSKELA, SUPERVISOR — AC
L. G. FARRAR, ASSISTANT SUPERVISOR — AC
C. P. BAKER — AC
R. E. CORCORAN — AC
S. R. DINSMORE — AC
G. M. CAMPBELL — AC
G. I. GAULT — AC
F. K. HEACKER — AC
M. H. MCCORQUODALE — AC
H. L. WEBB — AC
H. L. WHITTINGTON — AC
J. L. SHARP — AC

RADIOCHEMICAL ANALYSIS

E. I. WYATT,** SUPERVISOR — AC

HRT DEVELOPMENT

P. F. THOMASON,** GROUP LEADER — AC
R. E. BIGGERS** — AC
F. J. MILLER** — AC
S. A. REYNOLDS,** GROUP LEADER — AC
J. S. ELDRIDGE** — AC
T. H. HANDLEY** — AC
W. S. LYON** — AC

HIGH RADIATION LABORATORY

J. E. MORTON,** SUPERVISOR — AC

NUCLEAR ANALYSIS LABORATORY

G. W. LEDDICOTTE,** SUPERVISOR — AC
L. C. BATE** — AC
R. W. HARVEY** — AC

OPTICAL AND ELECTRON MICROSCOPY

T. E. WILLMARTH,** GROUP LEADER — AC

HOMOGENEOUS REACTOR TEST

S. E. BEALL, PROJECT ENGINEER — REE
B. EUBANK, SEC. — REE
D. SCOTT, JR., SPECIAL ASSIGNMENT — REE

J. W. HILL, JR., ASSISTANT SECTION CHIEF — REE
J. R. BUCHANAN, ASSISTANT FOR PLANNING — CT
R. H. GUYMON, CHIEF — CT
J. D. FLYNN, ASSISTANT FOR OPERATIONS — REE
H. C. ROLLER — REE
J. D. JONES — REE
R. J. HARVEY, SHIFT SUPERVISOR — REE
R. SMITH, JR., CONTROL ROOM SUPERVISOR — REE
D. T. GODWIN — REE
T. G. HILL — REE
A. L. JOHNSON — REE
H. F. BAUMAN, SHIFT SUPERVISOR — CT
E. W. BROWN, CONTROL ROOM SUPERVISOR — CT
J. D. BARNES — REE
E. D. BOLLING — REE
W. T. BOSTIC — CT
D. F. FRECH, SHIFT SUPERVISOR — REE
R. J. SHANNON, CONTROL ROOM SUPERVISOR — CT
P. B. DAVIS — REE
J. E. EVE — REE
L. J. SHERSKY — CT
J. E. WOLFE — REE
N. C. BRADLEY, SHIFT SUPERVISOR — CT
J. L. STEPP, CONTROL ROOM SUPERVISOR — REE
H. D. CURTIS — REE
T. W. HODGE — REE
F. L. ROUSER — REE

MAINTENANCE PLANNING

W. TERRY, SUPERVISOR — REE
G. H. JOHNSTONE — REE
L. P. PUGH — REE

INSTRUMENTATION

J. L. REOFORD, GROUP LEADER — I&C

P. N. HAUBENREICH,* ASSISTANT SECTION CHIEF — REE

REACTOR ANALYSIS

P. N. HAUBENREICH,* GROUP LEADER — REE
S. R. BUXTON — REE
J. HIROTA — JAPANESE ATOMIC ENERGY RESEARCH INSTITUTE
J. O. KOLB — REE
J. A. WATTS — REE

REACTOR CHEMISTRY

D. M. RICHARDSON, GROUP LEADER — REE
D. G. PEACH* — REE
R. M. WALLER* — REE

CHEMICAL PLANT

W. D. BURCH, GROUP LEADER — CT
O. O. YARBRO — CT

PERSONNEL SUMMARY

	FULL TIME	PART TIME	INDUSTRIAL PARTICIPATION	TOTAL
ADMINISTRATION	5	4	0	9
ANALYTICAL CHEMISTRY	27	19	0	46
CHEMICAL RESEARCH	11	0	0	11
CHEMICAL TECHNOLOGY	14	12	0	26
DESIGN AND ENGINEERING	47	11	0	58
HOMOGENEOUS REACTOR TEST	41	0	1	42
REACTOR MATERIALS RESEARCH	41	13	0	54
TOTAL	186	59	1	246

INTERNAL DISTRIBUTION

1. C. E. Center
2. Biology Library
3. Health Physics Library
4. Metallurgy Library
5-6. Reactor Experimental Engineering Library
7-9. Central Research Library
10-14. Laboratory Records Department
15. Laboratory Records, ORNL R.C.
16. G. M. Adamson
17. A. L. Bacarella
18. J. E. Baker
19. S. J. Ball
20. J. C. Banter
21. S. E. Beall
22. L. L. Bennett
23. A. M. Billings
24. D. S. Billington
25. E. P. Blizard
26. R. Blumberg
27. E. G. Bohlmann
28. S. E. Bolt
29. C. J. Borkowski
30. G. E. Boyd
31. J. C. Bresee
32. F. R. Bruce
33. J. R. Buchanan
34. W. D. Burch
35. C. A. Burchsted
36. S. R. Buxton
37. A. D. Callihan
38. T. A. Carlson
39. W. L. Carter
40. G. H. Cartledge
41. R. H. Chapman
42. R. A. Charpie
43. R. D. Cheverton
44. C. J. Claffey
45. H. C. Claiborne
46. T. E. Cole
47. C. W. Collins
48. E. L. Compere
49. F. L. Culler
50. D. G. Davis
51. R. J. Davis
52. V. A. DeCarlo
53. W. K. Eister
54. L. B. Emlet (K-25)
55. J. L. English
56. D. E. Ferguson
57. D. F. Frech
58. J. H. Frye, Jr.
59. C. H. Gabbard
60. J. L. Gabbard
61. W. R. Gall
62. R. B. Gallaher
63. E. H. Gift
64. H. E. Goeller
65. R. S. Greeley
66. A. T. Gresky
67. J. C. Griess
68. W. R. Grimes
69. E. Guth
70. R. H. Guymon
71. L. A. Haack
72. P. A. Haas
73. J. Halperin
74. P. H. Harley
75. R. J. Harvey
76. P. N. Haubenreich
77. D. N. Hess
78. J. W. Hill
79. E. C. Hise
80. A. Hollaender
81. P. P. Holz
82. H. P. House
83. A. S. Householder
84. S. Jaye
85. G. H. Jenks
86. D. T. Jones
87. E. V. Jones
88. W. H. Jordan
89. P. R. Kasten
90. C. P. Keim
91. M. T. Kelley
92. F. Kertesz
93. J. O. Kolb
94. U. Koskela
95. K. A. Kraus
96. N. A. Krohn
97. J. A. Lane
98. C. G. Lawson
99. S. C. Lind
100. R. B. Lindauer
101. R. S. Livingston
102. R. A. Lorenz
103. M. I. Lundin
104. R. N. Lyon
105. J. L. Marsh (C&CC, South Charleston)
106. W. L. Marshall

107. J. P. McBride
108. H. F. McDuffie
109. H. A. McLain
110. J. R. McWherter
111. O. Menis
112. E. C. Miller
113. C. S. Morgan
114. K. Z. Morgan
115. L. E. Morse
116. J. P. Murray (Y-12)
117. M. L. Nelson
118. P. D. Neumann
119. A. R. Olsen
120. L. F. Parsly
121. F. N. Peebles
122. M. L. Picklesimer
123. B. E. Prince
124. L. R. Quarles
125. S. A. Reed
126. W. D. Reel
127. P. M. Reyling
128. S. A. Reynolds
129. L. Rice
130. D. M. Richardson
131. R. C. Robertson
132. W. Robinson
133. H. C. Roller
134. M. W. Rosenthal
135. H. C. Savage
136. C. E. Schilling
137. H. E. Seagren
138. C. H. Secoy
139. C. L. Segaser
140. E. D. Shipley
141. M. D. Silverman
142. M. J. Skinner
143. A. N. Smith
144. E. S. Snavely
145. A. H. Snell
146. I. Spiewak
147. H. H. Stone
148. R. W. Stoughton
149. C. D. Susano
150. J. A. Swartout
151. A. Taboada
152. E. H. Taylor
153. W. Terry
154. D. G. Thomas
155. P. F. Thomason
156. M. Tobias
157. W. E. Unger
158. W. C. Ulrich
159. R. Van Winkle
160. D. W. Vroom
161. R. E. Wacker
162. H. O. Weeren
163. A. M. Weinberg
164. S. H. Wheeler
165. E. P. Wigner (consultant)
166. H. D. Wills
167. G. C. Williams
168. J. C. Wilson
169. R. H. Winget
170. C. E. Winters
171. L. F. Woo
172. F. C. Zapp
173. ORNL - Y-12 Technical Library, Document Reference Section
174. HRP Director's Office, Y-12

EXTERNAL DISTRIBUTION

175. Division of Research and Development, AEC, ORO
176-752. Given distribution as shown in TID-4500 (15th ed.) under Reactors-Power category (75 copies - OTS)

Reports previously issued in this series are as follows:

ORNL-527	Date Issued, December 28, 1949
ORNL-630	Period Ending February 28, 1950
ORNL-730	Feasibility Report - Date Issued, July 6, 1950
ORNL-826	Period Ending August 31, 1950
ORNL-925	Period Ending November 30, 1950
ORNL-990	Period Ending February 28, 1951
ORNL-1057	Period Ending May 15, 1951
ORNL-1121	Period Ending August 15, 1951
ORNL-1221	Period Ending November 15, 1951
ORNL-1280	Period Ending March 15, 1952
ORNL-1318	Period Ending July 1, 1952
ORNL-1424	Period Ending October 1, 1952
ORNL-1478	Period Ending January 1, 1953
ORNL-1554	Period Ending March 31, 1953
ORNL-1605	Period Ending July 31, 1953
ORNL-1658	Period Ending October 31, 1953
ORNL-1678	Period Ending January 31, 1954
ORNL-1753	Period Ending April 30, 1954
ORNL-1772	Period Ending July 31, 1954
ORNL-1813	Period Ending October 31, 1954
ORNL-1853	Period Ending January 31, 1955
ORNL-1895	Period Ending April 30, 1955
ORNL-1943	Period Ending July 31, 1955
ORNL-2004	Period Ending October 31, 1955
ORNL-2057	Period Ending January 31, 1956
ORNL-2096	Period Ending April 30, 1956
ORNL-2148	Period Ending July 31, 1956
ORNL-2222	Period Ending October 31, 1956
ORNL-2272	Period Ending January 31, 1957
ORNL-2331	Period Ending April 30, 1957
ORNL-2379	Period Ending July 31, 1957
ORNL-2432	Period Ending October 31, 1957
ORNL-2493	Period Ending January 31, 1958
ORNL-2561	Periods Ending April 30 and July 31, 1958
ORNL-2654	Period Ending October 31, 1958
ORNL-2696	Period Ending January 31, 1959
ORNL-2743	Period Ending April 30, 1959